

**CONSTRUCTION AND CHARACTERIZATION OF HYBRID
NANOPARTICLES VIA BLOCK COPOLYMER BLENDS AND
KINETIC CONTROL OF SOLUTION ASSEMBLY**

by

Yingchao Chen

A dissertation submitted to the Faculty of the University of Delaware in partial fulfillment of the requirements for the degree of Doctor of Philosophy in Material Science and Engineering

2015 Spring

© 2015 Yingchao Chen
All Rights Reserved

ProQuest Number: 3730204

All rights reserved

INFORMATION TO ALL USERS

The quality of this reproduction is dependent upon the quality of the copy submitted.

In the unlikely event that the author did not send a complete manuscript and there are missing pages, these will be noted. Also, if material had to be removed, a note will indicate the deletion.



ProQuest 3730204

Published by ProQuest LLC (2015). Copyright of the Dissertation is held by the Author.

All rights reserved.

This work is protected against unauthorized copying under Title 17, United States Code
Microform Edition © ProQuest LLC.

ProQuest LLC.
789 East Eisenhower Parkway
P.O. Box 1346
Ann Arbor, MI 48106 - 1346

**CONSTRUCTION AND CHARACTERIZATION OF HYBRID
NANOPARTICLES VIA BLOCK COPOLYMER BLENDS AND
KINETIC CONTROL OF SOLUTION ASSEMBLY**

by

Yingchao Chen

Approved: _____
Darrin J. Pochan, Ph.D.
Chair of the Department of Material Science and Engineering

Approved: _____
Babatunde A. Ogunnaike, Ph.D.
Dean of the College of Engineering

Approved: _____
James G. Richards, Ph.D.
Vice Provost for Graduate and Professional Education

I certify that I have read this dissertation and that in my opinion it meets the academic and professional standard required by the University as a dissertation for the degree of Doctor of Philosophy.

Signed:

Darrin J. Pochan, Ph.D.
Professor in charge of dissertation

I certify that I have read this dissertation and that in my opinion it meets the academic and professional standard required by the University as a dissertation for the degree of Doctor of Philosophy.

Signed:

David C. Martin, Ph.D.
Member of dissertation committee

I certify that I have read this dissertation and that in my opinion it meets the academic and professional standard required by the University as a dissertation for the degree of Doctor of Philosophy.

Signed:

Thomas H. Epps, III, Ph.D.
Member of dissertation committee

I certify that I have read this dissertation and that in my opinion it meets the academic and professional standard required by the University as a dissertation for the degree of Doctor of Philosophy.

Signed:

Chaoying Ni, Ph.D.
Member of dissertation committee

ACKNOWLEDGMENTS

I would like to begin my thanks for my advisor, Prof. Darrin Pochan, for inspiring me to think creatively, challenging me to do my best work and supporting me to finish my Ph.D. work. Prof. Pochan is always encouraging me and patient to me on my work in the past five years. I feel lucky and fun to work with Dr. Pochan that I had the precious education that will benefits my future life.

I would also like to thank my committee members, Prof. David Martin, Prof. Chaoying Ni and Prof. Thomas Epps, for their support and instruction over the past few years. Their advices provided great insights into my work and their questions helped me to think over my work and shape me to be an independent researcher and good presenter. I would also thank for the help I got from all faculties in UD.

I would give my great thanks to my collaborators who are experts on chemistry and synthesis. Without the help from outstanding chemists, I cannot finish my thesis. Thanks for the support from Prof. Karen Wooley and Wooley group members in Texas A&M University. Thanks for their help when I stayed in TAMU for the three weeks synthesis work. Thanks for Fuwu Zhang, Xun He, Jiong Zou, Adriana Pavia, Ang Li, Shiyi Zhang, Guorong Sun, Gye Seong and the past graduate students Prof. Ke Zhang and Kai Qi. I have learned a lot from the excellent chemists and I had great collaboration and enjoyed working with them. Most of the polymers I used in my work are from Karen Wooley lab. I would pass the good collaboration tradition to the junior students from the two research groups. I would give my thanks to Xiaojun Wang, Christopher Hurley, Andrew Goodwin, Kang, Namgoo and Prof. Jimmy Mays

from University of Tennessee. Their hard work provides the unsaturated block copolymer for the blend system, without which I cannot generate the research.

I felt I owe a full gratitude to all the Pochan group members, who has been accompany with me for the past few years study. I would like to give all my thanks to Congqi Yan, Jiahua Zhu, Sameer Sathaye, Sheng Zhong, Jessie Sun and Nikhil Sharma for their patience and answering all my questions when I started my research. I would specifically thank Sheng Zhong and Jiahua Zhu for their precious suggestions in my project. Time is one-dimensional kinetics and their advices helped me to understand it in a better way. I would like to thank the past group members Christopher Koehler for the paper revision. I would like to thank for the past group members Brendon Stewart, Honggang Cui and Zheng Zeng. I would like to thank for the current group members Jessie Sun for her help of connecting collaborations; thank for Michael Haider, Fr ank Polzer for the good coordination of the lab use and national lab trip etc. I would appreciate all the encouragements, inspirations and cares from them, making my past few years study enjoyable and pleasant.

I would also thank for the peers and collaborators I have worked with, met with and talked with in conferences, visiting for collaboration. I would thank for the great synthesis help and scientific discussion with Dr. Silvie Meeuwissen from Van Hest group; I thank for the diblock copolymers from Dr. Mingjiang Zhong from Matyjaszewski group at CMU; I thank for the cryo-imaging discussions and good instrument coordination with Thomas Smart from Epps group; I thank for Dr. Hao-jan Sun's help about 3D cartoon modeling and small angle x-ray scattering experiments at Argonne National lab. I would thank for Ngoc Nguyen for his instruction on AFM characterization. I would also thanks for the excellent researchers from MSE/CHEM

department, for any smile they gave me in the hallway and any care I received. I would remember the great time talking and working with people, shaping up me as an open, creative and collaborative researcher.

I would like to thank for the scientists I work with at NIST and Argonne National Lab, Dr. Paul Butler, Dr. Steve Weigand, Dr. Rita Graceffa and Olga Antipova. I would specifically thank for the continuous help from facility scientists and staff. Thanks for Prof. Chaoying Ni, even I had thanked him as being my committee member, for the support and management of advanced microscopy lab. Thanks for Frank Kriss for the patient and kind help of any problem I had. Thanks for the help of Dr. Fei Deng, Jennifer Sloppy for the FIB, TEM, and AFM help. I cannot remember how many times I bothered them for instrument issues and problem-solving. I am shaped up to be a proficient user with problem-solving abilities from a green hand who always made mistakes. The help I got from seniors, the challenges I received from peers, good discussions, laughs and depresses had shaped up me to be a mature research person.

I attribute all my excitement and self-accomplish moments, when I got good images in the dark room/ when good results-popped up from the beamline, to all the help I received from people. I feel thankful and lucky working with them.

Most importantly, I would like to thank my friends and family. I thank my friends for always believing me and forgiving me for being awful at keeping in touch over the past 6 years. I thank all of my friends for their support over the years, their encouragement and understanding when I met with some down points. Finally, I would like to thank my parents. Their unrequited love is my backup force for

solving any obstacles I met with and never saying give up in my study and life. I would not be the person I am today without their love and encouragement.

TABLE OF CONTENTS

LIST OF TABLES	xiii
LIST OF FIGURES	xiv
ABSTRACT	xxxi
1 INTRODUCTION OF BLOCK COPOLYMER SELF-ASSEMBLY.....	1
1.1 Introduction	1
1.2 Amphiphiles	2
1.2.1 Overview	2
1.2.2 Amphiphile Applications in Industry	3
1.3 Amphiphile Solution Assemblies	5
1.3.1 Fundamentals of Amphiphile Assemblies in Solution	5
1.3.2 Packing Parameters and Geometries	5
1.4 Block Copolymers and their Solution Assemblies	7
1.4.1 Shapes of Assemblies and their General Formation Mechanism ..	8
1.4.2 Theoretical Simulation of Block Copolymer Self-assembly.....	13
1.5 Multicompartment and Multigeometry Nanoparticle Assembly.....	15
1.6 Applications of Block copolymer Solution Assemblies.....	27
1.6.1 Nanocarriers as Drug Delivery Vehicle, DNA and other Molecule Encapsulations.....	28
1.6.2 Nanoreactors.....	30
1.7 Thesis Overview	31
REFERENCES	33
2 REVIEW OF CHARACTERIZATION METHODS FOR SOLUTION ASSEMBLIES.....	40
2.1 Introduction	40
2.2 Transmission Electron Microscopy Characterization Method	40

2.2.1	Overview of TEM.....	41
2.2.2	Sample Preparation and Selective Staining.....	42
2.2.3	Image Analysis	52
2.2.4	Cryogenic Transmission Electron Microscopy	52
2.3	Scattering Methods in Characterizing Solution Assemblies	57
2.3.1	Small Angle Neutron and X-ray Scattering in Solution Assembly Study.....	58
2.4	Scattering Methods in Characterization of Morphology Transitions in Block Copolymer Assembly with Kinetic Control	62
	REFERENCES.....	66
3	HYBRID VESICLE/CYLINDER NANOPARTICLES CONSTRUCTION: BLOCK COPOLYMER SOLUTION ASSEMBLY, KINETIC CONTROL AND NANOPARTICLE FORMATION MECHANISM.....	70
3.1	Introduction	70
3.2	Construction of Vesicle-Cylinder MCN/MGN	73
3.2.1	Materials	73
3.2.2	Self-assembly Procedure and Sample Characterization	73
3.2.3	Transmission Electron Microscopy and Selective Staining	75
3.2.4	Cryogenic Transmission Electron Microscopy (cryo-TEM) and Selective Staining	76
3.2.5	Atomic Force Microscopy	77
3.2.6	Small Angle x-ray Scattering Measurements	77
3.3	Results and Discussion of Vesicle/Cylinder MCN/MGN Construction .	78
3.3.1	Block copolymers for Binary Blending and Solution Assembly	78
3.3.2	Effect of Water Addition Rates on the Assembled Nanostructures at Different Blending Ratio	82
3.3.3	Structure Evolution of Multicompartment Nanoparticles	98
3.3.4	Small Angle X-ray Scattering Results.....	101
3.4	Discussion and Conclusion.....	114
	REFERENCES.....	116
4	CYLINDER-CYLINDER, DISK-DISK BINARY BLEND SYSTEMS AND LIMITATIONS OF BLENDING STRATEGY	119

4.1	Introduction	119
4.2	Cylinder-cylinder Multicompartment Nanoparticles via Binary Blends	123
4.2.1	Materials Design and Synthesis.....	123
4.2.2	Solution Self-assembly Procedure.....	125
4.2.3	Transmission Electron Microscopy and Selective Staining	125
4.2.4	Results and Discussion	126
4.3	Hybrid Disk-Disk Systems via Ternary Blends	131
4.3.1	Materials and Synthesis	131
4.3.2	Solution Self-assembly Procedure.....	131
4.3.3	Transmission Electron Microscopy and Selective Staining	132
4.3.4	Small Angle Neutron Scattering Measurement	132
4.3.5	Assembly results and discussion	133
4.4	Ternary blends of diblock copolymers with individual block copolymers that form spheres, cylinders and cylinders, respectively. ..	141
4.4.1	Experimental procedures	142
4.4.2	Experimental Results.....	142
4.5	Discussion and Conclusion.....	147
	REFERENCES	148
5	DESIGN OF FUNCTIONALIZED BLOCK COPOLYMER FOR NANOMATERIAL CONSTRUCTION VIA INTERPARTICLE CROSSLINKING.....	152
5.1	Introduction	152
5.1.1	Material Design and Synthesis	154
5.1.2	Synthesis of Thiol Functionalized Diblock Copolymer PAA ₉₀ - <i>b</i> -PS ₁₂₄	155
5.1.3	Synthesis of polyisoprene- <i>b</i> -poly(acrylic acid).....	157
5.1.4	Modification of PAA ₉₉ - <i>b</i> -PS ₇₆ with hydroxyethyl acrylate (HEA) and characterization	159
5.2	Multistep Self-assembly Experimental Procedures.....	160
5.2.1	Self-assembly of Single Diblock Copolymer	160
5.2.2	Co-assembly of PAA ₃₆ -PI ₁₆₀ and Functionalized HS ₁₈ -PAA ₇₂ - <i>b</i> -PS ₁₂₀	162

5.2.3	Interparticle Association via Thiolene Reaction	163
5.2.4	TEM and Cryo-TEM Experiments	163
5.3	Results and Discussions	164
5.3.1	Self-assembly of Single Diblock Copolymers	164
5.3.2	Co-assembly of HS ₁₈ -PAA ₇₂ - <i>b</i> -PS ₁₂₀ and PAA ₃₆ - <i>b</i> -PI ₁₆₀	167
5.4	Conclusion.....	170
REFERENCES	171
6	COLLABORATIVE WORK ON NANOSTRUCTURE CHARACTERIZATION.....	173
6.1	Polymersome Stomatocytes assembled from PEG ₄₄ -PS ₂₉₂	173
6.1.1	Introduction	173
6.1.2	Chemical Structure of Diblock Copolymers and Material Synthesis.....	174
6.1.3	Self-assembly Experimental Procedure.....	175
6.1.4	Results and Discussion	176
6.2	Self-Assembly of Amphiphilic Janus Glycodendrimers into Glycodendrimersomes and other Complex Architectures.....	179
6.2.1	Introduction	179
6.2.2	Molecular structure of Amphiphilic Dendrimers and their Self-assembly Behaviors	179
6.2.3	Conclusions of Glycodendrimer Assembly.....	186
6.3	“Single-Single” Amphiphilic Janus Dendrimers Self-Assemble into Narrow Distribution Dendrimersomes with Predictable Size	187
6.3.1	Molecular Architectures	188
6.3.2	Conclusions	193
6.4	Self-assembly of Amphiphilic Janus Dendrimers into Uniform Onion-like Dendrimersomes with Predictable Size and Number of Internalized Bilayers.....	194
6.4.1	Introduction	194
6.4.2	Molecular Structures of Dendrimers	195
6.5	Conclusions	198

REFERENCES	200
7 THESIS SUMMARY AND FUTURE WORK	203
7.1 Thesis Summary	203
7.1.1 Revealing Effects of Solvent Processing Rates on Block Copolymer Assemblies.....	204
7.1.2 Construction of Multicompartment and Multigeometry Nanoparticles	206
7.1.3 Exploration of Interparticle Crosslinking via Designed Functionalized Molecules.....	209
7.2 Recommendations for Future Work	209
7.2.1 Multidimensional Superstructure Construction via Hybrid Nanoparticle subunits containing Patchy, Anisotropic Surfaces	209
7.2.2 Complicated Morphology Transformations via long term aging under fast kinetic control	215
7.2.3 Summary of Future Directions	215
REFERENCES	217
A FORM FACTOR FITTING RESULTS OF SAXS TRACES	219
B COPYRIGHT PERMISSIONS	221

LIST OF TABLES

Table 2.1 Common staining agents and their functions.....	44
Table 2.2 The sizes of observed core, corona and overall of giant aggregates (unit: nm).....	48
Table 2.3 Statistic Counts of the paper related to cryo-TEM topic (total: 1316)..	52
Table 3.1 Average polymer concentration changing rates in different water addition rates.....	76
Table 3.2 χ parameters between polymer-solvent at room temperatures (25 °)...	80
Table 3.3 χ parameters between polymer-solvent at room temperatures (25 °)...	81
Table 3.4 χ parameters between polymer-polymer at room temperatures (25 °)..	81
Table 3.5 Summary of PAA₁₀₀-PI₁₅₀/PAA₉₉-PS₁₆₉ blending results in different conditions.....	96
Table 3.6 Morphologies at different water contents in PAA₉₉-PS₁₆₉ and PAA₁₀₀-PI₁₅₀ assembly.....	109
Table 4.1 χ parameters between two hydrophobic blocks at 25°.....	143
Table 5.1 M_n and \bar{D} of PAA-<i>b</i>-PI.....	159
Table 7.1 Diblock copolymers and their assembled nanostructures (amine:acid=0.5:1, 80% H₂O).....	208
Table 7.2 Designed diblock copolymers targeting specific sizes and shapes.....	212
Table 7.3 Predicted block length of SH-PAA-PS for achieving different geometries.....	212

LIST OF FIGURES

- Figure 1.1** Five proposed micelle shapes, as interpreted from experimental data. (a) spherical; (b) lamellar; (c) inverted (or reversed) micelle; (d) disk; (e) cylindrical or rodlike. Adapted from Wiley, Book⁴: Surfactant science and technology. 3
- Figure 1.2** Some important, high-impact areas of surfactant applications. Adapted from Reference⁴. Copyright permitted from Wiley-Interscience. 4
- Figure 1.3** Different Geometries formed by block copolymer assembled in selective solvent. P represents the packing parameter. Red color and green color: hydrophobic chains; Blue color: hydrophilic chains. Cryogenic Transmission Electron Microscopy (cryo-TEM) images are copied from reference¹⁷ with the permission from 2003 American Association for the Advancement of Science. 6
- Figure 1.4** Assemblies formed in selective solvent conditions by different block copolymers: (a) toroids³¹, (b) helix⁷, (c) double helix⁴⁴, (d) jellyfish structure⁴⁶, (e) multilayer vesicles⁴⁹, (f) monodisperse toroids⁴¹. (Reproduced with permissions from: 2004 American Association for the Advancement of Science³¹, 2009 Royal Society of Chemistry Journals, and 2006, 2009, 2014 American Chemistry Society⁴¹. 11
- Figure 1.5** 2D large nano-sheets with internal hexagonal packed pattern. (A): cryo-TEM images of large 2D nano-sheets, data unpublished. (C): The corresponded normal TEM image of the large 2D nano-sheet structure, figure adapted from reference⁴⁸ with copyright approved by 2015 American Chemistry Society. 13
- Figure 1.6** Morphologies possible for triblock copolymers as determined theoretically by Li⁶⁴ *et al.* Copyright approved by 2009 American Chemistry Society. 15
- Figure 1.7** Strategies for building multicompartiment micelles with different architecture of triblock copolymers. Figure adapted from reference⁶⁵ with the permission of copyright. 17

- Figure 1.8** Chemical structure of triblock copolymer (EHA)₁₂₀-(OEGA)₅₀-(FDA)₄₀ and cryo-TEM image of its 0.5 wt% aqueous dispersion. The micelles appear as high-contrast spherical particles surrounded by a fringed corona (indicated by arrows). 18
- Figure 1.9** Multicompartment micelles from miktoarm star terpolymers, μ -EOF(x-y-z). Cryo-TEM images of 1 wt % aqueous solutions of (A) μ -EOF(2-13-3.5), (B) μ -EOF(2-4-2.5), (C) μ -EOF(2-9-5), and (D) μ -EOF(2-6-2.5); scale bars indicate 50 nm⁷⁰. Cryo-TEM images adapted from reference⁶⁹. Copyright Approved from 2006 American Chemical Society..... 19
- Figure 1.10** TEM images of single (a) and aggregated (b) Janus cylinders on a carbon-coated TEM grid after staining with RuO₄ for 2 h. Grey-scale analyses (c-e) correspond to the section analyses as shown in the images from left to right. The schematic drawings at the bottom exhibit the orientation of the Janus cylinders within the cross-sections (PB) black, (PS) red, (PMMA) green. Figure adapted from reference⁶, with approved copyright from 2009 ACS publication..... 20
- Figure 1.11** TEM images of multicompartment micelles from B₈₀₀-b-V₁₉₀-b-T₅₅₀ (A) drop-coated and (B) freeze dried from 0.1 g/L acetone onto carbon coated gold TEM grids. (C) Single micelle at high magnification. (D) Proposed solution structure of the micelles. Figure adopted from reference⁷⁴, with approved permission from 2009 American Chemical Society..... 21
- Figure 1.12** Cryo-TEM micrographs of PB₈₀₀-b-P2VP₁₉₀-b-PMAA₅₅₀ in buffer aqueous solution with pH10 (0.05M CsCl, c=1 g/L), overview(A) and single core-shell-corona micelle (B); at pH4 (c=1 g/L) (C), the inset shows an enlargement; schematic depiction of the proposed solution structure of PB₈₀₀-b-P2VP₁₉₀-b-PMAA₅₅₀ depending on the pH; core-shell-corona structure with an expanded PMAA corona at pH10 (E) and micelles with a collapsed PMAA corona at pH 4 (D). Figure Adapted from reference⁷⁴, with approved permission from 2009 American Chemical Society..... 22
- Figure 1.13** (a, b) Non-stained and (c, d) RuO₄ stained TEM images of undulated cylinders, obtained from ethanol. Adapted from reference⁷⁵. Copyright permission approved from 2009 Wiley Publication. 23

Figure 1.14 (A,B) Cryo-TEM micrograph of IPECs pH 10 after 1 h mixing time at different locations of the same sample; (C,D) SFM height images of an IPEC solution at pH 10 after deposition on a carbon-coated TEM grid; z-scale in both cases is 6 nm, with D displaying an enlargement of C. Adapted from reference⁷⁸. Copyright permission approved from 2009 American Chemical Society.	24
Figure 1.15 Schematic representations of triblock co-micelle and its self-assembly into a supermicelle. (B) Low-magnification TEM micrograph of a cluster of supermicelles (C) Higher-magnification TEM micrograph of a supermicelle showing the core, (D) Optical micrograph of the supermicelles. Adapted from reference²⁴. Approved copyright from AAAS 2012.	26
Figure 1.16 Filomicelles and their persistent circulation. A, Filomicelles are self-assembled from diblock copolymers. B, Injection of fluorescent filomicelles into rodents. Figures adapted from reference⁹³, copyright approved by 2007 Nature Publication.	29
Figure 1.17 (a) Schematic illustration of enzymatic nanoreactor in the processing of the external non-fluorescent substrate into an internalized fluorescent substrate. (b) Fluorescent micrographs illustrating both the protein channel and pH-dependence on nanoreactor functionality. Reproduced with permission from ref. 2006 American Chemical Society¹⁰⁷	31
Figure 2.1 Schematic of important components in traditional TEM and the electron beam pathways.....	42
Figure 2.2 Chemical structures of triblock copolymer PAA₃₃₅-PI₃₃₅-PS₈₄ (with 1, 4 addition around 40-50%, 1, 2-addition around 50%-60%); chemical structures of EDDA molecule.....	46
Figure 2.3 Cryo-TEM images of the giant spherical aggregates assembled from PAA₃₃₅-PI₃₃₅-PS₈₄ at different amine to acid ratios, 80% H₂O/20% THF. A, 0.3:1; B, 0.5:1; C, 1:1; D, 2:1; E, 5:1.	48
Figure 2.4 Cast film TEM images of different staining methods applied to the giant aggregates, at amine to acid 0.3:1. A: OsO₄ stain. After cast-film TEM, the grid is staining exposed to OsO₄ for 6-8 hours; B: RuO₄ stain. After the sample was dried out on the TEM grid, RuO₄ was used to vapor stain the grid for 10-20 minutes. C: UA stain. After the solution sample was dried out on top of the grid, a small amount of UA was applied on top of the grid.....	49

Figure 2.5	Cryo-TEM images of spherical aggregates assembled from triblock copolymer PAA₃₃₅-PI₃₃₅-PS₈₄, with amine:acid=0.5:1, 80% H₂O/20% THF. A: Cryo-TEM images of giant spherical aggregates. B: Cryo-TEM image of giant aggregates with addition of ruthiniumhexamine (Ru (NH₃)₆Cl₂), the ruthiniumhexamine was added to reach amine:acid=1:1 for the total amine amount from EDDA and ruthiniumhexamine. C: Cryo-TEM image of giant aggregates with OsO₄ staining, double layers were observed similar as the image in Figure 2.4A. D: Chemical structure of rutheniumhexamine complexed with HCl.	51
Figure 2.6	Cryo-EM reconstruction of 30-nm chromatin fibers assembled from DNA molecule. Figure adapted from reference³¹, with the copyright permission from AAAS.....	54
Figure 2.7	Cryo-TEM analysis of spherical micelles formed from brush polymer LO-2. Figure adapted from reference³⁴ with the permission approved from 2014 American Chemical Society.	54
Figure 2.8	Common artifacts in cryo-TEM. (A) Hexagonal packed particles due to the shear force present during sample blotting. The disordered particles near the edge indicate that it is not real hexagonal structure in solution but shear-induced artifacts. (B, C, D) poorly vitrified samples and giant ice. (E) Beam damage.	57
Figure 2.9	Schematic of wavevectors and scattering vector (q) in elastic scattering.	58
Figure 2.10	Schematic of SANS and SAXS instrument in transmission. X and Y indicate the x axis and y axis.	60
Figure 2.11	SAXS traces of the assemblies formed in different water contents from PAA₉₉-b-PS₁₆₉, amine to acid=0.5:1 in different water contents. Scattering peaks were observed in middle water contents, corresponding to d-spacing which is around 30-33 nm ($q=0.018 \text{ \AA}^{-1}$). Pre represents precipitation.....	64

Figure 2.12 Cast film TEM images of the nanostructures assembled by PAA₉₉-b-PS₁₆₉ with amine to acid=0.5:1. A: 15% H₂O condition, giant membrane, precipitated suspensions. B: 24% H₂O condition, cylinder bundles suspended in cloudy solution. C: 28% H₂O condition, close packed cylindrical bundles suspended in cloudy solutions. D: 40% H₂O condition, lamellar structure with the d-spacing at 32 nm. E: 50% H₂O condition, intermediate nanostructures of lamellar to vesicle transition. F: 75% condition, vesicle to cylinder intermediate structures. Inserted scale bar: 500 nm. 65

Figure 3.1 Schematic of multicompartiment and multigeometry nanoparticles *via* binary blends of PAA₁₀₀-b-PI₁₅₀ and PAA₉₉-b-PS₁₆₉ diblock copolymers with different water addition rates, in THF/H₂O mixtures (v/v=1:4). Pure vesicles and pure cylinders are assembled from single assembly of PAA-PI and PAA-PS, respectively. Separate population of cylinders and vesicles are formed with extreme slow water addition *via* co-assembly of block copolymer blends; vesicle-cylinder connected particles are assembled with middle rate; Disk-cylinders and hybrid vesicles are formed with fast and extremely fast water addition rates. The blue color represents PAA block complexed with organic diamine; the red represents PI block and the green represents PS block..... 72

Figure 3.2 TEM images of nanoparticles assembled from PAA₁₀₀-b-PI₁₅₀, PAA₉₉-b-PS₁₆₉ diblock copolymers in mixed solvent with THF: water volume ratio v/v=1:4 and an amine to acid ratio=0.5:1.0 due to added EDDA. A: cryo-TEM images of vesicles assembled by PAA₁₀₀-b-PI₁₅₀ with vesicle wall thickness=35 nm, formed with a water addition rate of 5mL/h. B: Thin-film TEM images of cylinders assembled by PAA₉₉-b-PS₁₆₉ with the diameter=40 nm, water addition rate at 5 mL/h. C: cryo-TEM images of vesicle-cylinder connected MCNs with the middle water addition rate at 5 mL/h and equavelent blending ratio (PAA₁₀₀-b-PI₁₅₀: PAA₉₉-b-PS₁₆₉=1:1). C was taken of the sample without staining, and D was taken of the same sample as C after staining by OsO₄..... 81

- Figure 3.3** Representative TEM and cryo-TEM images of assemblies in different water addition rates in individual diblock assembly, with amine: acid=0.5:1, 80% v/v H₂O/THF. A: cryo-TEM images of vesicles assembled from PAA₁₀₀-*b*-PI₁₅₀, 0.8 mL/h. B: TEM images of cylinders formed from PAA₉₉-*b*-PS₁₆₉ at 0.8 mL/h, with the diameter equals to 40 nm C: TEM images of PAA₁₀₀-*b*-PI₁₅₀ forms vesicles 5 mL/h, with the wall thickness equals to 35 nm, some of the vesicles were aggregated together due to the drying effect in sample preparation. D: PAA₉₉-*b*-PS₁₆₉ forms cylinders with water addition rate at 5 mL/h. 83
- Figure 3.3** Representative TEM and cryo-TEM images of assemblies in different water addition rates in individual diblock assembly, with amine: acid=0.5:1, 80% v/v H₂O/THF. E: PAA₁₀₀-*b*-PI₁₅₀ forms vesicles with water addition rate at 30 mL/h; F: PAA₉₉-*b*-PS₁₆₉ forms cylinders, vesicles with water addition rate at 30 mL/h. G: PAA₁₀₀-*b*-PI₁₅₀ forms vesicles at extreme fast water addition. H: PAA₉₉-*b*-PS₁₆₉ forms cylinders, short cylinders, disk, vesicles and spheres with extreme fast water addition (>>100 mL/h). 84
- Figure 3.4** Cryo-TEM images of hybrid nanoparticles assembled from blends of PAA₁₀₀-*b*-PI₁₅₀ and PAA₉₉-*b*-PS₁₆₉ diblock copolymers (molar ratio=1:1) with EDDA at amine to acid ratio=0.5:1, in a mixed solvent of THF: water at a volume ratio=1:4 (1 mL THF initial, 5 mL final mixed solution) with different water addition rates. A: Separated vesicles (dominant nanostructure) and cylinders at water addition rate 0.8 mL/h H₂O. B: vesicle-cylinder connected nanoparticles assembled at 5 mL/h water titration rate. C: Disk-cylinder hybrid nanoparticles assembled at 30 mL/h H₂O. D: Disk-Cylinder hybrid nanoparticles assembled at the fasted water addition rate by pipette addition (>>100 mL/h). All solutions were imaged 1 day after the assembly process and vapor stained by OsO₄ for 10-20 minutes. 85
- Figure 3.5** A: cast-film TEM images of assemblies of PAA₁₀₀-*b*-PI₁₅₀ and PAA₉₉-*b*-PS₁₆₉, blending ratio=1:1, without amine, in a fast water addition rate (30 mL/h), v/v 80% H₂O/20%THF. A, Aggregations without any morphology control were observed as compared to samples with the diamine complexation; B, cast-film TEM images of blends of PAA₁₀₀-*b*-PI₁₅₀:PAA₉₉-*b*-PS₁₆₉=1:1, without amine, in a slow addition rate pathway (0.8 mL/h). 87

- Figure 3.6** Additional representative TEM and cryo-TEM images of assemblies in different water addition rates in blends of PAA₁₀₀-*b*-PI₁₅₀ : PAA₉₉-*b*-PS₁₆₉=1:1, amine:acid=0.5:1, 80% v/v H₂O/ THF. A: separate vesicles and cylinders at extreme slow water addition rate of 0.8 mL/h. B: vesicle-cylinder connected MCN formed at middle water addition rate of 5 mL/h. C: Disk-Cylinder MC disks formed at fast water addition rate of 30 mL/h. D: Disk-Cylinder MC disks formed at extremely fast water addition rate of >>100 mL/h..... 88
- Figure 3.7** (A, B): cast-film TEM image of Disk-cylinder MC disk nanoparticles, same sample as it is in Figure 3.6 C. B: tilted sample stage to 45 ° to observe the ellipse MCN nanoparticles. C. AFM images indicating the height information of disk-cylinder nanoparticles..... 89
- Figure 3.8** Cryo-TEM images of hybrid nanoparticles assembled from blends of PAA₁₀₀-*b*-PI₁₅₀ and PAA₉₉-*b*-PS₁₆₉ diblock copolymers (molar ratio=9:1) with EDDA at an amine to acid ratio=0.5:1. The final solvent mixture is THF: water volume ratio=1:4. Each image resulted from a different water addition rate. A: separated vesicles and cylinders at water addition rate of 0.8 mL/h; B: vesicle-cylinder connected hybrid nanoparticles, assembled at 5 mL/h, DI water was titrated to THF; C: Hybrid vesicles with dark wall domain (PI) and light wall domain (PS) assembled at 30 mL/h H₂O. D: Hybrid vesicles assembled with the extremely fast water addition rate, H₂O was added into THF by using pipette. All solutions were imaged 1 day after the assembly process and vapor stained by OsO₄ for 10-20 minutes. 91
- Figure 3.9** Additional representative TEM and cryo-TEM images of assemblies in different water addition rates in blends of PAA₁₀₀-*b*-PI₁₅₀: PAA₉₉-*b*-PS₁₆₉=9:1, amine:acid=0.5:1, 80% v/v H₂O/THF. A: separate vesicles and cylinders formed at extreme slow water addition rate of 0.8 mL/h. B: vesicle-cylinder connected MCN formed at middle water addition rate of 5 mL/h. C: Hybrid vesicles formed at fast water addition rate of 30 mL/h. D: Hybrid vesicle MCN formed at extreme fast water addition rate of >>100 mL/h..... 92

Figure 3.10 TEM images of hybrid nanoparticles assembled from blends of PAA₁₀₀-*b*-PI₁₅₀ and PAA₉₉-*b*-PS₁₆₉ diblock copolymers (molar ratio=1:9) with EDDA at an amine to acid ratio=0.5:1, THF: water volume ratio=1:4 and different water addition rate. A: separated vesicles and cylinders at water addition rate of 0.8 mL/h H₂O, B: vesicle-cylinder connected nanoparticles assembled at 5 mL/h water titration rate. C cylinder-disk hybrid nanoparticles assembled at 30 mL/h H₂O. D: disk-cylinder hybrid nanoparticles assembled at extreme fast water addition, >>100 mL/h. Arrows point to the short cylinders in disk-cylinder structure. All solutions were observed 1 day after assembly process and vapor stained by OsO₄ for 10-20 minutes. 94

Figure 3.11 Additional representative TEM and cryo-TEM images of assemblies in different water addition rates in blends of PAA₁₀₀-*b*-PI₁₅₀ : PAA₉₉-*b*-PS₁₆₉=1:9, amine:acid=0.5:1, 80% v/v H₂O/THF. A: separate vesicles and cylinders formed at extreme slow water addition rate of 0.8 mL/h. B: vesicle-cylinder connected MCN formed at middle water addition rate of 5 mL/h. C: Disk-Cylinder MCN/MGN formed at fast water addition rate of 30 mL/h. D: Disk-cylinder MCN formed at extreme fast water addition >>100 mL/h..... 96

Figure 3.12 Comparison of diameters of the nanoparticles at fast water addition and extremely fast water addition rates. Numbers were collected from multiple nanoparticles in different imaging areas. Left column: The graph shows the average diameter of hybrid vesicles at fast water addition and extremely fast water addition rates. The diameters of 118 hybrid vesicles were measured in different imaging areas at fast water addition rate (30 mL/h). The diameters of 113 hybrid vesicles were measured in different imaging areas at extremely fast water addition rate (>>100 mL/h). Right column: The graph shows the average diameter of disk-cylinder hybrid nanoparticles at fast water addition and extremely fast water addition. The diameters of 146 hybrid disk-cylinder nanoparticles were measured in different imaging areas. The diameters of 120 hybrid disk-cylinder nanoparticles were measured in different imaging areas. The diameters of both hybrid vesicles and disk-cylinder nanoparticles decreased in faster water addition condition. 97

- Figure 3.13** Aging results of multicompartment hybrid vesicles. Image A: cryo-TEM image of hybrid vesicles constructed from blends of PAA₁₀₀-*b*-PI₁₅₀: PAA₉₉-*b*-PS₁₆₉=9:1 with extremely fast water addition (>>100 mL/h) after sample ageing for 1 day. B: same sample after aged for one month. C: sample aged for two months. D: sample aged for three months. 1-4, selected snapshots from image A, B, C, D to show the signature micelle evolution status in different ageing points. 1: hybrid vesicles; 2: asymmetric hybrid vesicles with extended PS wall and PI phase; 3: asymmetric wheel-like hybrid vesicle; 4: larger magnification of asymmetric wheel-like hybrid vesicle from aggregates of hybrid vesicles. Inserted scale bar: 100 nm. 101
- Figure 3.14** SAXS traces of the assemblies formed in different water contents from PAA₉₉-*b*-PS₁₆₉, amine to acid=0.5:1 in separate water regimes. Scattering peaks were observed in middle water concentration regimes, corresponding to a d-spacing in the range of 30-33 nm. In the inner window markers, pre represents precipitation. 105
- Figure 3.15** Representative cast film TEM images of nanostructures assembled by PAA₉₉-*b*-PS₁₆₉ with amine to acid=0.5:1. A: 15% H₂O condition, giant membrane, precipitated suspensions. B: 24% H₂O condition, cylinder bundles suspended in cloudy solution. C: 28% H₂O condition, close packed cylindrical bundles suspended in cloudy solutions. D: 40% H₂O condition, lamellar structure with the d-spacing of 32 nm confirmed by TEM and SAXS. E: 50% H₂O condition, intermediate nanostructures of lamellar transitioning to vesicle transition. F: 75% condition, vesicle to cylinder intermediate structures. Inserted scale bar: 200 nm. 106
- Figure 3.16** SAXS traces of PAA₁₀₀-*b*-PI₁₅₀ assemblies in different water contents with extreme slow water titration, amine to acid=0.5:1. .. 107
- Figure 3.17** SAXS traces of blends of PAA₁₀₀-*b*-PI₁₅₀: PAA₉₉-*b*-PS₁₆₉ molar ratio=1:1 at detailed water points. Water adding at extreme slow rate (0.8 mL/h). 109
- Figure 3.18** SAXS traces of single assembly of PAA₉₉-*b*-PS₁₆₉ at interval water contents, single assembly of PAA₁₀₀-*b*-PI₁₅₀ at interval water contents, and blends of PAA₁₀₀-*b*-PI₁₅₀:PAA₉₉-*b*-PS₁₆₉ molar ratio=1:1 at intermediate water contents, respectively. Water adding at middle water titration rate (30 mL/h). 112

- Figure 4.1** Synthesis route of PtBA-*b*-PMMA from PtBA-Br..... 124
- Figure 4.2** GPC result of PtBA-PMMA, data provided by Ang Li, Wooley Lab.124
- Figure 4.3** TEM images of cylinder micelles assembled from PAA₉₉-*b*-PS₁₆₉ and PAA₁₀₅-*b*-PMMA₁₇₀. A, cylinders assembled by PAA₉₉-*b*-PS₁₆₉ at amine: acid=0.5:1, 1 mL THF containing polymer and amine, water added at 0.8 mL/h to reach 80% H₂O/20% THF. B: cylinders assembled from PAA₁₀₅-*b*-PMMA₁₇₀ at amine: acid=0.5:1, 1 mL THF containing polymer and amine, water added at 0.8 mL/h to reach 80% H₂O/20% THF. 127
- Figure 4.4** TEM images of multicompartiment cylinders assembled after blending PAA₉₉-*b*-PS₁₆₉ and PAA₁₀₅-*b*-PMMA₁₇₀ in THF/amine at a relative molar ratio of 1:3 of the two block copolymers and different rates of water addition. A: Separate populations of cylinders assembled after diblocks were blended in THF, diamine is added to reach an amine to acid molar ratio of 0.5:1 and water is added in a slow rate at 0.8 mL/h. B: Same solution mixing method as A but water added at ultra-fast rate using pipette addition at a rate >>100 mL/h. RuO₄ staining was used after the sample aged for 2 hours after water titration and the cast-film TEM grids dried. The grids were stained to RuO₄ vapor for 10 minutes. 128
- Figure 4.5** Dry film TEM images of the multicompartiment cylinders assembled *via* combination of two different water addition rates. Water (1 mL) was firstly added quickly to the pure THF solution (1 mL) *via* pipette to reach an intermediate water content of 50% water. Then water (3 mL) was added slowly (3 mL/h) to the system to eventually reach 80% water relative content. A, B: PAA₉₉-*b*-PS₁₆₉ and PAA₁₀₅-*b*-PMMA₁₇₀ were blended in molar ratio 1:3, amine: acid=0.5:1. C, D: PAA₉₉-*b*-PS₁₆₉ and PAA₁₀₅-*b*-PMMA₁₇₀ were blended in molar ratio 1:1, amine: acid=0.5:1. Samples were aged for two hours after water titration before cast-film TEM grids preparation. The grids were then stained with RuO₄ vapor for 10 minutes..... 129

Figure 4.6 Dry-film TEM images of disk formers assembled from PAA₉₉-*b*-PS₁₆₉/PAA₁₀₀-*b*-PI₁₅₀ blends and PAA₉₉-*b*-PMA₁₀₃-*b*-PS₁₈₈, respectively. A: PAA₉₉-*b*-PS₁₆₉/PAA₁₀₀-*b*-PI₁₅₀ molar ratio of 1:1, and water was added with ultra-fast rate by using pipette addition (>>100 mL/h). Diameter of the overall disk-cylinder nanoparticles are around 80-120 nm. B: Disks assembled from PAA₉₉-*b*-PMA₁₀₃-*b*-PS₁₈₈, amine: acid=0.5:1 with water added in a rate 5 mL/h to 1 mL THF to reach a final relative water composition of 80% water and a total of 5 mL final solution volume. Diameter of the disks is in the range of 60-120 nm. 3D cartoons are drawn to indicate the disk geometry, internal core domain, and chain organization in the disk-shaped nanoparticles. The blue color represents the PAA/amine condensed shell; the green color represents the PS domain in A and the PMA-PS domain in B, respectively; the red color represents the PI domain in A. 134

Figure 4.7 Dry-film TEM images of Disk-Disk multicompartiment nanoparticles assembled from the ternary diblock and triblock blend. A: ternary blends of PAA₁₀₀-*b*-PI₁₅₀/PAA₉₉-*b*-PS₁₆₉/PAA₉₄-*b*-PMA₁₀₃-*b*-PS₁₈₈ at molar ratio of 9:1:10 (or, an overall molar ratio of 1:1 of each disk-forming system), the volume fractions of different compartments of hybrid disks are designed to be ~50% volume PI phase/50% PMA and PS phases. Water was added with an ultra-fast rate by pipette, H₂O/THF v/v=4:1; B: ternary blends of PAA₁₀₀-*b*-PI₁₅₀/PAA₉₉-*b*-PS₁₆₉/PAA₉₉-*b*-PMA₁₀₃-*b*-PS₁₈₈ at molar ratio of 9:1:17, the volume fraction ratio of the dark phase and light phase was targeted to be around 2:8. Water was added in an ultra-fast rate by using pipette, H₂O/THF v/v=4:1. C: ternary blends of PAA₁₀₀-*b*-PI₁₅₀/PAA₉₉-*b*-PS₁₆₉/PAA₉₉-*b*-PMA₁₀₃-*b*-PS₁₈₈ at molar ratio of 9:1:5, the volume fractions of dark phase and light phase was around 40%:60%. The determination of the volume fractions of dark phase and light phase will be addressed later in the paper. D: Separate populations of disks assembled from blends of diblock and triblock copolymer at extreme slow water addition, at same molar ratio with image A. Separate disks are circled in the image. 136

Figure 4.8 Additional higher magnificent dry-film TEM images for the hybrid disk-disk nanoparticles assembled from diblocks and triblock blends. A: Same sample as in Fig 4.7A; B: Same sample as in Figure 4.7 B; C, D: Same sample as in Figure 4.7C. 137

Figure 4.9	Tilt dry-film TEM grids containing the disk structure assembled from PAA₉₄-<i>b</i>-PMA₁₀₃-<i>b</i>-PS₁₈₈. A: zero degree of sample holder. B: 60 degree tilted of sample holder.	138
Figure 4.10	Tilt images of dry-film TEM grids containing the disk-disk structure. A: hybrid disk-disk assembled from blends of diblocks and triblock, same sample as in the Figure 4.8A. B: image taken after holder was tilted at 45°.....	139
Figure 4.11	Small angle neutron scattering (SANS) data of disk formers assembled from PAA₉₉-<i>b</i>-PMA₁₀₃-<i>b</i>-PS₁₈₈ (AMS₁₈₈) and blends of PAA₁₀₀-<i>b</i>-PI₁₅₀/PAA₉₉-<i>b</i>-PS₁₆₉, respectively.....	140
Figure 4.12	Dry-TEM images of micelles assembled from three different diblock copolymers. In all the assemblies: amine: acid=0.5:1, H₂O:THF=4:1, water was added to THF-amine-block copolymer solution (1 mL) to reach 80% relative volume fraction water to THF for a total of 5 mL at a relative medium rate of water addition (10 mL/h). (A): spheres assembled from PAA₇₅-<i>b</i>-PB₁₀₄; the diameter of spheres is ~50 nm; (B): cylinders assembled from PAA₉₉-<i>b</i>-PS₁₆₉; the diameter of cylinders is ~40 nm; (C): cylinders assembled from PAA₁₀₀-<i>b</i>-PMMA₁₇₀; the diameter of cylinders is ~45 nm.	143
Figure 4.13	A, B: Lower magnification TEM images of asymmetric nanoparticles assembled from ternary blends of diblock copolymers: 1:1:1 molar ratio of PAA₇₅-<i>b</i>-PB₁₀₄:PAA₉₉-<i>b</i>-PS₁₆₉:PAA₁₀₀-<i>b</i>-PMMA₁₇₀. Samples were aged one day after water addition. TEM grids were prepared by dropping the solutions on the grid to make cast film after solution evaporation. OsO₄ vapor was used to stain the PB phase after carbon coated TEM grids were dried. C, D: High Mag TEM images of asymmetric nanoparticles. 3D cartoon represents the possible core-shell packing of asymmetric nanoparticles. The blue color represents PAA/amine shell, the red color represents the PB phase, the dark color represents the PS phase and the green color represents the PMMA phase.	144
Figure 4.14	Sequential staining using RuO₄ after OsO₄ staining. A, B, C: TEM images of asymmetric nanoparticles. Grids were sequentially stained by OsO₄ and RuO₄. D: Lower Mag image. Larger domains of dark phases were then observed, comparing with the images in Fig.4.13. Presumably, the PB and PS phases are all stained by sequentially staining using OsO₄ and RuO₄.	145

Figure 4.15	Cryo-TEM images of asymmetric nanoparticles from the same sample as in Figure 4.13. The solution was stained by OsO₄ vapor for 10 minutes before cryogenic TEM sample preparation. The dark domain is from PB phase. The light domain is interpreted to be PMMA and PS phases.....	146
Figure 5.1	Designed interparticle association between hybrid disk nanoparticles with thiol functionality on the periphery and small particles with diene present in the surface. In the left cartoon, the dark blue edge represents the thiol functionalized PAA shell and PS core from HS-PAA-<i>b</i>-PS, and the light blue core represents the PAA shell connected to the PI block disk interior from PAA-<i>b</i>-PI diblock copolymer when blended with HS-PAA-<i>b</i>-PS. In this particular design, the larger particles exhibit a disk geometry with an anisotropic surface (the PAA on the edge contain the thiol functionalities, while the PAA shell in the middle disk domain does not.). In the middle cartoon, the dark sphere represents the small assemblies from HEA modified PAA-<i>b</i>-PS with diene on the surface. After thiolene reaction, hybrid disks are presumably linked together through the dark spheres and two-dimensional large sheet-like structure can be formed.	155
Figure 5.2	NMR result of PI₁₆₀-<i>b</i>-PAA₃₆.....	158
Figure 5.3	GPC result of PI₁₆₀-<i>b</i>-PAA₃₆.....	158
Figure 5.4	UV-vis spectroscopy of cystamine in different buffer solutions. Data provided by Xun He	161
Figure 5.5	TEM images of the solution assemblies of PAA₉₀-<i>b</i>-PS₁₂₄ and HS₁₈-PAA₇₂-<i>b</i>-PS₁₂₀. A: Cylinders assembled from PAA₉₀-<i>b</i>-PS₁₂₄ with diamine: acid=0.5:1, 80% H₂O/20% THF. The diameter of the cylinders is 45 nm. Water was added with the rate of 1 mL/h. B: Stacked disks assembled from HS₁₈-PAA₇₂-<i>b</i>-PS₁₂₀ with diamine: acid=0.5:1, 80% H₂O/20% THF, water was added in a slow rate of 1 mL/h. C, D: disk structure assembled from HS₁₈-PAA₇₂-<i>b</i>-PS₁₂₀ with diamine: acid=1:1, 80% H₂O/20% THF. Water was added into THF with a slow rate at 1 mL/h. The diameter range of the disks is between 60 nm-80 nm.	165
Figure 5.6	TEM images of nanoparticles assembled from PAA₃₆-<i>b</i>-PI₁₆₀. A, B: TEM images of nanoparticles assembled from PAA₃₆-<i>b</i>-PI₁₆₀, with amine to acid=1:1, 80% H₂O/20% THF. The diameters of the particles are around 70 to 80 nm.	166

- Figure 5.7** TEM images of the spherical particles assembled from HEA₂₉-PAA₇₀-*b*-PS₇₆. A: cast-film TEM images of the spheres assembled from HEA₂₉-PAA₇₀-*b*-PS₇₆. Images were stained using uranyl acetate. B: cast-film TEM images of the spheres assembled from HEA₂₉-PAA₇₀-*b*-PS₇₆. Images were not stained. The diameter of the spheres is 30 nm..... 167
- Figure 5.8** TEM images of hybrid disks assembled from blends of HS₁₈-PAA₇₂-*b*-PS₁₂₀ and PAA₃₆-PI₁₆₀. HS₁₈-PAA₇₂-*b*-PS₁₂₀ and PAA₃₆-*b*-PI₁₆₀ were blended with the molar ratio 1:1, amine: acid=0.5:1, 80% H₂O/20% THF, 0.4 mL water was added to 0.1 mL in a rate of 30 mL/h, OsO₄ was used for staining the PI domain. A, B: cast-film TEM images of hybrid disks in different imaging areas. The inserted 3D cartoon represents for the hybrid disk-like nanoparticle with anisotropic surface. The dark blue edge represents the thiol functionalized PAA from HS₁₈-PAA₇₂-*b*-PS₁₂₀, the lighter blue color represents the PAA block from PAA₃₆-*b*-PI₁₆₀, the red color represents the PS block, and the inner green color represents the PI block..... 168
- Figure 5.9** Cryo-TEM images of solution assemblies after photo initiating thiolene reaction. A: cryo-TEM images of unstained solution assemblies after photo initiation, showing a type of 2D planar structure. B: 2D planar structure in different imaging area. C: cryo-TEM image of the same solution assembly sample. Solution was stained by OsO₄. D: cryo-TEM image of the same solution assembly sample, in different image are. Three-dimensional agglomerates were observed. Two-dimensional planar sheets and three-dimensional agglomerates are observed after photo-initiated crosslinking by cryo-TEM. 169
- Figure 6.1** Cartoon of shape transformation of stomatocytes into three different morphologies, from top to bottom: kippahs, indented uniconcave discocytes and polymersomes. Figures adapted from reference⁵, with approved copyright from Wiley Publications 2011. 175

- Figure 6.2** Shape transformation of stomatocytes of PEG-*b*-PS block copolymers over time illustrated by ambient TEM (left at 0 h, 1 h and 18 h), cryo-TEM (right at 1 h, middle at 18 h) and cryo-SEM images (right at 18 h). The stomatocytes were dialyzed against a mixture of water and organic solvent (1/1, v/v) using three different ratios of THF to dioxane by volume: a) 75:25, b) 55:45, and c) 25:75. Scale bars: 200 nm. Figures adapted from reference⁵, with copyright approved from Wiley 2011. The cryo-TEM images were obtained in UD Keck lab by Yingchao Chen. The SEM and cryo-SEM data was provided by Silvie Meeuwissen from Radboud University. 177
- Figure 6.3** Cryo-TEM images of stomatocytes. The stomatocytes were dialyzed for 18 h in MilliQ/(THF:dioxane) (v/v:v) is a) 50/(75:25); b) 50/(50:50) and c) 50/(25:75). Scale bars a-c: 200 nm. Figures adapted from reference⁵, with copyright approved from Wiley 2011. The images were taken in UD Keck lab by Yingchao Chen. .. 178
- Figure 6.4** Selected Cryo-TEM images of lamellar crystals assembled from (a) (3,4)₁₂G₁-PE-TRZ-Gal₂ 46aa; (b) solid glycodendrimersomes assembled from (3,4)₁₂G₁-PE-TRZ_i-Man₂ 47ab; (c) rectangular crystals assembled from (3,4,5)₁₂G₁-PE-TRZ-Gal₂ 46ca; (d) glycodendrimermicelles assembled from (3,5)₁₂G₁-PE-TRZ-Man₂ 46bb; (e, f) mixture of tubular and polygonal glycodendrimersomes and glycodendrimermicelles assembled from (3,4,5)₁₂G₁-PE-TRZ-Gal₂ 46cb. Figures adapted from reference⁷, with copyright approved from ACS publications 2013. The images a, b, d were obtained by yingchao chen at UD keck lab. The images b, c, e were obtained by Hao-jan from UPenn. 181
- Figure 6.5** Selected Cryo-TEM images of glycodendrimersomes assembled from (a) (3,5)₁₂G₁-PE-TRZ_i-3EOGal₂ 51ba, (b) (3,5)₁₂G₁-PE-TRZ_i-3EOMan₂ 51bb, and (c) (3,5)₁₂G₁-PE-TRZ_i-2EOMan₂ 51bc; glycodendrimercubosomes assembled from (d) (3,5)₁₂G₁-PE-TRZ_i-1EOMan₂ 51bd; lamellar crystals assembled from (e) (3,4,5)₁₂G₁-PE-TRZ_i-3EOGal₂ 51ca and (f) (3,4,5)₁₂G₁-PE-TRZ_i-3EOMan₂ 51cb. Figure adapted from reference⁷, with copyright approved from ACS publications 2013. The cryo-TEM images d,e,f were obtained from UD keck lab by Yingchao Chen; the cryo-TEM images a, b,c were provided by the Percec lab at UPenn. 185

- Figure 6.6** Selected cryo-TEM images of the self-assembled morphologies from libraries 1 and 2. (a) (3,4,5)12G1-L-Ala-CH₂-(3,4,5)-3EO-G1-(OCH₃)₃, 9cf. (b) (3,5)12G1-CH₂-L-Ala-(3,4)-3EO-G1-(OCH₃)₂, 10bd; (c) (3,5)12G1-L-CH₂-Ala-(3,4,5)-3EO-G1-(OCH₃)₃, 10bf; (d) (3,4,5)12G1-L-Ala-CH₂-(3,4,5)-3EO-G1-(OCH₃)₃, 10cf. Image adapted from reference¹⁰, with copyright approved from ACS 2014. The cryo-TEM images were obtained in UD by Yingchao Chen, Hao-jan Sun and Shaodong Zhang. 189
- Figure 6.7** Representative cryo-TEM images of self-assembled morphologies in libraries 3, 4 and 5. (a) (3,5)12G₁-CH₂-Gly-(3,4,5)G₁-3EOMe₃, 11bf; (b) (3,4,5)12G₁-CH₂-Gly-(3,4,5)G₁-3EOMe₃, 11cf; (c) (3,4)12G₁-I-PPD-(3,4,5)G₁-3EOMe₃, 12af; (d) (3,4,5)12G₁-I-PPD-(3,4,5)G₁-3EOMe₃, 12cf; (e) (3,4)12G₁-II-PPD-(3,4,5)G₁-3EOMe₃, 13af; (f) (3,4,5)12G₁-II-PPD-(3,4,5)G₁-3EOMe₃, 13cf. Image adapted from reference¹⁰, with copyright approved from ACS 2014. The images a-c were obtained in UD by Yingchao Chen, Hao-jan sun and Shaodong Zhang. The images d-f were provided by the Percec lab at UPenn. 191
- Figure 6.8** The concentration dependence of the size of dendrimersomes formed by (3,4)12G₁-I-PPD-(3,4,5)-3EO-G₁-(OCH₃)₃, 12af. (a) Square diameter-concentration relationship of the dendrimersomes. Cryo-TEM images of the dendrimersomes with the indicated size (in nm) and polydispersity index (PDI, in between brackets) at final concentration of (b) 0.25 mg/mL; (c) 1 mg/mL; (d) 2 mg/mL; (e) 4 mg/mL. Image adapted from reference¹⁰, with copyright approved from ACS 2014. The DLS data was provided by the Percec lab, and the images b and c were generated at UD. 193
- Figure 6.9** Multilayer onion-like vesicles assembled from dendrimers. Images adapted from reference²¹, with copyright approved from PNAS 2014. The image c was obtained at UD and images a, b, d were obtained at UPenn. 196
- Figure 6.10** Cryo-TEM images and 3D modeling of multilayer onion-like vesicles with predictable layer numbers. The images (a-b) were obtained at UD and the images (c-g) were obtained at UPenn. 196
- Figure 7.1** Varied morphologies assembled from blends of PAA-PI and PAA-PS in different water addition rates. The y axis represents the relative free energy of the formed nanoparticle system. Higher energy is observed when water addition rate is faster. 206

Figure 7.2	Construction of Multicompartment and Multigeometry nanoparticles <i>via</i> block copolymer blends. The black square represents the multicompartment nanoparticles. The red square represents the multicompartment and multigeometry nanoparticles.....	207
Figure 7.3	Sphere-sphere superstructures from hybrid sphere nanoparticles <i>via</i> multistep assembly.....	211
Figure 7.4	Three dimensional toroidal flowers build from hybrid toroids.	212
Figure 7.5	Packing disks assembled from hybrid disks with anisotropic and functionalized surface and gold nanoparticles.	214
Figure A1	Form factor fitting of the pure cylinders assembled from PAA-PS, with the extreme slow water addition rate. Core-shell cylinder form factor was used to fit the SAXS trace corresponding to the cylinder nanostructures. The SAXS trace is according to the Figure 3. 2B.....	219
Figure A2	Form factor fitting of the separate populations of vesicle and cylinder nanoparticles formed at extremely slow water addition, with the PAA-PI/PAA-PS blend ratio at 9:1, vesicles are in the dominant volume ratio. The SAXS trace is corresponding to the TEM image of Figure 3.8A.	220

ABSTRACT

Amphiphilic block copolymers are able to self-assemble into well-defined nanostructures in aqueous solutions or aqueous/miscible organic solutions. These structures include traditional spheres, cylinders and vesicles, which mimic nanostructures formed by small molecule analogs like lipids and surfactants. The large molecular weight and complex macromolecular architectures provide several advantages over small molecule amphiphiles, including the large chemical versatility, control over the size and shape of the solution assemblies, unique slow chain exchange and exceptional increased versatility in possible nanostructures. These advantages have motivated the noteworthy study of constructing well-defined, controlled and, especially, multicompartment and multigeometry polymeric nanoobjects for potential multiple nanotechnology applications. To reach complexity and well-controlled nanostructures, the facile utility and fundamental understanding of the parameters that influence the effective construction of solution assemblies needs to be continued. Given these motivations, this dissertation demonstrated the design of block copolymers, manipulation of kinetic control parameters of solution assembly, and characterization of hybrid nanostructures with the aim of creating new, well-defined nanostructures. The first objective of this dissertation was to explore the effects of solvent processing rates in influencing multicompartment and multigeometry nanoparticle construction, structure evolution over long-time aging and nanoparticle formation mechanisms. The noticeable effects of water addition rates on the formation of various nanostructures were studied by cryogenic transmission electron microscopy,

selective staining and small angle scattering. It was revealed that the water addition rate have significant influence over the final assemblies in block copolymer blends. New shapes of multicompartment and multigeometry nanoparticles have been constructed including hybrid vesicles, vesicle-cylinder connected nanoparticles, and disk-cylinder nanoparticles. It is discovered that smaller, kinetically-trapped, blended nanoparticles are observed with faster water addition rates, compared with larger, non-blended distinct nanoparticles with separate, unique geometries formed with slower water addition rate. The revealed rules were then applied in constructing new multicompartment hybrid nanoparticles with designed geometries, including the hybrid disks, hybrid cylinders and star-like nanoparticles. The second objective of this work was to explore a method for making hierarchical nanoparticle superstructures with designed functionality and subsequent multistep assembly and interparticle crosslinking. Advanced imaging of various nanostructures in different solution assembly systems was also generated. Together, the ideas of parameter control, kinetic study, and design of molecules and functionality presented in this dissertation will facilitate future work and nanotechnology development.

Chapter 1

INTRODUCTION OF BLOCK COPOLYMER SELF-ASSEMBLY

1.1 Introduction

Amphiphiles are chemical compounds having hydrophilic and hydrophobic domains linked together covalently. Due to the unique chemical structure and self-assembly ability in specific environments, amphiphiles play an important role in people's lives. Natural amphiphiles include many lipid molecules such as lipoproteins and saponins¹. The lipids can be self-assembled into membranes as observed in natural cells when the lipids are exposed to water and the hydrophilic head groups are exposed to the membrane surface and the hydrophobic tails are positioned inside of the membranes. It is reported that there are hundreds of phospholipids assembled together to form membranes in the cell, protecting and keeping the cell from the outside physiological environment². Synthetic small amphiphiles such as surfactants mostly can be assembled into different structures³ and are widely used in daily life. Industrial products made from various surfactants include cosmetics for personal care, detergents for cleaning, and wetting agents and emulsifiers for paints^{4,5}. Large molecular weight synthetic amphiphiles have distinct advantages over small amphiphiles when it comes to nanostructure assembly properties, such as enhanced mechanical properties and increased stability⁶. Various nanostructures assembled from large amphiphiles have been well-studied for the past few decades due to emerging applications in biomedical, biosensor, and also optical and electronic applications⁷. For example, vesicles assembled from block copolymers have been applied in acting as drug delivery vehicles⁸. These nanomaterial systems demand further fundamental research including deeper understanding of parameters controlling the solution assembly into new, well-defined nanostructures not yet explored. In this thesis, the

kinetic control of block copolymer assembly behaviors enables the fabrication of new nanostructures for promising nanotechnology.

1.2 Amphiphiles

1.2.1 Overview

Amphiphilic molecules have two chemically distinct (hydrophilic *vs.* hydrophobic) regions covalently linked together in the same molecule. Due to this characteristic, amphiphiles spontaneously assemble into a variety of structures in selective solvent ranging from spherical micelles to elongated cylindrical micelles and bilayer vesicular or membrane structures^{3, 9, 10} as depicted in figure 1.1. In this section, a brief overview of small amphiphiles is discussed, including the applications of amphiphiles in industry; the basic shapes of small amphiphile molecule assemblies as well as important parameters such as molecular packing parameters and critical micellization concentration. Block copolymer solution assembly, the main topic of the thesis, will be discussed later.

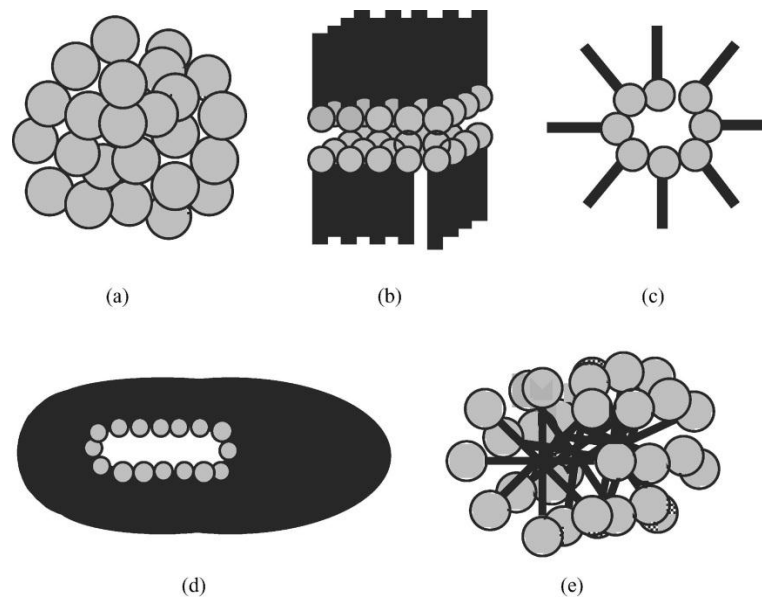


Figure 1.1 Five proposed micelle shapes, as interpreted from experimental data. (a) spherical; (b) lamellar; (c) inverted (or reversed) micelle; (d) disk; (e) cylindrical or rodlike. Adapted from Wiley, Book⁴: Surfactant science and technology.

1.2.2 Amphiphile Applications in Industry

Amphiphiles such as surfactants, are widely used in industry. The primary, traditional application for surfactants is their use as soaps and detergents for a wide variety of cleaning processes. Cosmetics and personal care products is also a vast million-dollar market. Another one of the most important applications of surfactants is in coating products. Surfactants also are active ingredients broadly used in the pharmaceutical industry. The current existing products in the surfactant industry are summarized in Figure 1.2⁴. Large amphiphiles, including amphiphilic block copolymers, are currently of interest in light of their increasing range of application and their interesting properties. Often used are the trademarked amphiphiles such as Pluronic[®], Synperionic[®], or Poloxamer[®]. Pluronics[®], one kind of block copolymer consisting of hydrophilic poly(ethylene oxide) (PEO) and hydrophobic poly(propylene oxide) (PPO) blocks arranged in an A-B-A tri-block structure, or PEO-

PPO-PEO, are widely used as biomaterials for drug delivery. The incorporation of drugs into the core of the micelles formed from Pluronic[®] results in increased solubility, metabolic stability and circulation time for drugs in the patients^{11, 12}.

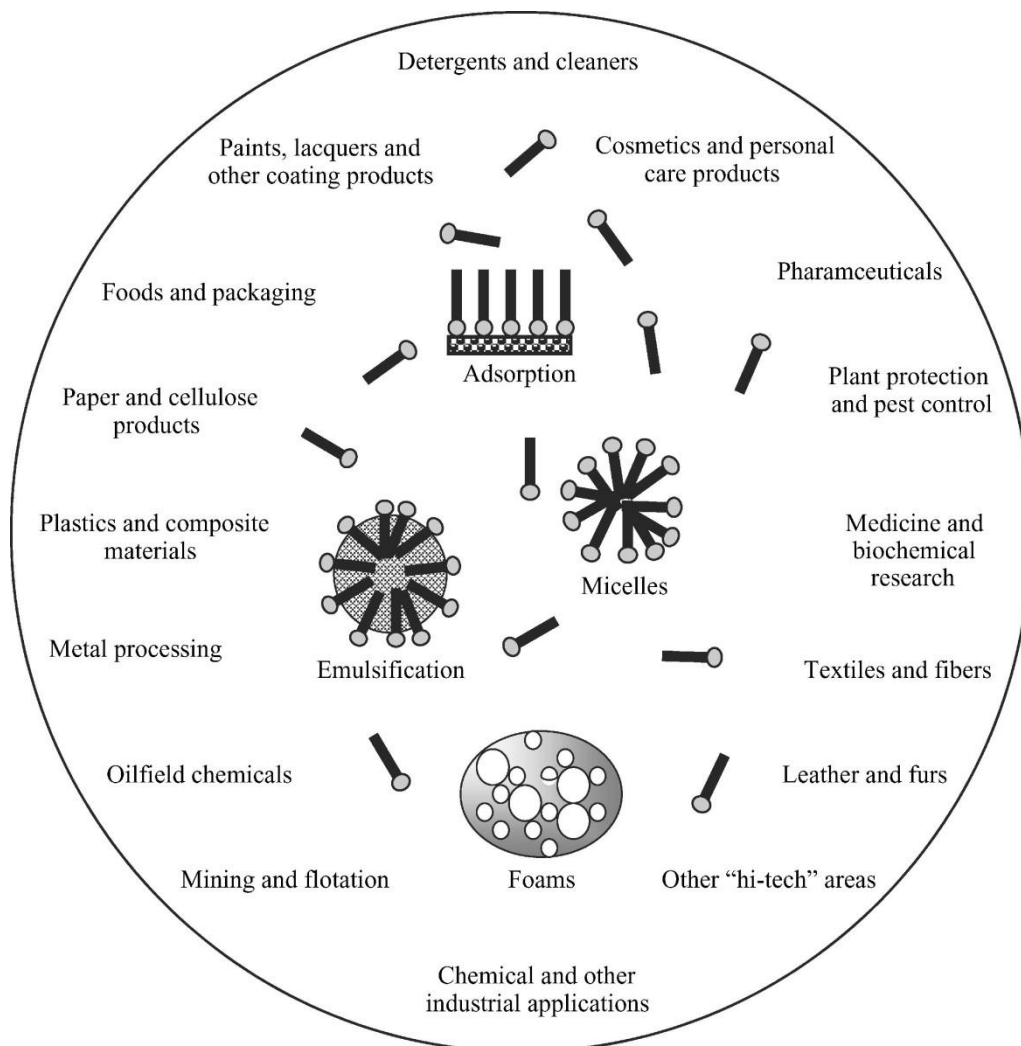


Figure 1.2 Some important, high-impact areas of surfactant applications. Adapted from Reference⁴. Copyright permitted from Wiley-Interscience.

1.3 Amphiphile Solution Assemblies

1.3.1 Fundamentals of Amphiphile Assemblies in Solution

The observed tendency of amphiphiles to aggregate in aqueous solution and exclude water molecules is named the hydrophobic effect¹³. Because of the hydrophobic effect, amphiphilic molecules assemble into a variety of nanoscale structures in aqueous solution when the molecular concentration is above a critical micelle concentration (CMC). Amphiphilic molecules are dispersed as unimers below the CMC but also form assembled nanostructures when above the CMC. For small amphiphiles, the CMC value is relatively large due to the small molecular weight and high configurational entropy/entropy of mixing of the small amphiphiles. For block copolymers, the CMC is relatively small due to the intrinsic large values of repeating units of each block linked in one polymer chain that greatly lowers the entropy of mixing of block copolymers.

1.3.2 Packing Parameters and Geometries

Final assembled geometries in amphiphiles are determined by the hydrophobic-interfacial curvature in the assembly arising from the relative volume fraction ratio between the soluble and insoluble domain due to both the length/size of the respective molecular domains due to their inherent molecular size as well as their respective interaction with the solvent. As depicted in Figure 1.3, vesicles, cylinders and spheres are assembled in different relative volume fraction zones of hydrophilic blocks *vs.* hydrophobic blocks in diblock copolymers in a water solvent¹⁴. The dimensionless packing parameter, p , originally derived for small amphiphiles, can be used qualitatively to describe the behavior of block copolymers. The packing parameter p is defined as:

$$p=v/a_0d.$$

where v is the volume, d is the length of the insoluble hydrophobic block and a_0 represents the surface area between hydrophobic and hydrophilic block.

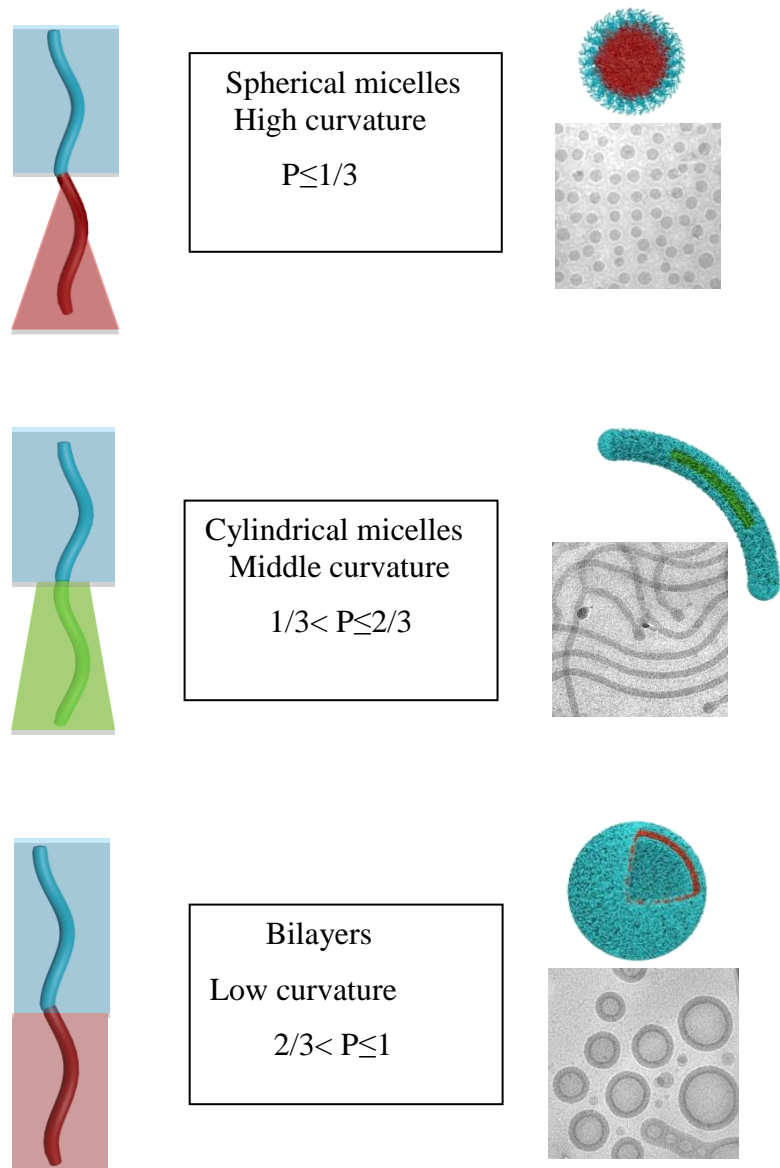


Figure 1.3 Different Geometries formed by block copolymer assembled in selective solvent. P represents the packing parameter. Red color and green color: hydrophobic chains; Blue color: hydrophilic chains. Cryogenic Transmission Electron Microscopy (cryo-TEM) images are copied from reference¹⁷ with the permission from 2003 American Association for the Advancement of Science.

1.4 Block Copolymers and their Solution Assemblies

Amphiphilic block copolymers have the same dual nature as their small amphiphile analogues but have a much larger molecular weight. By controlling the architecture of individual molecules, it is possible to generate nanostructures either in an undiluted melt or in solution. Similar to their small amphiphile analogues, classic nanostructures can be assembled from amphiphilic block copolymers in dilute solution such as spheres¹⁷, cylinders and vesicles¹⁶. Importantly, there are more chemical or physical parameters that can be manipulated in solution assembly to achieve a vast library of uncommon and well-controlled nanostructures. Through design of block type and number (diblock, triblock, multiblock, etc), changing of the block length and block length ratio, changing of the solvent conditions, or addition of external stimuli (such as changing pH¹⁸ or temperature environments¹⁹), one can achieve numbers of different solution nanostructures. The seemingly innumerable numbers of combinations of the parameters opens the possibility of accessing complex morphologies that cannot be attainable in small molecule amphiphiles. In addition to the parameters discussed above, management of assembly strategies offers an alternative for novel nanostructure formation. Protocols involving solvent processing²⁰⁻²², flash nanoprecipitation²³, or polymerization of crystalline-coil micelles²⁴ are good examples of new processes in engineering nanoscale materials. However, there are still clear opportunities for exploring new, facile self-assembly strategies and construction of new structures of nanostructured systems. More importantly, the advantages of large molecular weight assemblies with respect to certain properties, such as polymersomes that have significantly better mechanical properties relative to vesicles made from small molecule amphiphilic analogues, provides potential use in biomedical applications such as responsive drug delivery vehicles²⁵. In this thesis, new systems of block copolymer blends of construction of new multicompartiment and multigeometry nanoparticles are presented.

1.4.1 Shapes of Assemblies and their General Formation Mechanism

The classic shapes of molecule assemblies, cylinders and spheres contain a soluble shell from the hydrophilic molecule domains and an insoluble core from the hydrophobic domains. The other classic structure, the bilayer membrane, consists of two monolayers aligned so as to form a sandwich-like structure with a solvophobic core: soluble block-insoluble block next to insoluble block-soluble block. The bilayer membranes can become disks when the membranes have finite size and a resultant round, flat shape, and can also become vesicles when they close up to minimize membrane surface energy.

From a theoretical point of view²⁶, it is generally more energetically favorable to have infinitely long cylinders and infinitely large membranes in order to minimize the creation of end-caps and edges²⁷, respectively. However, the fluid nature of the block copolymer nanostructure and compositional fluctuations usually cause the breaking up of these aggregates to form smaller, finite sized aggregates²⁸. These finite-sized aggregates will form a high-energy defect at the ends/edges to avoid contact between the hydrophobic domain and the selective solvent (usually aqueous). For example, cylinders are stabilized by spherical end-caps into wormlike structures²⁷ and membranes are stabilized by a curved, half-cylinder edge to form disks²⁹. A unique example of energy minimization is the toroid structure formed from cylinders bending to completely close into a ring³⁰. This toroid formation is the cylinder equivalent to what happens to bilayer membranes when they close to form vesicles. For the typical structures formed through the breaking up of larger structure, it is more typical to observe finite cylinders formation while it is less typical to observe disk formation³¹, statistically and experimentally. And, for the scenarios involving the closing up of cylindrical or membrane nanostructures, it is more common to observe the closing up of membranes to form vesicles than it is to observe toroid formation³¹.

Pioneering work from Eisenberg established the field of block copolymer (BCP) self-assembly in dilute solution³². Research on block copolymer solution assembly has

been very active in recent years combined with the development of advanced characterization techniques such as cryogenic transmission electron microscopy (cryo-TEM) and small angle neutron or x-ray scattering (SANS or SAXS) to help with the deep understanding of new morphologies. Besides the well-known common morphologies already discussed, there are also other, unusual morphologies that have been discovered, designed and published previously³³. In the next section, a brief review of recent published morphologies is given. New, emerging, multicompartment, multigeometry, and asymmetric nanostructures will be discussed later in Section 1.4.

The exploration of novel nanostructures is an interesting topic growing in importance with many new morphologies having been reported. The addition of extra small molecules or application of external stimuli have been explored intensively in block copolymer self-assembly systems. The Pochan and Wooley research groups have worked on the polyacrylic-acid-*b*-polymethyl acrylate-*b*-polystyrene (PAA-*b*-PMA-*b*-PS) triblock copolymer system with the introduction of basic small molecules for an extra, added interaction between acidic hydrophilic blocks³⁴. Toroid structures^{31, 35-37}, spheres, packed disks, spheres with internal phase separation³⁸, cylinders³⁹, striped cylinders⁴⁰ and helical cylinders structures⁷ have been assembled with different length of triblock copolymers via kinetically controlled pathways. The Jiang group has used the complexation between DNA and oppositely charged micelles to make toroids⁴¹ and cylinders⁴² with low dispersity of shape and size. Small molecule complexation has also been used by Hayward and coworkers. Helical ribbons were assembled in conjugated poly(3-hexylthiophene)-*b*-poly(3-triethylene glycol thiophene) crystalline-coil diblock copolymer system *via* the complexation between the hydrophilic block with added potassium ions⁴³. The Liu group has also built up double or triple helices in an ABC triblock copolymer assembly system that was assembled in organic solvent mixtures that were marginal for A block, poor for B block and good for C block^{44, 45}. Besides the classic sphere, cylinder, bilayer structures, many intermediate transition structures have also been observed. Jellyfish structures between worm-like and vesicular nanoparticles have also been captured via kinetic

control in polybutadiene-*b*-poly(methylacrylic acid) diblock systems by the Battaglia lab^{46,47}. The recent discovery of large, 2D sheets between cylinders and vesicles has been reported by the Cheng group⁴⁸. Functionality possible with copolymers provides a variety of other possible nanostructures. For example, annular multilayer vesicles were prepared from RGD-functionalized poly (ethylene oxide)-*b*-polybutadiene by Hillmyer group⁴⁹.

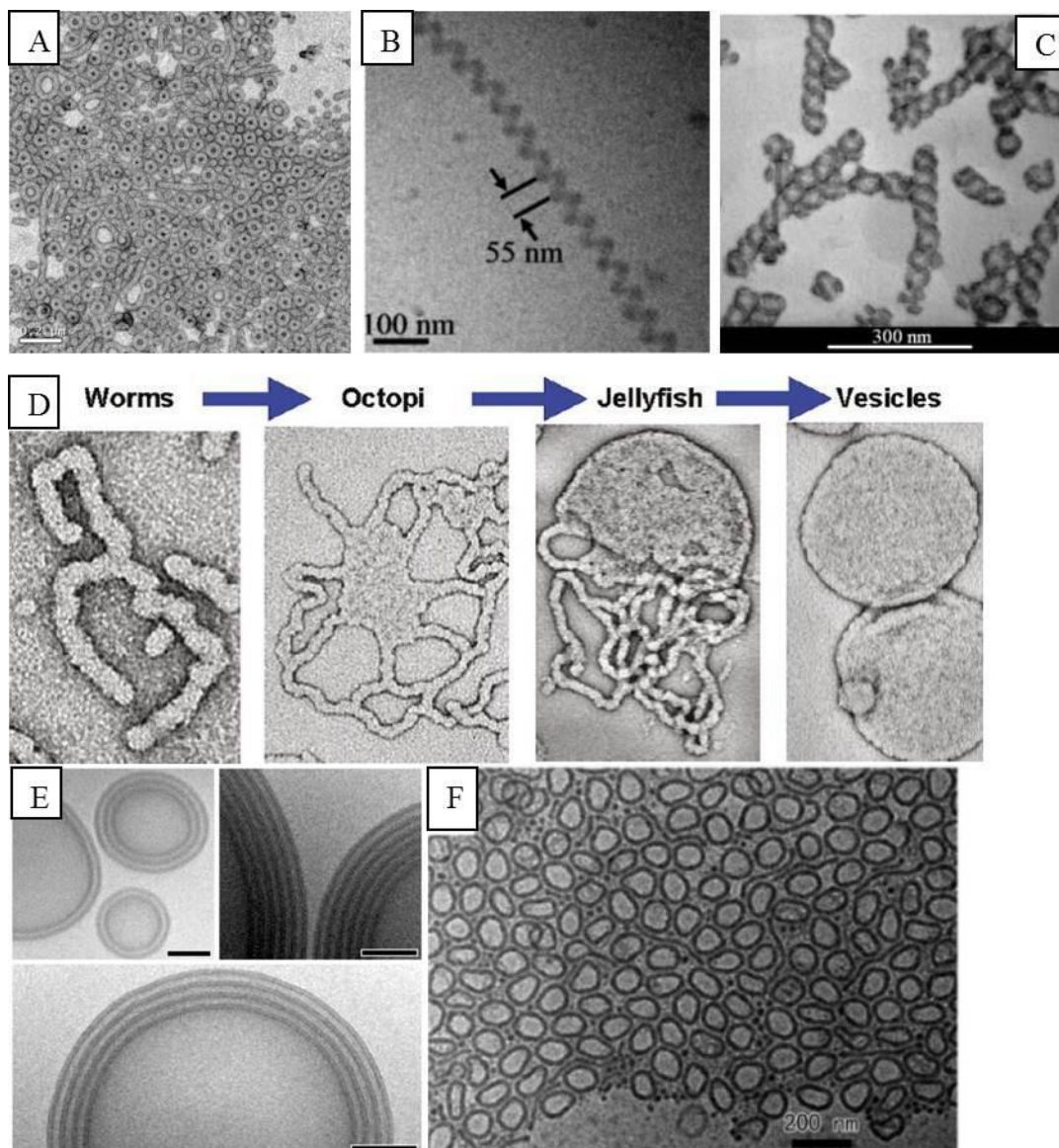


Figure 1.4 Assemblies formed in selective solvent conditions by different block copolymers: (a) toroids³¹, (b) helix⁷, (c) double helix⁴⁴, (d) jellyfish structure⁴⁶, (e) multilayer vesicles⁴⁹, (f) monodisperse toroids⁴¹. (Reproduced with permissions from: 2004 American Association for the Advancement of Science³¹, 2009 Royal Society of Chemistry Journals, and 2006, 2009, 2014 American Chemistry Society⁴¹).

As mentioned previously, the formation of large, flat 2D nano-sheet structures is not readily accessible; sheets usually break up into small pieces of membrane⁵⁰, disks or close up to form vesicles. The recent discovery from the Cheng group showed a unique way to make 2D sheets where cylinders could be wrapped up to form large 2D nano-sheets with an underlying, unique hexagonal packed honeycomb-like pattern⁴⁸. The slow solvent exchange performed with the giant triblock amphiphile poly(styrene)-*b*-poly(ethylene oxide)-tethered-fluorinated polyhedral oligomeric silsesquioxane (FPOSS) was the key to hierarchical sheet formation through slow chain segregation that eventually formed the intermediate hexagonal patterned nano-sheet. Cryo-TEM was used to observe the unique structure *in-situ*, Figure 1.5. Other groups have employed hierarchical assembly methods to form 2D sheet-like structure in a bottom-up fashion. Work from the Winnik and Manners groups effectively constructed 2D sheets from cylindrical crystalline-coil fiber sub-units⁵¹. Other free-standing 2D sheets have been reported by the Eisenberg group. By taking advantage of polymer single crystal growth mechanisms, the diblock copolymer poly(ethylene oxide)-*b*-polycaprolactone was co-assembled with homopolycaprolactone and 2D large sheets were formed from fiber seeds after co-assembly⁵².

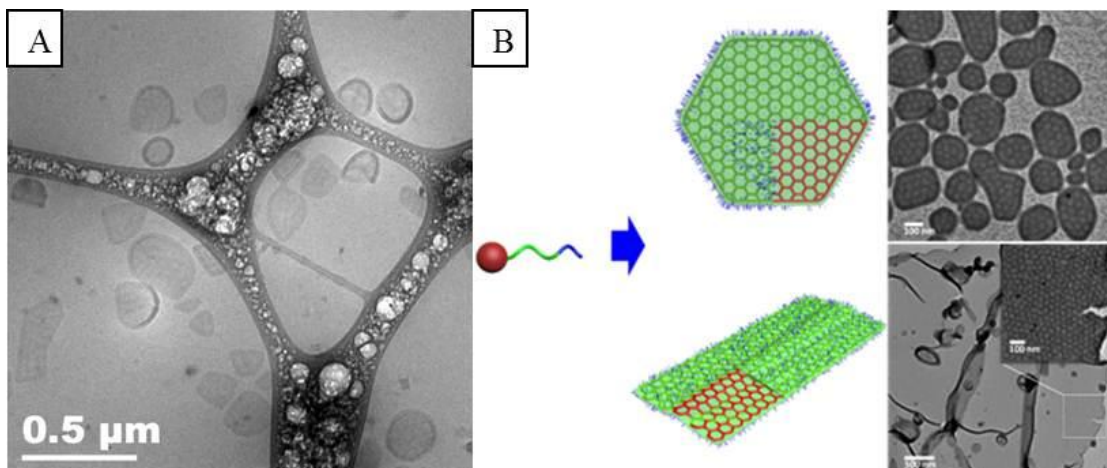


Figure 1.5 2D large nano-sheets with internal hexagonal packed pattern. (A): cryo-TEM images of large 2D nano-sheets, data unpublished. (B): The corresponded normal TEM image of the large 2D nano-sheet structure, figure adapted from reference⁴⁸ with copyright approved by 2015 America Chemistry Society.

Besides the molecular weight, the other significant difference between small molecule amphiphiles and block copolymers is the polydispersity of molecular weight. While current, advanced anionic polymerization and controlled living polymerization methods provide block copolymers with low \mathcal{D} (polydispersity index), it is still one factor that influences the formation of well-defined shaped and sized solution assemblies⁵³⁻⁵⁵. People have taken advantages of the polydispersity of large amphiphiles in constructing unconventional nanostructures. Prolate-spheroid micelles were assembled in poly(ethylene oxide-*b*-1,4-butadiene-*b*-ethylene oxide) (OBO) system and was reported by Mahanthappa group⁵⁶.

1.4.2 Theoretical Simulation of Block Copolymer Self-assembly

Besides the experimental investigation of new nanostructures, theoretical simulation has also been used to predict new structures and help to further understand more exotic experimental structures. Different computer simulation methods have

been used such as Monte Carlo methods, the simulated annealing method⁵⁷, self-consistent field theory (SCFT)⁵⁸ among others. Toroids^{59, 60}, segmented cylinders, patchy spheres⁶¹, gyroid structures in bulk block copolymer assembly⁶², as well as short cylinders and disks⁶³ have been reported previously. Intermediate shape transformations of membrane vesicles have been predicted, such as the pear-shaped, dumbbell, starfish, and stomatocyte and inverted vesicles⁶⁴. Confinement-induced novel morphologies of block copolymer particles such as helices have been predicted by the Li group from Nankai University by using a lattice model with simulated annealing technique⁵⁸. Single left and right handed helices, a double helix, and toroids have been observed in their simulated results. Recently their simulated results showed that helical vesicles, segmented semivesicles, and noncircular bilayer sheets could be assembled from ABC miktoarm star terpolymers in the solution-state⁵⁷. The new findings of theoretical simulation work will be important going forward in helping to predict new structures as well as to understand experimental results.

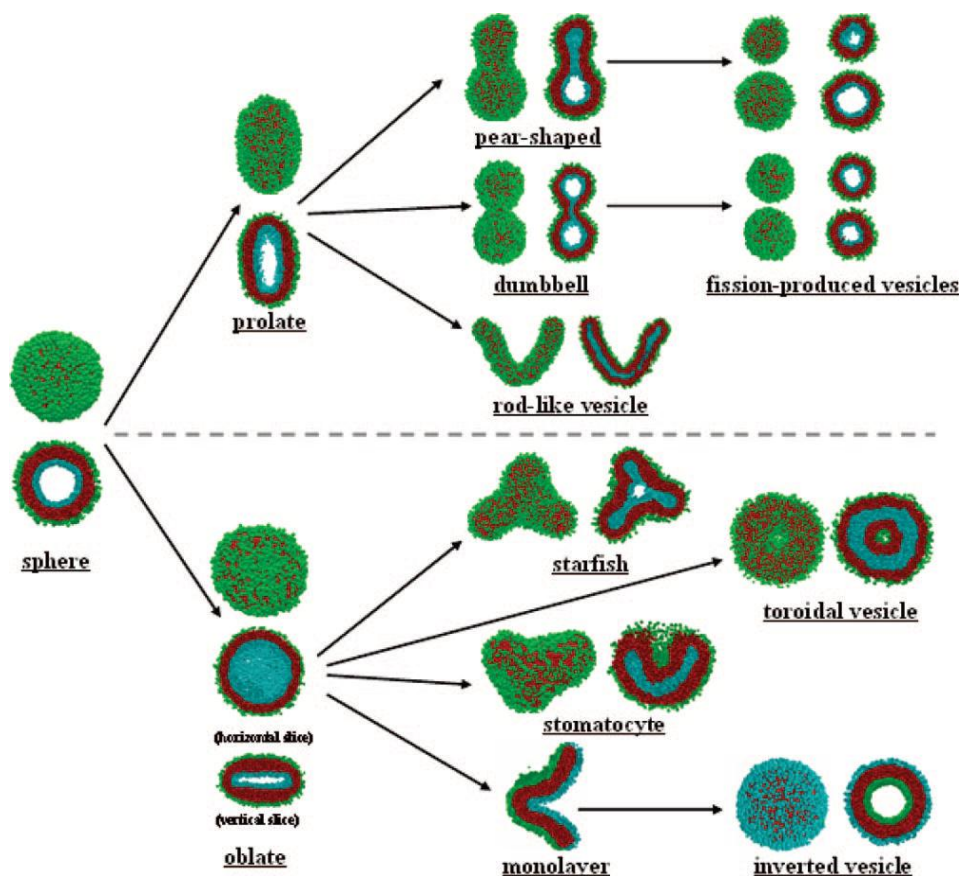


Figure 1.6 Morphologies possible for triblock copolymers as determined theoretically by Li⁶⁴ *et al.* Copyright approved by 2009 America Chemistry Society.

1.5 Multicompartment and Multigeometry Nanoparticle Assembly

Compared with the classic core-shell like micelles with a single core domain and single shell domain, multicompartment and, sometimes, multigeometry nanoparticles (MCN & MGN) have the signature character of having multiple hydrophobic/hydrophilic phases trapped and locally separated within one, nanosized domain. The multicompartment nanoparticles hold potential for being multifunctional nanomaterials due to the incorporation of subdivided, multiple phases. For instance, two or more incompatible compounds such as two drugs could be stored in the distinct

core domains and then released to specific targeted sites. Many methods have been reported to achieve novel shapes of multicompartiment and multigeometry nanoparticles, not only because of the possible applications but also due to the exploration of a larger complexity of untraditional morphologies. Synthesis of new, complicated molecules is one major way to realize this goal⁶⁵. The simplest molecular structure for MCN formation is the linear triblock copolymer, ABC, with A hydrophilic block and B, C hydrophobic blocks. Specifically, B and C are immiscible hydrophobic blocks with poor thermodynamic compatibility. For MCN formation, B and C have a large Flory-Huggins interaction parameter that will provide for the local phase separation within the hydrophobic nanoparticle core in an aqueous-rich solvent. People have been designing different linear triblock copolymers with unusual morphologies having been assembled. For instance, the Laschewsky group has a series of reports on MCN systems assembled from different linear triblock copolymers. For example, raspberry-like, spherical nanoparticles with patches on the surface of the spheres were assembled from the linear triblock copolymer poly(4-methyl-4-(4-vinylbenzyl) morpholin-4-ium chloride)-*b*-poly-styrene-*b*-poly(pentafluorophenyl 4-vinylbenzyl ether)⁶⁶, Figure 1.8. A further approach to compartmentalized micelles was developed by Laschewsky *et al.* through the aqueous assembly of poly(4-methyl-4-(4-vinylbenzyl)morpholin-4-ium chloride)-*block*-poly-styrene-*block*-poly(pentafluorophenyl 4-vinylbenzyl ether).

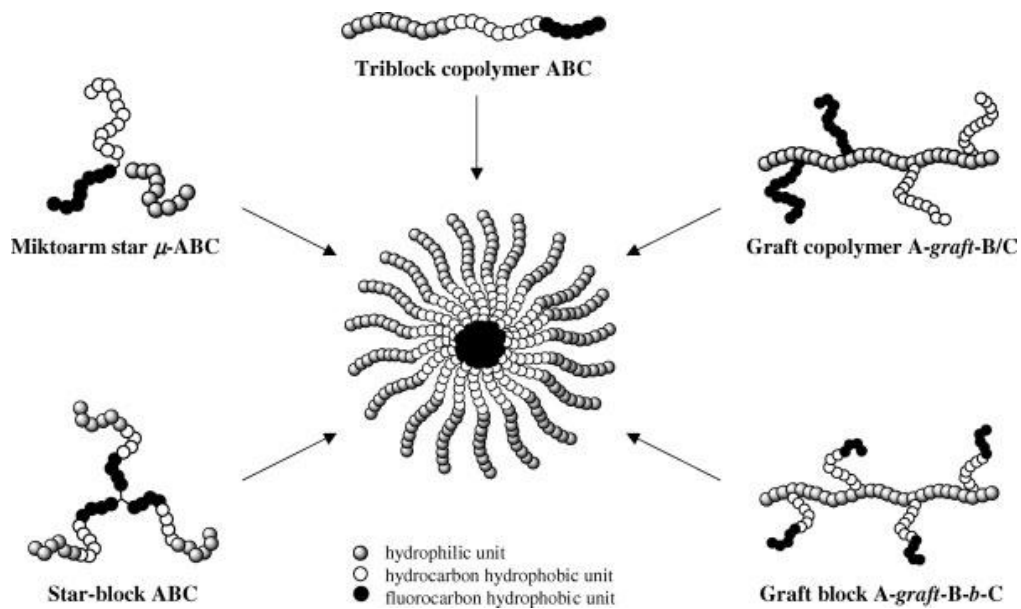


Figure 1.7 Strategies for building multicompartiment micelles with different architecture of triblock copolymers. Figure adapted from reference⁶⁵ with the permission of copyright.

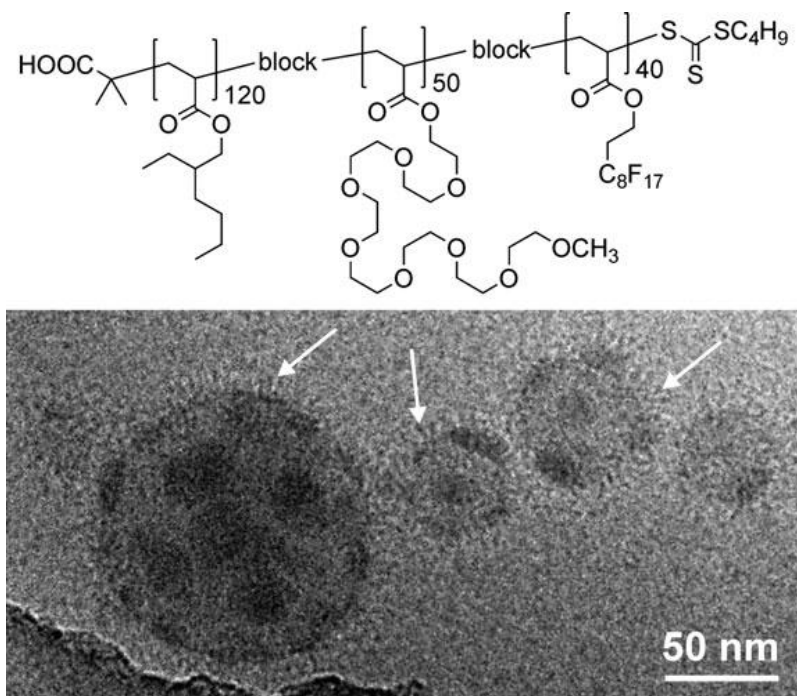


Figure 1.8 Chemical structure of triblock copolymer (EHA)₁₂₀-(OEGA)₅₀-(FDA)₄₀ and cryo-TEM image of its 0.5 wt% aqueous dispersion. The micelles appear as high-contrast spherical particles surrounded by a fringed corona (indicated by arrows).

More complex morphologies have been achieved through the use of miktoarm star block, star and graft block copolymers⁶⁷⁻⁶⁹. The Lodge group has a series of work on miktoarm star block terpolymers with hydrophilic poly(ethylene oxide) and two hydrophobic, but immiscible, components (a polymeric hydrocarbon and a perfluorinated polyether) at a common junction. Worm-like structures with a segmented core⁶⁷, hamburger-like structures⁶⁸, and bilayer structures⁶⁹ have been assembled with unlike hydrophobic chains segmented, as depicted in Figure 1.9.

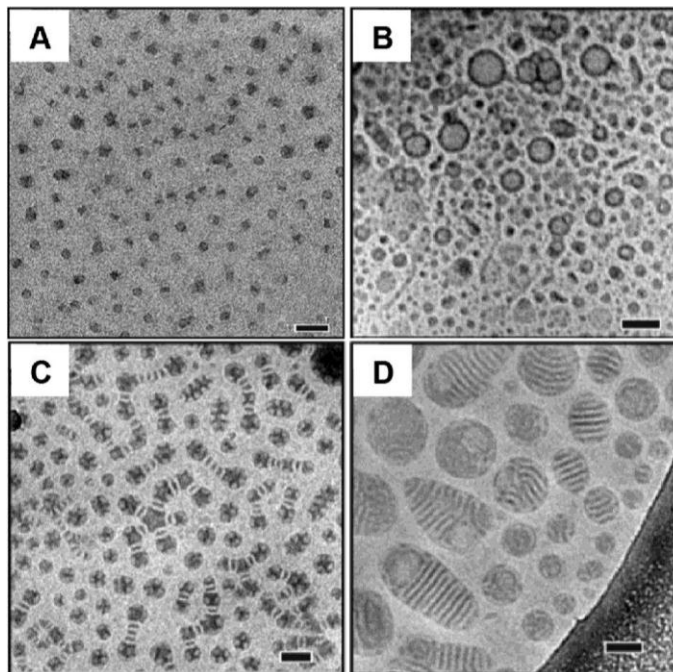


Figure 1.9 Multicompartment micelles from miktoarm star terpolymers, μ -EOF(x-y-z). Cryo-TEM images of 1 wt % aqueous solutions of (A) μ -EOF(2-13-3.5), (B) μ -EOF(2-4-2.5), (C) μ -EOF(2-9-5), and (D) μ -EOF(2-6-2.5); scale bars indicate 50 nm⁷⁰. Cryo-TEM images adapted from reference⁶⁹. Copyright Approved from 2006 American Chemical Society.

The group of Axel Müller started work on Janus nanoparticles in early 2000⁷⁰. Janus nanoparticles are named to describe multicompartment nanoparticles with a phase-separated corona, like the structure of a Janus-face. Janus micelles were assembled from triblock copolymer and contained a polybutadiene (PB) core and a compartmentalized corona consisting of a poly(methacrylic acid) (PMAA) and a polystyrene (PS) hemisphere. Taking advantage of the different solubility properties of the three blocks in mixed organic solvent, a slow exchange of solvents was used to produce the assembly. The final assemblies were obtained by dialysis of the mixed organic solvent against water⁷¹. Janus disks were prepared with similar methods used to make the Janus micelles⁷². And Janus cylinders were also prepared by cross-linking

the lamelle-cylinder morphology of a poly(styrene)-*b*-poly(butadiene)-*b*-poly(methyl methacrylate) block terpolymer⁶. Janus cylinders possess a phase segregation of two hemicylinders as depicted in Figure 1.10.

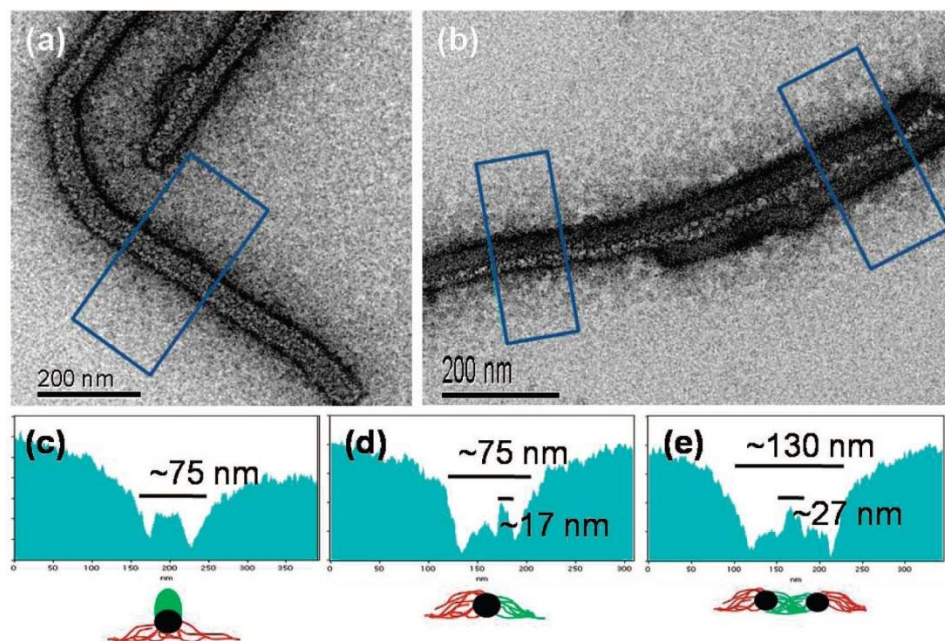


Figure 1.10 TEM images of single (a) and aggregated (b) Janus cylinders on a carbon-coated TEM grid after staining with RuO₄ for 2 h. Grey-scale analyses (c-e) correspond to the section analyses as shown in the images from left to right. The schematic drawings at the bottom exhibit the orientation of the Janus cylinders within the cross-sections (PB) black, (PS) red, (PMMA) green. Figure adapted from reference⁶, with approved copyright from 2009 ACS publication.

The use of the solubility differences of three blocks in one triblock copolymer has been extended to other assembly systems. Multicompartment micelles featuring a “sphere on sphere” core morphology is achieved through the assembly of a ABC triblock terpolymer, poly(butadiene)-*b*-poly(2-vinyl pyridine)-*b*-poly(*tert*-butyl methacrylate) (BCT). Cross-linking of the polybutadiene block was accomplished, and the core domain was stabilized. PB and P2VP were phase separated locally in the core

domain to form sphere-on-sphere structure⁷³, Figure 1.11. Different triblock terpolymers polybutadiene-*b*-poly(2-vinyl pyridine)-*b*-poly(methacrylic acid) (PB₈₀₀-*b*-P2VP₁₉₀-*b*-PMAA₅₅₀) were synthesized to assemble into dynamic multicompartment-core micelles in basic or acidic buffer solution⁷⁴. A core-shell-corona structure was clearly observed by cryo-TEM, Figure 1.12.

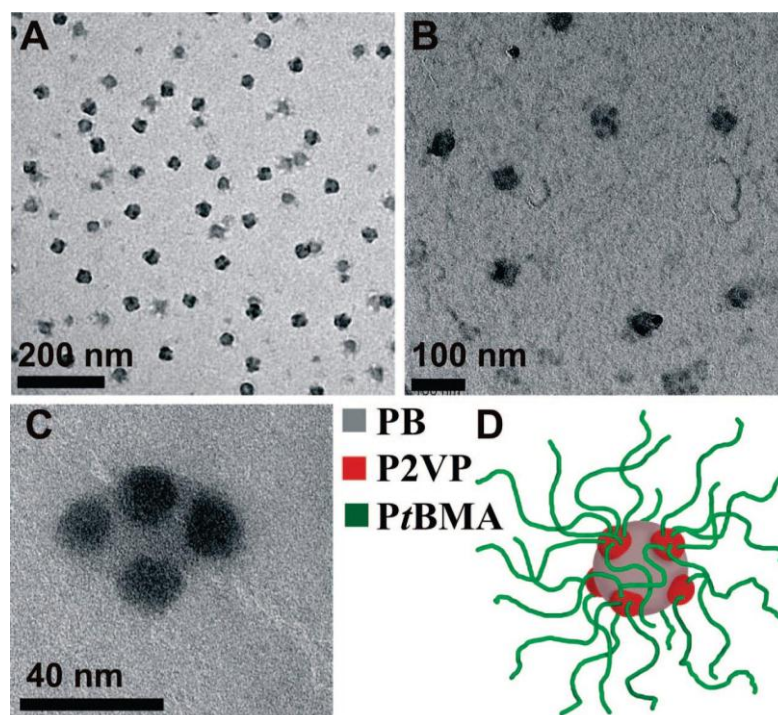


Figure 1.11 TEM images of multicompartment micelles from B₈₀₀-*b*-V₁₉₀-*b*-T₅₅₀ (A) drop-coated and (B) freeze dried from 0.1 g/L acetone onto carbon coated gold TEM grids. (C) Single micelle at high magnification. (D) Proposed solution structure of the micelles. Figure adopted from reference⁷⁴, with approved permission from 2009 American Chemical Society.

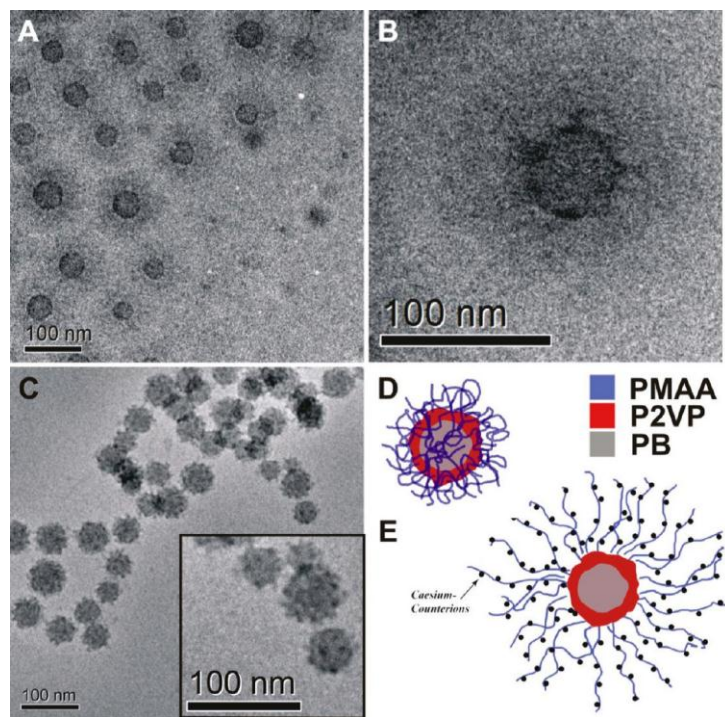


Figure 1.12 Cryo-TEM micrographs of $PB_{800}\text{-}b\text{-}P2VP_{190}\text{-}b\text{-}PMAA_{550}$ in buffer aqueous solution with pH10 (0.05M CsCl, $c=1$ g/L), overview(A) and single core-shell-corona micelle (B); at pH4 ($c=1$ g/L) (C), the inset shows an enlargement; schematic depiction of the proposed solution structure of $PB_{800}\text{-}b\text{-}P2VP_{190}\text{-}b\text{-}PMAA_{550}$ depending on the pH; core-shell-corona structure with an expanded PMAA corona at pH10 (E) and micelles with a collapsed PMAA corona at pH 4 (D). Figure Adapted from reference⁷⁴, with approved permission from 2009 American Chemical Society.

The phase-separation in the corona was taken advantage of to form undulating multicompartiment cylinders from a triblock copolymer poly(4-*tert*-butoxystyrene)-*block*-polybutadiene-*block*-poly(*tert*-butyl methacrylate) (PtBS-*b*-PB-*b*-PtBMA) basic block, in which the central PB block was modified with a fluorinated side group by the thiolene reaction of the vinyl groups with 1-mercapto-1*H*, 1*H*, 2*H*, 2*H*-perfluorooctane⁷⁵. Multistep solvent exchange was applied to produce the undulated cylinders from sphere seeds, Figure 1.13.

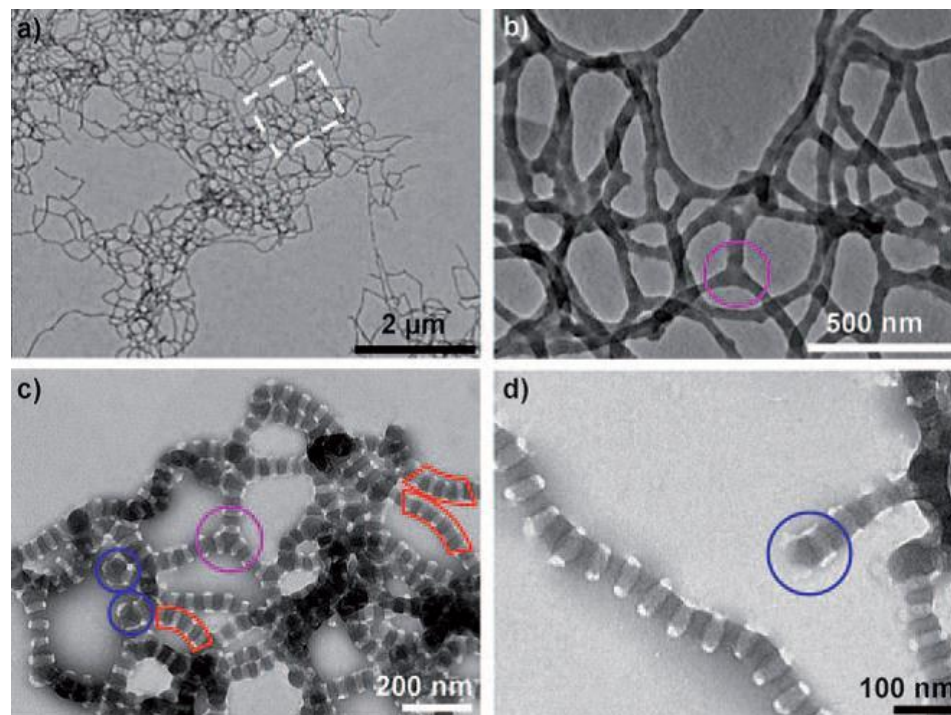


Figure 1.13 (a, b) Non-stained and (c, d) RuO₄ stained TEM images of undulated cylinders, obtained from ethanol. Adapted from reference⁷⁵. Copyright permission approved from 2009 Wiley Publication.

MCNs can be made not only by assembling one triblock copolymer with immiscible blocks but also through physical blends of distinct block copolymers⁷⁶. For example, by mixing distinct block copolymers containing oppositely charged hydrophilic domains, people have successfully assembled interpolyelectrolyte complexes of dynamic multicompartment spherical micelles. Complexed hydrophilic chains are observed clearly via cryo-TEM⁷⁷. Blends of triblock terpolymers were also made, on which formed highly ordered multicompartment patchy particles. Hierarchical, particle-based assembly was performed recently to construct multicompartment cylindrical superstructures with sphere patches precisely distributed on the shell²², Figure 1.14. The Hayward group has observed a peasecod-like structure

by blending two distinct diblock copolymers that have the immiscible hydrophilic phases (polyethylene oxide (PEO) and poly (2-vinylpyridine) (P2VP) and the same hydrophobic polystyrene block in a PS favorable solvent⁷⁶. Generally, by blending two or more different block copolymers, one can tune the nanoparticle morphology without synthesizing a range of multiblock copolymers. Even though the possibility of macrophase separation can limit the efficacy of this strategy, the simple mixing of polymers in different ratios presents a feasible way to produce a broad of structures with the same block copolymers (this will be discussed more in Chapter 3, 4 and 5).

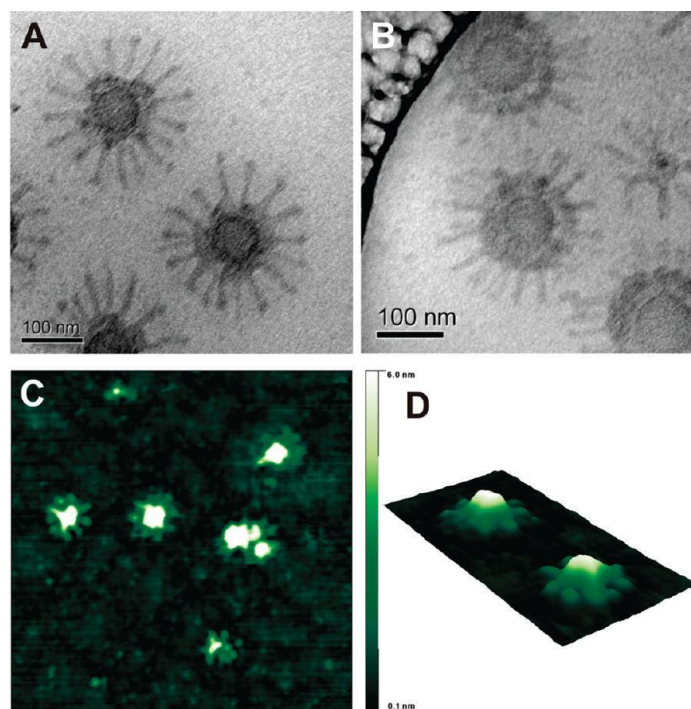


Figure 1.14 (A,B) Cryo-TEM micrograph of IPECs pH 10 after 1 h mixing time at different locations of the same sample; (C,D) SFM height images of an IPEC solution at pH 10 after deposition on a carbon-coated TEM grid; z-scale in both cases is 6 nm, with D displaying an enlargement of C. Adapted from reference⁷⁸. Copyright permission approved from 2009 American Chemical Society.

Due to the large complexity potentially achieved via different assembly methods, asymmetric and anisotropic polymeric nanoparticles are not a dream⁷⁸. Now, one can possibly extend the solution assembly of polymers into potentially arbitrary structures and not only be limited to highly symmetric structures. An excellent example of using hierarchical assembly and block copolymer blending to produce asymmetric structures is from the Winnik and Manners groups who have built non-centrosymmetric cylinder structures via multistep assembly. Monodisperse cylinder micelle sub-units, which were fabricated through crystallization-driven self-assembly (CDSA), were grown into two and three segmented cylinders through sequential addition of new block copolymers that subsequently assembled onto the initial, seed micelle subunit. Further assemblies have been produced through linking together of the active cylinder ends to make large-star like cylinder aggregates, Figure 1.15. More recent work has been reported on constructing multidimensional cylindrical comicelle superstructures based on hierarchical assembly of cylinder subunits. One-dimensional single-stranded chains, two-dimensional and three-dimensional cylinder networks were reported⁷⁹.

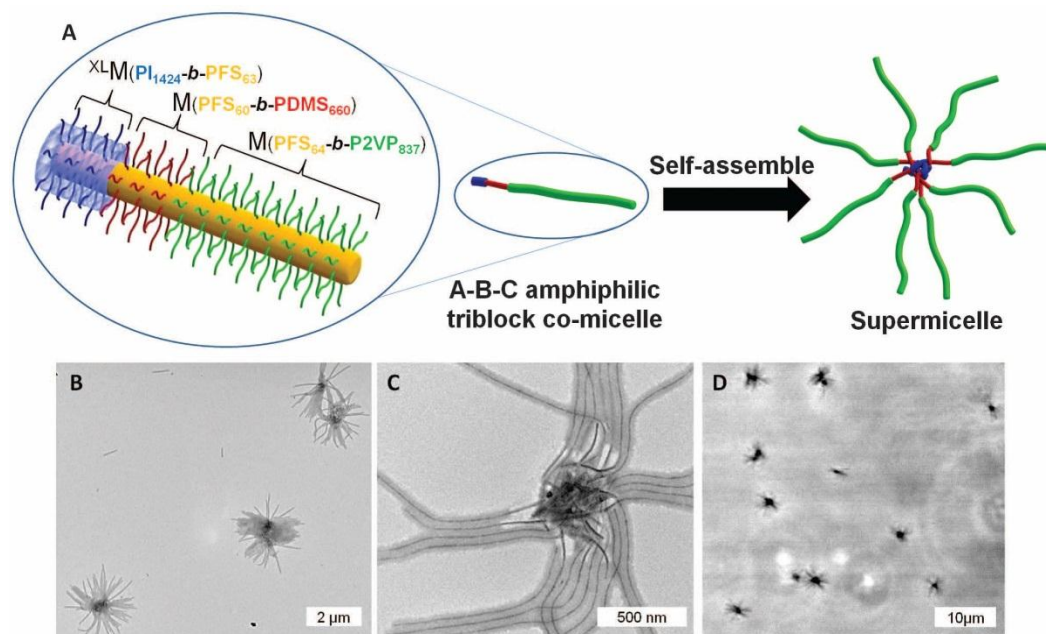


Figure 1.15 Schematic representations of triblock co-micelle and its self-assembly into a supermicelle. (B) Low-magnification TEM micrograph of a cluster of supermicelles (C) Higher-magnification TEM micrograph of a supermicelle showing the core, (D) Optical micrograph of the supermicelles. Adapted from reference²⁴. Approved copyright from AAAS 2012.

Our research group takes inspiration from the above described literature and performs block copolymer solution assembly via kinetic control to produce new nanostructures⁴⁰. Avoiding the time-consuming synthesis process for complicated molecules, kinetic control of assembly was developed as an advanced tool to introduce well-defined, novel and more complicated nanostructures via either a single diblock or triblock assembly or coassembly of two different block copolymers. Originally, one triblock copolymer with an acidic hydrophilic block was used for assembly with small organic amine molecules added to complex with the hydrophilic block. By changing the amount and type of the amine, one can achieve various kinds of morphologies³⁸. More importantly, the self-assembly pathway was further controlled by slow or fast water addition to an original polymer/amine THF solution. During the water addition

process, reproducible, intermediate, kinetically-trapped and controlled nanostructures were observed^{39, 80-82}. For example, control of the assembly parameters can produce quite interesting striped cylinder structures³⁰. More recently, kinetic control was used for construction of multicompartiment and multigeometry nanoparticles through co-assembly of block copolymer materials. Multicompartiment cylinders⁴¹, spheres, sphere-cylinders⁸³, and multigeometry patchy disks and disk-cylinders²⁹ were assembled and reported. Functionality (primarily the introduction of interactions through the hydrophilic shells of particles) of the building blocks was introduced to achieve hierarchical assembly of multicompartiment nanoparticles including rings, linear arrays and three-dimensional aggregates²⁹. Detailed studies of solvent manipulation and the addition of chemical functionality to introduce intermicelle chemical crosslinking will be presented in this dissertation.

1.6 Applications of Block copolymer Solution Assemblies

The versatility in molecular architecture, composition and solution-assembled structures of block copolymers allow specific applications to be designed. The tunable shapes and sizes⁸⁴⁻⁸⁶ of the solution assemblies have opened the door for emerging nanotechnologies including aqueous nanoreactors, nanocarriers and other applications. It is suggested that the optimal nanoparticle size range for cancer treatment is 10-100 nm, length scales feasibly achieved by block polymer assemblies^{87, 88}. The lower size limit is set according to the filtering effects of kidneys⁸⁹, as particles smaller than 10 nm are easily filtered and cleared by kidneys. The upper size limit is set by many factors such as the liver filtration and particle diffusion^{88, 90, 91}. The manipulation of block copolymer lengths and solution conditions can easily achieve the size requirements of nanocarriers.

The achievement of novel, well-controlled nanostructures is important as the predictable manipulation of solution-assembly parameters in order that technology becomes feasible. Some examples of potential technology with nanoparticle assemblies are described in the following section.

1.6.1 Nanocarriers as Drug Delivery Vehicle, DNA and other Molecule Encapsulations

Solution assemblies formed from amphiphilic block copolymers have been explored in recent years as nanocarriers for nanomedicine study⁹². Firstly, the inside core of a micelle can serve as a nanoenvironment for the carrying of drugs, while the corona shell can serve as a stabilizing interface between the internal hydrophobic core and the external medium. Secondly, nanosized solution assemblies being gene or drug carriers tend to circulate in vivo for at least couples of hours, compared with the practically immediate clearance of their micrometer-sized analogs⁹³. Thirdly, block copolymer assemblies have better mechanical properties, stabilities and larger topological and chemical diversity compared with other amphiphile^{94, 95}. Self-assembled polymer structures such as micelles and vesicles are mostly used for drug transporting and release in drug delivery systems. Some systems are currently on the market, such as Lumirem from Guebert s.A or Abraxane from American Bioscience Inc. etc⁹⁶. Considering its biocompatibility, polyethylene glycol is one of the FDA (US Food and Drug Administration) approved molecules and is more widely used relative to other polymer candidates in real applications and fundamental study of nanocarriers.

The morphologies of assemblies, size of assemblies⁸⁵, loading capacity and their stability will have influence over their performance as nanocarriers.

Morphology and size influence:

Among the various structured assemblies⁹, spherical core-shell micelles are good candidates for loading drug and the release in the body⁹⁷. Vesicles, as good mimics of cell bilayer structures, are inherently good drug delivery vehicles⁹⁸. The responsive and functionalized vesicular polymersomes attract intense attention due to good permeability, pH responsive property and specificity in site targeting⁹⁹.

The emerging studies of other morphological nanoparticles provide other high-performance nanocarrier candidates. Non-spherical nanoparticles have received significant attention recently. Cylindrical filomicelles loaded with drugs persisted up

to one week after intravenous injection which is ten times longer than spherical counterparts⁹³. Further results indicated that cylindrical filomicelles can deliver anticancer drugs and shrink human-derived tumors in mice, showing significantly promise for the future of novel nanocarrier.

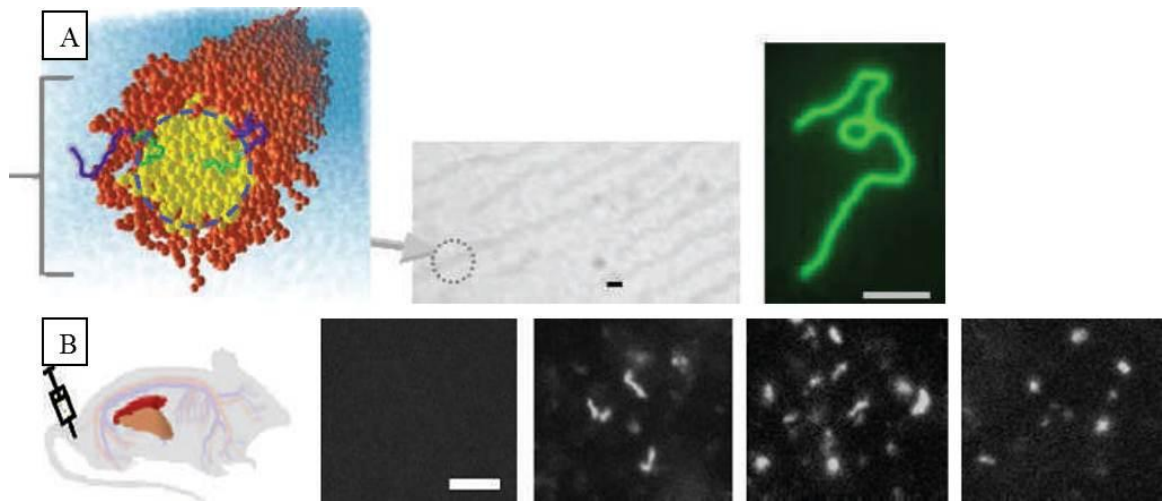


Figure 1.16 Filomicelles and their persistent circulation. A, Filomicelles are self-assembled from diblock copolymers. B, Injection of fluorescent filomicelles into rodents. Figures adapted from reference⁹³, copyright approved by 2007 Nature Publication.

Higher degree of morphology sophistication is needed from block copolymer-based drug delivery systems that can act as multiple drug carriers with pH, and temperature-responsive compartments and even in vivo site targeting. Multicompartment micelles could fill this role. Müller recently used triblock terpolymer multicompartment nanoparticles as advanced drug delivery systems for photodynamic therapy (PDT). The tunable poly(ethylene glycol) shell in the multicompartment nanoparticles demonstrated up to 24 hours circulation time when fully PEGylated but rapid clearance for the only partially PEGylated ones¹⁰⁰. This

study is an excellent example of promising applications of the hierarchical, complex structured nanocarrier systems.

1.6.2 Nanoreactors

Block copolymer micelles can also be used for nanoreactors^{101, 102}. The specific, internal hydrophobic/external hydrophilic dual properties of amphiphilic assemblies provide a suitable environment for certain reactions. Micelles, which can be spherical or cylindrical, have a compartment that is capable of accommodating solutes. Menger and co-workers firstly published transition metal-catalyzed reactions in surfactant aqueous solution in late 1970¹⁰³. Additional work has been reported on surfactant-enhanced reductive reaction and micelle-increased reaction rates of metal catalysts¹⁰⁴. Micelles can also be used for metal nanoparticle stabilization and can provide the interior cage for metal nanoparticle synthesis¹⁰⁵. Thus, nanoscale metal particles are potentially being applied in electronic, magnetic, optical and catalytic applications. Besides metal nanoparticles, metal oxides such as Fe₂O₃, TiO₂, ZnO and quantum dots, *e.g.* CdS, CoS can be formed within micellar nanoreactors¹⁰⁶.

Copolymer vesicles are not just limited to being used as nanocarriers, but are also being used as numerous vesicular nanoreactors. It has been demonstrated that vesicle nanoreactors loaded with an enzyme proved to be catalytically active within the vesicle interior, converting a soluble non-fluorescent substrate into a non-soluble fluorescent substrate, Figure 1.17¹⁰⁷. pH sensitive vesicular nanoreactors have also successfully transformed the extra-vesicular superoxide radical (O₂⁻) into O₂¹⁰⁸.

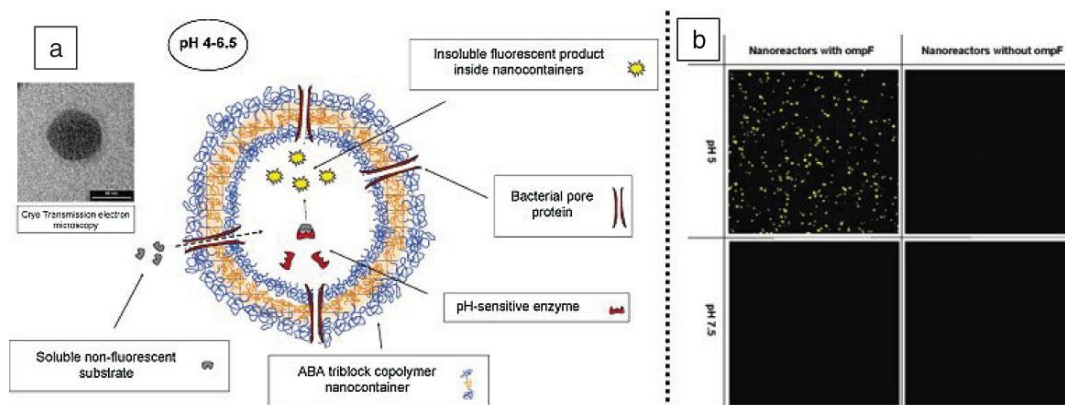


Figure 1.17 (a) Schematic illustration of enzymatic nanoreactor in the processing of the external non-fluorescent substrate into an internalized fluorescent substrate. (b) Fluorescent micrographs illustrating both the protein channel and pH-dependence on nanoreactor functionality. Reproduced with permission from ref. 2006 American Chemical Society¹⁰⁷.

The inner nanocavity of the polymersome provided not only for encapsulation but also acted as a physical barrier to protect interior compounds from degradation. Thus, stomatocyte polymersomes with tunable openings under external stimuli allow these supramolecular structures to capture and release cargo in a reversible and controlled manner¹⁰⁹. Polymer stomatocytes were also used to entrap platinum nanoparticles within their nanocavities, and, subsequently, generate autonomous movement by controlling the opening and closing of the stomatocyte mouth¹¹⁰.

1.7 Thesis Overview

The remainder of this dissertation presents the construction of multicompartiment and multigeometry nanoparticles (MCN and MGN, respectively) via blends of unlike block copolymers during solution assembly. New multicompartiment hybrid vesicles, hybrid disks, hybrid cylinders, and multigeometry disk-cylinders, vesicle-cylinders, and asymmetric star-like micelles were assembled via blends of amphiphilic block copolymers having the same PAA hydrophilic block and immiscible hydrophobic

blocks. Specifically, key results demonstrated that the detailed tuning of selective solvent addition rates resulted in different solution assemblies even with the same block copolymer blends. For example, smaller nanoparticles with immiscible blocks trapped in the core but nanophase separated are formed via faster solvent addition rates during assembly. Larger multicompartment nanoparticles, or even populations of discrete nanoparticles, are formed at slower solvent addition rates. The additional understanding described herein makes more possible material design for new, potential applications such as nanocarriers and nanoreactors, hopefully helping to lead to significant developments of nanotechnologies.

A review of foundational and recent block copolymer solution assembly, especially multicompartment and multigeometry nanoparticle assembly was presented in Chapter 1. An overview of *in situ* characterization methodologies for solution assemblies is presented in Chapter 2, including advances in electron microscopy, selective staining, *in-situ* imaging and 3D imaging. The effects of selective solvent addition rates on the final assembled structures of block copolymer blends are discussed in Chapter 3. Further study on binary blends and ternary blends that resulted in new structures is presented in Chapter 4. An increasing number of reports indicate that both the assembly pathway and the surface functionality would aid for novel nanostructure construction through interparticle, hierarchical assembly. Thus, Chapter 5 explores the potential of functionalized diblock copolymers being used for hierarchical, interparticle crosslinking. Collaborative work on *in-situ* imaging of solution assemblies are presented in Chapter 6. Finally, Chapter 7 summarizes the main results of this dissertation and recommends future research targeting novel, well-defined and multifunctional nanostructures.

REFERENCES

1. J. H. Lorent, J. Quetin-Leclercq and M. P. Mingeot-Leclercq, *Org. Biomol. Chem.*, 2014, **12**, 8803-8822.
2. D. Deamer, J. P. Dworkin, S. A. Sandford, M. P. Bernstein and L. J. Allamandola, *Astrobiology*, 2002, **2**, 371-386.
3. R. Nagarajan and E. Ruckenstein, *J. Colloid Interface Sci.*, 1979, **71**, 580-604.
4. D. Myers, *Surfactant Science and Technology* A JOHN WILEY & SONS, INC., 2006.
5. L. Romsted, *Surfactant Science and Technology : Retrospects and Prospects*, CRC Press, 2014.
6. A. Walther, M. Drechsler, S. Rosenfeldt, L. Harnau, M. Ballauff, V. Abetz and A. H. E. Muller, *J. Am. Chem. Soc.*, 2009, **131**, 4720-4728.
7. S. Zhong, H. Cui, Z. Chen, K. L. Wooley and D. J. Pochan, *Soft Matter*, 2008, **4**, 90.
8. A. S. Mikhail and C. Allen, *J. Controlled Release*, 2009, **138**, 214-223.
9. K. Letchford and H. Burt, *Eur. J. Pharm. Biopharm.*, 2007, **65**, 259-269.
10. D. E. Discher and A. Eisenberg, *Science*, 2002, **297**, 967-973.
11. A. V. Kabanova, E. V. Batrakovaa and V. Y. Alakhov, *J. Controlled Release*, 2002, **82**, 189-212.
12. E. V. Batrakova and A. V. Kabanov, *J. Controlled Release*, 2008, **130**, 98-106.
13. C. Tanford, *Science*, 1978, **200**, 1012-1018.
14. B. L. P. Alexandridis, *Amphiphilic Block Copolymers: Self-Assembly and Applications*, Elsevier, 2000.
15. R. Nagarajan, *Langmuir*, 2002, **18**, 31-38.

16. S. Hyde, Z. Blum, T. Landh, S. Lidin, B. W. Ninham, S. Andersson and K. Larsson, *The Language of Shape: The Role of Curvature in Condensed Matter: Physics, Chemistry and Biology* Elsevier, 1996.
17. S. Jain and F. S. Bates, *Science*, 2003, **300**, 460-464.
18. L. Zhang and A. Eisenberg, *Science*, 1995, **268**, 1728-1731.
19. C. Liu, M. A. Hillmyer and T. P. Lodge, *Langmuir*, 2009, **25**, 13718-13725.
20. X. Jiang and B. Zhao, *Macromolecules*, 2008, **41**, 9366-9375.
21. K. T. Kim, J. Zhu, S. A. Meeuwissen, J. J. L. M. Cornelissen, D. J. Pochan, R. J. M. Nolte and J. C. M. v. Hest, *J. Am. Chem. Soc.*, 2010, **132** 12522-12524.
22. S. A. Meeuwissen, K. T. Kim, Y. Chen, D. J. Pochan and J. C. M. v. Hest, *Angew. Chem. Int. Ed.*, 2011, **50**, 7070-7073.
23. A. H. Groschel, A. Walther, T. I. Lobling, F. H. Schacher, H. Schmalz and A. H. Müller, *Nature*, 2013, **503**, 247-251.
24. C. Zhang, V. J. Pansare, R. K. Prud'homme and R. D. Priestley, *Soft Matter*, 2012, **8**, 86.
25. P. A. Rupar, L. Chabanne, M. A. Winnik and I. Manners, *Science*, 2012, **337**, 559-562.
26. R. P. Brinkhuis, F. P. J. T. Rutjes and J. C. M. van Hest, *Polymer Chemistry*, 2011, **2**, 1449.
27. R. A.L.Jones, *Soft Condensed Matter*, 2002.
28. V. Castelletto, P. Parras and I. W. Hamley, *Langmuir*, 2007, **23**, 6896-6902.
29. T. Smart, H. Lomas, M. Massignani, M. V. Flores-Merino, L. R. Perez and G. Battaglia, *Nano Today*, 2008, **3**, 38-46.
30. J. Zhu, S. Zhang, F. Zhang, K. L. Wooley and D. J. Pochan, *Advanced Functional Materials*, 2013, **23**, 1767-1773.
31. D. J. Pochan, Z. Chen, H. Cui, K. Hales, K. Qi and K. L. Wooley, *Science*, 2004, **306**, 94-97.
32. L. Zhang and A. Eisenberg, *Science*, 1995, **268**, 1728-1731.

33. A. O. Moughton, M. A. Hillmyer and T. P. Lodge, *Macromolecules*, 2012, **45**, 2-19.
34. H. Cui, Z. Chen, K. L. Wooley and D. J. Pochan, *Macromolecules*, 2006, **39**, 6599-6607.
35. H. Cui, Z. Chen, K. L. Wooley and D. J. Pochan, *Soft Matter*, 2009, **5**, 1269-1278.
36. Z. Wang and W. Jiang, *Soft Matter*, 2010, **6**, 3743.
37. H. Yu and W. Jiang, *Macromolecules*, 2009, **42**, 3399-3404.
38. K. Hales, Z. Chen, K. L. Wooley and D. J. Pochan, *Nano Letter*, 2008, **8**, 2023-2026.
39. H. Cui, Z. Chen, K. L. Wooley and D. J. Pochan, *Macromolecules* 2006, **39**, 6599-6607.
40. H. Cui, Z. Chen, S. Zhong, K. L. Wooley and D. J. Pochan, *Science*, 2007, **317**, 647-650.
41. K. Zhang, H. Miao and D. Chen, *J. Am. Chem. Soc.*, 2014, **136**, 15933-15941.
42. K. Zhang, M. Jiang and D. Chen, *Angew. Chem. Int. Ed.*, 2012, **51**, 8744-8747.
43. E. Lee, B. Hammer, J.-K. Kim, Z. Page, T. S. Emrick and R. C. Hayward, *J. Am. Chem. Soc.*, 2011.
44. J. Dupont, G. Liu, K. Niihara, R. Kimoto and H. Jinnai, *Angew. Chem. Int. Ed.*, 2009, **48**, 6144-6147.
45. H. Dou, G. Liu, J. Dupont and L. Hong, *Soft Matter*, 2010, **6**, 4214.
46. A. Blanazs, J. Madsen, G. Battaglia, A. J. Ryan and S. P. Armes, *J. Am. Chem. Soc.*, 2011, **133**, 16581-16587.
47. C. Fernyhough, A. J. Ryana and G. Battaglia, *Soft Matter*, 2009, **5**, 1674-1682.
48. B. Ni, M. Huang, Z. Chen, Y. Chen, C.-H. Hsu, Y. Li, D. Pochan, W.-B. Zhang, S. Z. D. Cheng and X.-H. Dong, *J. Am. Chem. Soc.*, 2015, **137**, 1392-1395.
49. F. S. B. John A. Zupancich, and Marc A. Hillmyer, *Biomacromolecules*, 2009, **10**, 1554-1563.

50. V. Percec, P. Leowanawat, H. J. Sun, O. Kulikov, C. D. Nusbaum, T. M. Tran, A. Bertin, D. A. Wilson, M. Peterca, S. Zhang, N. P. Kamat, K. Vargo, D. Moock, E. D. Johnston, D. A. Hammer, D. J. Pochan, Y. Chen, Y. M. Chabre, T. C. Shiao, M. Bergeron-Brelek, S. Andre, R. Roy, H. J. Gabius and P. A. Heiney, *J. Am. Chem. Soc.*, 2013, **135**, 9055-9077.
51. Z. M. Hudson, C. E. Boott, M. E. Robinson, P. A. Rugar, M. A. Winnik and I. Manners, *Nat. Chem.*, 2014, **6**, 893-898.
52. G. Rizis, T. G. M. v. d. Ven and A. Eisenberg, *Angew. Chem. Int. Ed.*, 2014, **53**, 1-5.
53. N. A. Lynd, A. J. Meuler and M. A. Hillmyer, *Progress in Polymer Science*, 2008, **33**, 875-893.
54. M. A. Hillmyer, *Journal of Polymer Science Part B: Polymer Physics*, 2007, **45**, 3249-3251.
55. A. J. Meuler, C. J. Ellison, J. Qin, C. M. Evans, M. A. Hillmyer and F. S. Bates, *J. Chem. Phys*, 2009, **130**, 234903.
56. A. L. Schmitt, M. H. Repollet-Pedrosa and M. K. Mahanthappa, *ACS Macro Letters*, 2012, **1**, 300-304.
57. W. Kong, B. Li, Q. Jin, D. Ding and A.-C. Shi, *J. Am. Chem. Soc.*, 2009, **131**.
58. B. Yu, P. Sun, T. Chen, Q. Jin, D. Ding, B. Li and A.-C. Shi, *Physical Review Letters*, 2006, **96**.
59. R. Wang, Z. Jiang, Y.-L. Chen and G. Xue, *Journal of Physical Chemistry B*, 2006, **110**, 22726-22731.
60. X. Li, P. Tang, F. Qiu, H. Zhang and Y. Yang, *Journal of Physical Chemistry B*, 2006, **110**, 2024-2030.
61. J. W. Ma, P. T. Xuan Li and Y. Yang, *J. Phys. Chem. B*, 2007, **111**, 1552-1558.
62. W. Kong, B. Li, Q. Jin, D. Ding and A.-C. Shi, *Langmuir*, 2010, **26**, 4226-4232.
63. L. Zhang, J. Lin and S. Lin, *J. Phys. Chem. B*, 2007, **111**, 9209-9217.

64. X. Li, I. V. Pivkin, H. Liang and G. E. Karniadakis, *Macromolecules*, 2009, **42**, 3195-3200.
65. J.-F. Lutz and A. Laschewsky, *Macromolecular Chemistry and Physics*, 2005, **206**, 813-817.
66. S. Kubowicz, J. F. Baussard, J. F. Lutz, A. F. Thunemann, H. von Berlepsch and A. Laschewsky, *Angew. Chem. Int. Ed.*, 2005, **44**, 5262-5265.
67. Z. Li, E. Kesselman, Y. Talmon, M. A. Hillmyer and T. P. Lodge, *Science*, 2004, **306**, 98-101.
68. Z. Li, M. A. Hillmyer and T. P. Lodge, *Macromolecules*, 2006, **39**, 765-771.
69. Z. Li, M. A. Hillmyer and T. P. Lodge, *Langmuir*, 2006, **22**, 9409-9417.
70. R. Erhardt, A. Böker, H. Zettl, H. Kaya, W. Pyckhout-Hintzen, G. Krausch, V. Abetz and A. H. E. Müller, *Macromolecules*, 2001, **34**, 1069-1075.
71. R. Erhardt, M. Zhang, A. Boker, H. Zettl, C. Abetz, P. Frederik, G. Krausch, V. Abetz and A. H. E. Müller, *J. Am. Chem. Soc.*, 2003, **125**, 3260-3267.
72. A. Walther, X. Andre, M. Drechsler, V. Abetz and A. H. E. Müller, *J. Am. Chem. Soc.*, 2007, **129**, 6187-6198.
73. F. Schacher, A. Walther, M. Ruppel, M. Drechsler and A. H. E. Müller, *Macromolecules*, 2009, **42**, 3540-3548.
74. F. Schacher, A. Walther and A. H. E. Müller, *Langmuir*, 2009, **25**, 10962-10969.
75. B. Fang, A. Walther, A. Wolf, Y. Xu, J. Yuan and A. H. Müller, *Angew. Chem. Int. Ed.*, 2009, **48**, 2877-2880.
76. J. Zhu and R. C. Hayward, *Macromolecules*, 2008, **41**, 7794-7797.
77. E. B. Felix Schacher, Andreas Walther, Holger Schmalz, Dmitry V. Pergushov, and A. H. E. Müller, *ACS Nano*, 2009, **3**, 2095-2102.
78. L. Cademartiri and K. J. Bishop, *Nature Mater.*, 2014, **14**, 2-9.
79. H. Qiu, Z. M. Hudson, M. A. Winnik and I. Manners, *Science*, 2015, **347**, 1329-1332.

80. Z. Chen, H. Cui, K. Hales, Z. Li, Kai Qi, D. J. Pochan and K. L. Wooley, *J. Am. Chem. Soc.*, 2005, **127**, 8592-8593.
81. Z. Li, Z. Chen, H. Cui, K. Hales, K. L. Wooley and D. J. Pochan, *Langmuir*, 2007, **23**, 4689-4694.
82. S. Zhong, H. Cui, Z. Chen, K. L. Wooley and D. J. Pochan, *Soft Matter*, 2008, **4**, 90-93.
83. D. J. Pochan, J. Zhu, K. Zhang, K. L. Wooley, C. Miesch and T. Emrick, *Soft Matter*, 2011, **7**, 2500-2506.
84. E. G. Kelley, T. P. Smart, A. J. Jackson, M. O. Sullivan and T. H. Epps, III, *Soft Matter*, 2011, **7**.
85. E. G. Kelley, R. P. Murphy, J. E. Seppala, T. P. Smart, S. D. Hann, M. O. Sullivan and T. H. Epps, *Nat. Commun.*, 2014, **5**, 3599.
86. R. P. Murphy, E. G. Kelley, S. A. Rogers, M. O. Sullivan and T. H. Epps, 3rd, *ACS Macro Lett*, 2014, **3**, 1106-1111.
87. M. E. Davis, Z. G. Chen and D. M. Shin, *Nat. Rev. Drug Discov.*, 2008, **7**, 771-782.
88. J. D. Heidel and M. E. Davis, *Pharmaceut. Res.*, 2011, **28**, 187-199.
89. J. A. Champion and S. Mitragotri, *Proc. Natl. Acad. Sci.*, 2006, **103**, 4930-4934.
90. J. Fang, H. Nakamura and H. Maeda, *Adv. Drug Delivery Rev.*, 2011, **63**, 136-151.
91. I. Canton and G. Battaglia, *Chem. Soc. Rev.*, 2012, **41**, 2718-2739.
92. E. G. Kelley, J. N. Albert, M. O. Sullivan and T. H. Epps, III, *Chem. Soc. Rev.*, 2013, **42**, 7057-7071.
93. Y. Geng, P. Dalhaimer, S. Cai, R. Tsai, M. Tewari, T. Minko and D. E. Discher, *Nat. Nanotechnol.*, 2007, **2**, 249-255.
94. L. Y. Qiu and Y. H. Bae, *Pharmaceut. Res.*, 2006, **23**, 1-30.
95. H. Cui, M. J. Webber and S. I. Stupp, *Biopolymers*, 2010, **94**, 1-18.

96. O. Onaca, R. Enea, D. W. Hughes and W. Meier, *Macromol. Biosci.*, 2009, **9**, 129-139.
97. D. M. Christine Allen, Adi Eisenberg, *Colloids and Surfaces B: Biointerfaces*, 1999, **16**, 3-27.
98. D. E. D. a. A. Eisenberg, *Science*, 2002, **297**, 967-973.
99. S. Ganta, H. Devalapally, A. Shahiwala and M. Amiji, *J. Controlled Release*, 2008, **126**, 187-204.
100. C. V. Synatschke, T. Nomoto, H. Cabral, M. Fortsch, K. Toh, Y. Matsumoto, K. Miyazaki, A. Hanisch, F. H. Schacher, A. Kishimura, N. Nishiyama, A. H. E. Müller and K. Kataoko, *ACS Nano*, 2014, **8**, 1161–1172.
101. G. Oehme, I. Grassert, E. Paetzold, H. Fuhrmann, U. S. T. Dwars and I. Iovel, *Kinetics and Catalysis*, 2003, **44**, 766-777.
102. M. J. Boerakker, J. M. Hannink, P. H. H. Bomans, P. M. Frederik, R. J. M. Nolte, E. M. Meijer and N. A. J. M. Sommerdijk, *Angew. Chem. Int. Ed.*, 2002, **41**, 4122-4239.
103. F. M. Menger, I. J. U. Rhee and H. K. Rhee, *J. Org. Chem.*, 1975, **40**, 3803-3805.
104. I. Grassert, E. Paebold and G. Oehme, *Tetrahedron* 1993, **49**, 6605-6612.
105. S. Forster and M. Konrad, *J. Mater. Chem.*, 2003, **13**, 2671.
106. I. Whamley, *Nanotechnology*, 2003, **14**, R39–R54.
107. P. Broz, S. Driamov, J. Ziegler, N. Ben-Haim, S. Marsch, W. Meier and P. Hunziker, *Nano Lett.*, 2006, **6**, 2349-2353.
108. F. Axthelm, O. Casse, W. H. Koppenol, T. Nauser, W. Meier and C. G. Palivan, *J. Phys. Chem. B*, 2008, **112**, 8211-8217.
109. P. G. van Rhee, R. S. Rikken, L. K. Abdelmohsen, J. C. Maan, R. J. Nolte, J. C. van Hest, P. C. Christianen and D. A. Wilson, *Nat. Commun.*, 2014, **5**, 5010.
110. D. A. Wilson, R. J. M. Nolte and J. C. M. v. Hest, *Nat. Chem.*, 2012, **4**, 268-274

Chapter 2

REVIEW OF CHARACTERIZATION METHODS FOR SOLUTION ASSEMBLIES

2.1 Introduction

The demand for more complex nanostructures in materials and soft matter nanoscience requires even more sophisticated characterization tools for reliable visualization and understanding of nanostructure. In this chapter, a brief overview of the imaging and scattering techniques used to characterize assembled nanostructures, especially nanostructures in solution, is presented.

2.2 Transmission Electron Microscopy Characterization Method

Electron microscopy (EM)¹ is a powerful tool to study structure-property relationships of materials over a large size range. The most commonly used EM methods include transmission electron microscopy (TEM)² and scanning electron microscopy (SEM)^{3, 4}. In a TEM, an electron beam is spread to uniformly illuminate a thin film of materials at a perpendicular angle. The image is collected from the transmitted beam, and the contrast comes from the interaction of electrons with the local variations in sample film thickness, density, mass and any crystalline phase orientations. TEM is widely used in material science. Specifically, TEM is an irreplaceable tool that provides incomparable insights into block copolymer assemblies' morphologies in the nanosize range. Cryogenic TEM is an *in-situ* TEM technique that can image assemblies in solvent suspension, providing invaluable information of the nanostructures that cannot be resolved by other methods.

2.2.1 Overview of TEM

TEM is one of the best techniques for nanostructure observation and image collection. In a TEM instrument, a monochromatic electron beam is focused on a thin layer of sample distributed on a substrate. High vacuum is used in the whole pathway of the beam to avoid scattering of the beam by air, dust and other contaminations. The electron beam goes through a series of lenses and apertures. The lenses control the focus and magnification. The apertures control the brightness, meaning the electron dose spread on the samples and collected by detector cameras. As the beam passes through the sample, electrons are scattered by the atoms in the sample. Charge-coupled device (CCD) cameras are currently the mostly widely used camera to collect the scattered, transmitted beam to get images. Imaging contrast can be separated into three categories: mass-thickness (amplitude) contrast; phase contrast and Bragg contrast. In mass-thickness contrast, more electrons are scattered by heavier atoms (with a larger atomic number) or by thicker regions of a sample film, resulting in darker image regions. Phase contrast is caused by introducing a path difference between the scattered and unscattered waves before allowing them to interfere, which is enhanced by imaging a sample at slight underfocus.

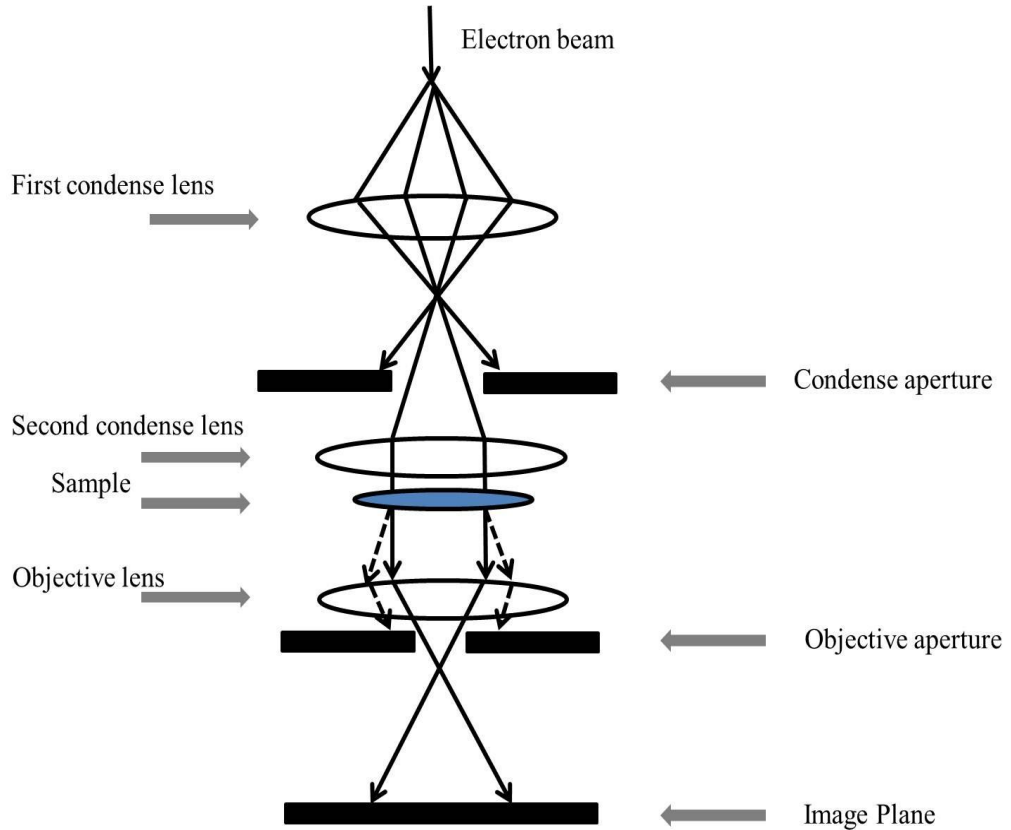


Figure 2.1 Schematic of important components in traditional TEM and the electron beam pathways.

In cryo-TEM imaging, underfocus is used to increase the phase contrast without distorting the image. Based on the different contrast forming mechanism, TEM is widely used in material characterization^{5, 6}.

2.2.2 Sample Preparation and Selective Staining

The high vacuum condition in TEM requires specific sample preparation. Liquid samples cannot be directly adapted to the traditional TEM. Instead, *in-situ* TEMs and *in-situ* TEM holders have been developed in recent years and are used more and more broadly in industrial and academic fields. Regardless of the type of instruments used,

well-prepared samples are essential for obtaining high-quality, reliable and reproducible results. For polymer-based solution assemblies, the sample can be dried out on top of a TEM grid or other substrate to form a cast-film. Selective staining is commonly used afterward to increase the mass-thickness contrast. However, the cast film method brings along unavoidable structure change during the drying process with even more artifacts introduced sometimes by staining. Cryo-TEM provides for *in-situ* structure imaging of solution-state samples through fast vitrification of liquid samples into a thin, glassy layer. The details of the cryo-TEM technique and recent developments will be discussed in the next section. Other *in-situ* TEM techniques such as dynamic TEM are becoming more and more popular to visualize the samples in the liquid state with the ability to track the dynamic motion of the samples⁷. Currently, metal nanoparticles need to be covalently linked to samples to increase the contrast of the solution assemblies in a liquid cell⁸. Recently, the electron transparent substrate graphene oxide has been used for enhancing contrast without using the heavy staining⁸⁻¹⁰.

Cryo-TEM provides a powerful tool to visualize solution assemblies in the *in-situ* state, which is intensively used in structural biology¹¹ and material science^{12, 13}. In cryo-TEM, the sample preparation process is somewhat tedious and highly dedicated. Cryo-TEM maintains the solution structure by fast vitrification of the sample to produce a thin-film glass (normally 0-300 nm thick)¹⁴. The brief sample preparation process is: A small amount of suspension (1-3 μL) is applied onto a lacey carbon grid. At UD, the FEI Vitrobot instrument is used for sample preparation. Excessive solution is removed by blotting the grid with filter paper. The blotting times and period can be tuned. The grid is then quickly plunged into a liquid ethane holder with an approximate cooling rate of 10^5 K/S ¹⁴ resulting in a vitrified liquid sample. The grid is then transferred into a liquid nitrogen dewar for preservation until transfer to the holder. After the cryo-TEM holder is cooled down to $-176 \text{ }^\circ\text{C}$, the sample is then transferred into the cryo-holder for imaging. Low electron dose with longer exposure time usually is used to acquire better images with good contrast. There are certain

considerations and tips in preparing successful cryo-TEM grids, which generally requires patience and practice. For example, during the sample preparation, the grid is better to be kept in the liquid nitrogen after it is vitrified. The less time the grid is exposed to the air, the less chance of ice to form on the grid from the atmosphere and the more possibility of getting a well-prepared grid. Cryo-TEM enhances the ability to directly image nanoparticles in the solution state and also eliminate external staining artifacts. However, there are also certain artifacts that can be introduced, such as ice formation due to solvent crystallization from poor heat transfer, that one must watch out for ¹⁴. Cryo-TEM is used intensively and irreplaceably in this dissertation and will be discussed in more detail in next section.

Selective staining is widely used in transmission electron microscopy sample preparation. One can roughly separate staining methods into two kinds: positive staining and negative staining. The positive stains are basically high-atomic number element-containing compounds that bind either chemically or physically to materials providing for more electrons scattering from the regions that have been stained. Negative stains are usually acidic dyes that provide for a high atomic number element-rich background in order to provide contrast through a darker background relative to desired structures for imaging. In the Table 2.1, common staining methods and their respective mechanisms are listed that are commonly used in nanoparticle imaging¹⁵.

Table 2.1 Common staining agents and their functions

Staining Agent	Functions
RuO ₄	Positive stain; stains aromatic rings.
OsO ₄ (osmium tetroxide)	Positive stain; stains double bond, OsO ₄ react with double bond to form 16 electron complex.
UA (uranyl acetate)	Negative stain; stains background.
PTA (Phosphotungstic acid)	Negative stain; Adsorption onto tissue or the surface of viruses and its electron density are the bases of PTA action as a negative stain.

To clearly illustrate the different staining effects of different staining agents, a series of staining experiments of the same complicated nanoparticles are presented here. The triblock copolymer poly(acrylic acid)-*b*-polyisoprene-*b*-polystyrene (PAA-*b*-PI-*b*-PS) was synthesized in the Jimmy Mays research group¹⁶ using anionic polymerization method. Initially, the triblock copolymer was designed to have the immiscible hydrophobic blocks in one triblock copolymer, with the hypothesis of having PI and PS nanophase-separated when assembled in selective solvent. Kinetic control self-assembly (described in more detail in upcoming chapters) was used to construct micelles in high water solution conditions (the remainder of the solvent being THF). The experimental process of the self-assembly is: triblock copolymer PAA₃₃₅-*b*-PI₃₃₅-*b*-PS₈₄ was dissolved in THF, and the solution was stirred for 24 hours, with the polymer weight concentration at 2 mg/mL. Then, EDDA (2, 2'-ethylenedioxy bis(ethylamine)) and extra THF were added to the THF solution to reach a polymer concentration of 0.1% at a desired ratio of amine to acid functionality. Water was then added in a slow rate (1 mL/h water to 1 mL THF solution) to initiate the self-assembly process. A cloudy solution with self-assembled aggregates was obtained. Samples were aged for one day before imaging. Different amine: acid ratios were applied to

investigate the effects of the diamine molecule on the assembled nanostructures and possible new nanostructures.

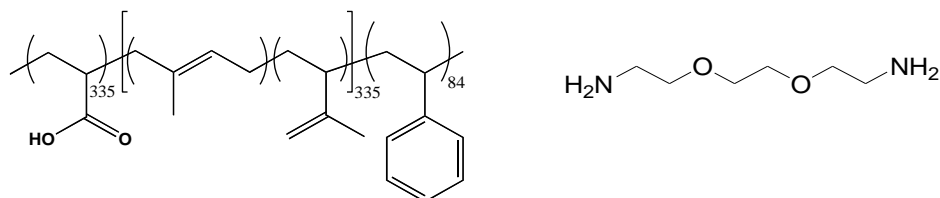


Figure 2.2 Chemical structures of triblock copolymer PAA₃₃₅-PI₃₃₅-PS₈₄ (with **1, 4** addition around 40-50%, **1, 2**-addition around 50%-60%); chemical structures of EDDA molecule.

Cryogenic TEM was used to observe the nanostructures and the expected nanophase separated domains inside the core. At different amine to acid ratios, giant spherical aggregates with large diameter (200-400 nm) were assembled, as shown in Figure 2.3. A shell with lighter contrast outside of a spherical core is observed in most images (A, B, C, D). The shell is attributed to the complexation of PAA and amine. The spherical core is attributed to the collapsed PS and PI phases. It is observed that the halo outside of the dark core become less obvious when the amine amount increased to a higher ratio (5:1). The stronger, more complete complexation between the amines and acid side chains is the cause of this halo collapse. The size of the halo, core and entire particles are listed in Table 2.2. To observe the nanophase separations of PS and PI in the particle core domains, different selective staining was then used.

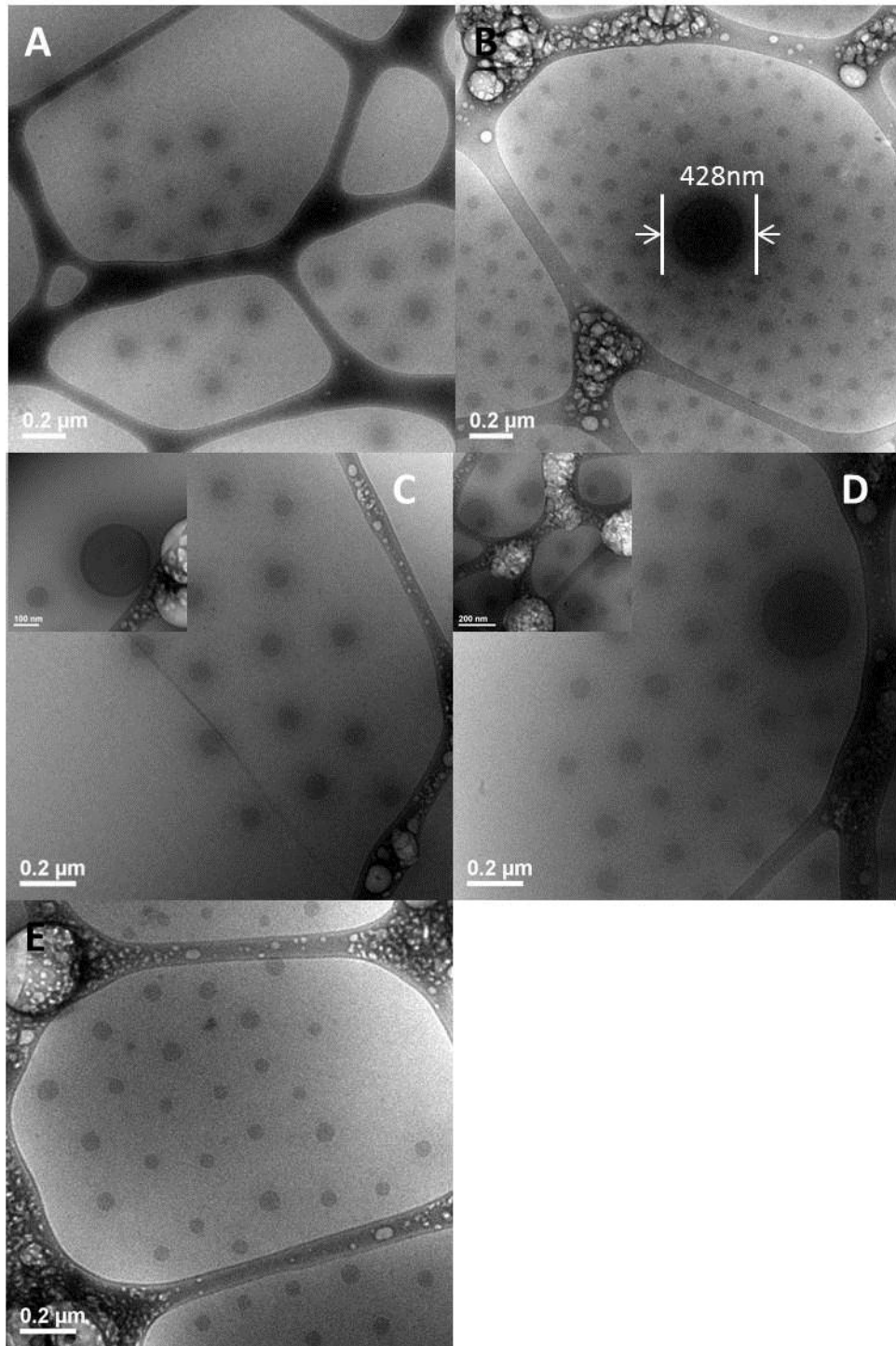


Figure 2.3 Cryo-TEM images of the giant spherical aggregates assembled from PAA₃₃₅-PI₃₃₅-PS₈₄ at different amine to acid ratios, 80% H₂O/20% THF. A, 0.3:1; B, 0.5:1; C, 1:1; D, 2:1; E, 5:1.

Table 2.2 The sizes of observed core, corona and overall of giant aggregates (unit: nm)

Amine: acid ratio	Size	core	Halo corona
0.3:1	160	100	60
0.5:1	150	98.3±11.8	58
1:1	134±6.8	76±6.8	57.5
2:1	137±11	79±11	58
5:1	80	69±9.5	Less obvious

OsO₄, RuO₄ and uranyl acetate (UA) were used to stain the cast-film TEM grids after the solution sample was dried out on the grids. For negative staining, a small amount of UA (0.1 μL) was applied on top of the dried out grid for the staining. For positive OsO₄ and RuO₄ staining, a small amount of aqueous solution (4% OsO₄ or RuO₄ aqueous solution, purchased from EMS) was put in the bottom of a vial, and TEM grids containing dried sample films were exposed to the OsO₄ or RuO₄ vapor by being placed in the vial above the staining solution. This method is called vapor staining. For OsO₄ vapor staining, 6 to 24 hours is required for staining of the dried TEM grids. For RuO₄ staining, only 10-20 minutes of vapor staining is required. After removing the samples and allowing the grids to completely dry, imaging was performed. As shown in Figure 2.4 A, multilayer structures are observed after OsO₄ staining, in which the dark layers are attributed to PI phases. From image B, the entire core appears dark due to both PI and PS being stained simultaneously with RuO₄. UA staining provides a dark ring outside the nanostructured highlighting the edge which is altered from cryo-TEM with the differences attributed to the drying during cast-film preparation.

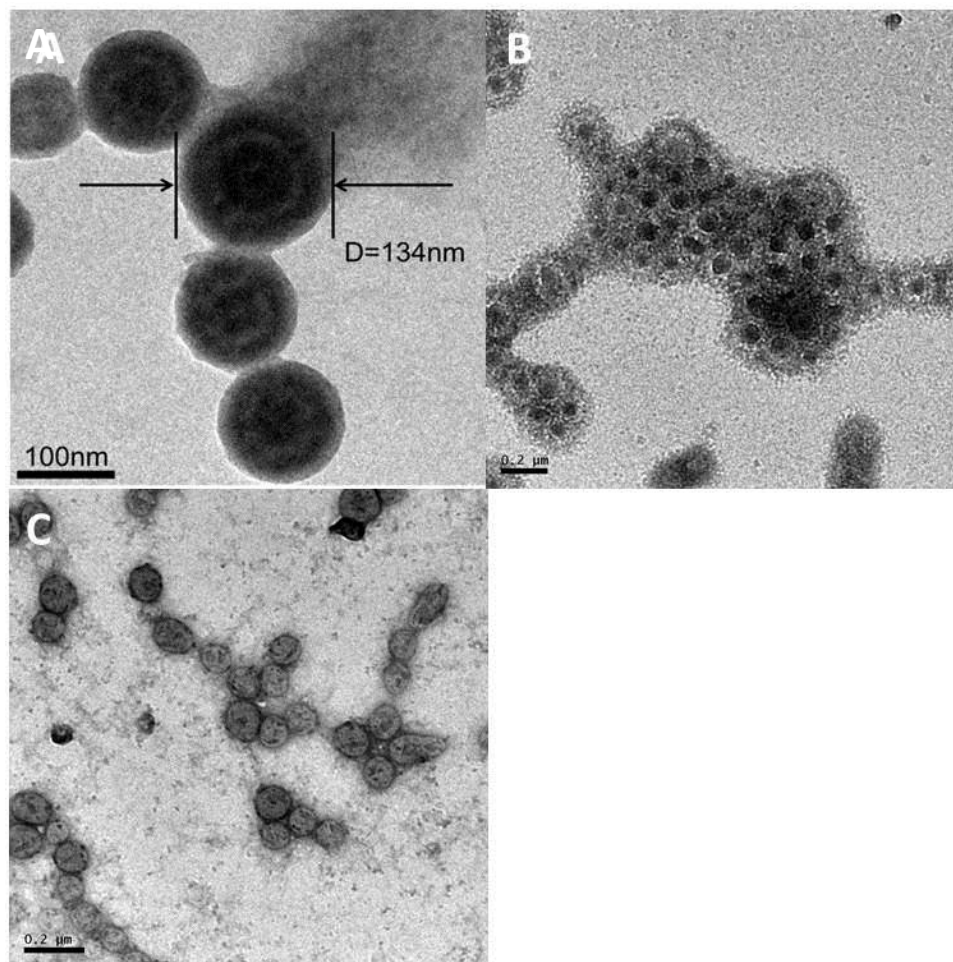


Figure 2.4 Cast film TEM images of different staining methods applied to the giant aggregates, at amine to acid 0.3:1. **A:** OsO₄ stain. After cast-film TEM, the grid is staining exposed to OsO₄ for 6-8 hours; **B:** RuO₄ stain. After the sample was dried out on the TEM grid, RuO₄ was used to vapor stain the grid for 10-20 minutes. **C:** UA stain. After the solution sample was dried out on top of the grid, a small amount of UA was applied on top of the grid.

To observe the *in-situ* state of the local nanophase separation, cryo-TEM with selective staining was used. The solution samples were put into a chamber having a small amount of OsO₄ or RuO₄ in the bottom (0.5~1 μL). The direct solution staining

lasted for 10-20 minutes for OsO₄ staining and around 5 minutes for RuO₄ staining. Cryo-TEM images were generated right after staining. Cryo-TEM images before and after staining are shown in Figure 2.5. Similar multilayer internal structures are observed via OsO₄ staining in cryo-TEM as was observed in normal TEM (Figure 2.4A). A heavy metal staining agent, ruthiniumhexamine (structure shown in Figure 2.5D, purchased from EMS), was added to the assembled particle solution with initial amine to acid at 0.5:1 to reach the saturated amine to acid ratio at 1:1. Here, ruthiniumhexamine is used as positive stain for the hydrophilic domain. In the images stained by ruthiniumhexamine, the dark rings outside the spheres result from the complexation of ruthiniumhexamine with the acrylic acid functionality.

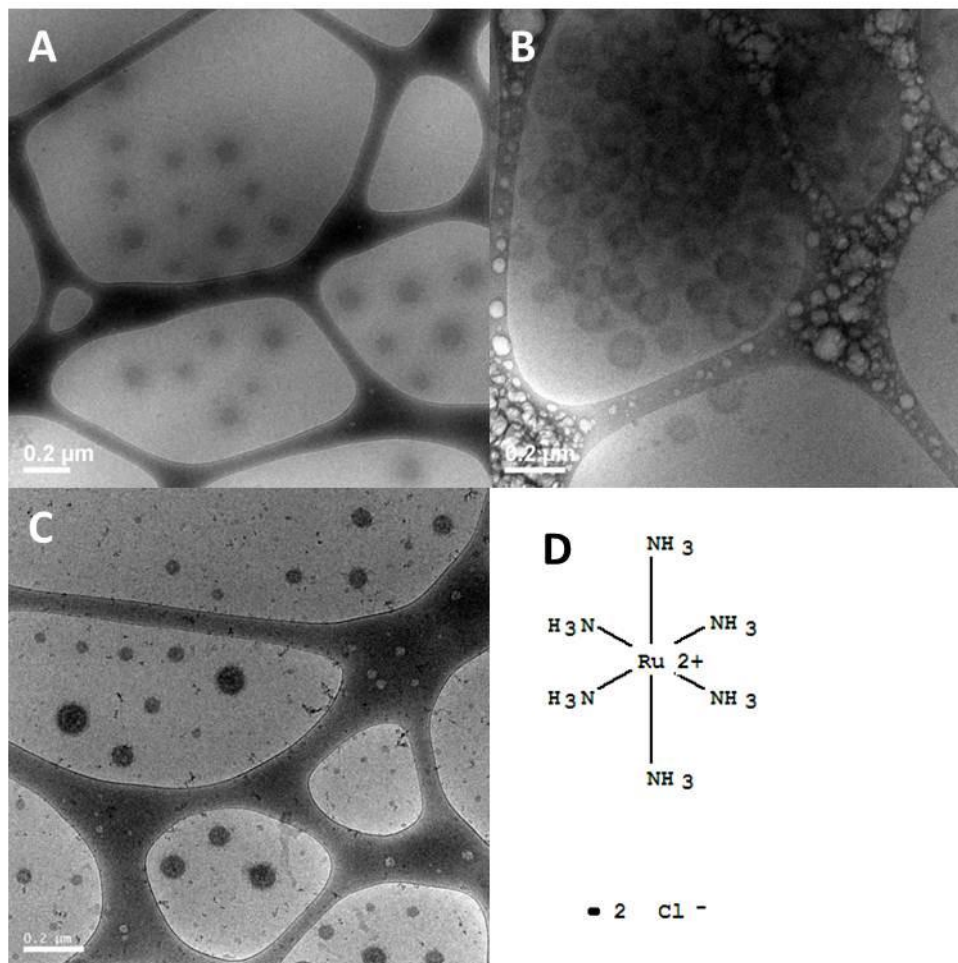


Figure 2.5 Cryo-TEM images of spherical aggregates assembled from triblock copolymer PAA₃₃₅-PI₃₃₅-PS₈₄, with amine:acid=0.5:1, 80% H₂O/20% THF. **A:** Cryo-TEM images of giant spherical aggregates. **B:** Cryo-TEM image of giant aggregates with addition of rutheniumhexamine (Ru (NH₃)₆Cl₂), the rutheniumhexamine was added to reach amine:acid=1:1 for the total amine amount from EDDA and rutheniumhexamine. **C:** Cryo-TEM image of giant aggregates with OsO₄ staining, double layers were observed similar as the image in Figure 2.4A. **D:** Chemical structure of rutheniumhexamine complexed with HCl.

2.2.3 Image Analysis

Becoming more popular is the quantitative analysis of TEM images. By using software for analysis of assembled nanostructure, one can perform statistical analyses of the size and shapes of nanoparticles as well as more careful greyscale analysis of local compartments inside the nanoparticles. The size and shape can be directly obtained from the TEM and cryo-TEM images. The gray scale of TEM micrographs can be evaluated to yield the electron density of the sample^{17, 18}. Thus amplitude contrast and phase contrast can be quantified, in addition to the information obtained from other methods that are sensitive to local electron density. Software, like Image J or GIMP is used to assign gray-scale value. The diameter of the classic shapes from assemblies including spheres and cylinders can be easily obtained from the grey scale value, as well as the wall thickness of vesicles. For the other uncommon shapes, people have developed several methods to quantify particle shapes and sizes. For example, distance measurement-based methods have been developed to quantify clay particles with the shape of curved lines in the nanocomposites^{19, 20}. The lengths of the curved lines can then be obtained and the length distribution can also be quantified by probability model fitting²¹. Statistical analysis of particle size and size distribution can be achieved using MATLAB and Image J²¹ as well as more sophisticated, algorithmic analysis²².

2.2.4 Cryogenic Transmission Electron Microscopy

For many years, TEM has been one of the most powerful techniques for the study of nanostructured materials. In recent decades, cryogenic TEM has greatly enlarged the scope of the TEM technique and has, thus, become an irreplaceable tool for detecting the *in-situ* nanostructures of biological samples^{11, 23, 24}, solution polymeric assemblies^{13, 25-28}, inorganic biomimetic nanomaterials^{12, 29} and others. There are growing numbers of morphological studies using cryo-TEM^{13, 28, 30}, with publications related to cryo-TEM increasing remarkably in the past 10 years. Recent statistics with the key word of “cryo-TEM” topic from the Web of Science are listed in the following

table indicating that cryo-TEM plays more and more important roles in morphological study.

Table 2.3 Statistics of the papers related to the cryo-TEM topic (total: 1316)

Publication years	Record count	% of 1316
2014	142	10.8%
2013	130	9.9%
2012	130	9.8%
2011	121	9.2%
2010	120	7.5%
2009	98	6.7%
2008	89	5.8%
2007	76	5.7%
2006	69	5.2%
2005	49	3.7%

The elucidation of structural information of nanoscale materials in their in situ state is one challenging topic. Cryo-TEM can be complementary method to other characterization methods, such as small-angle scattering, to provide comprehensive information of the nanostructures. It can be used to investigate nanostructures in biology³¹, colloidal science^{17, 32}, polymeric solution assemblies³³⁻³⁸, giant amphiphiles^{39, 40}, polypeptide solution assemblies^{28, 41} and inorganic nanomaterials^{18, 42-44}.

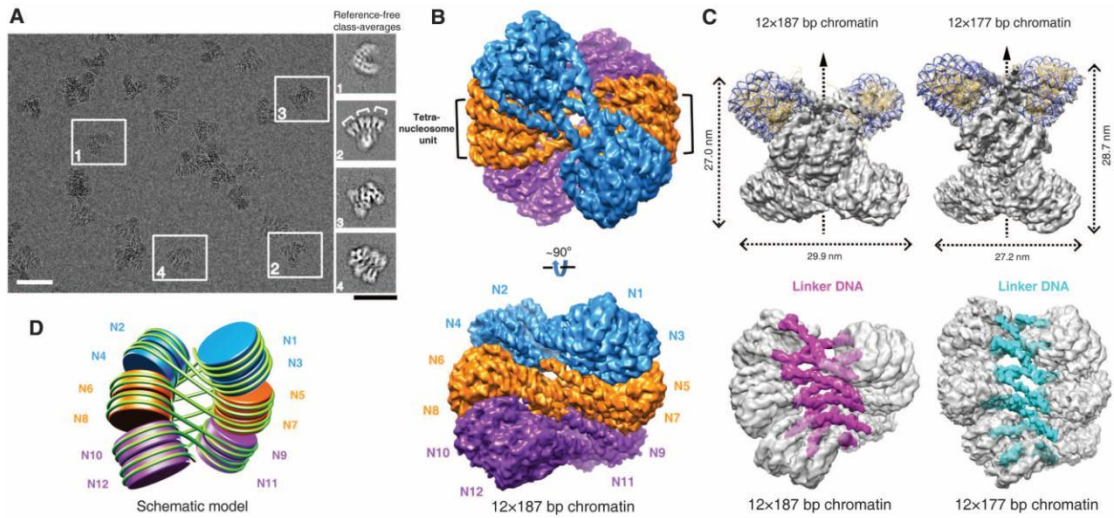


Figure 2.6 Cryo-EM reconstruction of 30-nm chromatin fibers assembled from DNA molecule. Figure adapted from reference³¹, with the copyright permission from AAAS.

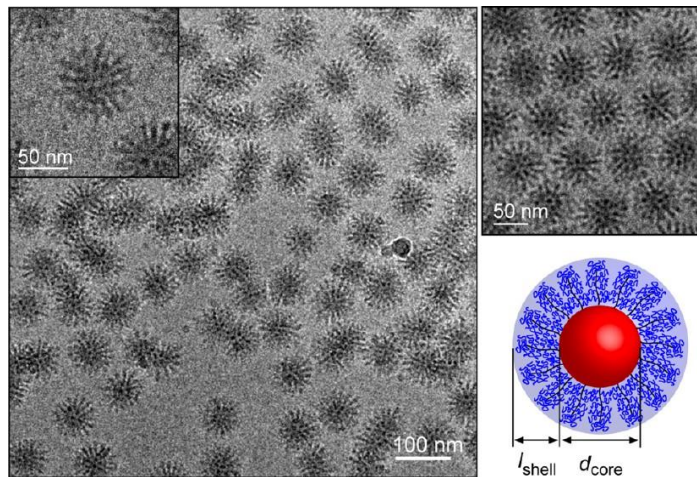


Figure 2.7 Cryo-TEM analysis of spherical micelles formed from brush polymer LO-2. Figure adapted from reference³⁴ with the permission approved from 2014 American Chemical Society.

Artifacts of images in cryo-TEM

Although cryo-TEM has a number of advantages over other characterization methods for investigating nanoscale features, there are a few concerns and limitations to consider. For instance, beam damage occurs rapidly during sample imaging. Since most solution assemblies are sensitive to electron radiation, low-electron dose methods should always be applied in cryo-TEM along with longer exposure time for imaging⁴⁵. However, longer exposure time means higher possibility to have beam or sample shift and lower resolution, out of focus images. Furthermore, low dose means worse signal-to-noise ratio. To help mitigate these problems, researchers have introduced new technology such as more sensitive cameras for collecting images with less electron dose as well as phase plates installed into the TEM instrument to enhance image contrast⁴⁶. Secondly, artifacts are easily caused during sample preparation and the imaging process. As mentioned earlier, during plunging, the solvent can freeze resulting in the formation of ice crystals that appear as dark, opaque areas within the sample film. Recent reviews have focused on how to interpret cryo-TEM images⁴⁷. Also, the size range that cryo-TEM can image is limited to several hundred nanometers⁴⁸, making large particles such as cells difficult to observe^{49,50}. Recent progress in the use of cryogenic sample preparation methods such as cryogenic fixing and cryo-sectioning has enabled the imaging of giant biological samples⁵¹. The common artifacts are summarized in Figure 2.8.

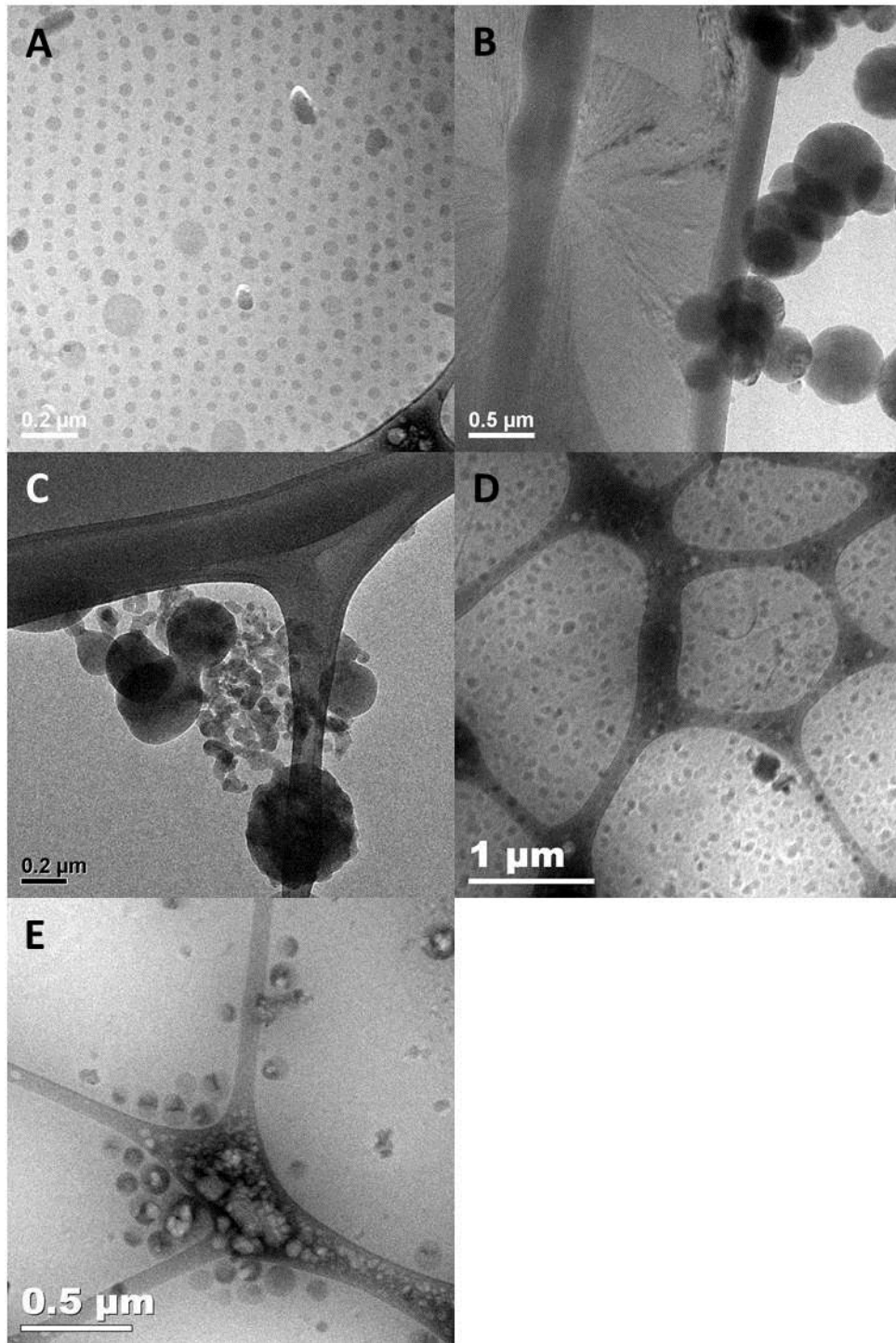


Figure 2.8 Common artifacts in cryo-TEM. (A) Hexagonal packed particles due to the shear force present during sample blotting. The disordered particles near the edge indicate that it is not real hexagonal structure in solution but shear-induced artifacts. (B, C, D) poorly vitrified samples and giant ice. (E) Beam damage.

2.3 Scattering Methods in Characterizing Solution Assemblies

Although imaging is a powerful tool in providing local nanostructure information, scattering is a complimentary method that provides global structure observation of materials. Specifically, scattering is invaluable for characterizing solution assemblies^{52, 53}. Scattering methods, especially elastic scattering methods in which the scattered radiation or particles have the same energy as the impinging radiation or particles, represents a change in the direction of a travelling wave (light, neutron or x-ray) due to contrast on the nano through micron length scales. The contrast in the sample environment may be due to the changes in refractive index (thus impacting light), nuclei (thus impacting neutrons) or electron density (thus impacting x-rays).

Even though microscopy provides unique, local structural insights difficult to identify through scattering analysis, scattering can provide much more global analysis ($\sim 10^{15}$ micelles) vs. ($\sim 10^3$ micelles in electron microscopy)³⁸. In block copolymer self-assembly study, mainly two scattering methods are used to provide global and overall structure features (*e.g.* size and shape of particles) of the assembled nanostructures in solution. In this dissertation, the two methods were used to characterize the global character of the hybrid multicompartment and multigeometry nanoparticles made through different kinetic pathways. Small-angle x-ray scattering (SAXS) and small-angle neutron scattering (SANS) measurements were completed at the Advanced Photon Synchrotron at Argonne National Lab (APS, ANL), and the National Institute of Science and Technology Center for Neutron Science (NIST, NCNR), respectively.

2.3.1 Small Angle Neutron and X-ray Scattering in Solution Assembly Study

The scattering vector is the most important parameter in scattering. When an incident beam of radiation (light beam, x-ray beam, or neutrons) interacts with a sample, the direction and the momentum of the beam will be changed with the changing vector named q (Figure 2.9).

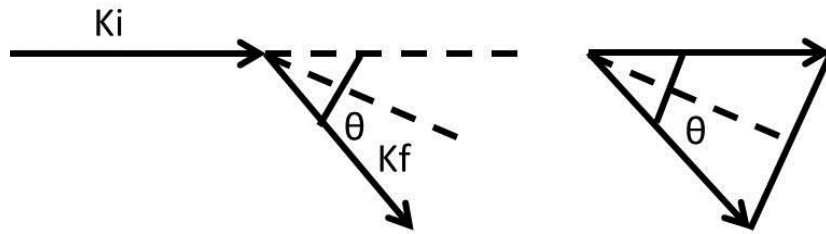


Figure 2.9 Schematic of wavevectors and scattering vector (q) in elastic scattering.

If the sample happens to have a repeating arrangement of nanostructure that gives rise to diffraction, Bragg's law shows that the scattering vector is inversely related to the spacing of the planes,

$$2\pi/q=d/n. \quad (1)$$

where q is the scattering vector and d is the space between the lattice. Larger objects scatter at smaller q . Accordingly, the d range indicating the length scales that can be reached by scattering experiments are described by q range, which is then determined by the incident beam wavelength λ and scattering angle θ .

$$q=(4\pi/\lambda) \sin \theta \quad (2)$$

Scattering that is independent of q is referred to as incoherent scattering, while scattering that is dependent on q is referred to coherent scattering.

To detect the detailed structure of block copolymer solution assemblies from 1 to 100 nm, very small scattering angle must be observed according to the inverse correlation between q and d ($\theta < 5^\circ$). The measured scattering intensity is a function of several parameters:

$$I(q)=\Phi\Delta\rho^2P(q)S(q) \quad (3)$$

Φ is the volume fraction of scattering agent. $\Delta\rho$ is the scattering contrast. This equation applies to both neutron and x-ray scattering with different mechanisms of the scattering contrast (nucleus character vs electron density for SANS and SAXS, respectively). $P(q)$ is the form factor, and $S(q)$ is the structure factor⁵⁴. The form factor represents the scattering interference between different parts of the same particle, individual and, hence, provides information on the size and shape of the individual particle. The structure factor describes scattering interference between different particles and, thus, provides information on the particle-particle separation and interactions. In dilute solution with no interparticle interactions, $S(q)=1$.

Contrast in Scattering

In neutron scattering, neutrons interact with the nucleus of the atoms within particles and solvents, and the scattering is due to the distribution of nuclei within the sample. The neutron scattering length density is related to the coherent nuclear scattering length. The nuclear scattering length varies widely across the elements and also varies between the isotopes of the same elements. Another important point is that the scattering from a hydrogen nucleus (the scattering length density is -0.3742 in units of 10^{-12} cm) is distinct from that of a deuterium (the scattering length density is 0.6671 in units of 10^{-12} cm). In block copolymer solution assemblies, the particles and solvents contain large numbers of hydrogen atoms. Accordingly, the contrast in the system can be tuned by varying the hydrogen and deuterium content in the sample vs. the solvent. The size and shape of the particles and also specific parts of the particles (core or shell), can be highlighted by varying the contrast of the solvents vs. particles, and core vs. shell.

Thus the structure information can then be obtained from coherent scattering. Whereas, the incoherent scattering produces a flat, q -independent background that gives no significant structural information. For all intents and purposes, this incoherent scattering sets the lower bound on the accessible intensity in a SANS experiment. Accordingly, one tries to minimize the incoherent scattering by minimizing the

incoherent cross section of the sample, usually through solvent selection. Hydrogen contains a large incoherent cross section vs. the deuterium, which is a common element in many solvents such as water. Thus, one can then use the deuterated solvent to decrease the incoherent scattering and provide contrast with a particle containing hydrogen.

In x-ray scattering, the scattering contrast is coming from the electron density difference between the sample and the surrounding solvent. Scattering length density of a particular nanostructure can be obtained from on-line calculator from NCNR, NIST website that considers the elements that make up the nanoparticle.

Data Collection and Analysis

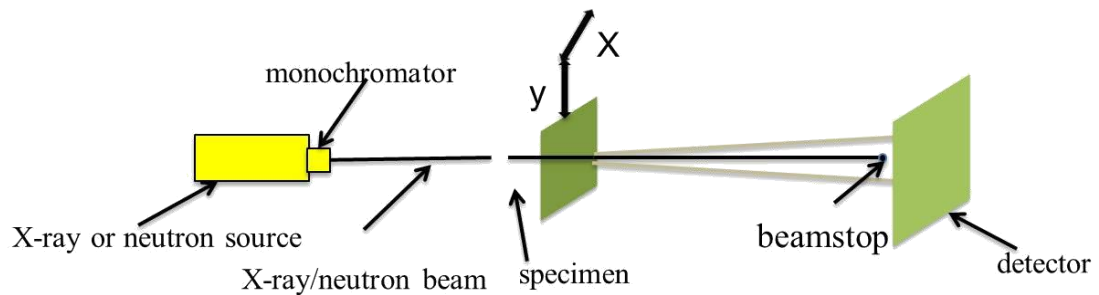


Figure 2.10 Schematic of SANS and SAXS instrument in transmission. X and Y indicate the x axis and y axis.

As shown in Figure 2.10, the basic set up for small angle scattering instruments is indicated. A monochromatic neutron or x-ray beam is focused onto a specimen. The incident beam is then scattered by the sample, and the scattered neutrons or x-rays are collected by a 2D detector. The sample-to-detector distance can be changed. Different scattering angles can then be observed, and different length scales of the samples can be interrogated. The longer the sample-detector distance is, the smaller the scattering angles are that can be resolved and, thus, the smaller the q values and the larger the structures that can be observed. The detector then collects the 2D scattering pattern

and the 2D pattern can be reduced to a 1D plot showing the relationship between the scattering intensity, I , and scattering vector, q .

Data analysis is needed to obtain the most information for structure analysis. The data analysis most frequently used in block copolymer solution assembly is a model-dependent fitting analysis. The different models for individual particles (*e.g.* spheres, cylinders, vesicles and many others) are provided by the NCNR at NIST. Each solution assembly system is unique having the unique scattering length density of the different components of the nanostructure (for example the core and shell) relative to the volume fraction of each component as well as the solvent conditions. Successful fitting of the nanostructure in each, unique solution assembly sometimes requires tweaking of the model, combination of different models and sometimes the building of new models. In summary, by analyzing the SAXS/SANS data, one can get a global picture of the structure shape and size that corresponds to the local information acquired from TEM imaging. The models in the fitting software provided by the NCNR can also be applied in SAXS fitting. The respective sample and experimental parameters need to be altered such as the scattering length density for x-rays is used as opposed to neutrons.

In this dissertation, SAXS was performed to understand the block copolymer solution assembly formation mechanism, especially observing phase behavior during different kinetic control methods of solution assembly. The data will be presented in section 2.4 and also in Chapters 3 and 4. SAXS measurements were performed at APS on 18-ID-D beamline. Solution samples were prepared in quartz capillaries (outside diameter=1.5 mm, inner diameter =1.3 mm) with all scattering measurements lasting for 45 seconds. SANS were performed in NG-7 30 m beamline at NCNR, NIST. Samples were loaded in titanium sample cells with 30 mm diameter quartz windows at a 2 mm path distance. Monochromatic neutrons at $\lambda = 6 \text{ \AA}$ and a wavelength spread ($\Delta\lambda/\lambda$) of 0.14 were incident on the sample. The scattered neutrons were captured by a 64 cm \times 64 cm 2D detector. Sample-to-detector distances were applied at 1.33, 4.5 and 13.17 m to cover a large scattering vector q range ($0.004 < q < 0.4 \text{ \AA}^{-1}$).

2.4 Scattering Methods in Characterization of Morphology Transitions in Block Copolymer Assembly with Kinetic Control

In Chapter 3 and Chapter 4, the construction of hybrid nanoparticles with new geometries and multiple compartments is described. Kinetic control was used to construct the nanoparticles via self-assembly of either a single block copolymer or block copolymer blends in solution. In the kinetic control self-assembly, amphiphilic block copolymer was firstly dissolved in THF to make a homogeneous solution. The small diamine molecule EDDA was added to complex with the acrylic acid side chains in the hydrophilic domain of the block copolymer such as PAA-*b*-PS or PAA-*b*-PI. Importantly and lastly, water was added to the THF solution to introduce the self-assembly process. During the water addition process, many intermediate, kinetically-trapped and reversible nanostructures are formed at different solvent compositions. Slightly different water contents (2~3%) can introduce different morphologies. TEM is used to characterize the nanostructures assembled in THF/H₂O mixed solvent. However, the sample size that can be investigated locally by microscopy is much smaller than the global sample size that can be examined by scattering techniques. Besides the large sample size, fast-throughput and high-efficiency are significant advantages of small-angle scattering methods. For example, the characterization of one solution sample costs around two minutes by the synchrotron x-ray beamline in Argonne National Lab, which is obviously less than imaging process. In this thesis, small angle x-ray/neutron scattering were used to characterize the solution assemblies in different assembly systems (different solvent compositions, water addition rates, single diblock copolymer assembly or co-assembly of blends of block copolymers).

As discussed above, gross differences of assembly behaviors are observed in different solvent compositions. To highlight the advantages of using scattering methods in characterizing solution assemblies, the SAXS traces of aggregates formed by PAA₉₉-*b*-PS₁₆₉ in different THF/H₂O contents are presented here, Figure 2.11. The corresponding TEM images are shown in Figure 2.12. In the assembly, PAA-PS was firstly dissolved in THF to form a homogeneous, clear solution. Then, amine is added

to complex with the PAA block. Water was then added using a syringe pump with an extremely slow rate (0.5 mL/h). The solution status changed as water was added into the solution, due to the formation of aggregates in different water contents. The characterization results of nanostructures formed at approximately 15%, 24%, 28%, 40%, 52%, and 75% are presented here. As shown from Figure 2.11, the intensity of the scattering curve increased as water composition changed from 1% to 15%, as well as the solution status changed from clear to precipitation which indicated the formation of large aggregates. Giant membrane structures were observed by TEM as shown in Figure 2.12. In the middle water regimes, large particles with local nanostructures were observed from TEM, such as the large cylinder bundles at 24% water composition and hexagonal packed cylinder bundles in 28%. Lamellar structure and lamellar-to-vesicle intermediate structures were then formed at higher water contents (40%, 50%). The layered structures were confirmed by the SAXS traces which provide clear Bragg peaks in the middle q range, corresponding to a periodic d -spacing equal to 30-33 nm. Cylinders were formed in higher water contents, as indicated by TEM and SAXS traces.

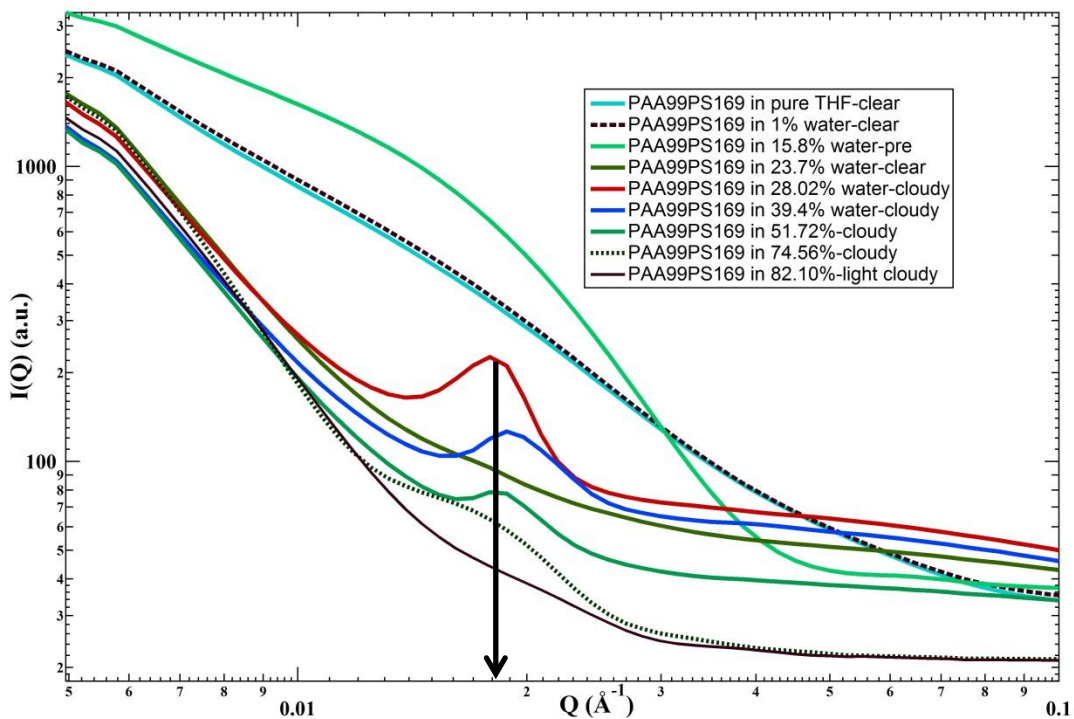


Figure 2.11 SAXS traces of the assemblies formed in different water contents from PAA₉₉-b-PS₁₆₉, amine to acid=0.5:1 in different water contents. Scattering peaks were observed in middle water contents, corresponding to d-spacing which is around 30-33 nm ($q=0.018 \text{ \AA}^{-1}$). Pre represents precipitation.

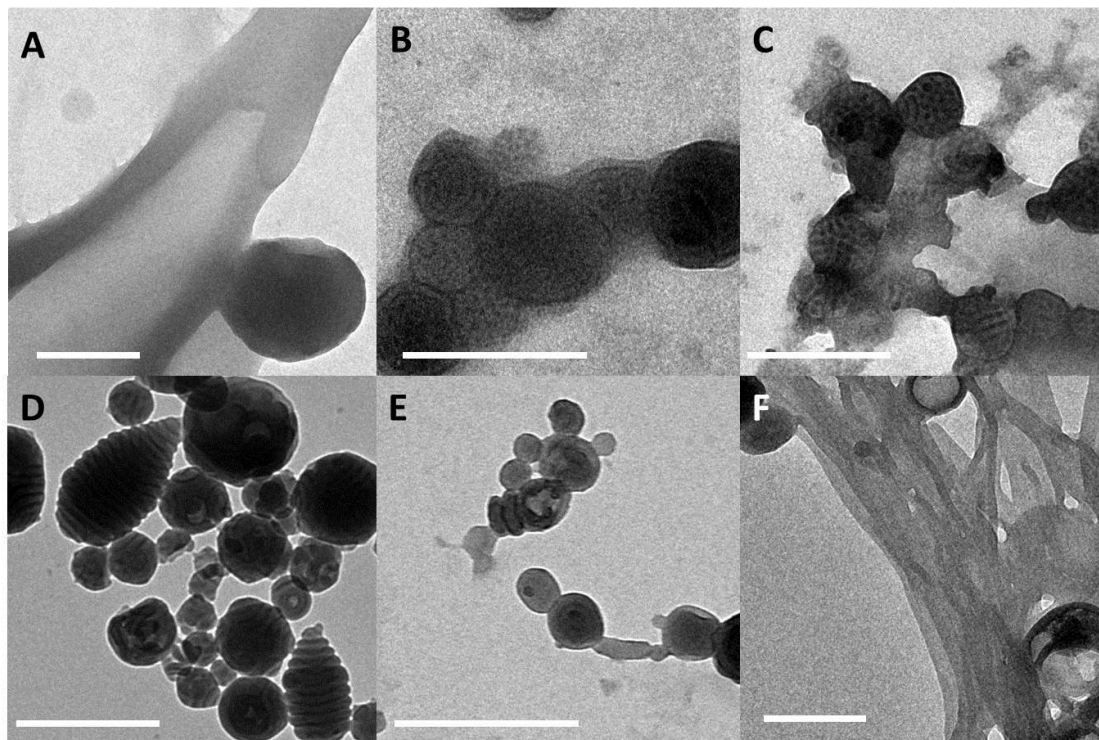


Figure 2.12 Cast film TEM images of the nanostructures assembled by PAA₉₉-b-PS₁₆₉ with amine to acid=0.5:1. **A:** 15% H₂O condition, giant membrane, precipitated suspensions. **B:** 24% H₂O condition, cylinder bundles suspended in cloudy solution. **C:** 28% H₂O condition, close packed cylindrical bundles suspended in cloudy solutions. **D:** 40% H₂O condition, lamellar structure with the d-spacing at 32 nm. **E:** 50% H₂O condition, intermediate nanostructures of lamellar to vesicle transition. **F:** 75% condition, vesicle to cylinder intermediate structures. Inserted scale bar: 500 nm.

Herein, the SAXS results provided a global picture of the nanostructures of solution assemblies, a crucial complement to the imaging results. The detailed morphology characterizations in even small water composition windows (3%-5%) are described in Chapter 3, as well as the assembly of other diblock copolymer and coassembly of blends of distinct diblock copolymers. The form factor fitting of the cylinders assembled in high water contents is also discussed in Chapter 3.

REFERENCES

1. J. Adamcik and R. Mezzenga, *Curr. Opin. Colloid Interface Sci.*, 2012, **17**, 369-376.
2. H. Jinnai, R. J. Spontak and T. Nishi, *Macromolecules*, 2010, **43**, 1675-1688.
3. D. Danino, *Curr. Opin. Colloid Interface Sci.*, 2012, **17**, 315-319.
4. R. F. Egerton, *Physical Principles of Electron Microscopy. An Introduction to TEM, SEM, and AFM*, Springer 2005.
5. L. Li, C. Y. Li, C. Ni, L. Rong and B. Hsiao, *Polymer*, 2007, **48**, 3452-3460.
6. K. H. Roh, D. C. Martin and J. Lahann, *Nat. Mater.*, 2005, **4**, 759-763.
7. J. S. Kim, T. LaGrange, R. K. B.W. Reed, T. P. Weihs, N. D. Browning and G. H. Campbell, *Acta Mater.*, 2011, **59**, 3571–3580.
8. Q. Chen, J. M. Smith, J. Park, K. Kim, D. Ho, H. I. Rasool, A. Zettl and A. P. Alivisatos, *Nano Lett.*, 2013, **13**, 4556-4561.
9. N. Petzetakis, M. P. Robin, J. P. Patterson, E. G. Kelley, P. Cotanda, P. H. Bomans, N. A. J. M. Sommerdijk, A. P. Dove, I. Thomas H. Epps and R. K. O'Reilly, *ACS Nano*, 2013, **7**, 1120–1128.
10. J. P. Patterson, A. M. Sanchez, N. Petzetakis, T. P. Smart, I. Thomas H. Epps, Ian Portman, N. R. Wilson and R. K. O'Reilly, *Soft Matter*, 2012, **8**, 3322-3328.
11. V. Alfredsson, *Curr. Opin. Colloid Interface Sci.*, 2005, **10**, 269-273.
12. A. Dey, G. de With and N. A. J. M. Sommerdijk, *Chem. Soc. Rev.*, 2010, **39**, 397-409.
13. S. Zhong and D. J. Pochan, *Polymer Reviews*, 2010, **50**, 287-320.
14. H. Cui, T. K. Hodgdon, E. W. Kaler, L. Abezgauz, D. Danino, M. Lubovsky, Y. Talmon and D. J. Pochan, *Soft Matter*, 2007, **3**, 945-952.

15. R. B. Dettmeyer, *Staining Techniques and Microscopy*, Elsevier, 2011.
16. X. Wang, J. Chen, K. Hong and J. W. Mays, *ACS Macro Letters*, 2012, **1**, 743-747.
17. J. J. Crassous, C. N. Rochette, A. Wittemann, M. Schrunner, M. Ballauff and M. Drechsler, *Langmuir*, 2009, **25**, 7862-7871.
18. J. P. Patterson, P. Cotanda, E. G. Kelley, A. O. Moughton, A. Lu, T. H. Epps, III and R. K. O'Reilly, *Polymer Chemistry*, 2013, **4**, 2033-2039.
19. Z. P. Luo and J. H. Koo, *Polymer*, 2008, **49**, 1841-1852.
20. B. M. Tyson, R. K. Abu Al-Rub, A. Yazdanbakhsh and Z. Grasley, *Composites Part B: Engineering*, 2011, **42**, 1395-1403.
21. Q. Gou, M. D. Wetzel and B. A. Ogunnaike, *Polymer*, 2014, **55**, 4216-4225.
22. V. Zeljković, C. Tameze, D. J. Pochan, Y. Chen and V. Valev, *Automated Nanostructure Microscopic Image Characterization and Analysis*, 2015.
23. P. P. Neelakandan, Z. Pan, M. Hariharan, Y. Zheng, H. Weissman, B. Rybtchinski and F. D. Lewis, *J. Am. Chem. Soc.*, 2010, **132**, 15808–15813.
24. W. H. Massover, *Micron*, 2011, **42**, 141-151.
25. Y. I. González and E. W. Kaler, *Curr. Opin. Colloid Interface Sci.*, 2005, **10**, 256-260.
26. A. J. Kim, M. S. Kaucher, K. P. Davis, M. Peterca, M. R. Imam, N. A. Christian, D. H. Levine, F. S. Bates, V. Percec and D. A. Hammer, *Adv. Funct. Mater.*, 2009, **19**, 2930-2936.
27. A. Yagmur and O. Glatter, *Adv. Colloid Interface Sci.*, 2009, **147-148**, 333-342.
28. D. Danino, *Curr. Opin. Colloid Interface Sci.*, 2012, **17**, 316-329.
29. I. Dáz, V. Alfredsson and Y. Sakamoto, *Curr. Opin. Colloid Interface Sci.*, 2006, **11**, 302-307.
30. J.-F. Berret, N. Schonbeck, F. Gazeau, D. E. Kharrat, O. Sandre, A. Vacher and M. Airiau, *J. Am. Chem. Soc.*, 2006, 1755-1761.

31. F. Song, P. Chen, D. Sun, M. Wang, L. Dong, D. Liang, R.-M. Xu, P. Zhu and G. Li, *Science*, 2014, **344**, 376-380.
32. J. Kuntsche, J. C. Horst and H. Bunjes, *Int. J. Pharm.*, 2011, **417**, 120-137.
33. C. J. Newcomb, T. J. Moyer, S. S. Lee and S. I. Stupp, *Curr. Opin. Colloid Interface Sci.*, 2012, **17**, 350-359.
34. R. Fenyves, M. Schmutz, I. J. Horner, F. V. Bright and J. Rzyayev, *J. Am. Chem. Soc.*, 2014, **136**, 7762-7770.
35. C. V. Synatschke, T. Nomoto, H. Cabral, M. Förtsch, K. Toh, Y. Matsumoto, K. Miyazaki, A. Hanisch, F. H. Schacher, A. Kishimura, N. Nishiyama, A. H. E. Müller and K. Kataoka, *ACS Nano*, 2014, **8**, 1161-1172.
36. T. I. Löblich, J. S. Haataja, C. V. Synatschke, F. H. Schacher, M. Müller, A. Hanisch, A. H. Gröschel and A. H. E. Müller, *ACS Nano*, 2014, **8**, 11330-11340.
37. C. V. Synatschke, T. I. Löblich, M. Förtsch, A. Hanisch, F. H. Schacher and A. H. E. Müller, *Macromolecules*, 2013, **46**, 6466-6474.
38. E. G. Kelley, R. P. Murphy, J. E. Seppala, T. P. Smart, S. D. Hann, M. O. Sullivan and T. H. Epps, *Nat. Commun.*, 2014, **5**, 3599-3607.
39. V. Percec, P. Leowanawat, H. J. Sun, O. Kulikov, C. D. Nusbaum, T. M. Tran, A. Bertin, D. A. Wilson, M. Peterca, S. Zhang, N. P. Kamat, K. Vargo, D. Moock, E. D. Johnston, D. A. Hammer, D. J. Pochan, Y. Chen, Y. M. Chabre, T. C. Shiao, M. Bergeron-Brelek, S. Andre, R. Roy, H. J. Gabius and P. A. Heiney, *J. Am. Chem. Soc.*, 2013, **135**, 9055-9077.
40. B. Ni, M. Huang, Z. Chen, Y. Chen, C.-H. Hsu, Y. Li, D. Pochan, W.-B. Zhang, S. Z. D. Cheng and X.-H. Dong, *J. Am. Chem. Soc.*, 2015, **137**, 1392-1395.
41. H. Cui, E. T. Pashuck, Y. S. Velichko, S. J. Weigand, A. G. Cheetham, C. J. Newcomb and S. I. Stupp, *Science*, 2010, **327**, 555-229.
42. R. J. Hickey, J. Koski, X. Meng, R. A. Riggelman, P. Zhang and S.-J. Park, *ACS Nano*, 2014, **8**, 495-502.

43. P. J. M. Smeets, K. R. Cho, R. G. E. Kempen, N. A. J. M. Sommerdijk and J. J. D. Yoreo, *Nat. Mater.*, 2015, **6**, 1-10.
44. P. H. H. B. Emilie M. Pouget, Jeroen A. C. M. Goos, Peter M. Frederik, and N. A. J. M. S. Gijsbertus de With, *Science*, 2009, **323**, 1455-1458.
45. J. E. Evans, C. Hetherington, A. Kirkland, L. Y. Chang, H. Stahlberg and N. Browning, *Ultramicroscopy*, 2008, **108**, 1636-1644.
46. R. Danev and K. Nagayama, in *Methods in Enzymology*, Elsevier, Elsevier, 2010, vol. 481, pp. 343-369.
47. H. Friedrich, P. M. Frederik, G. de With and N. A. Sommerdijk, *Angew. Chem. Int. Ed.*, 2010, **49**, 7850-7858.
48. S. Zhang, H.-J. Sun, A. D. Hughes, R.-O. Moussodia, A. Bertin, Y. Chen, D. J. Pochan, P. A. Heiney, M. L. Klein and V. Percec, *Proc. Natl. Acad. Sci.*, 2014, **111**, 9058-9063.
49. J.-K. H. Hye-Jin Cho, Jin-Gyu Kim, Hyeong Seop Jeong, Hyo Nam Park, Dong-Ju You and a. H. S. Jung, *Journal of Analytical Science and Technology*, 2013, **4**, 1-7.
50. S. Subramaniam, *Curr. Opin. Microbiol.*, 2005, **8**, 316-322.
51. I. Hurbain and M. Sachse, *Biol. Cell*, 2011, **103**, 405-420.
52. S. Jain and F. S. Bates, *Science*, 2003, **300**, 460-464.
53. F. Caputo, W. Burghardt, K. Krishnan, F. Bates and T. Lodge, *Physical Review E*, 2002, **66**, 041401-041418.
54. R. R.J., *Methods of X-ray and Neutron Scattering in Polymer Science*, Oxford University Press, 2000.

Chapter 3

HYBRID VESICLE/CYLINDER NANOPARTICLES CONSTRUCTION: BLOCK COPOLYMER SOLUTION ASSEMBLY, KINETIC CONTROL AND NANOPARTICLE FORMATION MECHANISM

3.1 Introduction

The ability of amphiphilic block copolymers to associate into complex morphologies depends not only on the molecules used but also on the intermolecular assembly strategy. Frequently-used methodologies to create novel, nano-sized morphologies include the design and synthesis of different block copolymers, changing the solution conditions (pH¹, temperature², ionic strength³) and variation of solution assembly kinetic pathways^{4, 5}. In an effort to minimize the need to develop new polymer synthetic routes⁶, management of assembly strategies offers an alternative for novel nanostructure formation. Protocols involving solvent processing⁷⁻⁹, flash nanoprecipitation¹⁰, and polymerization of crystalline-coil micelles¹¹ are good examples of new processes in engineering nanoscale materials. However, there is clear opportunity for new methods of forming MCN and MGN *via* simple assembly strategies.

Herein, by simply blending the amphiphilic block copolymers poly(acrylic acid)-*block*-polyisoprene (PAA-*b*-PI) and poly(acrylic acid)-*block*-polystyrene (PAA-*b*-PS), multigeometry vesicle-cylinder particles, multicompartment vesicles, or multigeometry cylinder-disk nanostructures were constructed *via* kinetic control. In the assembly strategy, the PAA common domain in both block copolymers was first complexed with organic diamine molecules in organic solution to form a particle core. Therefore, the two different hydrophobic blocks from the two different polymers were trapped into the outer shell of the same particle, overall with inverse micelle-like structure. After addition of water and eventual inversion of the particles to form

hydrophobic cores and PAA-amine hydrophilic shells, the two hydrophobic domains locally nanophase-separated to form the multicompartment and multigeometry nanoparticles. Importantly, detailed control of the solvent mixing rates helps dictate the final hybrid nanostructures formed at higher water content.

Four different water addition rates and three blending ratios of two different block copolymers were used in order to investigate new MCN and MGN and the rates/ratios influences. Two different block copolymers that form vesicles and cylinders, respectively, were selected as the building blocks for co-assembly. Strong correlations between water addition rates and assembled nanostructures were observed. Generally, faster water addition rates provide for hybrid nanoparticles with different block copolymers trapped within the same particle while slow solvent mixing rates produce populations of discrete nanoparticles with separate, constituent block copolymers. At intermediate solvent mixing rates, there are subtle effects on the morphologies of formed, hybrid nanoparticles in which different block copolymers are trapped together. Specifically, the new structures reported here shed light on multifunctional nanomedicine vehicle or nanoreactor construction with advantages from both vesicular and cylindrical shapes^{12, 13}. The particles observed inform construction strategies of other hybrid nanostructures with other block copolymer blend systems. Therefore, the use of solvent mixing rate is discussed as an additional and necessary tool to control the morphology of mixed block copolymer hybrid nanoparticles.

In the end, since all of the nanoparticles produced with kinetic control are in metastable, kinetically-trapped states, the evolution of nanoparticles over time is also discussed. Interestingly, unanticipated morphologies can develop over long periods of time (*e.g.* several months) of ageing during which block copolymers, still trapped locally within the particles due to block molecular weight, solvent composition and acid-base complexation in the particle shells, are able to further diffuse internally within the nanoparticles and relax into a lower free energy state. Significantly, while discussed in the context of the model amphiphilic block copolymers herein, the

solution assembly strategy is applicable to a wider variety of block copolymers and block copolymer mixtures for future nanomaterials construction.

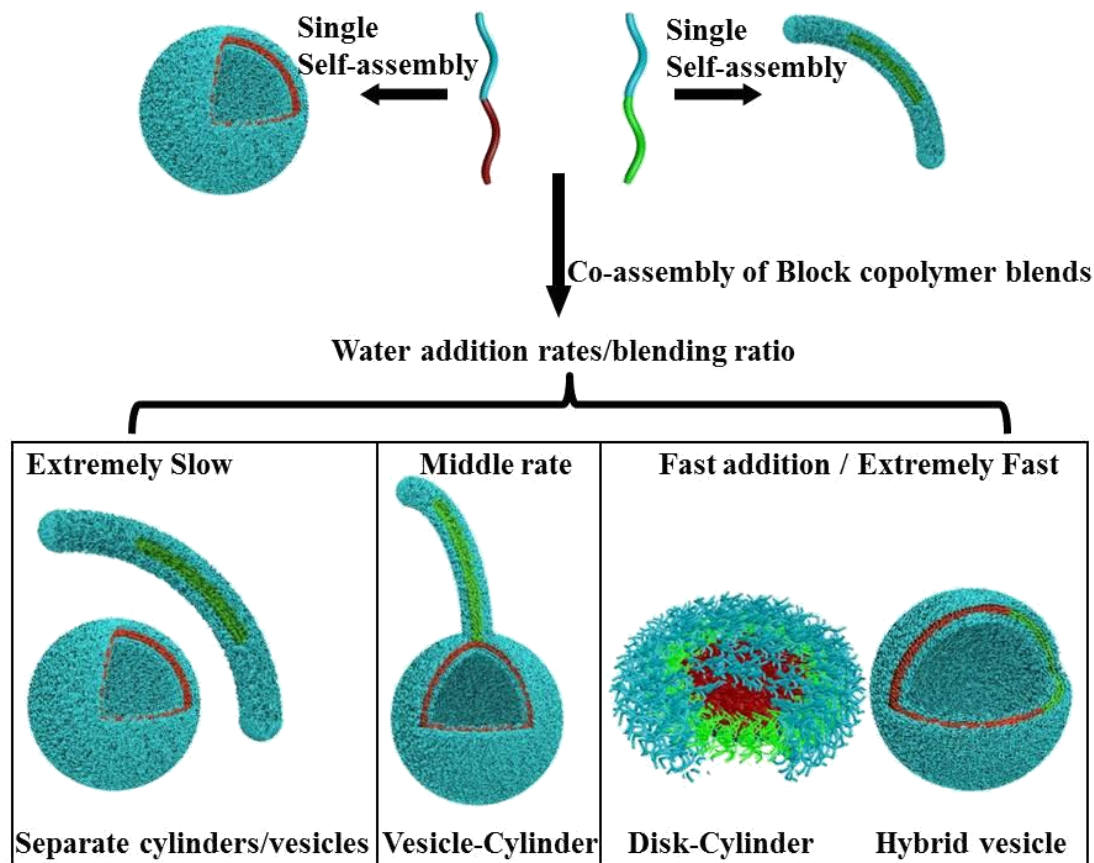


Figure 3.1 Schematic of multicompartament and multigeometry nanoparticles *via* binary blends of PAA₁₀₀-*b*-PI₁₅₀ and PAA₉₉-*b*-PS₁₆₉ diblock copolymers with different water addition rates, in THF/H₂O mixtures (v/v=1:4). Pure vesicles and pure cylinders are assembled from single assembly of PAA-PI and PAA-PS, respectively. Separate population of cylinders and vesicles are formed with extreme slow water addition *via* co-assembly of block copolymer blends; vesicle-cylinder connected particles are assembled with middle rate; Disk-cylinders and hybrid vesicles are formed with fast and extremely fast water addition rates. The blue color represents PAA block complexed with organic diamine; the red represents PI block and the green represents PS block.

The construction of multigeometry nanoparticles combining vesicle and cylinder geometries is presented in the first part of the chapter. To better understand the phase separation behaviors in the blend system at different water addition rates, small angle x-ray scattering was performed to track the morphology behavior at different relative water compositions through which the multicompartment and multigeometry nanoparticles are formed.

3.2 Construction of Vesicle-Cylinder MCN/MGN

3.2.1 Materials

The diblock copolymer PAA₁₀₀-PI₁₅₀ was synthesized by Dr. Xiaojun Wang from Jimmy Mays lab at University of Tennessee. The unsaturated diblock copolymer poly(*tert*-butyl acrylate)-polyisoprene was synthesized by anionic polymerization employing high vacuum techniques and sequential polymerization of isoprene and *tert*-butylacrylate according to a developed protocol¹⁴. The subsequent dialysis process to obtain poly(acrylic acid)-polyisoprene (PAA₁₀₀-*b*-PI₁₅₀; M_w: 27370 Da; M_w/M_n=1.19) was performed according to a method described elsewhere¹⁴. The PAA₉₉-*b*-PS₁₆₉ was synthesized by Dr. Ke Zhang from Karen Wooley lab at Texas A&M University. The diblock copolymer poly(*tert*-butyl acrylate)-polystyrene (PtBA-PS) was synthesized by successively incorporating *tert*-butyl acrylate (tBA), and styrene (S) through an atom transfer radical polymerization (ATRP) procedure¹⁵. The *tert*-butyl esters of PtBA-PS were selectively cleaved *via* reaction with trifluoroacetic acid (TFA) in dichloromethane, producing the amphiphilic block copolymer poly(acrylic acid)-*block*-polystyrene (PAA₉₉-*b*-PS₁₆₉; M_w: 26927 Da; M_w/M_n=1.09). The organic diamine, 2, 2'-ethylenedioxy bis(ethylamine) (EDDA, 99%) was purchased from Sigma-Aldrich and was used as obtained.

3.2.2 Self-assembly Procedure and Sample Characterization

Polymer solutions were firstly prepared by dissolving PAA₁₀₀-*b*-PI₁₅₀ and

PAA₉₉-*b*-PS₁₆₉ into tetrahydrofuran (THF) to reach a concentration of 2 mg/mL, respectively. The solution was stirred for 24 hours for complete dissolution. The blending solution was made by mixing the two polymer solutions at different molar ratios of the two diblocks (PAA₁₀₀-*b*-PI₁₅₀: PAA₉₉-*b*-PS₁₆₉=9:1, 1:1, 1:9) with THF. Organic diamine (1 vol% concentration in THF) was then added to reach a polymer concentration of 0.1 wt% and an amine: acid ratio of 0.5:1. The solution was stirred for 24 hours for sufficient mixing and complexation between amine and acid groups. Solutions of individual block copolymers for assembly were prepared the same way as the blend samples with EDDA added to either PAA₉₉-*b*-PS₁₆₉ or PAA₁₀₀-*b*-PI₁₅₀ solution. Next, water was added to the 1 mL THF solution to reach 80% water concentration at different addition rates as listed in Table 1. Final polymer assemblies were thus obtained in 5 mL total mixed solvent (THF/H₂O=1/4 v/v) with a final polymer concentration at around 0.018 wt%. Different water addition rates were achieved through use of a syringe pump (KD Scientific Syringe Pump, KDS 100). The assembly solutions were constantly stirred with a magnetic stir bar during water addition at the same stirring rate (100 r/m). The assembly solutions were stored in glass vials sealed with PTFE covers and Teflon tape to limit solvent evaporation to undetectable levels. During ageing, the solutions were not stirred further. The parameters of titration rates, blending ratios, and corresponding morphologies are listed in Table 1. Sample microscopy images were obtained after solutions aged for 1 day after water addition. The ageing effects shown in Figure 3.13 were performed after 1, 2, or 3 months of ageing.

Throughout the thesis, all the starting volumes for polymer/amine/THF dilute solutions are 1 mL contain 0.1wt% polymer. Water was added in particular rate to reach 5 mL THF/H₂O mixture. And the final polymer concentration reached 0.018wt% in 20% THF/80%H₂O. The 0.1 wt% concentration is suggested for one to repeat the experiments to eliminate concentration effects. If a different starting volume is used, then one should aim for titration rates that match the polymer concentration

wt% change/min that were used here. The polymer concentration changing rates in different water addition rates are listed in Table 3.1.

Table 3.1 Average polymer concentration changing rates in different water addition rates

Rates	0.8 mL/h	5 mL/h	30 mL/h	Extremely fast
Polymer concentration changing rates (average)	2.73×10^{-4} wt%/min	1.7×10^{-3} wt%/min	0.01 wt%/min	Instant change

The water addition rates (*e.g.* 5 mL/h) will be using in the rest of the thesis for clarity and consistency.

3.2.3 Transmission Electron Microscopy and Selective Staining

TEM observations of dried samples were performed on a FEI Tecnai G²-12 microscope operated at 120 kV, equipped with a Gatan CCD camera. Grids were pre-treated with oxygen plasma to increase the surface hydrophilicity. TEM samples were prepared by applying a drop of nanoparticle suspension (about 3 μ L) directly onto a carbon-coated copper TEM grid, and the drop was allowed to evaporate under ambient conditions. After the grids were completely dried, they were stained by exposure to a 1ml osmium tetroxide aqueous solution (purchased from Electron Microscopy Sciences, 4 wt% OsO₄) in a closed glass vessel. Different time periods (6-24 hours) were used for the staining of different samples.

3.2.4 Cryogenic Transmission Electron Microscopy (cryo-TEM) and Selective Staining

Cryo-TEM observations were performed on a FEI Tecnai G²-12 microscope, operated at 120 kV and equipped with a Gatan CCD camera. Lacey carbon grids were pre-treated using oxygen plasma to increase the surface hydrophilicity right before sample preparation. Approximately 0.6 mL of nanoparticle suspension was held in a centrifuge tube (2 mL). The tube was then put into the staining vessel having 0.5 mL 4 wt% OsO₄ solution in the bottom. Staining occurred for 10-20 minutes in a closed 100 mL glass vessel. It was observed that the clear solutions turned slightly yellow after 10-20 minutes staining. Cryo-TEM sample grids were prepared directly after staining using a Vitrobot vitrification system. A droplet of ~1.2 μ L of stained nanoparticle suspension was pipetted onto a lacey carbon grid. Multiple blotting times were used (usually 2 times) with each blot lasting 2 seconds in order to obtain suitable liquid film thickness for imaging. The sample was allowed to relax for ~3 seconds post-blotting, and then quickly plunged into a liquid ethane reservoir cooled by liquid nitrogen. The vitrified sample was transferred into a Gatan 626 cryo-holder and cryo-transfer stage cooled by liquid nitrogen. During the observation of the vitrified samples, the cryo-holder temperature was maintained around -176 $^{\circ}$ C to limit sublimation of vitreous water. The images were recorded digitally with a Gatan CCD camera. Longer exposure time (3-5 seconds) at a lower dose was used to acquire data and avoid beam damage.

For each assembly solution, 10-15 cryo-TEM/TEM images were taken from different areas, with more than 100 nanoparticles analyzed, in order to assess the distribution in structures observed and to discuss representative nanoparticle behavior in the results. Specifically in both extremely fast water addition (\gg 100 mL/h) and fast addition conditions (30 mL/h), the diameters of resultant hybrid vesicles and disk-cylinders formed were measured using Image J and summarized for comparison (Fig. 3.12).

3.2.5 Atomic Force Microscopy

Assembly solution (5 μL) was deposited on a freshly cleaved mica substrate and allowed to dry under nitrogen flow. Imaging was performed in Tapping Mode on a Dimension 3000 Instruments Multimode AFM. Sectional analysis on height micrographs was conducted using Nanoscope III AFM software.

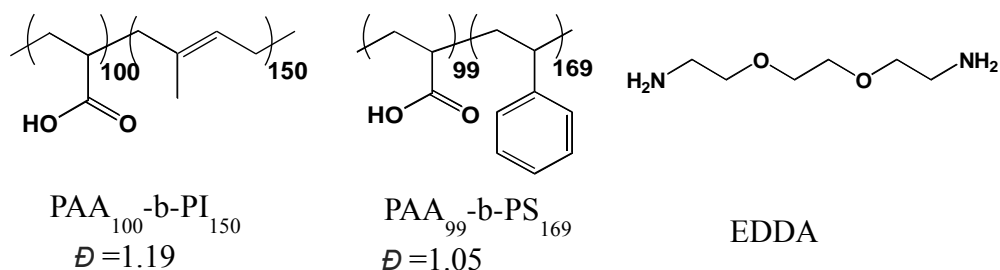
3.2.6 Small Angle x-ray Scattering Measurements

SAXS measurements were executed at the 18-IDB Bio-CAT beamline, Advanced Photon Source (APS), Argonne National Laboratory (ANL). Solution samples were withdrawn and put into cylindrical thin wall (0.2 mm) quartz capillaries with an outer diameter of 1.5 mm (purchased from Charles Super Company, MA) and sealed with wax to prevent THF evaporation. The monochromated x-ray beam had an energy of 12 keV and a wavelength of 1.033 Å. The x-ray beam was directed perpendicular through the center of the capillary. The scattered photons were collected on a two-dimensional CCD detector with typical acquisition times of 45 s. The sample-detector distance was fixed to 3 m resulting in a q range of $0.0055 < q$ (\AA^{-1}) < 0.25 , where q is the magnitude of the scattering vector ($q = (4\pi/\lambda) \sin \theta$) and 2θ is the scattering angle. The whole q range corresponds to a real-space range of 2.5-114 nm. SAXS measurements were performed to track the nanostructures of the assemblies spanning different water content (3%-4% by volume H_2O difference for each solution condition ranging from 0% by volume relative to THF to 80%) with samples placed in capillaries one day after the water titration processes. 2D image patterns were reduced to 1D data files ($I(q)$ versus q) on site. Background for each THF/water condition was subtracted using THF/water mixture solvent at different ratios. The scattering intensity $I(q)$ versus q was obtained by plotting and fitting using Igor software with the NIST NCNR analysis package¹⁶.

3.3 Results and Discussion of Vesicle/Cylinder MCN/MGN Construction

3.3.1 Block copolymers for Binary Blending and Solution Assembly

PAA-*b*-PI and PAA-*b*-PS diblocks were chosen as the two block copolymers to study binary blending *via* desired solution assembly pathway. PAA₁₀₀-*b*-PI₁₅₀ was selected due to its demonstrated ability to form vesicles at water-rich conditions in the presence of EDDA diamine (H₂O=80%, amine: acid=0.5:1). Also, PAA₁₀₀-*b*-PI₁₅₀ provides unsaturated double bonds for increasing mass-thickness contrast *via* OsO₄ selective staining. PAA₉₉-*b*-PS₁₆₉ was selected due to its ability to form cylinders at the same solution condition in which the PAA₁₀₀-*b*-PI₁₅₀ forms vesicles. The identical hydrophilic PAA domains shared by the two block copolymers are complexed with diamine in neat THF solution which acts to confine the PAA-*b*-PI and PAA-*b*-PS into the same aggregate with a PAA-diamine core and mixed PI and PS in the shell. After addition of water and consequent confinement of the PI and PS blocks into the core of formed nanoparticles, the immiscible nature of PI and PS affords local nanophase separation and separated PI and PS compartment formation.



Scheme 3.1 Chemical structures of diblock copolymers and diamine molecule.

The other important reason for selecting PS and PI as the two hydrophobic blocks is that they display Flory-Huggins χ parameters between the polymer blocks and the solvents (water, THF, respectively) that guarantee hydrophobic block assembly with water addition. As the selective solvent water is added to the cosolvent THF, the

mixed solvent becomes quickly and progressively poor for the core formed by PS or PI blocks. Quantitatively, the poor quality of the selective solvent with respect to the hydrophobic blocks can be described enthalpically by the χ interaction parameter, that can be estimated using the van Laar-Hildebran equation^{17, 18} of

$$\chi_{p-s}=[V_s/(RT)](\delta_p-\delta_s)^2$$

where V_s is the molar volume of the solvent and δ_p and δ_s are solubility parameters of polymer and selective solvent, respectively. Since the solubility parameters of PS is $9.04 \text{ (cal/cm}^3)^{0.5}$, PI is $8.1 \text{ (cal/cm}^3)^{0.5}$, while that of water is $23.4 \text{ (cal/cm}^3)^{0.5}$, and THF is $9.52 \text{ (cal/cm}^3)^{0.517, 19}$, the interaction parameters at room temperature can then be calculated according to references.

Table 3.2 χ parameters between polymer-solvent at room temperature (25 °C)

PS/THF ¹⁷²	PS/H ₂ O ¹⁷²	PI/THF	PI/H ₂ O
0.07	6.27	0.06	7.12

The χ parameter between PS and water is much larger than the χ parameter between PS/THF at room temperature, indicating that water is a poor solvent for PS compared to THF. Similar to PS, χ parameter between PI and water is much larger than χ parameter between PI/THF. As water is added into the solution, the solubility of the hydrophobic blocks quickly changes which initiates the micellization process. Well-defined nanoparticles such as cylinders and vesicles are formed at high water contents. The phase separation processes and morphology transitions for the two diblock copolymers are also affected by the introduction of amine molecule in the assembly system. The phase separation are not only depending on the interaction property between the polymer components and solvent but also influenced by the small molecule. The detailed morphology transitions in the kinetic control process are studied by SAXS and TEM, which are discussed in Section 3.2.4.

Other than PI and PS, polybutadiene (PB) and poly(methyl methacrylate) (PMMA) were also selected as the hydrophobic blocks for the assembly system. The solubility parameter for the PB is $8.38 \text{ (cal/cm}^3)^{0.5}$, and $9.25 \text{ (cal/cm}^3)^{0.5}$ for PMMA. The χ parameters between polymer and solvents are listed in Table 3.3.

Table 3.3 χ parameters between polymer-solvent at room temperature (25 °C)

PB/THF	PB/H ₂ O	PMMA/THF	PMMA/H ₂ O
0.038	6.76	6.06	0.003

The different polymer-polymer Flory-Huggins χ parameters pairwise between PS, PB, PMMA and PI guarantee the local phase separation after being trapped inside the same nanoparticles. The χ parameters can be calculated by SANS or SAXS experiments^{20, 21}. According to the published data, the χ parameters pairwise are listed as follows:

Table 3.4 χ parameters between polymer-polymer at room temperature (25 °C)

PS/PI	PS/PB	PS/PMMA	PB/PMMA
0.039	6.045	0.03	0.071

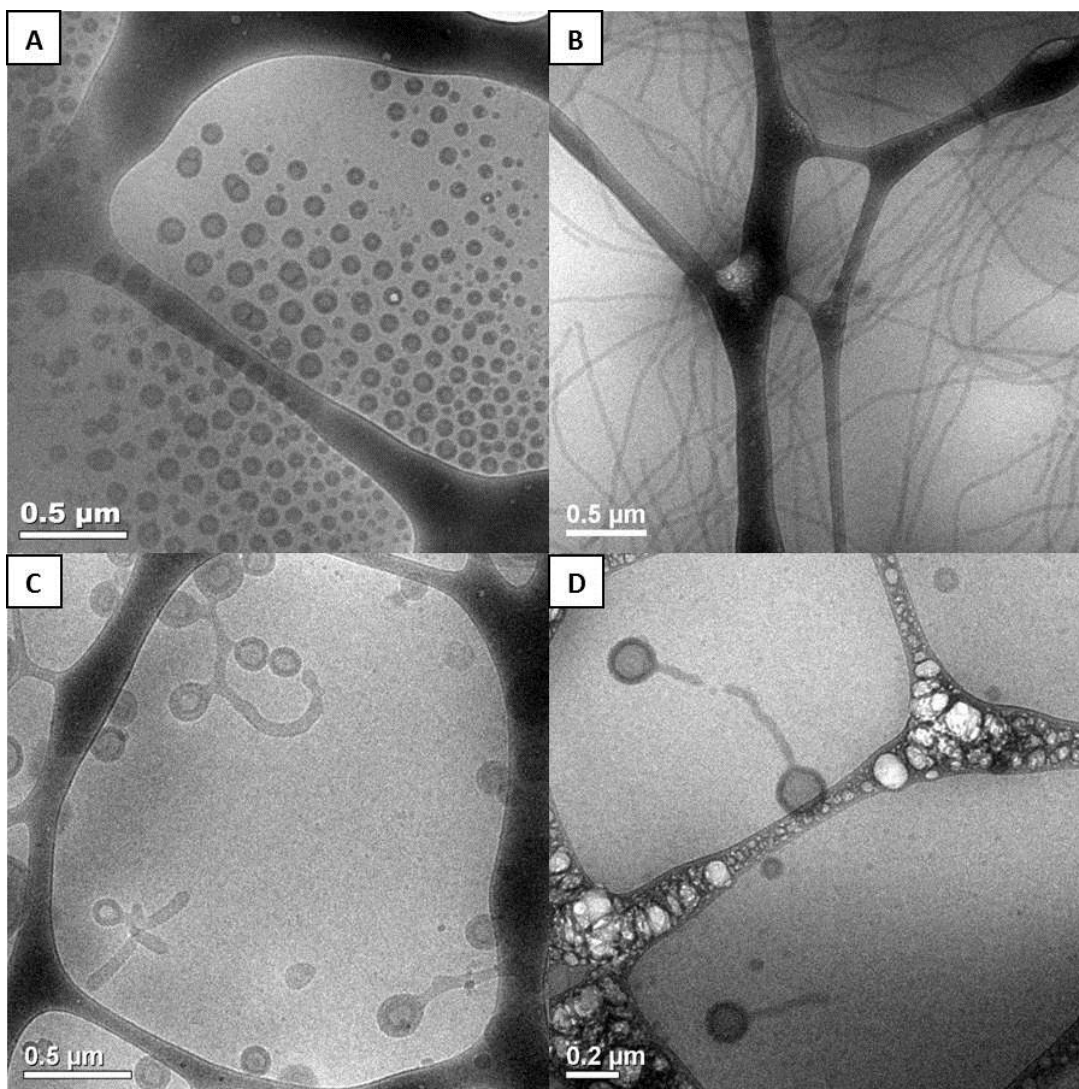


Figure 3.2 TEM images of nanoparticles assembled from PAA₁₀₀-*b*-PI₁₅₀, PAA₉₉-*b*-PS₁₆₉ diblock copolymers in mixed solvent with THF: water volume ratio $v/v=1:4$ and an amine to acid ratio=0.5:1.0 due to added EDDA. A: cryo-TEM images of vesicles assembled by PAA₁₀₀-*b*-PI₁₅₀ with vesicle wall thickness=35 nm, formed with a water addition rate of 5mL/h. B: Thin-film TEM images of cylinders assembled by PAA₉₉-*b*-PS₁₆₉ with the diameter=40 nm, water addition rate at 5 mL/h. C: cryo-TEM images of vesicle-cylinder connected MCNs with the middle water addition rate at 5 mL/h and equivalent blending ratio (PAA₁₀₀-*b*-PI₁₅₀: PAA₉₉-*b*-PS₁₆₉=1:1). C was taken of the sample without staining, and D was taken of the same sample as C after staining by OsO₄.

When assembled individually, PAA₁₀₀-*b*-PI₁₅₀ and PAA₉₉-*b*-PS₁₆₉ form vesicles and cylinders, respectively, at 80% water condition (Fig 3.2, Fig 3.3). Interestingly, after blending the two diblock copolymers in pure THF at 1:1 molar ratio, then adding EDDA for an amine to acid ratio of 0.5:1, and finally adding water at a same rate of 5 mL/h, vesicle-cylinder connected nanoparticles were observed (Fig 3.2, Fig 3.5B). Osmium tetroxide was then used to distinguish the PI and PS phases.

3.3.2 Effect of Water Addition Rates on the Assembled Nanostructures at Different Blending Ratio

Previous block copolymer blending results indicate that with proper kinetic control, unique nanoparticle geometries can be confined into one nanoparticle such as hybrid sphere-sphere, sphere-cylinder, disk-cylinder and disk-sphere particles^{22, 23}. However, the study of the effects of kinetic solvent mixing rates has not been presented. The solvent mixing rate plays a crucial role in the design and formation of metastable nanoparticles with new, hybrid shapes. Four different water addition rates were used to explore the impacts and possible nanostructure construction (0.8 mL/h, 5 mL/h, 30 mL/h, >>100 mL/h). Also, three blending ratios of the two block copolymers were used to observe the influence of block copolymer blend composition on final nanostructure formation.

In individual assembly of the two diblock copolymers, a majority of vesicles and cylinders are formed at different water addition rates, respectively (Figure 3.3). After blending, various kind of blended nanoparticles are formed at different combination of water addition rate and blending ratio.

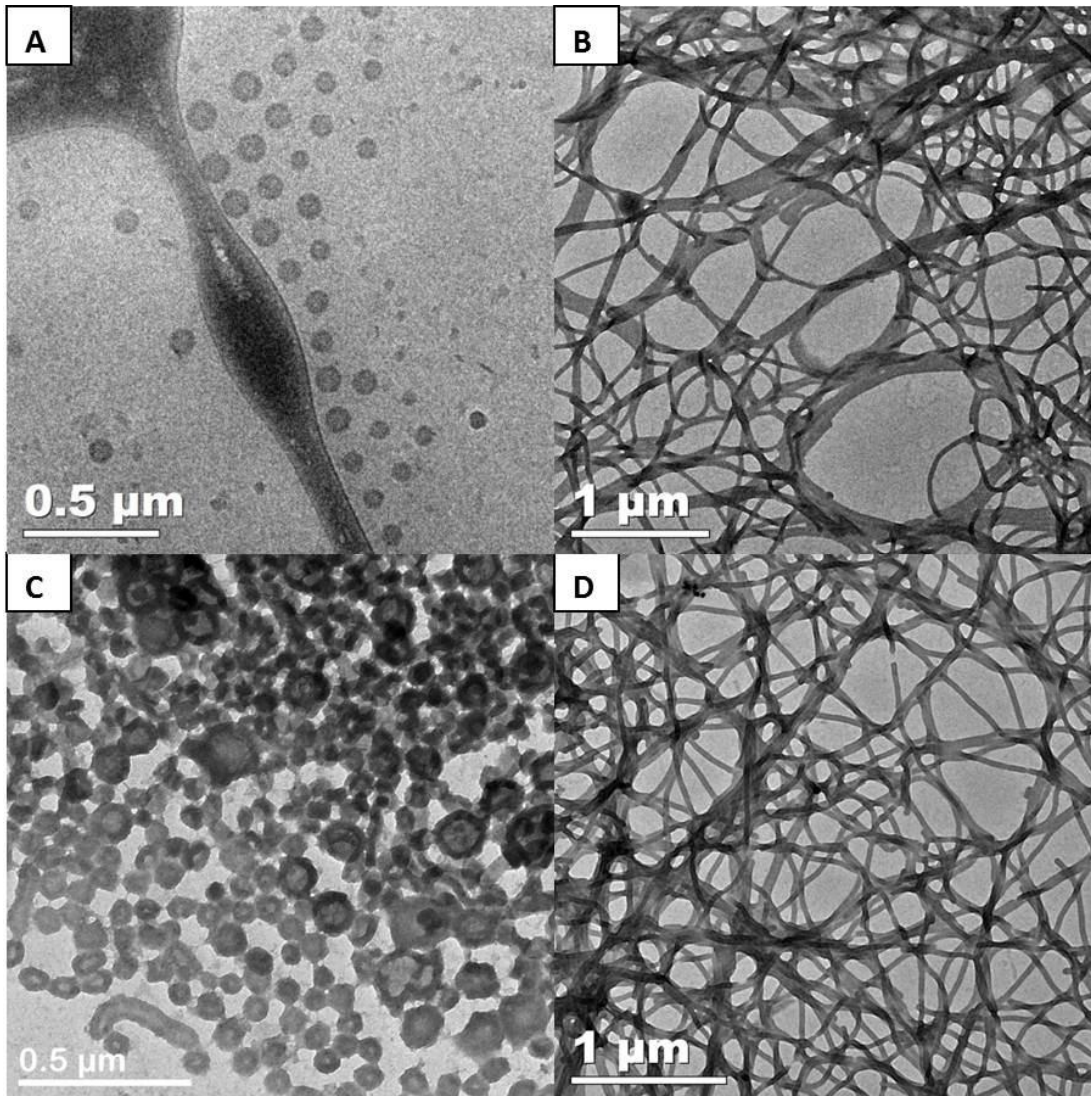


Figure 3.3 Representative TEM and cryo-TEM images of assemblies in different water addition rates in individual diblock assembly, with amine: acid=0.5:1, 80% v/v H₂O/THF. A: cryo-TEM images of vesicles assembled from PAA₁₀₀-*b*-PI₁₅₀, 0.8 mL/h. B: TEM images of cylinders formed from PAA₉₉-*b*-PS₁₆₉ at 0.8 mL/h, with the diameter equals to 40 nm C: TEM images of PAA₁₀₀-*b*-PI₁₅₀ forms vesicles 5 mL/h, with the wall thickness equals to 35 nm, some of the vesicles were aggregated together due to the drying effect in sample preparation. D: PAA₉₉-*b*-PS₁₆₉ forms cylinders with water addition rate at 5 mL/h.

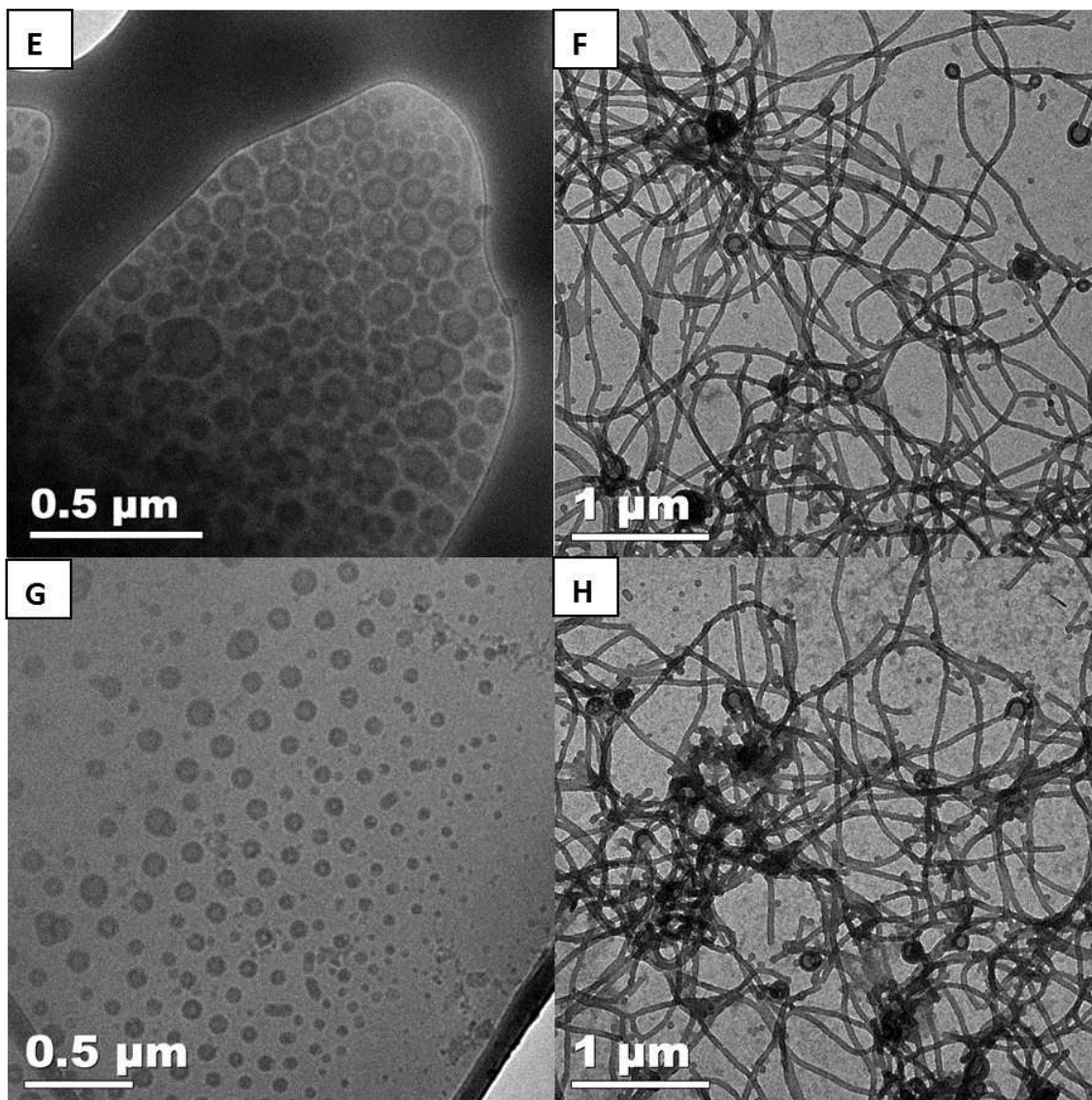


Figure 3.3 Representative TEM and cryo-TEM images of assemblies in different water addition rates in individual diblock assembly, with amine: acid=0.5:1, 80% v/v H₂O/THF. E: PAA₁₀₀-*b*-PI₁₅₀ forms vesicles with water addition rate at 30 mL/h; F: PAA₉₉-*b*-PS₁₆₉ forms cylinders, vesicles with water addition rate at 30 mL/h. G: PAA₁₀₀-*b*-PI₁₅₀ forms vesicles at extreme fast water addition. H: PAA₉₉-*b*-PS₁₆₉ forms cylinders, short cylinders, disk, vesicles and spheres with extreme fast water addition (>>100 mL/h).

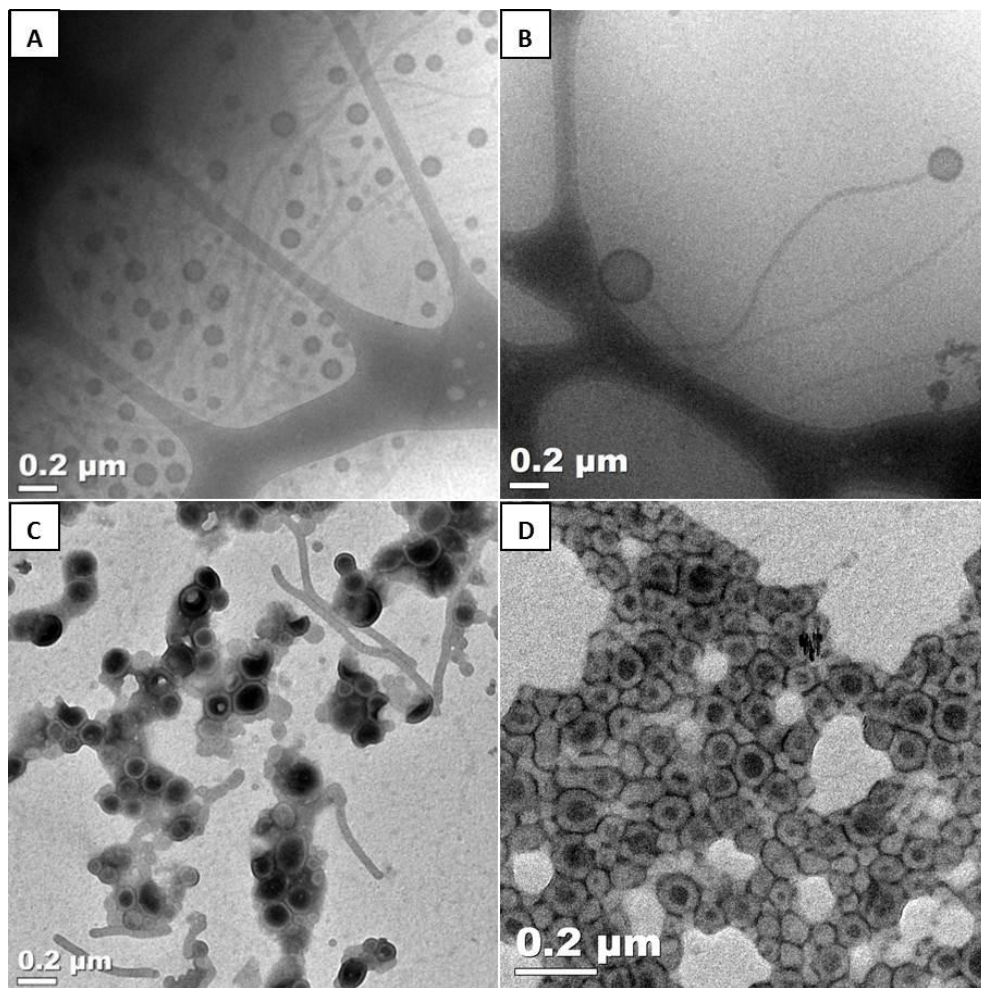


Figure 3.4 Cryo-TEM images of hybrid nanoparticles assembled from blends of PAA₁₀₀-*b*-PI₁₅₀ and PAA₉₉-*b*-PS₁₆₉ diblock copolymers (molar ratio=1:1) with EDDA at amine to acid ratio=0.5:1, in a mixed solvent of THF: water at a volume ratio=1:4 (1 mL THF initial, 5 mL final mixed solution) with different water addition rates. A: Separated vesicles (dominant nanostructure) and cylinders at water addition rate 0.8 mL/h H₂O. B: vesicle-cylinder connected nanoparticles assembled at 5 mL/h water titration rate. C: Disk-cylinder hybrid nanoparticles assembled at 30 mL/h H₂O. D: Disk-Cylinder hybrid nanoparticles assembled at the fasted water addition rate by pipette addition (>>100 mL/h). All solutions were imaged 1 day after the assembly process and vapor stained by OsO₄ for 10-20 minutes.

With the extremely slow addition rate (0.8 mL/h), cryo-TEM images show that separate populations of PAA₁₀₀-*b*-PI₁₅₀ vesicles and PAA₉₉-*b*-PS₁₆₉ cylinders are formed (Fig 3A; 3.5A). Clearly, each diblock copolymer was able to organize into separate particles with preferred curvature during slow water titration as opposed to the formation of multigeometry and multicompartment nanoparticles.

However, when the water addition rate was faster (5 mL/h), connected vesicle-cylinder MCN/MGNs were produced (Fig 3.4B; 3.5B). The PAA₁₀₀-*b*-PI₁₅₀ and PAA₉₉-*b*-PS₁₆₉ block copolymers expressed their own preferred curvatures locally while connected together and shared the same PAA/amine complexed shell. All vesicles in these hybrid nanoparticles exhibit the same wall thickness (~35 nm) as in the pure PAA₁₀₀-*b*-PI₁₅₀ vesicle assembly. Similarly, the cylinder former PAA₉₉-*b*-PS₁₆₉ exhibits the same diameter (~40 nm) as in the separate PAA₉₉-*b*-PS₁₆₉ assembly. Without OsO₄ staining, it is observed that the vesicular head and cylindrical tail in the blended nanoparticle have the same contrast (Fig 3.2 C). After staining, the vesicle domain is darker than the cylinder domains due to the staining of the isoprene block. Additional cryo-TEM images from different imaging areas are provided in supporting images to indicate the formation of vesicle-cylinder connected nanostructure (Fig.3.4 B). In the blended assemblies, diamine molecules play a significant role in helping to trap the different hydrophobic blocks inside the PAA/amine condensed shell. Without the diamine molecules, the diblock copolymer blends are assembled into ill-defined aggregates at different water addition rates (Fig 3.5). The construction of nanoparticles with desired formation of different compartments in the core domain relies on the amine/acid electrostatic complexation in the shared PAA/amine shell.

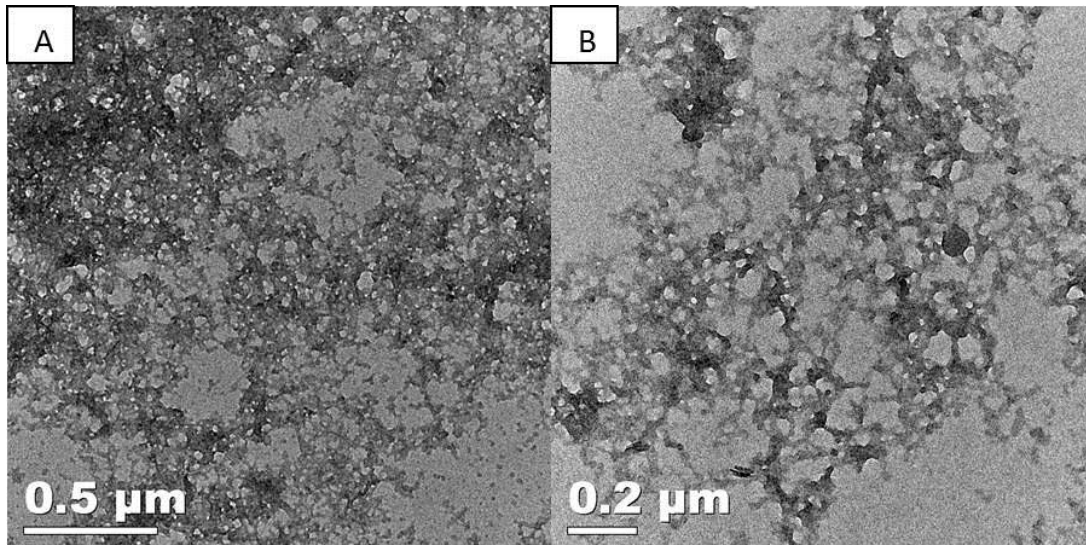


Figure 3.5 A: cast-film TEM images of assemblies of PAA₁₀₀-*b*-PI₁₅₀ and PAA₉₉-*b*-PS₁₆₉, blending ratio=1:1, without amine, in a fast water addition rate (30 mL/h), v/v 80% H₂O/20% THF. A, Aggregations without any morphology control were observed as compared to samples with the diamine complexation; B, cast-film TEM images of blends of PAA₁₀₀-*b*-PI₁₅₀:PAA₉₉-*b*-PS₁₆₉=1:1, without amine, in a slow addition rate pathway (0.8 mL/h).

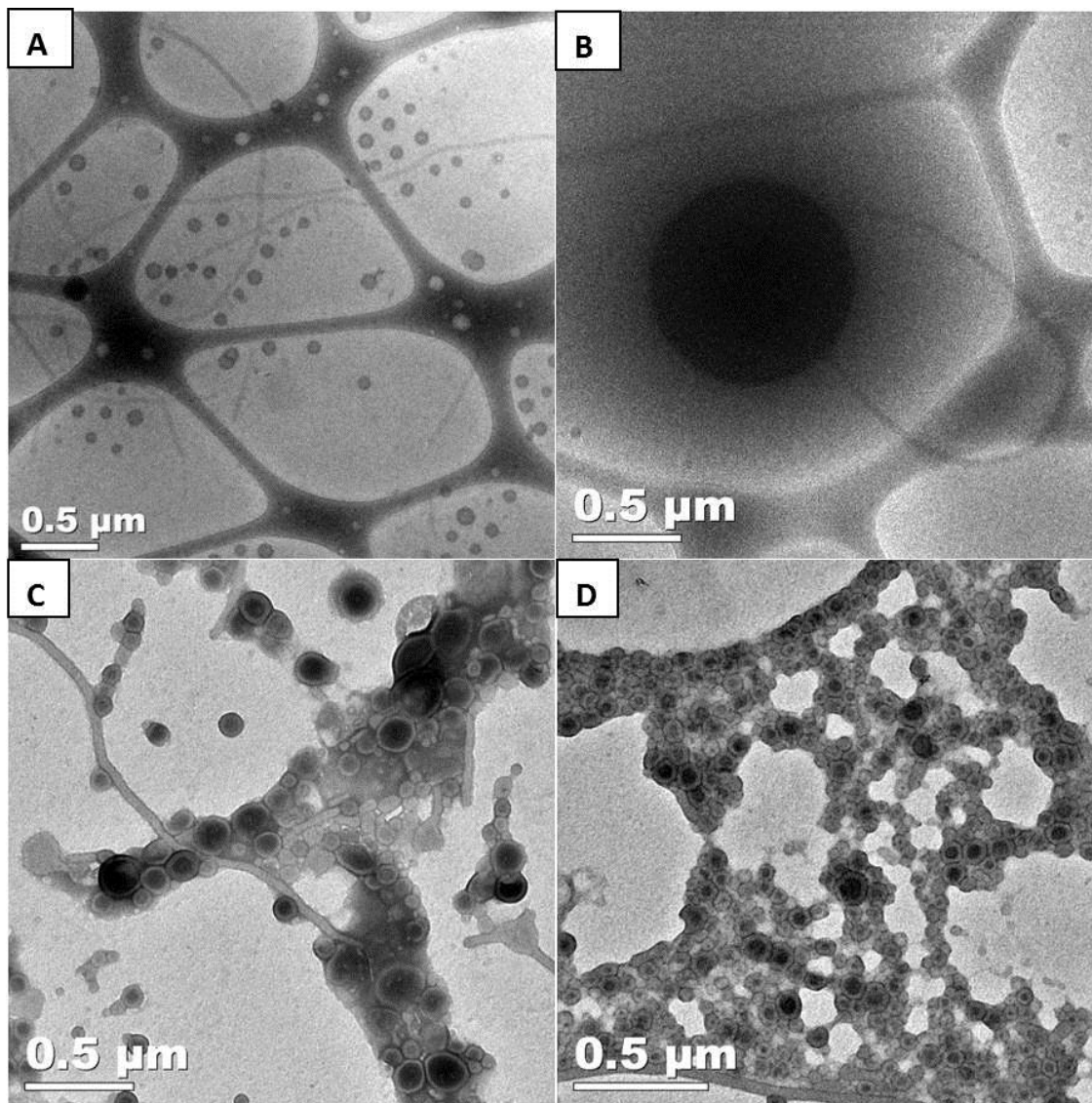


Figure 3.6 Additional representative TEM and cryo-TEM images of assemblies in different water addition rates in blends of PAA₁₀₀-*b*-PI₁₅₀ : PAA₉₉-*b*-PS₁₆₉=1:1, amine:acid=0.5:1, 80% v/v H₂O/ THF. A: separate vesicles and cylinders at extreme slow water addition rate of 0.8 mL/h. B: vesicle-cylinder connected MCN formed at middle water addition rate of 5 mL/h. C: Disk-Cylinder MC disks formed at fast water addition rate of 30 mL/h. D: Disk-Cylinder MC disks formed at extremely fast water addition rate of >>100 mL/h.

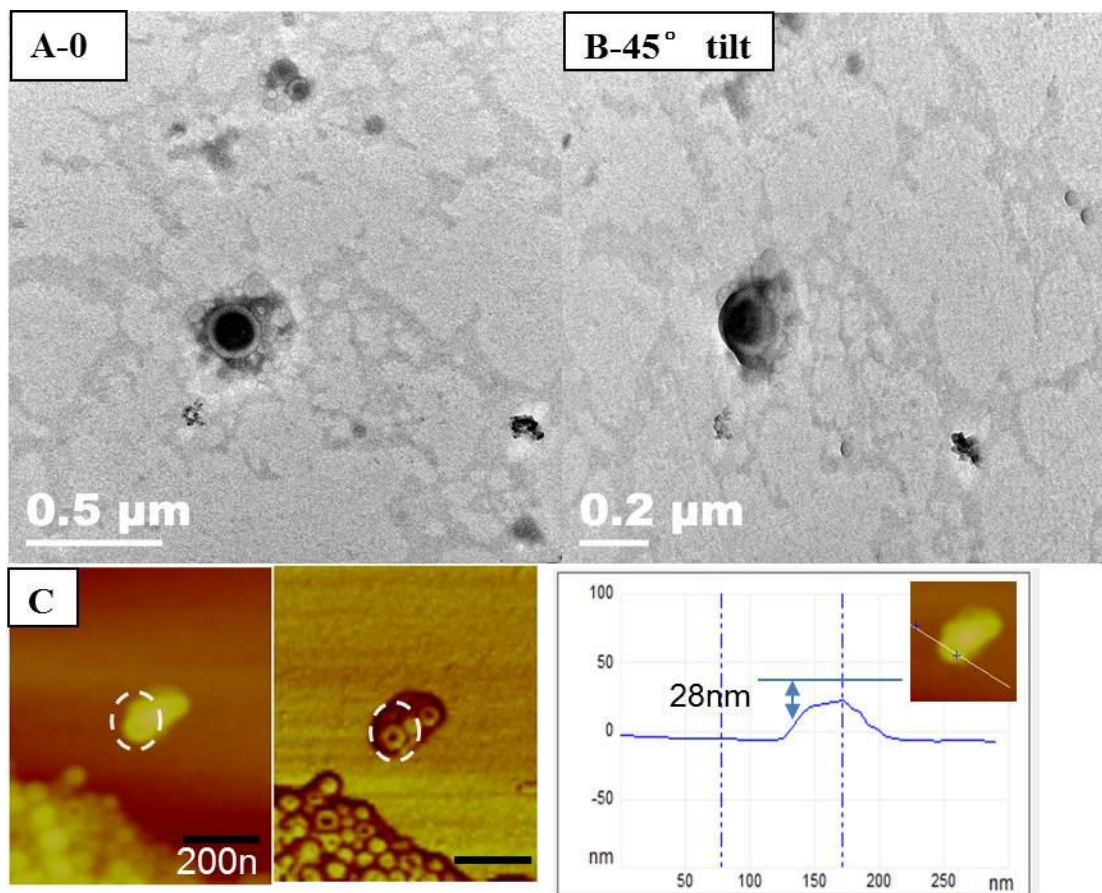


Figure 3.7 (A, B): cast-film TEM image of Disk-cylinder MC disk nanoparticles, same sample as it is in Figure 3.6 C. B: tilted sample stage to 45° to observe the ellipse MCN nanoparticles. C. AFM images indicating the height information of disk-cylinder nanoparticles.

To further verify the particle disk morphology and measure particle thickness, tilted TEM and AFM characterization were performed. If disks exist, the tilting stage will alter the 2-dimensional particle projection from circles to elliptical shape. An image with tilt angle of -45° is provided in Fig 3.7, and confirms the overall disk shape of the disk-cylinder MC disk nanoparticles. The theoretical thickness of the inner disk piece should be the same as the wall thickness of bilayer vesicles in PAA₁₀₀-PI₁₅₀ assembly (~ 35 nm). The height information from AFM measurement is

similar to theoretical value but consistently lower. This is due to the slight shrinking of the nanoparticles during solvent drying on sample preparation.

In the extreme fast water addition, water is added by using a pipette to immediately change the solvent condition ($\gg 100$ mL/h). Similar to the fast addition rate (30 mL/h), disk-cylinder shaped MCN/MGNs are formed with flat polyisoprene-core domains bordered by half polystyrene-core cylindrical rims. The disk-cylinder particles display a more homogeneous size as compared to the fast addition rate (30 mL/h) with a rare, discrete cylinder also observed (Fig 3.6D). A comparison of the overall sizes of the disk-cylinder MCNs at the two different water addition rates was performed by measuring the diameters of a sample of nanoparticle across different imaging areas (50-100 nanoparticles in 10 different images). Slight differences of the diameters are observed as shown in Figure 3.12. Additional cryo-TEM images from different imaging areas are provided to indicate the formation of vesicle-cylinder connected nanostructure (Fig 3.6, A-D).

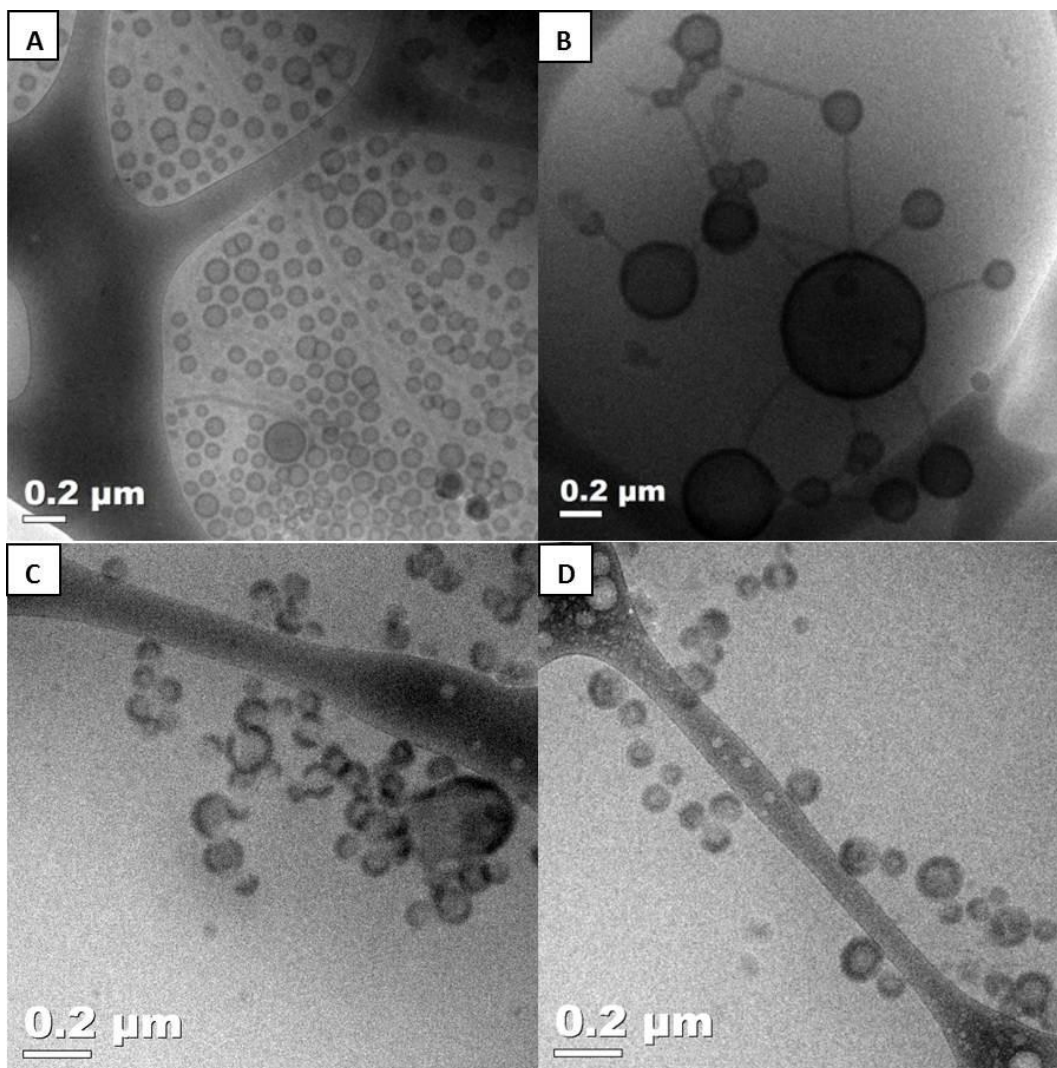


Figure 3.8 Cryo-TEM images of hybrid nanoparticles assembled from blends of PAA₁₀₀-*b*-PI₁₅₀ and PAA₉₉-*b*-PS₁₆₉ diblock copolymers (molar ratio=9:1) with EDDA at an amine to acid ratio=0.5:1. The final solvent mixture is THF: water volume ratio=1:4. Each image resulted from a different water addition rate. A: separated vesicles and cylinders at water addition rate of 0.8 mL/h; B: vesicle-cylinder connected hybrid nanoparticles, assembled at 5 mL/h, DI water was titrated to THF; C: Hybrid vesicles with dark wall domain (PI) and light wall domain (PS) assembled at 30 mL/h H₂O. D: Hybrid vesicles assembled with the extremely fast water addition rate, H₂O was added into THF by using pipette. All solutions were imaged 1 day after the assembly process and vapor stained by OsO₄ for 10-20 minutes.

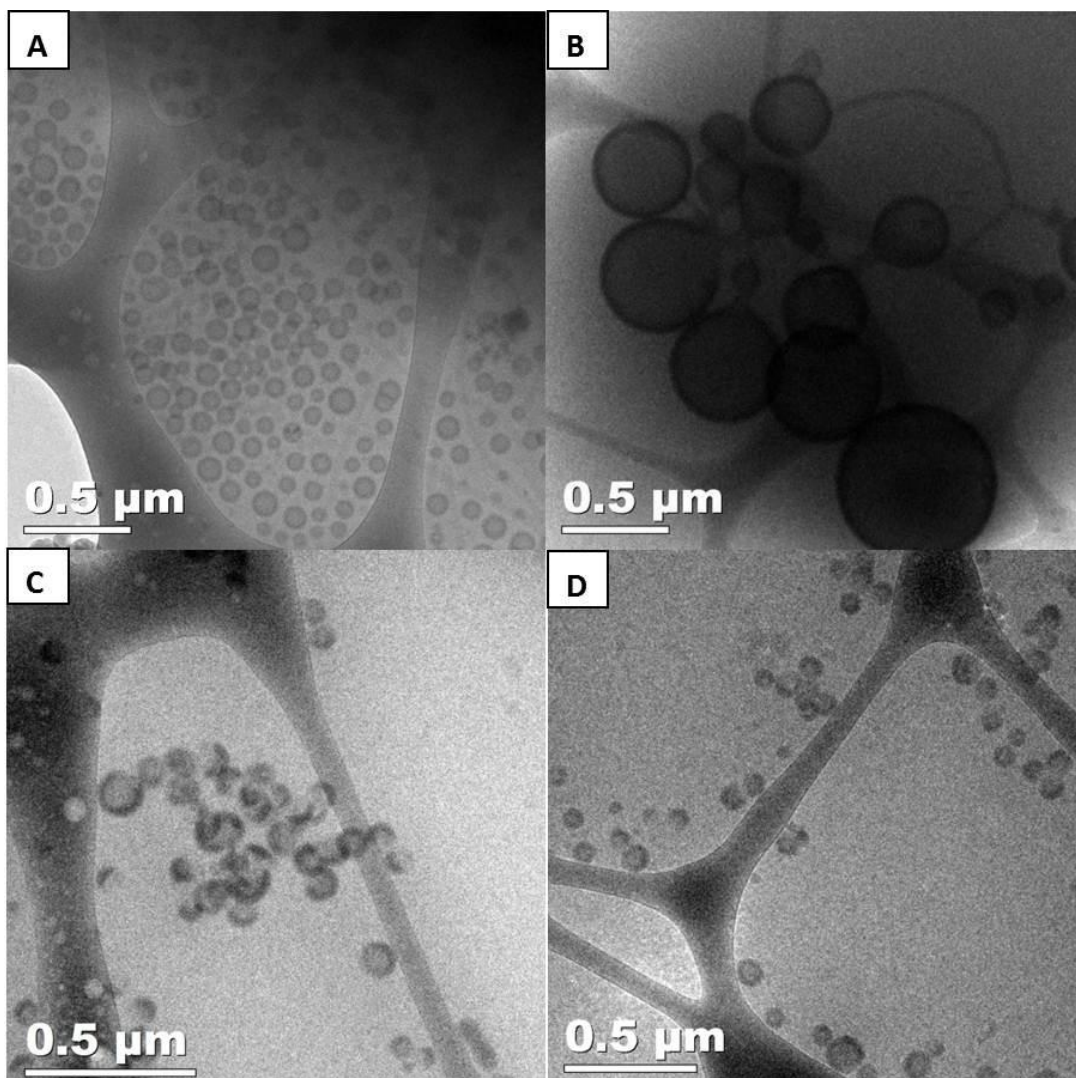


Figure 3.9 Additional representative TEM and cryo-TEM images of assemblies in different water addition rates in blends of PAA₁₀₀-*b*-PI₁₅₀: PAA₉₉-*b*-PS₁₆₉=9:1, amine:acid=0.5:1, 80% v/v H₂O/THF. A: separate vesicles and cylinders formed at extreme slow water addition rate of 0.8 mL/h. B: vesicle-cylinder connected MCN formed at middle water addition rate of 5 mL/h. C: Hybrid vesicles formed at fast water addition rate of 30 mL/h. D: Hybrid vesicle MCN formed at extreme fast water addition rate of >>100 mL/h.

By changing the blending ratio to a dominant vesicle former condition (PAA₁₀₀-*b*-PI₁₅₀:PAA₉₉-*b*-PS₁₆₉=9:1), unblended or blended MCN/MGNs are formed

depending on the different water addition rates. At the extreme slow water addition rate (0.8 mL/h), again separate populations of vesicles and cylinders are formed, Fig.3.8A. Vesicle-cylinder connected nanoparticles with more vesicles linked by fewer cylinders are observed in the middle water addition rate (5 mL/h), Fig 3.8B. However, when the fast rate (30 mL/h) is used, novel, kinetically-trapped, multicompartment vesicles are formed. Due to the dominant molar fraction of the PAA₁₀₀-*b*-PI₁₅₀ vesicle former, the overall particle morphology is a vesicular shape with the PAA₉₉-*b*-PS₁₆₉ cylinder former constrained inside the same bilayer wall. The partial dark and partial light domains shown in Fig 3.8C are attributed to the stained PI and unstained PS blocks, respectively. When the extreme fast water addition rate is used (>>100 mL/h), hybrid vesicles (Fig 3.8D) with a quite uniform diameter were observed. To compare the difference in size between the two populations of vesicles, diameters of the hybrid vesicles constructed with two different water addition rates were measured. Smaller and more monodisperse hybrid vesicles are formed with the extremely fast rate, Figure 3.12. In order to form the hybrid vesicles, mixed hydrophobic chains from two block copolymers must locally separate and migrate into different domains in the same vesicle wall. Since the dominant block copolymer component is a vesicle former, the overall morphology of the mixed nanoparticle remains a vesicle here as opposed to the stabilization of disk particles observed in the 1:1 blending ratio at faster water addition rates in Figure 3.4D. Additional representative images are provided in Figure 3.9A-D.

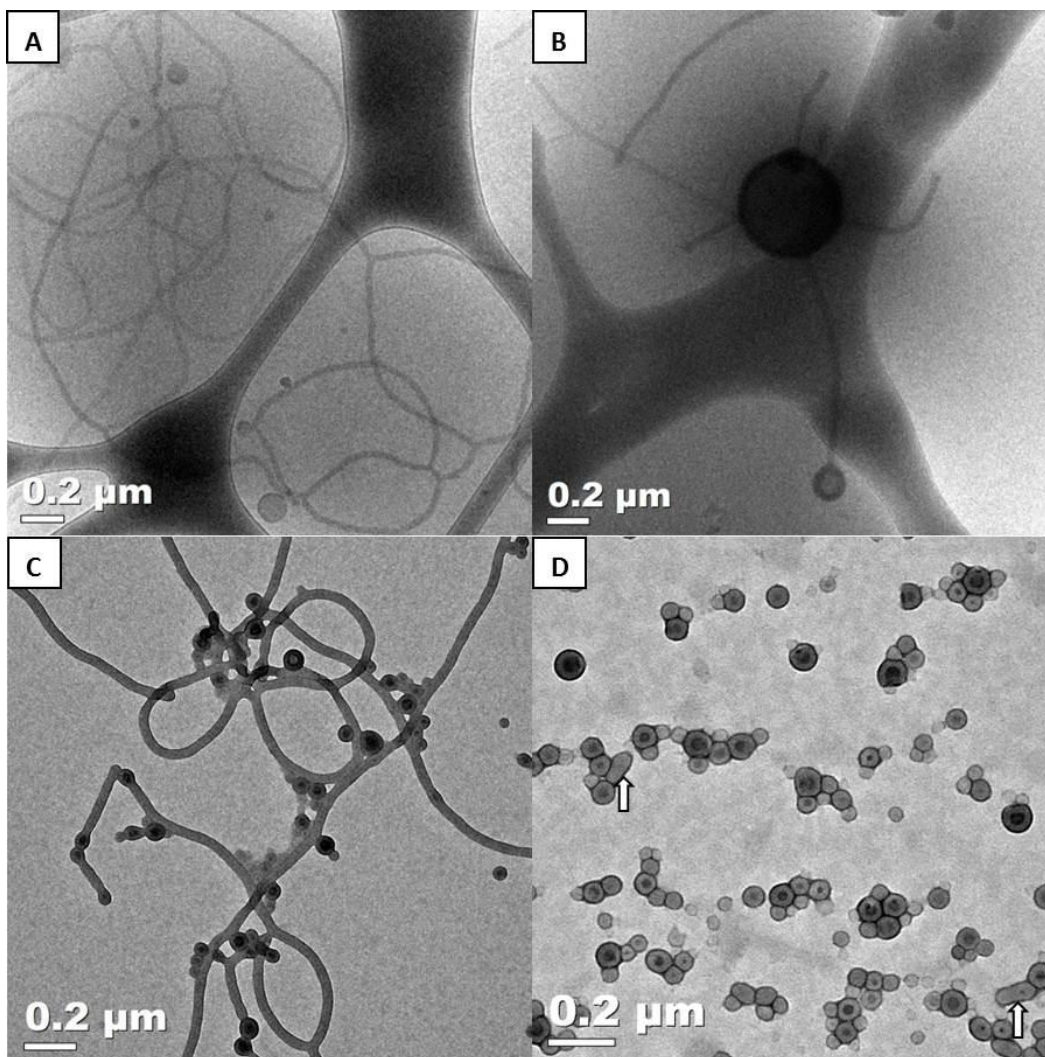


Figure 3.10 TEM images of hybrid nanoparticles assembled from blends of PAA₁₀₀-*b*-PI₁₅₀ and PAA₉₉-*b*-PS₁₆₉ diblock copolymers (molar ratio=1:9) with EDDA at an amine to acid ratio=0.5:1, THF: water volume ratio=1:4 and different water addition rate. A: separated vesicles and cylinders at water addition rate of 0.8 mL/h H₂O, B: vesicle-cylinder connected nanoparticles assembled at 5 mL/h water titration rate. C cylinder-disk hybrid nanoparticles assembled at 30 mL/h H₂O. D: disk-cylinder hybrid nanoparticles assembled at extreme fast water addition, >>100 mL/h. Arrows point to the short cylinders in disk-cylinder structure. All solutions were observed 1 day after assembly process and vapor stained by OsO₄ for 10-20 minutes.

At the blending ratio of 1:9 of PAA₁₀₀-*b*-PI₁₅₀ to PAA₉₉-*b*-PS₁₆₉, a trend of nanostructure formation similar to what was observed at the same water addition rates but at different block copolymer blending ratio is obtained. Separate populations of vesicles and cylinders (now with fewer vesicles and more cylinders) are formed with the extreme slow water addition rate (0.8 mL/h, Fig 3.10A). Connected vesicle-cylinder multicompartment and multigeometry nanoparticles with more cylinders around each vesicle are observed in the middle water addition rate (5 mL/h, Fig 3.10B). In the fast water addition rate (30 mL/h, Fig 3.10C), a small population of disk-cylinder nanoparticles was observed along with many separate cylinders as well as cylinders with disk endcaps. When water is added in an ultra-fast way (>>100 mL/h), disk-cylinder shaped nanoparticles are formed with rare short cylinders as indicated by the arrows (Fig 3.10D). The inner disk pieces are much smaller (5 nm-50 nm) than observed in the disks (10 nm-80 nm) assembled with the equivalent blending ratio of block copolymers in Fig 3.4D. Additional representative images are provided in Figure 3.11. By adjusting the initial blending ratio, well-defined MCN/MGNs nanoparticles with controlled overall size and also the size of different compartments are achieved.

Table 3.5 Summary of PAA₁₀₀-PI₁₅₀/PAA₉₉-PS₁₆₉ blending results in different conditions

PAA ₁₀₀ - <i>b</i> -PI ₁₅₀ : PAA ₉₉ - <i>b</i> -PS ₁₆₉ molar ratio/ H ₂ O to THF volume ratio	9:1	1:1	1:9
Extremely slow (0.8 mL/h)*	Vesicle+cylinder	Vesicle+cylinder	Vesicle+cylinder
Middle rate (5 mL/h)	Vesicle-cylinder	Vesicle-cylinder	Vesicle-cylinder
Fast rate water (30 mL/h)	Hybrid vesicle	MC Disks	MC Disks
Extreme fast (>>100 mL/h)	Hybrid vesicle	Disk-cylinder	MC Disks

*: water addition rates were listed in a way of volume of water added per hour to 1ml initial THF solution. MC disks represent for the disk shaped exotic nanoparticles having disk-cylinder immiscible domains.

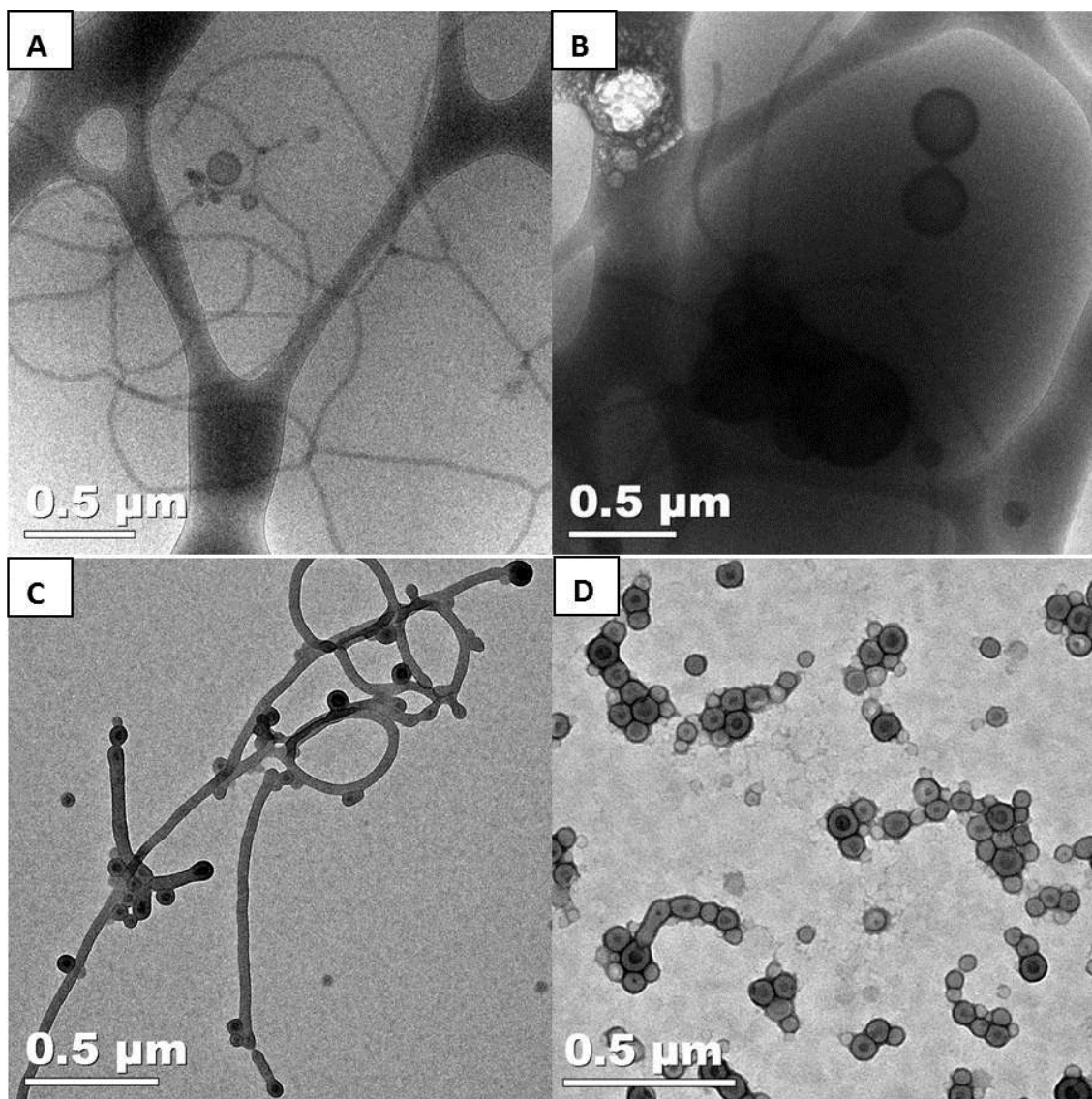
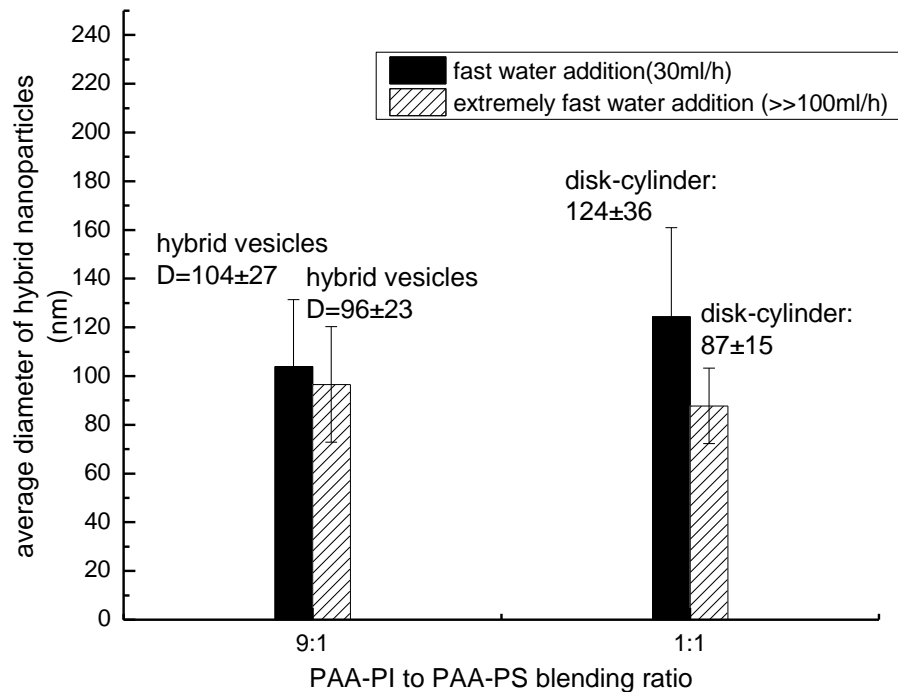


Figure 3.11 Additional representative TEM and cryo-TEM images of assemblies in different water addition rates in blends of PAA₁₀₀-*b*-PI₁₅₀ : PAA₉₉-*b*-PS₁₆₉=1:9, amine:acid=0.5:1, 80% v/v H₂O/THF. A: separate vesicles and cylinders formed at extreme slow water addition rate of 0.8 mL/h. B: vesicle-cylinder connected MCN formed at middle water addition rate of 5 mL/h. C: Disk-Cylinder MCN/MGN formed at fast water addition rate of 30 mL/h. D: Disk-cylinder MCN formed at extreme fast water addition >>100 mL/h.



Comparison of the average sizes of nanoparticle in fast water addition and water quenching

Figure 3.12 Comparison of diameters of the nanoparticles at fast water addition and extremely fast water addition rates. Numbers were collected from multiple nanoparticles in different imaging areas. Left column: The graph shows the average diameter of hybrid vesicles at fast water addition and extremely fast water addition rates. The diameters of 118 hybrid vesicles were measured in different imaging areas at fast water addition rate (30 mL/h). The diameters of 113 hybrid vesicles were measured in different imaging areas at extremely fast water addition rate (>>100 mL/h). Right column: The graph shows the average diameter of disk-cylinder hybrid nanoparticles at fast water addition and extremely fast water addition. The diameters of 146 hybrid disk-cylinder nanoparticles were measured in different imaging areas. The diameters of 120 hybrid disk-cylinder nanoparticles were measured in different imaging areas. The diameters of both hybrid vesicles and disk-cylinder nanoparticles decreased in faster water addition condition.

It is clear when comparing nanoparticles formed by different water addition rates that there are gross differences in the assembly behavior observed, which are dependent on the degree to which the blended block copolymers are kinetically trapped locally within a particle. For example, macrophase separation clearly is possible between unlike block copolymers during the extreme slow water addition despite the fact that the unlike block copolymers were initially complexed together in pure THF solution by the presence of the organic amines. This macrophase separation consistently produced separate nanoparticles of exclusively vesicle or cylinder geometry with no hybrid structures observed. However, at faster water addition rates, the unlike block copolymers are forced to reside in the same nanoparticle and produce particles with hybrid geometry. Even within the faster water addition rates, there is a rich variety of assembly behavior in the hybrid particles formed, showing the importance of the differences in local nanophase separation on the final particle structure. In all hybrid particles formed, the presence of the EDDA diamine is significant to trap the different hydrophobic blocks within the same final particles. Without the EDDA, the well-defined hybrid nanoparticles are not achievable (Fig. 3.5).

3.3.3 Structure Evolution of Multicompartment Nanoparticles

Since the hybrid particle formation is the result of a kinetic process, the structure is only metastable and may change over time. The structure evolution of nanoparticles is an important topic in macromolecule self-assembly, due to the formation of unusual nanostructures resulting from diverse evolution mechanisms. Structure evolutions could be caused by a change in chemical structure, addition of external stimuli to the assembly solution and interparticle or intraparticle chain exchange in selective solvent²⁴. For example, the Hillmyer group has reported incorporation of pH-sensitive degradable blocks in star-like triblock copolymer and the subsequent pH-tuning of block degradation and micelle evolution²⁵. Another good example is the micelle-to-micelle morphology evolution reported by the Lodge group

in which immiscible PEE (polyethylene) and PMCL (polymethyl-caprolactone) hydrophobic blocks are covalently-linked in a triblock copolymer, and intramicelle structure evolution happened in selective solvents *via* dynamic slow chain exchange²⁶.

In the current assembly system, multicompartment nanoparticle evolution occurred in the hybrid vesicle systems observed in Figure 3.13 C and 3.13 D. During the ultra-fast water addition process, two immiscible hydrophobic blocks were confined into a vesicular geometry. The trapped PI and PS blocks experience chain reorganization in mixed solvent. It is shown clearly in Figure 3.13 that the mixed vesicles contain the segregated phases of the PI and PS blocks in the vesicle walls. However, after ageing, further transformations occurred with the hybrid vesicles (Fig 3.13 A) where the particles joined together to form larger, compound vesicles with a preference of the PI membrane portions to lie on the interior of the hybrid particles (Fig 3.13 C, D). The wheel-like structures stay stable after three months of ageing (Fig 3.13 D). The diameter of the nanoparticles changes from around 100 nm (Fig 3.13 A) to 140 nm (Fig 3.13 D). The wheel-like structures seem like aggregates of several small vesicles from early time points. The majority phase is still PI and the minority phase PS may join together to stabilize the inter-vesicle junction. Since all of the nanoparticles are kinetically trapped, fluid assemblies, transitions with ageing are always possible. The transition of the hybrid vesicles is the only clear transition observed in the currently discussed set of blended particles and simply shown for illustrative, descriptive purposes at this point. The transition only occurs with apparent interparticle interaction over time since the PI-rich membrane portions seem to remain intact as well as the PS-rich domains. If one wishes to guarantee the persistence of a particular hybrid particle size/shape after formation, then covalent trapping of the particle is suggested^{27, 28} in order to prevent ageing and further structure evolution. Further evolution of the hybrid vesicles may occur over time as the PS-containing block copolymer seeks a higher interfacial curvature and cylindrical geometry, although we have not observed this transition over several months of aging.

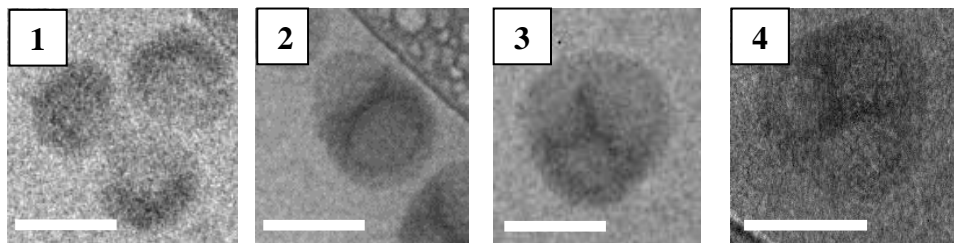
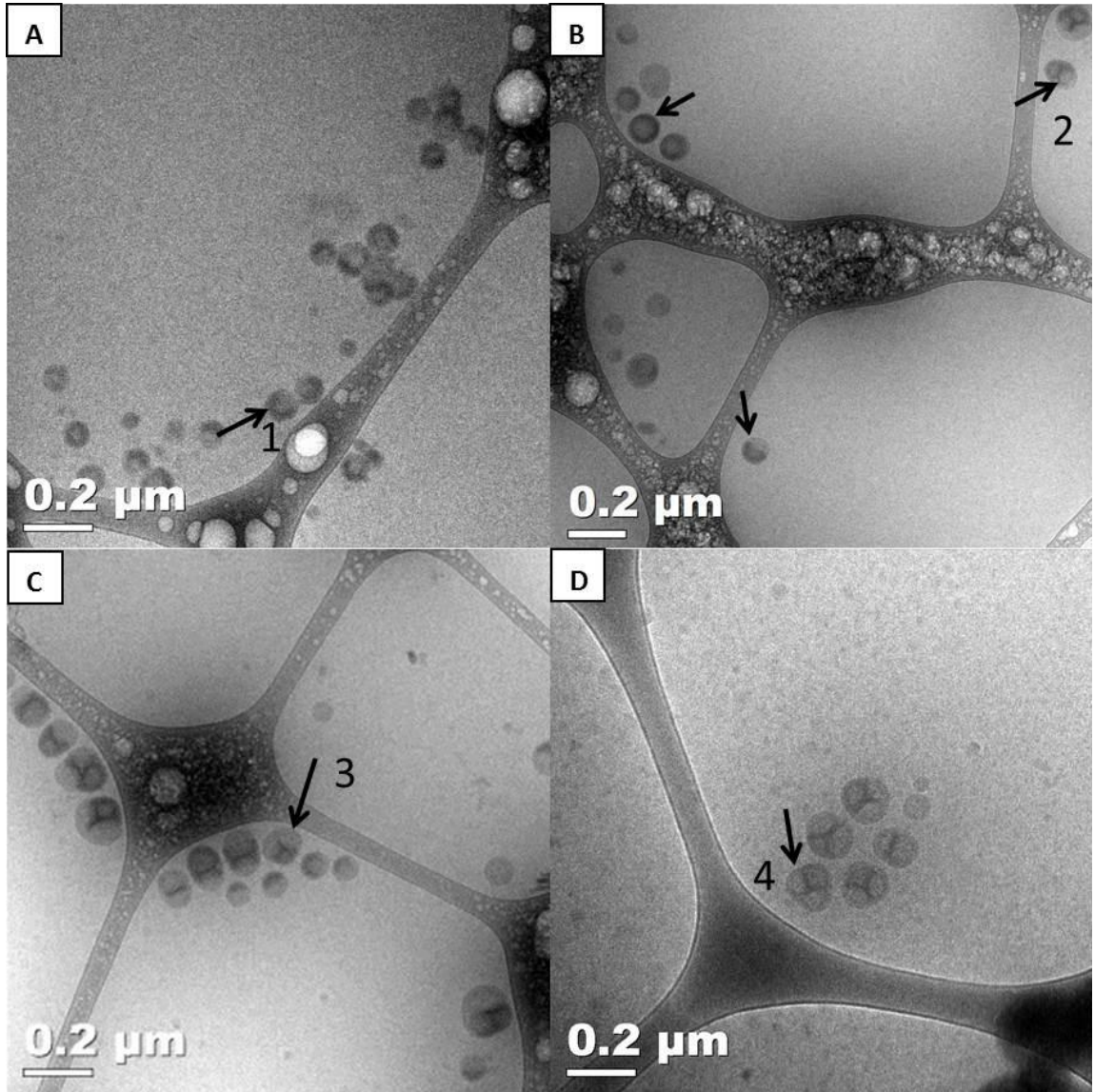


Figure 3.13 Aging results of multicompartiment hybrid vesicles. Image A: cryo-TEM image of hybrid vesicles constructed from blends of PAA₁₀₀-*b*-PI₁₅₀: PAA₉₉-*b*-PS₁₆₉=9:1 with extremely fast water addition (>>100 mL/h) after sample ageing for 1 day. B: same sample after aged for one month. C: sample aged for two months. D: sample aged for three months. 1-4, selected snapshots from image A, B, C, D to show the signature micelle evolution status in different ageing points. 1: hybrid vesicles; 2: asymmetric hybrid vesicles with extended PS wall and PI phase; 3: asymmetric wheel-like hybrid vesicle; 4: larger magnification of asymmetric wheel-like hybrid vesicle from aggregates of hybrid vesicles. Inserted scale bar: 100 nm.

3.3.4 Small Angle X-ray Scattering Results

Although microscopy provides unique and intuitive structural insights, the sample size that can be investigated locally by microscopy is much smaller than the global sample size that can be examined with scattering techniques. To understand the assembled nanostructures in a more comprehensive way, SAXS was performed to characterize the global structure of the particles in solution.

As mentioned above, gross differences of self-assembly behaviors are observed at different water addition rates. During the water addition process, the two diblock copolymers are subject to continuous solvent condition changes and, thus, solubility fluctuations. Many intermediate structures are produced during the assembly pathway (water addition, inter-micelle growth, intra-micellar segregation, morphology evolution) in seconds to minutes. Continuous phase separation and morphological transitions occur during the process. From the imaging results, it is hypothesized that the binary blend system undergoes macrophase separation in extremely slow water addition conditions but produces blended particles with internal nanophase separation in fast water addition rate conditions through which unlike block copolymers are trapped together in the same particle. In an attempt to observe the above different processes, a detailed morphology study of the nanostructures assembled during the entire water addition processes was required. To investigate the nanostructures at different solvent conditions, SAXS measurements were performed at many different

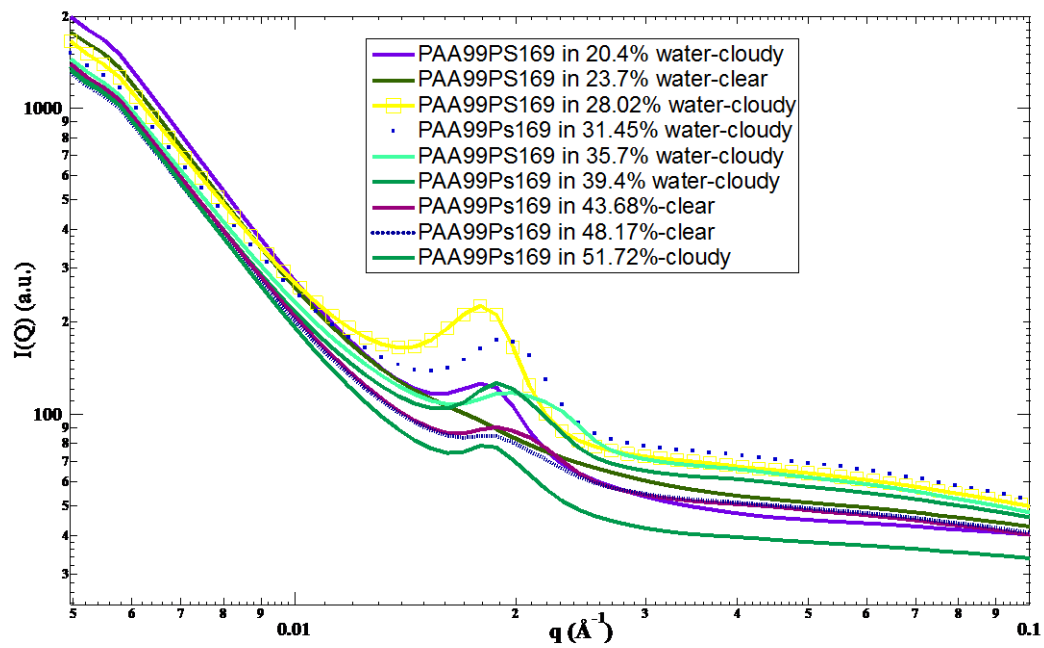
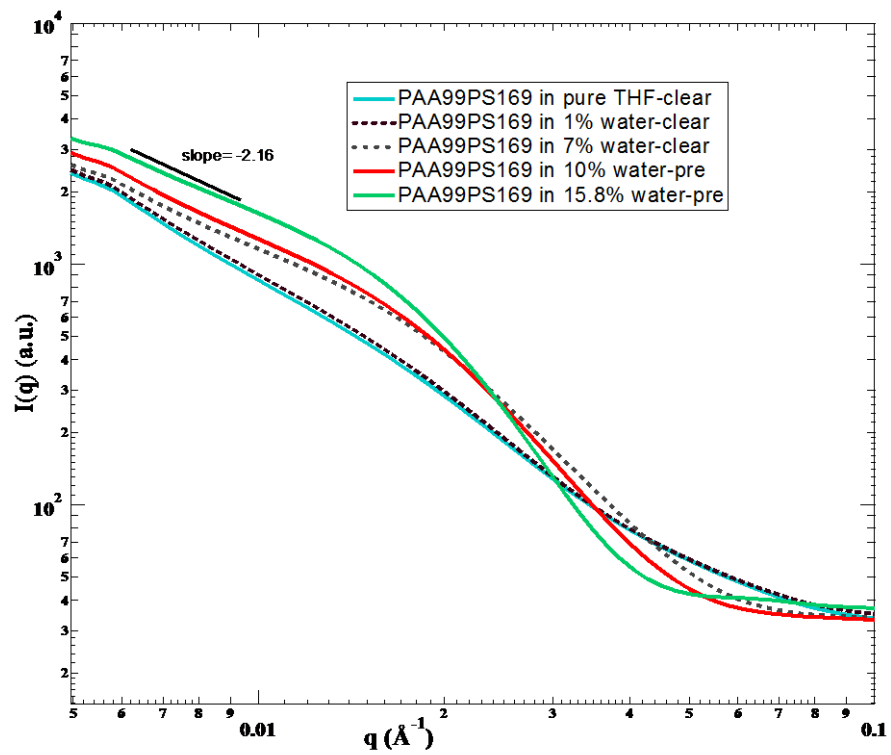
solution conditions during particle assembly. Morphologies corresponding to the structures shown in the imaging results in high water condition (80% H₂O) and the morphologies in many lower water conditions (from 0% water to 80% water with every 2~3% water interval) were interrogated by SAXS.

Four groups of nanostructures across all water addition rates were observed by SAXS and then compared: the solution assemblies of single PAA₉₉-*b*-PS₁₆₉ with extreme slow water addition; the solution assemblies of single PAA₁₀₀-*b*-PI₁₅₀ with extreme slow water addition; the solution assemblies of blends of PAA₉₉-*b*-PS₁₆₉ and PAA₁₀₀-*b*-PI₁₅₀ with extreme slow water addition; the solution assemblies of individual assembly of PAA₉₉-*b*-PS₁₆₉ and PAA₁₀₀-*b*-PI₁₅₀, respectively, and blends of PAA₉₉-*b*-PS₁₆₉ and PAA₁₀₀-*b*-PI₁₅₀ with fast water addition rates. All the solution assemblies are prepared in the same procedure as described earlier, with amine to acid at 0.5:1.

The SAXS curves of the aggregates formed from PAA₉₉-*b*-PS₁₆₉ at each water condition are presented in Figure 3.14. The corresponding TEM results are shown in Figure 3.15. In the assembly, PAA₉₉-*b*-PS₁₆₉ is firstly dissolved completely in THF to form a homogeneous, optically clear solution. Then, diamine is added to complex with the PAA block to produce PAA-amine aggregates. Water was then added using a syringe pump in an extreme slow rate (0.5 mL/h). The diblock is still solvated at low water conditions (1%-7% H₂O), and the solution is still clear. Aggregates are then expected with the addition of organic amine with the structure of an amine/acid complexed core and PS shell which are formed at 7% H₂O. Higher scattering intensity was observed in this water content (7%) relative to lower contents (1-6%), which means larger scatters are formed at this water condition commensurate with the precipitation of polymer rich particles at these low-to-middle water concentrations. The successive addition of water into the system changed the clear solution to a precipitated, phase separated state above 15.8% water content, with the PAA-amine core aggregated changed to extended giant membrane structures at around 15% water content (Fig 3.14). As can be seen, no clear structure factor/diffraction peaks are

observed at low water contents, suggesting that the contribution of the interparticle scattering is negligible in dilute solution. The fitting of mid- q data to a power-law in the low water content solutions (here the slope of SAXS curve at 10% was calculated as a representative) shows that the slope of $\log(I)$ vs $\log(q)$ is near 2 implying that two dimensional membrane-like assemblies are the main scatters²⁹.

The addition of water to above ~20% triggers the PAA-amine core particles to further associate together resulting in precipitated large particles (Fig 3.14). Sequential addition of higher relative amounts of water prompts the formation of large particles with some type of local nanostructure, which was indicated by the Bragg diffraction peak clearly observed at mid- q . The scattering peaks correspond to a periodic spacing equal to 30-33 nm for the solution assemblies from 28% to 52% H₂O (Fig 3.14). Sequentially, the lamellar to vesicle (63%), vesicle to cylinder transitions are expected at higher water conditions (75% H₂O) and are confirmed *via* cast-film TEM imaging (Fig 3.15). The periodic nanostructure within the precipitated particle is difficult to assign with SAXS alone and requires TEM to help in understanding the nanostructure present. While Figure 3.15 provides TEM evidence for bicontinuous or lamellar-like nanostructures within the precipitated particles, more work needs to be done to unambiguously determine the precipitated particle internal morphology²⁸. At higher water content (63%), the diffraction peak disappears coinciding with the solution becoming optically clear with polymer resuspended in the solvent as nanoparticles. Cylinders are observed at higher water conditions (75% H₂O) and confirmed *via* cast-film TEM imaging.



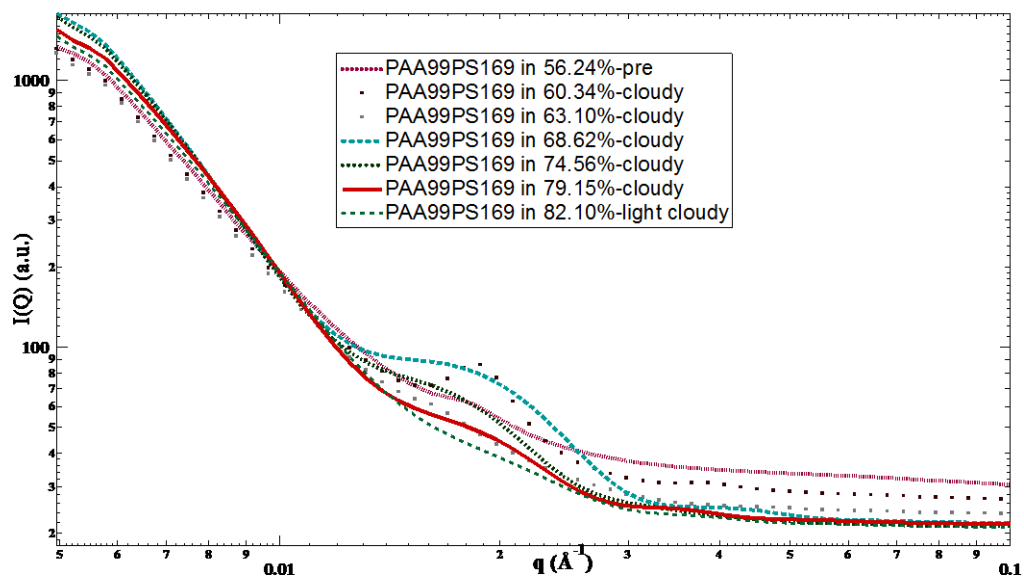


Figure 3.14 SAXS traces of the assemblies formed in different water contents from PAA₉₉-*b*-PS₁₆₉, amine to acid=0.5:1 in separate water regimes. Scattering peaks were observed in middle water concentration regimes, corresponding to a d-spacing in the range of 30-33 nm. In the inner window markers, pre represents precipitation.

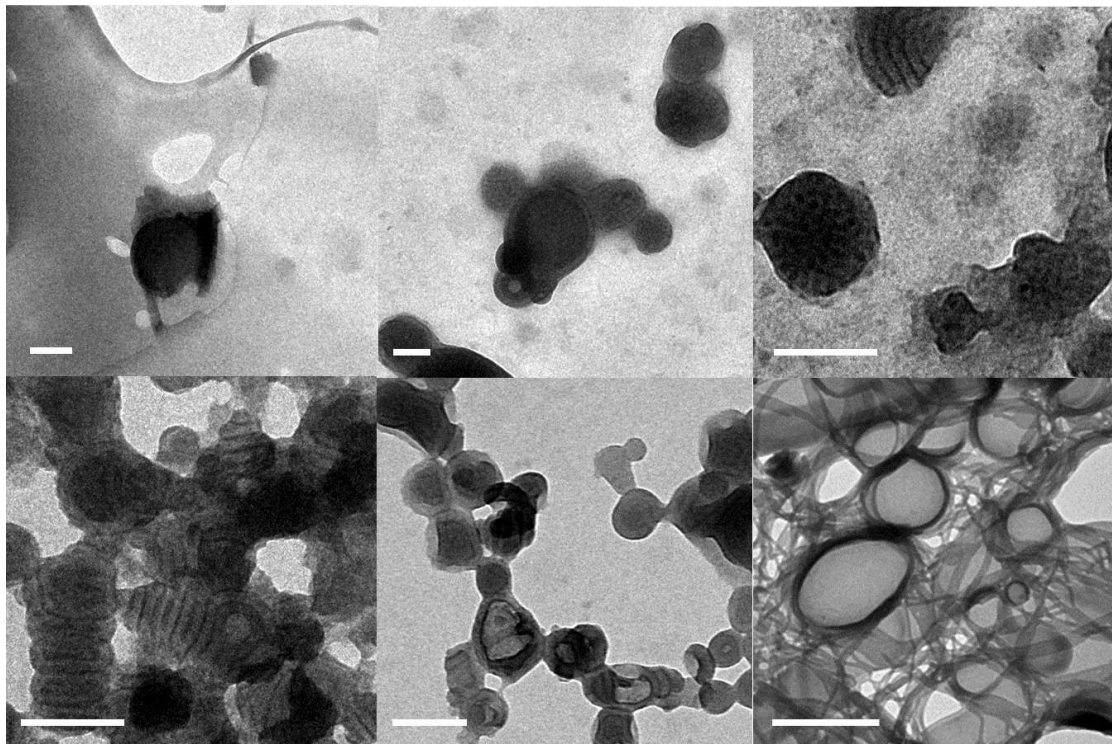


Figure 3.15 Representative cast film TEM images of nanostructures assembled by PAA₉₉-*b*-PS₁₆₉ with amine to acid=0.5:1. A: 15% H₂O condition, giant membrane, precipitated suspensions. B: 24% H₂O condition, cylinder bundles suspended in cloudy solution. C: 28% H₂O condition, close packed cylindrical bundles suspended in cloudy solutions. D: 40% H₂O condition, lamellar structure with the d-spacing of 32 nm confirmed by TEM and SAXS. E: 50% H₂O condition, intermediate nanostructures of lamellar transiting to vesicle transition. F: 75% condition, vesicle to cylinder intermediate structures. Inserted scale bar: 200 nm.

PAA₁₀₀-*b*-PI₁₅₀ assembled with diamine at the same water contents with slow water addition yielded different results as the PS-based block copolymer. No clear scattering peaks were observed in the middle relative water contents, possibly due to the fluid nature of the PI phase which would be swollen with solvent and, perhaps, not well nanophase separated from the PAA-amine phase (Figure 3.16). However, high intensity at low q still suggests the presence of large particles in solution at middle

relative water contents. More work is needed to unambiguously observe the low to mid-level relative water composition nanostructures that eventually become vesicles at high water content. It is observed that SAXS traces with clear vesicle form factor starts to show up at around 80% H₂O.

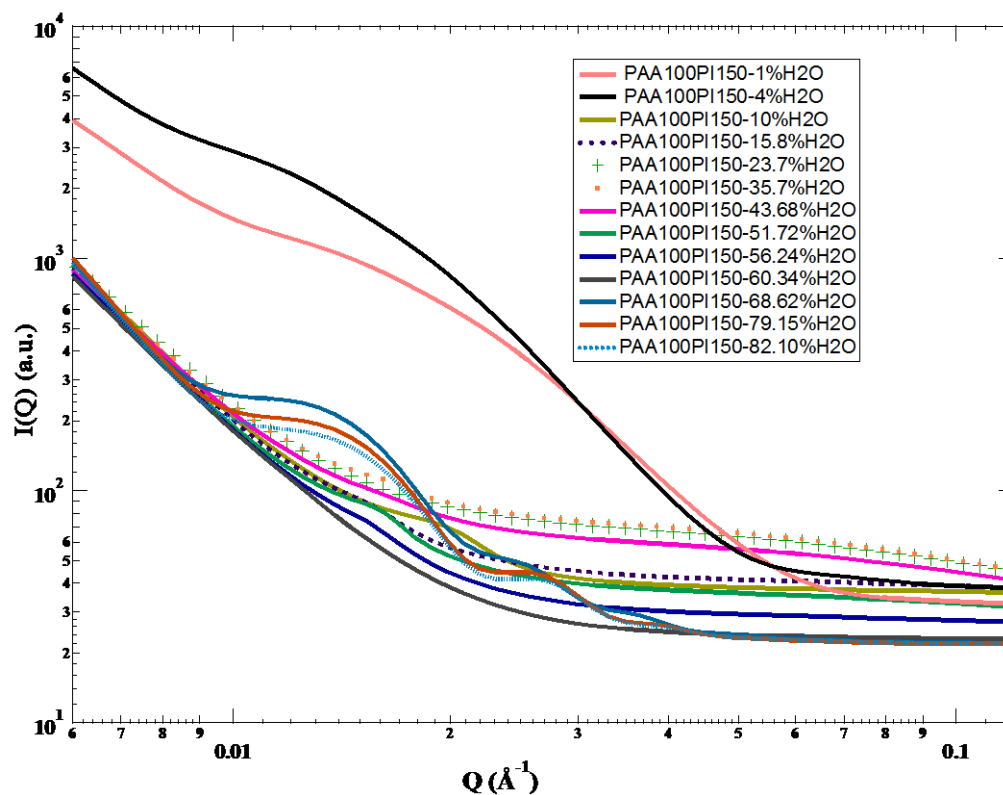


Figure 3.16 SAXS traces of PAA₁₀₀-*b*-PI₁₅₀ assemblies in different water contents with extreme slow water titration, amine to acid=0.5:1.

Comparing the morphology transitions of the two diblock copolymers in different water contents, it is noticed that the nanostructures formed at each water composition depends on the block copolymer types and block length ratios. The summary of the morphology windows is presented in Table 3.3. In this system, PAA-PS starts to form cylinders at around 75% (Figure 3.14) and PAA-PI starts to form vesicles at around 70%.

Table 3.6 Morphologies at different water contents in PAA₉₉-PS₁₆₉ and PAA₁₀₀-PI₁₅₀ assembly (results organized from TEM and SAXS).

	0%	10%	20%	30%	40%	50%	60%	70%	80%
PAA- PS	Inverse micelle	Giant membrane	Cylinder bundles	Cylinder bundles to lamellar	lamellar	L-V	L-V	V-C	C
PAA- PI	Inverse micelle	Giant membrane	-----	-----	-----	---	----	C+V	V

L represents lamellar; V represents vesicle; C represents cylinder.

After blending, the two diblock copolymers can undergo bulk phase separation into separate particles or intramicellar phase separation depending on the different water addition rates. SAXS results showed the sensitive correlation of the water addition rate with the eventual morphology formed across the entire relative water composition (from 0 to 80%, shown in Figure 3.17, 3.18). One blend with PAA₁₀₀-*b*-PI₁₅₀/PAA₉₉-*b*-PS₁₆₉ molar ratio at 1:1 was interrogated as a blend example. The SAXS traces of the blend system during extremely slow water addition display similarities (Figure 3.17) to the SAXS results of the single assembly of PAA₁₀₀-*b*-PI₁₅₀. Combining the cryo-TEM results at 80% water, it is reasonable to conclude that distinct diblocks undertake macrophase separation, thus forming separated nanoparticles from each building block in extremely slow water addition rate.

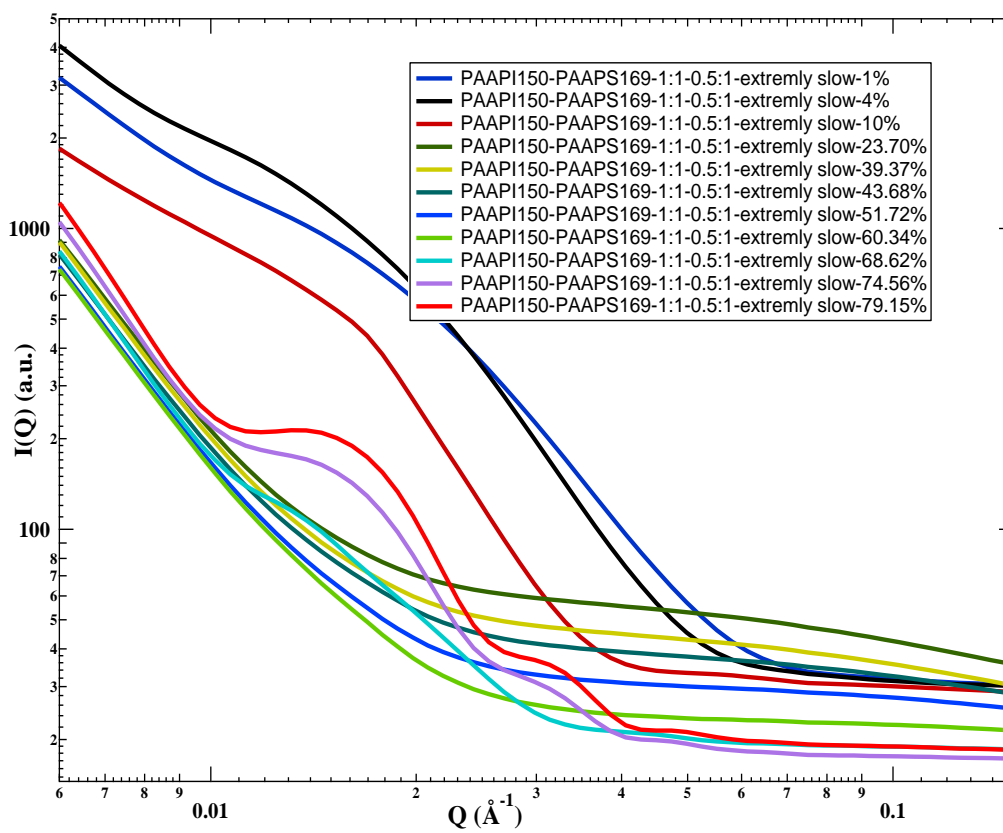
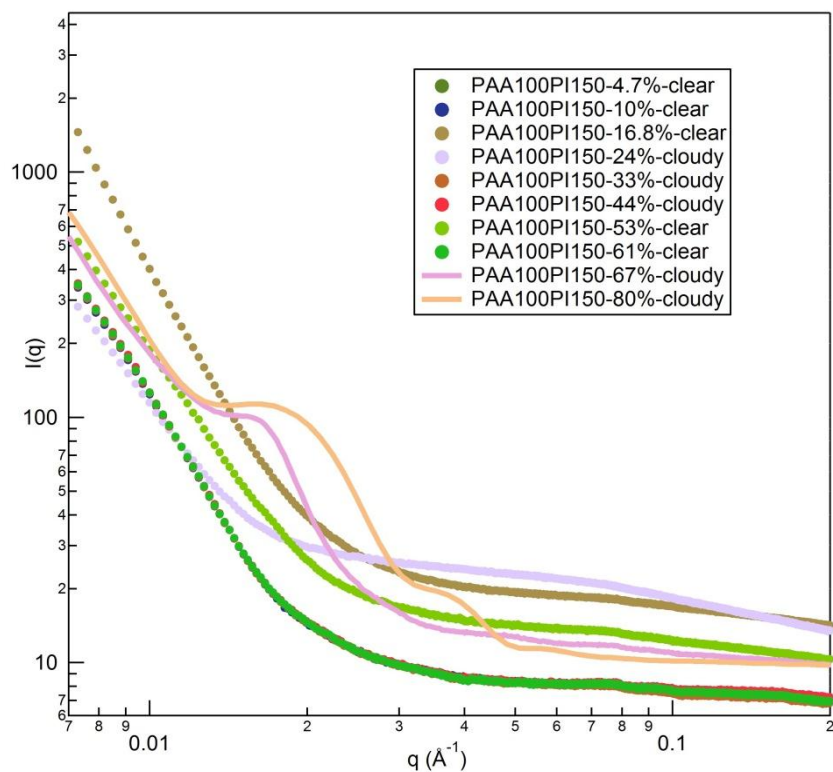
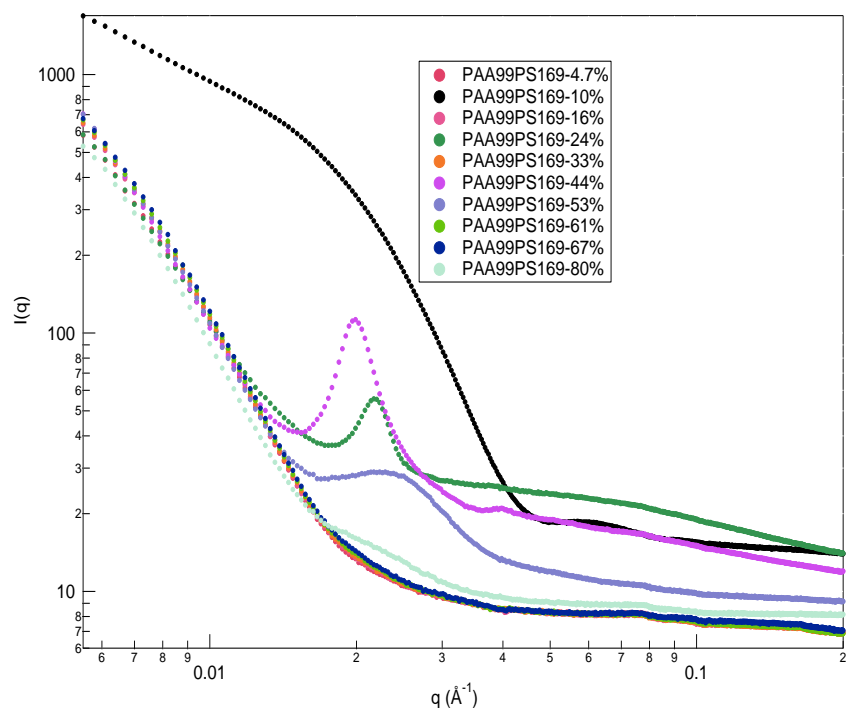


Figure 3.17 SAXS traces of blends of PAA₁₀₀-*b*-PI₁₅₀: PAA₉₉-*b*-PS₁₆₉ molar ratio=1:1 at detailed water points. Water adding at extreme slow rate (0.8 mL/h).

Different form factor models were used to fit the SAXS traces for the nanostructures formed at extremely slow water addition condition. For the pure cylinders assembled from single PAA-PS at 80% water with extremely slow water addition rate, core-shell cylinder form factor model was used to fit the SAXS data. The result is attached in the Appendix Figure A1. The SLD for different components in the core-shell cylinders, and the fitting parameters are also included. The variations of the length, core and shell radius are explained to result from the polydispersity of the cylinders formed in solution.

For the vesicle and cylinder mixture with dominant vesicle composition assembled at extremely slow water addition, core-multi-shell model was used to fit the SAXS trace considering the large volume of vesicles in the system. The result is shown in Figure A2. To fit the core-multi-shell model, H₂O/THF solvent was considered as the core. The PAA/amine layers outside the PI were considered as the layer 1 and layer 3. And the PI hydrophobic domain was considered as the layer 2. Several assumptions were considered when fitting the SAXS results. First, the SLD in each regime is constant, meaning the SLD in the core, here it is the solvent H₂O/THF (4/1), is constant. And the SLD values for the three shell layers, the PAA/amine inner layer, the PI middle layer, and the PAA/amine inner layer are constant. Gaussian distribution polydispersity was considered in this system to include the polydispersity of the core radius, and also the radius for the three layers. As shown from the Figure A2, more work needs to be done to get perfectly fitting results. From the current fitting, the radius of the core is in the range of the initial set (300-700 Å), and shown as 400 Å in the fitting result. The fitting result of radius of the layer one was shown as 27 Å, and the fitting result of the radius of the layer three was shown as 17 Å. The radius of the layer two, corresponding to the PI core, is shown as 156 Å. It is then hypothesized that the gradient SLD in the interface of each layer need to be considered due to the gradient boundaries formed from polymer chains. Also, possibly free polymer chains exists in the system which will contribute to the scattering. Combination of both multilayer shell model and cylinder model is also suggested to fit the SAXS in this specific condition. Finally, in the current q range, nano-objects with the size range of between 2.5-114 nm are able to be detected. The diameters of the polydisperse vesicles can reach 200 nm which needs ultra-small angle scattering methods.

Water addition rates influences on the assembly and coassembly



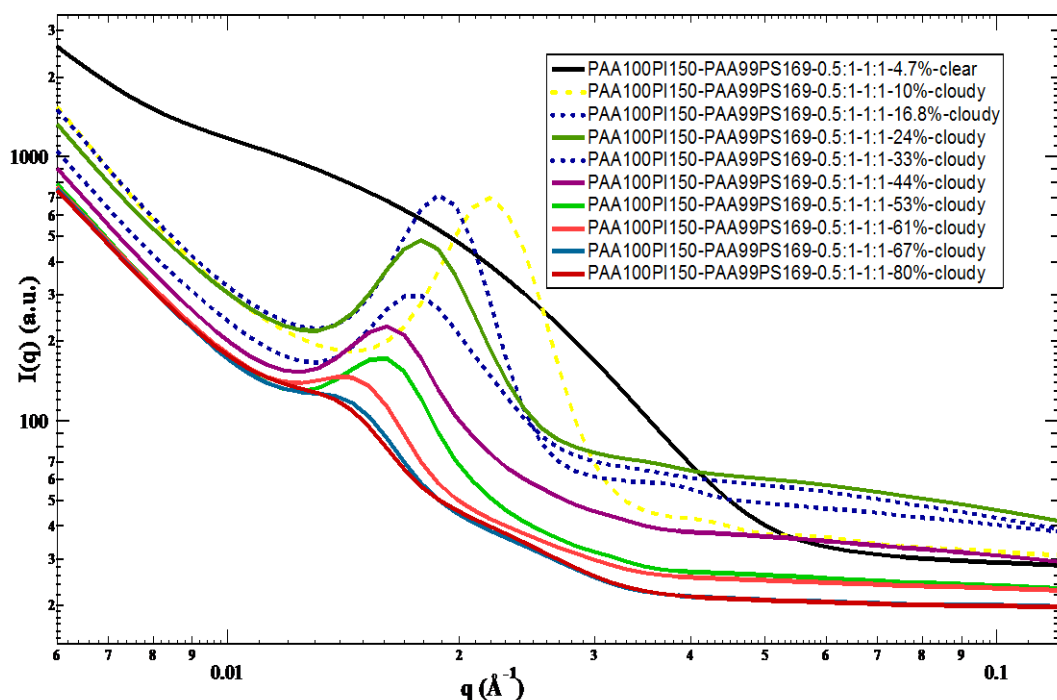


Figure 3.18 SAXS traces of single assembly of PAA₉₉-*b*-PS₁₆₉ at interval water contents, single assembly of PAA₁₀₀-*b*-PI₁₅₀ at interval water contents, and blends of PAA₁₀₀-*b*-PI₁₅₀:PAA₉₉-*b*-PS₁₆₉ molar ratio=1:1 at intermediate water contents, respectively. Water adding at middle water titration rate (30 mL/h).

When water addition rate was increased to 30 mL/h (Figure 3.18), similar scattering results are observed in individual block copolymer assembly system as they are in the extremely slow water addition rates, and different scattering results were observed in blend system. Compared with the individual block copolymer assemblies in extremely slow water addition rate, we observe the Bragg peaks appeared in the middle water range in PAA-PS assembly (10%-60% H₂O) and the curve transitions are similar as they are in extremely slow addition. The scattering peaks start earlier (10% water content) in faster water addition rates than in slow water addition rates (24%), indicating that larger aggregates with layered structure started to form earlier. In the

PAA-PI assembly, the clear vesicle form factor oscillations were also observed in high water contents (80%). Clearly, more work needs to be done on successful fitting of the form factors of cylinders and vesicles in individual diblock copolymer assembly, which would be complements to the imaging results provided above.

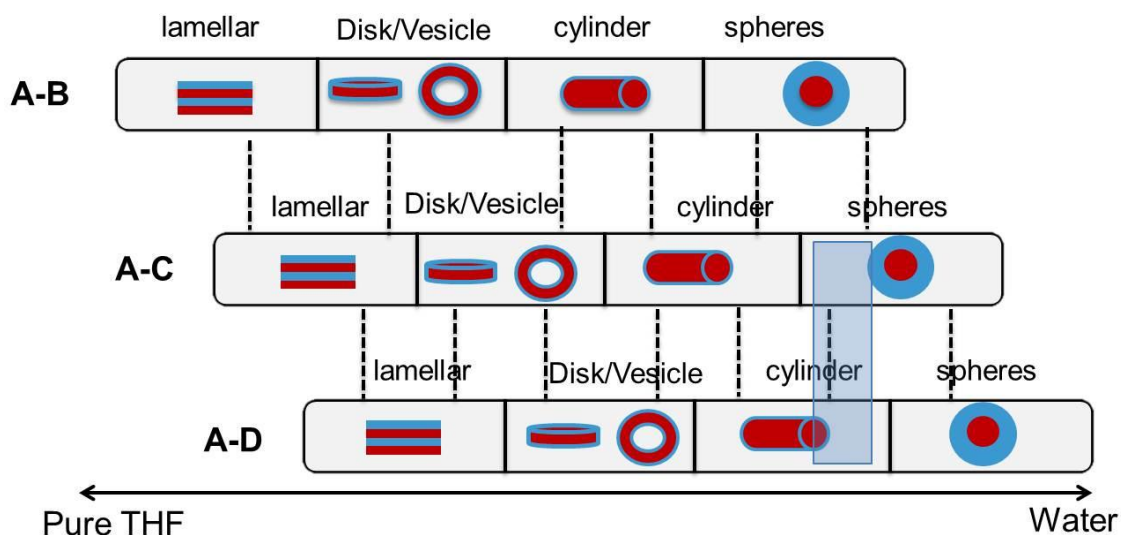
In the blend system, quite different results are observed. Broad scattering peaks were detected in low to middle relative water concentrations (10%-67%). From the scattering peaks and high intensity at low q , it is clear that large hybrid aggregates with internal periodic structures are formed. The two diblock copolymers are kinetically trapped together at this water addition rate without macrophase separation. As water was added to reach the higher amount, the peak position shifts from high q range to low q range, implying that the local nanostructure display PAA-diamine swelling with added water. The expanding of the hydrophilic domain overwhelms the collapsing of the hydrophobic domain, so that the spacing of the aggregates keeps on increasing as water is added to higher amount. The solution changes observed at extremely slow rate were not observed with this faster rate. The clear solution containing polymer/THF quickly changes to cloudy when subjecting to the quicker water addition. As discussed earlier, the two diblock copolymers start to form vesicles and cylinders at slightly different water composition (70% for PAA-PI and 75% for PAA-PS), the early stage kinetically-trapped hybrid nanoparticles would evolve to hybrid multicompartiment and multigeometry vesicle-cylinder, hybrid vesicles, or disk-cylinders in 80% water content.

The influence of the water addition rates to the solution phase behavior, nanoparticle assembly behavior, and local intraparticle phase separation behavior were investigated by small angle x-ray scattering. We can conclude that there exists strong rate-morphology correlations. The fundamental understanding of the phase separation behaviors in a single diblock assembly helps to inform the further morphological study and novel nanostructure construction in block copolymer blends. More work is needed in the new area of using SAXS to monitor nanostructure along the kinetic pathway.

3.4 Discussion and Conclusion

Formation of various multicompartment and multigeometry nanoparticles are presented here by binary blends of PAA-*b*-PI and PAA-*b*-PS. Different kinetic controlling parameters were utilized: the solvent addition rate, the block copolymer blending ratio and ageing effects. Separate vesicles and cylinders, novel connected vesicle-cylinder multigeometry nanoparticles, multicompartment disk-cylinders, and multicompartment hybrid vesicles are formed at specific solution conditions. Overall rate-morphology correlations showed that blended and nano-objects with smaller, overall size are formed at faster water addition rates. The evolutions of hybrid vesicles were presented here to fully understand the advantages of kinetic control methods. Nanoparticles with nontraditional shapes were evaluated over long time aging. The observed gross differences in assembly behaviors showed the importance of kinetic control. And the structure exploration paves the way of constructing shape specified drug delivery vehicles, nanosensors and even nanoreactors.

To produce complexity, the systematic construction of multicompartment and multigeometry nanoparticles *via* block copolymer blends can be predicted with the use of specific water addition rate ranges. In scheme 3.2, the engineering of hybrid nanoparticles *via* binary or ternary blends is presented. In the scheme, A-B, A-C, and A-D represent diblock copolymers that have the same hydrophilic block but immiscible hydrophobic blocks. They are designed with desired block length. Separately, they form different nanostructures in the same water composition and amine to acid conditions. For instance, they form spheres and cylinders in the high water composition as shown in the scheme. By blending and kinetic control, new shapes of hybrid nanoparticles are predicted by forcing the different block copolymers and their respective geometry into the same nanoparticle. The scheme is a map for the targeting of specific morphologies assembled from different block copolymers that exist at the same solvent composition so that the molecules can be combined into nanoparticles.



Scheme 3.2 Multicompartment and multigeometry nanoparticle construction *via* block copolymer blends. A-B, A-C and A-D represent for different diblock copolymers. The x axis represents the water contents from 0% to 100%.

It was reported that specific morphology formation depend on the block copolymer types, block length ratios, amine: acid ratios and also water compositions³². The empirical rules of thumb can be used for other experimental designs. By taking advantage of the kinetic control method, other hybrid multicompartment nanoparticles are predicted to be possible such as hybrid cylinders, hybrid disks, and hybrid lamellar particles can be assembled *via* other material blends. Moreover, systems that incorporate more building units such as degradable blocks and functional groups for post-assembly modification are promising and are under investigation, targeting for well-defined asymmetric and anisotropic multifunctional nanomaterials. The continuous work on assembly of new shapes of hybrid nanoparticles is presented in Chapter 4.

REFERENCES

1. C. Liu, M. A. Hillmyer and T. P. Lodge, *Langmuir*, 2009, **25**, 13718-13725.
2. X. Jiang and B. Zhao, *Macromolecules*, 2008, **41**, 9366-9375.
3. J. Jansson, K. Schillen, G. Olofsson, R. C. d. Silva and W. Loh, *J. Phys. Chem. B*, 2004, **108**, 82-92.
4. R. C. Hayward and D. J. Pochan, *Macromolecules*, 2010, **43**, 3577-3584.
5. H. Cui, Z. Chen, S. Zhong, K. L. Wooley and D. J. Pochan, *Science*, 2007, **317**, 647-650.
6. A. H. Gröschel, F. H. Schacher, H. Schmalz, O. V. Borisov, E. B. Zhulina, A. Walther and A. H. E. Müller, *Nat. Commun.*, 2012, **3**, 1-10.
7. S. A. Meeuwissen, K. T. Kim, Y. Chen, D. J. Pochan and J. C. M. van Hest, *Angew. Chem. Int. Ed.*, 2011, **50**, 7070-7073.
8. K. T. Kim, J. Zhu, S. A. Meeuwissen, J. J. L. M. Cornelissen, D. J. Pochan, R. J. M. Nolte and J. C. M. v. Hest, *J. Am. Chem. Soc.*, 2010, **132**, 12522-12524.
9. A. H. Groschel, A. Walther, T. I. Lobling, F. H. Schacher, H. Schmalz and A. H. Müller, *Nature*, 2013, **503**, 247-251.
10. C. Zhang, V. J. Pansare, R. K. Prud'homme and R. D. Priestley, *Soft Matter*, 2012, **8**, 86.
11. P. A. Rugar, L. Chabanne, M. A. Winnik and I. Manners, *Science*, 2012, **337**, 559-562.
12. R. Duncan and R. Gaspar, *Macromol. Biosci.*, 2011, **8**, 2101-2141.
13. D. M. Vriezema, M. C. Aragonès, J. A. A. W. Elemans, J. J. L. M. Cornelissen, A. E. Rowan and R. J. M. Nolte, *Chem. Rev.*, 2005, **105**.
14. X. Wang, J. Chen, K. Hong and J. W. Mays, *ACS Macro Letters*, 2012, **1**, 743-747.

15. Q. Ma and K. L. Wooley, *J. Polym. Sci. A Polym. Chem.*, 2000, **38**, 4805-4820.
16. S. R. Kline, *Journal of Applied Crystallography*, 2006, **39**, 895-900.
17. A. F.M.BARTON, *CRC Handbook of Solubility Parameters and other Cohesion Parameters, Second Edition*, CRC Press, 1991.
18. J.BRANDRUP, E.H.IMMERGUT and E.A.GRULKE, *POLYMER HANDBOOK*, JOHN WILEY&SONS, INC, 1999.
19. B. A. Miller-Chou and J. L. Koenig, *Progress in Polymer Science*, 2003, **28**, 1223-1270.
20. T. P. Russell, J. Rex P. Hjelm and P. A. Seeger, *Macromolecules* 1990, **23**,, 890-893.
21. Reimund Stadler, Tt Clemens Auschra, Ts Jrg Beckmann, U. Krappe, I. Voigt-Martin and L. Leiber-L, *Macromolecules*, 1996, **28**, 3080-3091.
22. D. J. Pochan, J. Zhu, K. Zhang, K. L. Wooley, C. Miesch and T. Emrick, *Soft Matter*, 2011, **7**, 2500-2506.
23. J. Zhu, S. Zhang, K. Zhang, X. Wang, J. W. Mays, K. L. Wooley and D. J. Pochan, *Nat. Commun.*, 2013, **4**, 1-7.
24. A. G. Denkova, E. Mendes and M. O. Coppens, *Soft Matter*, 2010, **6**, 2351-2357.
25. N. Saito, C. Liu, T. P. Lodge and M. A. Hillmyer, *ACS Nano*, 2010, **4**, 1907–1912.
26. C. Liu, M. A. Hillmyer and T. P. Lodge, *Langmuir*, 2008, **24**, 12001-12009.
27. R. K. O'Reilly, C. J. Hawker and K. L. Wooley, *Chem. Soc. Rev.*, 2006, **35**, 1068-1083.
28. F. Zhang, M. Elsbahy, S. Zhang, L. Y. Lin, J. Zou and K. L. Wooley, *Nanoscale*, 2013, **5**, 3220-3225.
29. R. R.J., *Methods of X-ray and Neutron Scattering in Polymer Science*, Oxford University Press, 2000.

30. K. Hales, Z. Chen, K. L. Wooley and D. J. Pochan, *Nano Lett.*, 2008, **8**, 2023-2026.
31. B. Hammouda, *PROBING NANOSCALE STRUCTURES-THE SANS TOOLBOX*, National Institute of Standards and Technology 2010.
32. H. Cui, Z. Chen, K. L. Wooley and D. J. Pochan, *Macromolecules*, 2006, 39, 6599-6607.

Chapter 4

CYLINDER-CYLINDER, DISK-DISK BINARY BLEND SYSTEMS AND LIMITATIONS OF BLENDING STRATEGY

Inspired by the results from the vesicle-cylinder system in Chapter 3, the following work involves binary blends of block copolymers combining disk-disk and cylinder-cylinder geometries. In this chapter, the design and synthesis of molecules and their assembly results are presented. Kinetic control of the solution assembly through tuning of selective solvent addition rates has been applied in successfully constructing hybrid nanoparticles with targeted geometries. In addition to presenting the advantages of the blending strategy, the limitations of the blend strategy in forming well-defined nanoparticles will also be shown in a ternary blend system combining sphere, cylinder, and cylinder geometries.

4.1 Introduction

Research of classic cylindrical nanostructures has been reported prolifically in the past few decades¹. Y-junction cylinders², worm-like cylinders, rod-like cylinders¹ and fibril-like cylinders³ have been observed through the assembly of amphiphilic block copolymers⁴, polypeptides³, surfactants⁵ and even inorganic materials⁶. Many solution processing methods have been applied to fabricate cylindrical micelles. For instance, kinetic control⁷ has been applied in the Pochan research group to form cylindrical micelles through the PAA-PMA-PS triblock copolymer self-assembly in mixed solvent and addition of organic amines. Other methods such as direct dissolution into selective solvent have also been utilized to trigger the organization of worm-like

cylindrical micelles in a triblock copolymer system with large hydrophobic/hydrophilic length ratios⁸.

Compared with other, classic core-shell-like nanostructures such as spheres, one signature geometric property of cylindrical nanostructures is the prevalent polydispersity in length, which is hard to control by using common solution assembly means. To solve this problem, many research groups have been working on employing novel assembly strategies. The Jiang group has reported on the creation of monodisperse-length cylinders assembled from a DNA/polymeric micelle complex. Monodisperse length DNA molecule with negative charges on the surface was used as the substrate to complex with spherical micelles with oppositely charged shell⁹. Controlled-length cylinders are then incubated through DNA/polymeric sphere complexation. Under this topic, work from the Winnik and Manners groups should also be mentioned. A unique, crystallization driven self-assembly method was programmed in the polyferrocenyldimethylsilane-polyisoprene (PFS-PI) diblock copolymer assembly system⁹⁻¹¹. By using the crystalline seeds as initiators, cylinders with uniform length are formed through the sequential addition of block-copolymers. By adding distinct copolymers sequentially, co-micelles can be assembled with tunable architecture and lengths⁹. Complex cylinder-cylinder and platelet-cylinder connected hybrid structures have been built up hierarchically by epitaxial crystallization of the core-forming metal block and polymerization self-assembly¹². A group of novel and functionalized cylinder nanostructures have been constructed *via* tuning of different parameters. The published results include the controlled-length cylinders assembled *via* polythiophene-based block copolymer poly(3-hexylthiophene)-b-polydimethylsiloxane¹³; branched micelles formed by the growth of thinner-core cylindrical micelles at the termini of the thicker-core cylindrical micelle seeds¹⁴; multi-armed micelles and co-micelles that are initiated from homopolymer nanocrystals¹⁵; cylinder networks formed from cylindrical block copolymer micelles with a crystalline PFS core *via* end-to-end coupling¹⁶; color-tunable fluorescent multiblock micelles built up from fluorescent block copolymer¹⁷; 2D planer nano-

sheets built up from a series of platelet forming block copolymers¹⁸. Asymmetric cylindrical micelles with multiarms, which are rare and hard to construct *via* solution assembly, have also been fabricated¹⁹. The almost arbitrary design and accurate achievement of new and well-defined cylinder-based nanostructure systems show the utility of solution assemblies²⁰.

Importantly, the solution assemblies could be potentially used as nanocarriers or nanoreactors in the nanomedicine²¹ field for many reasons. Cylinder micelles with a long length and narrow diameter are useful relative to other structures of micelles². For example, cylindrical aggregates of peptide-amphiphile have been used as fibrous scaffold for the mineralization of hydroxyapatite³. The effects of the cylinder shape on the interaction between cylinder micelles and animals *in vivo* have been studied in the filomicelle system. Compared with a spherical shape, the long, cylindrical filomicelle can effectively deliver the anticancer drug paclitaxel and shrink human-derived tumors in mice²². The recent increasing need of multifunctional nanomaterials require multiple components incorporated in one nanovehicle²³. The Müller group has reported dynamic core-shell-corona micelles formed from two oppositely charged block copolymer systems. Star-shaped nanostructures were observed²⁴. Recently they reported the long-range multicompartment cylinders with soft patchy spheres precisely positioned along, by co-assembly of triblock copolymers²⁵. The Manners group has used crystalline-driven polymerization self-assembly to include multiple fluorescent block copolymers to fabricate color-tunable fluorescent multiblock cylindrical micelles²⁶. However, there are few works of multicompartment cylindrical nanoparticles combining different blocks with multiple physical properties reported. In this chapter, a blend system will be discussed that produced new cylinder-cylinder multicompartment co-micelles (Figure 4.1-5). Kinetic control and material design are applied as powerful tools for “bottom-up”¹ self-assembly.

Compared with the facile formation of cylindrical nanoparticles, disk-shaped or sheet-like nanoparticles are not commonly formed in solution assembly systems. Disk-like nanoparticles normally contain two layers of amphiphilic molecules with the

bilayer hydrophobic blocks packed in the center and hydrophilic blocks facing outside²⁷. Several reports of disk-like micelles come from the assembly of coil-rod-coil molecules²⁸, supramolecular block copolymer²⁹, coil-coil diblock copolymers with a perfluoropolymer segments³⁰, glycodendrimer molecules³¹ and diblock copolymers with a crystallizable domain³². Recent publications report the formation of disk and stacked-disks assembled from cholesterol-functionalized amphiphilic polycarbonate diblock copolymer³³ and the disk micelles with highly ordered internal pattern assembled from molecular bottlebrushes³⁴. The difficulties of achieving disk-like or sheet-like structures are attributed to the high free energy of the hydrophobic edges, which normally causes the formation of vesicles. The Pochan group has used PAA-PMA-PS triblock copolymers in the presence of organic amine additives to form disks and stacked disks under kinetic control³⁵. The blending of PAA-PB diblock copolymer, a sphere former and PAA-PMA-PS triblock, a vesicle former, resulted in exotic patchy disk particles due to the immiscible hydrophobic blocks of the two block copolymers³⁶ causing multiple compartments trapped in one core domain.

Disk-shaped particles from block copolymers, colloids, and hydrogels have potential usage in nanocomposite materials³⁷ and biological studies²⁷. The study of disk-like hydrogel beads for cell encapsulation and manipulation indicates that a disk shape could be promising candidate for nanomedicine devices³⁸. Multicompartment and multigeometry patchy disks from material blends not only enrich the complexity of novel morphologies available but also provide potential multifunctional nanomaterials for potential applications. In this chapter, we will discuss the facile assembly of disk-disk multicompartment and multigeometry nanoparticles *via* purposely designed molecules and manipulation of solvent addition kinetics. With the simple changing of the initial molecules blending ratio, one can then tune the internal volume of immiscible compartments in the final nanoparticles (Figure 4.6-10).

As previously mentioned, the self-assembly of amphiphilic molecules in solution has been studied for decades with hundreds of assembled structures reported. However, there are scarce publications of asymmetric nanostructures. Work from the Winnik

and Manners groups has successfully built the non-centrosymmetric cylinders with crystalline core cylinder micelles linked together¹⁹. Nanostars with an asymmetric shape have been fabricated by in situ assembly of fully conjugated polythiophene diblock copolymers³⁹. In addition, some research has been focused on polymer/inorganic material co-assembly introducing asymmetric hybrid nanoparticles with anisotropic properties^{40, 41}. Herein, we present the formation of new, asymmetric star-like multicompartiment and multigeometry nanoparticles by ternary blends of three diblock copolymers with immiscible hydrophobic blocks. The limitations of the blending strategy are also discussed.

4.2 Cylinder-cylinder Multicompartiment Nanoparticles via Binary Blends

4.2.1 Materials Design and Synthesis

As discussed in Chapter 3, PAA₉₉-*b*-PS₁₆₉ assembles into cylinder micelles at specific solution conditions. To build a cylinder-cylinder MCN system, the diblock copolymer PAA₁₀₀-*b*-PMMA₁₇₀ was then designed with the block lengths similar to PAA₉₉-*b*-PS₁₆₉ and was expected to assemble into cylinders in the same solution conditions as PAA₉₉-*b*-PS₁₆₉. The dimensional similarity of molecules and assemblies are important for forming hybrid nanoparticles. The match and mismatch of geometries from each block copolymer will influence the final formed nanoparticles.

Synthesis of diblock PAA-PMMA by Halogen exchange method and ATRP

PAA₁₀₀-*b*-PMMA₁₇₀ was synthesized by Ang Li from the Wooley lab. The synthesis procedure is as follows: macromolecular initiator poly(*tert*-butyl acrylate)-Br was synthesized using *tert*-butyl acrylate (tBA) as the monomer through an atom transfer radical polymerization (ATRP) procedure. Then, methylene methacrylate was added sequentially following the halogen exchange method. The *tert*-butyl esters of PtBA-PMMA were selectively cleaved *via* reaction with trifluoroacetic acid (TFA) in dichloromethane, producing the amphiphilic block copolymer poly (acrylic acid)-

block-poly(methylene methacrylate) (PAA₁₀₅-*b*-PMMA₁₇₀: M_w: 25824 Da; M_w/M_n=1.09). GPC was used to characterize PtBA-PMMA. The procedure of synthesizing PAA₉₉-*b*-PS₁₆₉ has been described in Chapter 3.

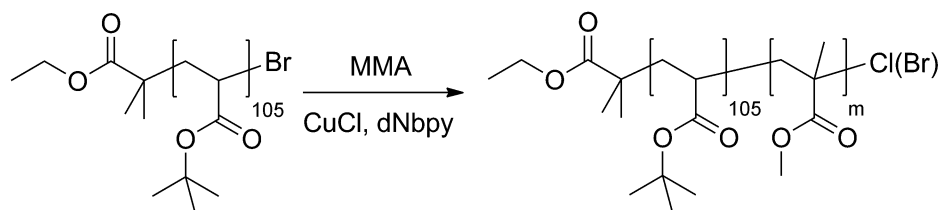


Figure 4.1 Synthesis route of PtBA-*b*-PMMA from PtBA-Br.

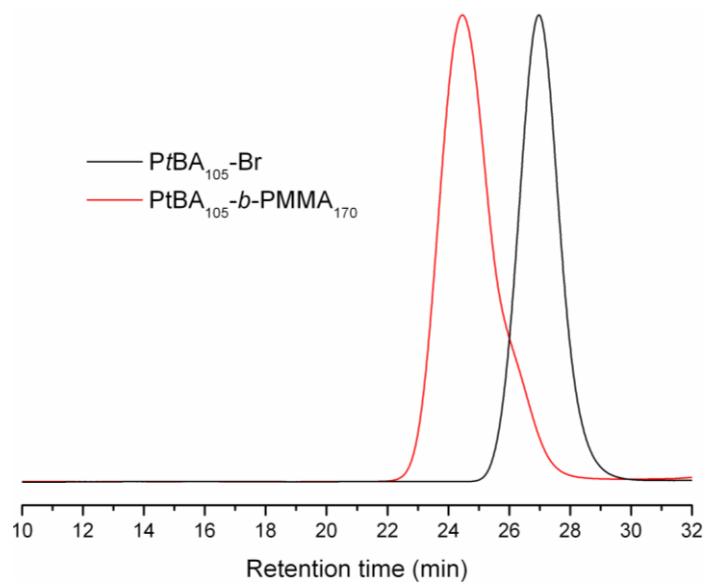


Figure 4.2 GPC result of PtBA-PMMA, data provided by Ang Li, Wooley Lab.

4.2.2 Solution Self-assembly Procedure

Individual polymer solutions were firstly prepared by dissolving PAA₉₉-*b*-PS₁₆₉ and PAA₁₀₅-*b*-PMMA₁₇₀ separately into tetrahydrofuran (THF) to reach a 2 mg/mL concentration. The solutions were stirred for 24 hours for complete dissolution. Blend solutions were made by mixing the individual polymer solutions with a desired, final molar ratio of the two block copolymers. Organic diamine (1 vol% concentration in THF) was then added to reach a final block polymer concentration of 0.1 wt% and an amine: acid ratio of 0.5:1. Resultant solutions were stirred for 24 hours for sufficient mixing and complexation between amine and acid groups. Solutions of individual block copolymers for assembly were prepared the same way as the blend samples with EDDA added to either PAA₉₉-*b*-PS₁₆₉ or PAA₁₀₅-*b*-PMMA₁₇₀ solution. Next, water was added to the 1 mL THF solution to reach 80% water concentration at different water addition rates as discussed later in chapter. Final polymer assemblies were observed after reaching 5 mL of mixed solvent (THF/H₂O=1/4 v/v) with a final polymer concentration at 0.018 wt%. Different water addition rates were achieved through the use of a syringe pump (KD Scientific Syringe Pump, KDS 100). The assembly solutions were constantly stirred with a magnetic stir bar during water addition. The assembly solutions were stored in glass vials sealed with PTFE covers and Teflon tape to limit solvent evaporation to undetectable levels. During aging, the solutions were not stirred further. Sample microscopy images were obtained after solutions aged for 2 hours after water addition.

4.2.3 Transmission Electron Microscopy and Selective Staining

TEM observations of dried samples were performed on the FEI Tecnai G²-12 microscope operated at 120 kV, equipped with a Gatan CCD camera. Grids were pre-treated with oxygen plasma to increase the surface hydrophilicity. TEM samples were prepared by applying a drop of nanoparticle suspension (about 3 μ L) directly onto a carbon-coated copper TEM grid, and the drop was allowed to evaporate under ambient conditions. After the grids were completely dry, they were stained by exposure to a

ruthenium tetroxide aqueous vapor solution for 5-10 minutes (purchased from electron Microscopy Sciences, 4 wt% RuO₄) in a closed glass vessel.

4.2.4 Results and Discussion

Single assembly of designed diblock copolymers

PAA-*b*-PS and PAA-*b*-PMMA diblocks were chosen as the two block copolymers to study binary blending *via* a desired solution assembly pathway. PAA₉₉-*b*-PS₁₆₉ was selected due to the studied assembly behavior of cylinder formations at water-rich conditions in the presence of EDDA diamine (H₂O=80%, amine: acid=0.5:1). Also, PAA₉₉-*b*-PS₁₆₉ has aromatic rings that can be used for RuO₄ staining to increase the mass-thickness contrast of PS phase. PAA₁₀₅-*b*-PMMA₁₇₀ was selected due to its ability to form cylinders at the same solution conditions as PAA₉₉-*b*-PS₁₆₉. The identical hydrophilic PAA domains shared by the two block copolymers are complexed with diamine that acts to confine the PAA₉₉-*b*-PS₁₆₉ and PAA₁₀₅-*b*-PMMA₁₇₀ into the same aggregate. The immiscible nature of PS and PMMA blocks (and possible PB or other hydrophobic blocks) affords the local nanophase separation in expected hybrid nanoparticles.

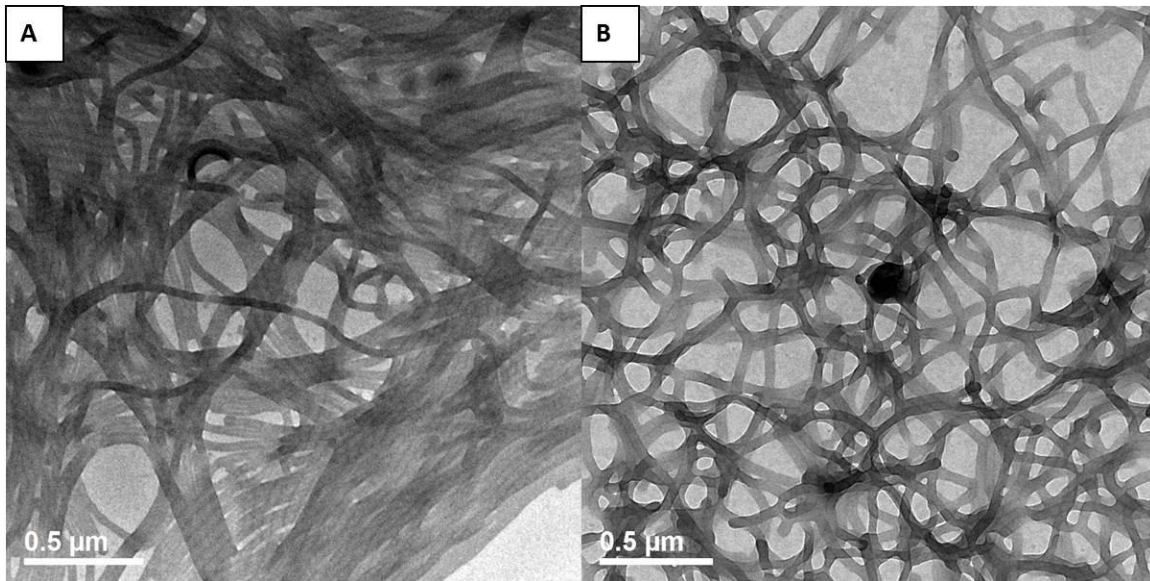


Figure 4.3 TEM images of cylinder micelles assembled from PAA₉₉-*b*-PS₁₆₉ and PAA₁₀₅-*b*-PMMA₁₇₀. A, cylinders assembled by PAA₉₉-*b*-PS₁₆₉ at amine: acid=0.5:1, 1 mL THF containing polymer and amine, water added at 0.8 mL/h to reach 80% H₂O/20% THF. B: cylinders assembled from PAA₁₀₅-*b*-PMMA₁₇₀ at amine: acid=0.5:1, 1 mL THF containing polymer and amine, water added at 0.8 mL/h to reach 80% H₂O/20% THF.

In the same solution conditions, PAA₉₉-*b*-PS₁₆₉ and PAA₁₀₅-*b*-PMMA₁₇₀ form cylinders, respectively. The diameters of the cylinders are all around 45 nm measured from the images in Fig 4.3.

Co-assembly results after blending.

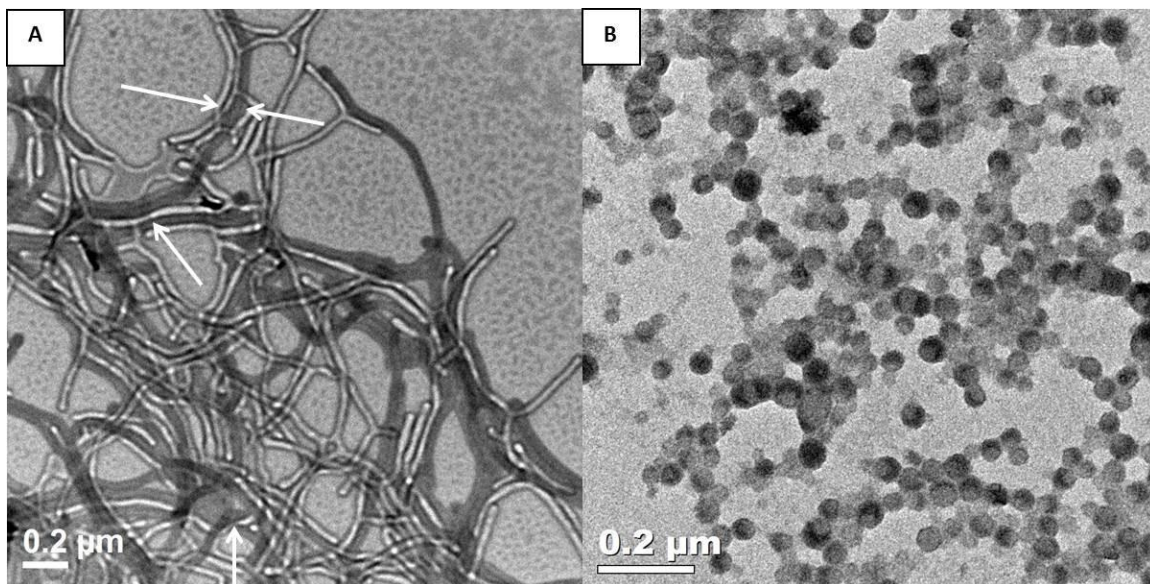


Figure 4.4 TEM images of multicompartiment cylinders assembled after blending PAA₉₉-*b*-PS₁₆₉ and PAA₁₀₅-*b*-PMMA₁₇₀ in THF/amine at a relative molar ratio of 1:3 of the two block copolymers and different rates of water addition. **A:** Separate populations of cylinders assembled after diblocks were blended in THF, diamine is added to reach an amine to acid molar ratio of 0.5:1 and water is added in a slow rate at 0.8 mL/h. **B:** Same solution mixing method as A but water added at ultra-fast rate using pipette addition at a rate $\gg 100$ mL/h. RuO₄ staining was used after the sample aged for 2 hours after water titration and the cast-film TEM grids dried. The grids were stained to RuO₄ vapor for 10 minutes.

In Figure 4.4 and Figure 4.5, we observed separate populations of cylinders assembled at extreme slow water addition, which is attributed to the macrophase separation between diblock copolymers. Similar results (not shown) were obtained with a 1:1 blend of PAA₉₉-*b*-PS₁₆₉ and PAA₁₀₅-*b*-PMMA₁₇₀ with the exact same assembly protocol. In contrast, when water is added at an ultra-fast rate, short cylinders and spherical hybrid nanoparticles were formed. Given these results, combination of different kinetics of water addition was then performed to form

multicompartment cylindrical hybrid nanoparticles including different hydrophobic blocks in one cylinder (Fig 4.6).

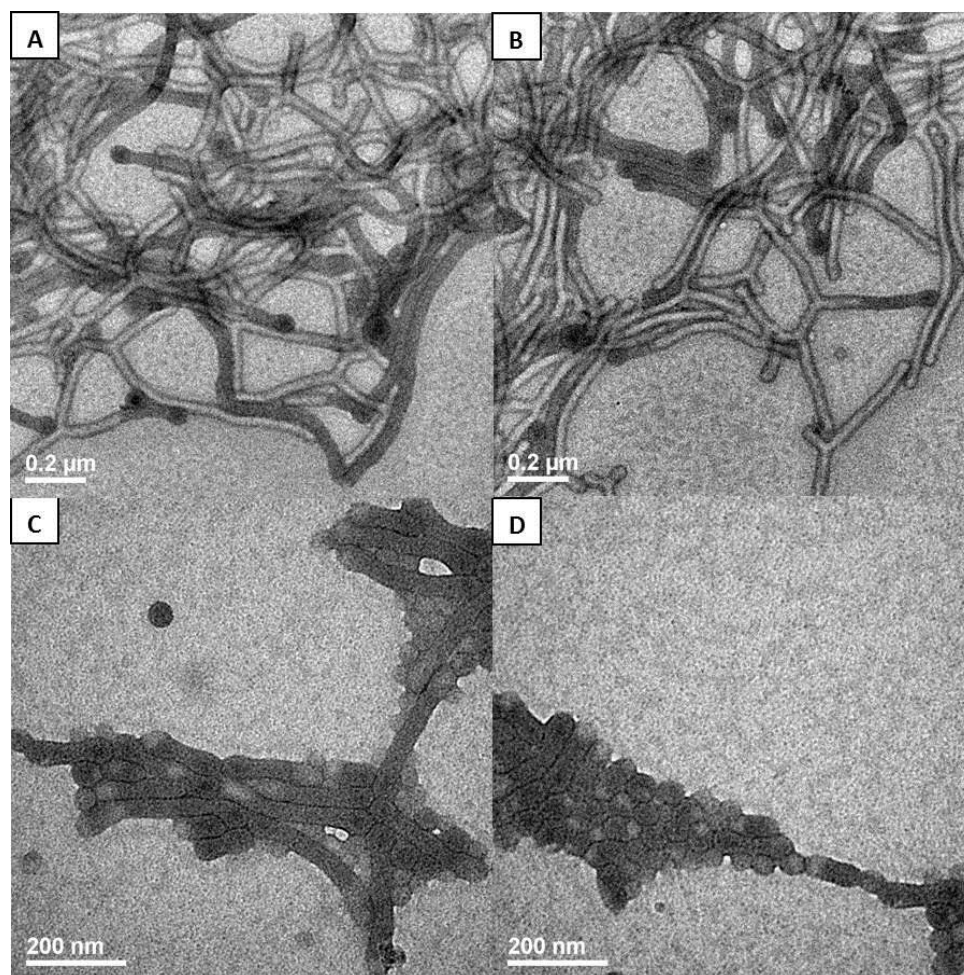


Figure 4.5 Dry film TEM images of the multicompartment cylinders assembled *via* combination of two different water addition rates. Water (1 mL) was firstly added quickly to the pure THF solution (1 mL) *via* pipette to reach an intermediate water content of 50% water. Then water (3 mL) was added slowly (3 mL/h) to the system to eventually reach 80% water relative content. A, B: PAA₉₉-*b*-PS₁₆₉ and PAA₁₀₅-*b*-PMMA₁₇₀ were blended in molar ratio 1:3, amine: acid=0.5:1. C, D: PAA₉₉-*b*-PS₁₆₉ and PAA₁₀₅-*b*-PMMA₁₇₀ were blended in molar ratio 1:1, amine: acid=0.5:1. Samples were aged for two hours after water titration before cast-film TEM grids preparation. The grids were then stained with RuO₄ vapor for 10 minutes.

To trap the different hydrophobic phases into the same core of hybrid cylinder nanoparticles, fast water and slow water addition were performed sequentially. For the first step of fast water addition, the intermediate targeted water content point was decided by the observed morphology solvent composition windows of each diblock copolymer (for example, Figure 3.15). In single diblock assembly, the PAA-PS in THF/water solvent went through different stages of phase separation and morphology formation at different solvent compositions. For instance, at 30% relative water composition, a precipitated lamellar particle structure was formed. With water added to reach higher relative water content, vesicles and disks eventually appeared with cylinders forming at high relative water content of ~80%. The same morphology transition behavior was observed for PAA₁₀₀-*b*-PMMA₁₇₀ individual assembly *via* slow water addition. Predictably, by quickly addition water to reach 50% condition, the distinct diblock copolymers will be quickly trapped together to form one lamellar aggregate. And, by slow, subsequent addition of water to 80% relative content, cylindrical shapes are grown with the different hydrophobic phases trapped inside the same nanoparticle. At different blending ratios of 1: and 1:3 of the two block copolymers, the combined fast and then slow kinetic pathway succeeded in forming hybrid cylinders. However, due to not being able to control cylinder length or the specific local composition within the blended cylinders, we would not be able to correlate the initial blending ratio to the final volume fraction of different hydrophobic phases in the hybrid cylinders. Future work will involve quantitative image analysis of the different cylinder phases in order to quantify the distribution of the two block copolymers within the assembled cylinders (collaborated work with Prof. Vesna Zeljkovic from Lincoln University).

Based on the understanding of the morphology transition behaviors of each diblock copolymer, controllable unblended and blended cylinders are constructed *via* different water addition rates. Separate cylinders, sphere-sphere, short hybrid cylinders, multicompartment cylinder-cylinder nanoparticles are assembled.

4.3 Hybrid Disk-Disk Systems via Ternary Blends

Inspired by the results of earlier vesicle-cylinder and cylinder-cylinder blend systems, another blending system with targeted geometries was designed: the disk-disk hybrid multicompartment nanoparticle system. The triblock copolymer poly(acrylic acid)-*block*-poly(methyl acrylate)-*block*-polystyrene (PAA₉₉-*b*-PMA₁₀₃-*b*-PS₁₈₈) was used as a known disk former to blend with the other disk former PAA₁₀₀-*b*-PI₁₅₀/PAA₉₉-*b*-PS₁₆₉ blended disk-cylinder nanoparticle, as described in Chapter 3. Multicompartment hybrid disk-disk nanoparticles are formed *via* control of the water addition rates in this ternary block copolymer system.

4.3.1 Materials and Synthesis

The synthesis process of diblock copolymers PAA₁₀₀-*b*-PI₁₅₀ and PAA₉₉-*b*-PS₁₆₉ were provided in Chapter 3. The other triblock copolymer PAA₉₉-*b*-PMA₁₀₃-*b*-PS₁₈₈ was synthesized according to literature⁴² ($M_n=35264$, with $\bar{D}=1.10$).

4.3.2 Solution Self-assembly Procedure

The pre-blending polymer solutions were firstly prepared by dissolving PAA₉₉-*b*-PS₁₆₉/PAA₁₀₀-*b*-PI₁₅₀ (mixed diblock) and PAA₉₉-*b*-PMA₁₀₃-*b*-PS₁₈₈ separately into tetrahydrofuran (THF) to reach a polymer concentration of 2 mg/mL at desired molar ratio. The solutions were stirred for 24 hours for complete dissolution. Blending solutions were made by mixing the two disk-forming solutions at desired molar ratio of polymers from each solution. Organic diamine (1 vol% concentration in THF) was then added to reach a total polymer concentration of 0.1 wt% and an amine: acid ratio of 0.5:1. The solution was stirred for 24 hours for sufficient mixing and complexation between amine and acid groups. The two individual disk former block copolymer solutions were prepared the same way as the blend samples with EDDA added to either PAA₉₉-*b*-PS₁₆₉/PAA₁₀₀-*b*-PI₁₅₀ mixture or PAA₉₉-*b*-PMA₁₀₃-*b*-PS₁₈₈ solution. Next, water was added to the 1 mL THF solution to reach a final 80% relative water

composition at different water addition rates. Polymer assemblies in a final volume of 5 mL mixed solvent (THF/H₂O=1/4 v/v) with a final polymer concentration at 0.018 wt% were obtained in all cases. Different water addition rates were achieved through use of a syringe pump. The assembly solutions⁴³ were constantly stirred with a magnetic stir bar during water addition and were then stored in glass vials sealed with PTFE covers and Teflon tape to limit solvent evaporation to undetectable levels. During aging, the solutions were not stirred further. For the separate disk forming solutions made with PAA₉₉-*b*-PS₁₆₉/PAA₁₀₀-*b*-PI₁₅₀ or PAA₉₉-*b*-PMA₁₀₃-*b*-PS₁₈₈, images were taken after three days aging. For the blend solutions, images were also taken three days after water addition.

4.3.3 Transmission Electron Microscopy and Selective Staining

TEM observations of dried samples were performed on the FEI Tecnai G²-12 microscope operated at 120 kV, equipped with a Gatan CCD camera. Grids were pre-treated with oxygen plasma to increase the surface hydrophilicity. TEM samples were prepared by applying a drop of nanoparticle suspension (about 3 μ L) directly onto a carbon-coated copper TEM grid, and the drop of solution was allowed to evaporate under ambient conditions. After the grids were completely dried, they were stained by exposure to a 1 mL osmium tetroxide 4 wt% aqueous solution vapor for 8-24 hours (purchased from Electron Microscopy Sciences, 4 wt% OsO₄) in a closed glass vessel.

4.3.4 Small Angle Neutron Scattering Measurement

Small angle neutron scattering (SANS) experiments were performed on the 30 m instrument (NG-3) at the NIST center for Neutron Research (NCNR), National Institute of Standards and Technology (NIST). A series of fresh multicompartiment disk nanoparticle samples were prepared in D₂O and TDF for the SANS studies. The sample preparation was the same as described above, except that TDF and D₂O were used instead of THF and H₂O. The final concentration of the particles in mixed

TDF/D₂O (v/v=1/4) is 0.25 mg/mL. Samples were loaded in titanium sample cells with 30 mm diameter quartz windows and a 2 mm path distance. Approximately monochromatic neutrons at $\lambda=6\text{\AA}$ and a wavelength spread ($\Delta\lambda/\lambda$) of 0.14 were incident on the sample. The scattered neutrons were captured by a $64\times 64\text{ cm}^2$ 2D detector. Sample-to-detector distances used were at 1.33, 4.5 and 13.17 m to cover a wide scattering wave vector, q range ($0.004 < q < 0.4\text{ \AA}^{-1}$), with $q=(4\pi/\lambda)\sin(\theta/2)$, where λ is the neutron wavelength and θ is the scattering angle. Sample data were corrected for background and empty cell scattering. The initial scattering length densities (\AA^{-1}) used for PAA, PAA/EDDA, PS, PMA-PS, PI and the final TDF/D₂O mixture for fitting purpose are 1.39e^{-6} , 5.82e^{-6} , 1.22e^{-6} , 1.10e^{-6} , 2.0e^{-7} , 6.2e^{-6} respectively. Intensities were normalized to an absolute scale using main beam transmission measurements and were reduced according to published protocol. The disk form factor model from the NCNR SANS package was used to fit the SANS curves obtained.

4.3.5 Assembly results and discussion

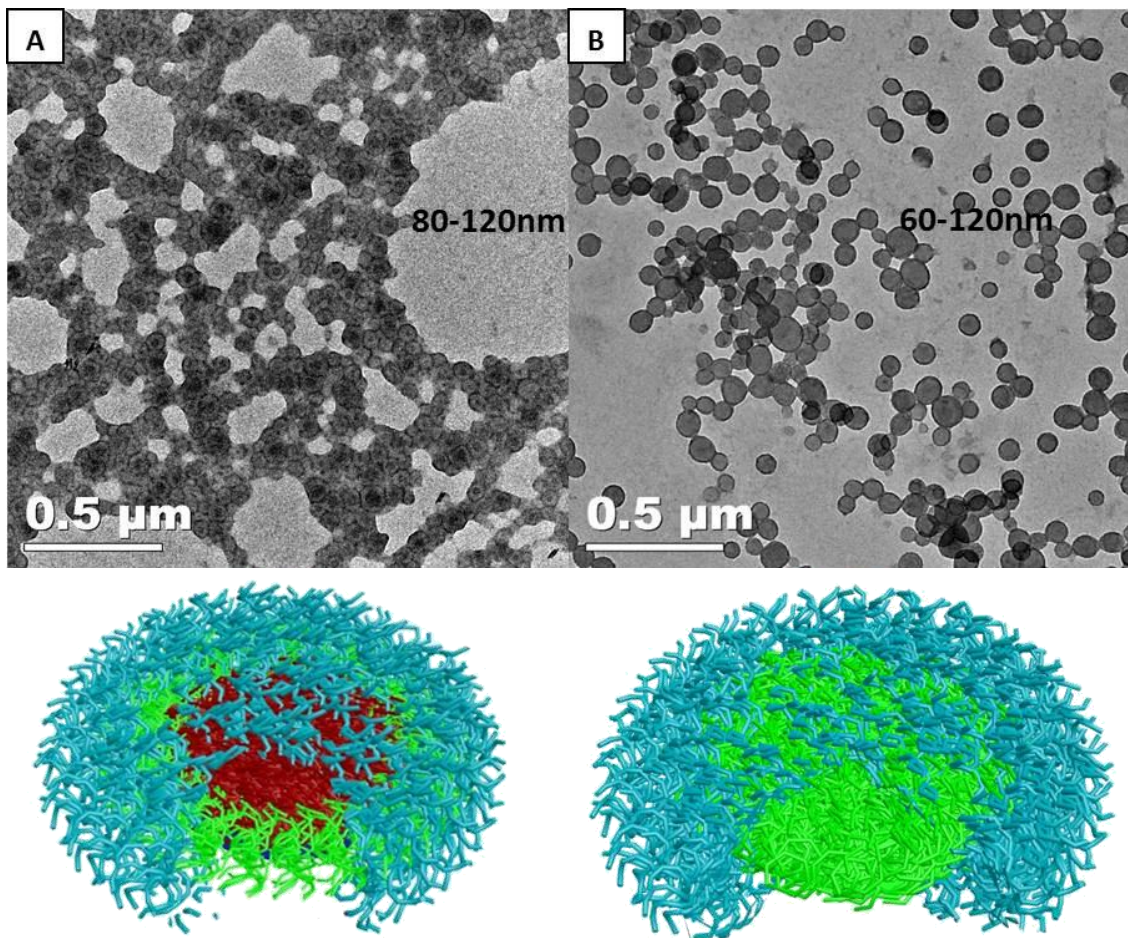


Figure 4.6 Dry-film TEM images of disk formers assembled from PAA₉₉-*b*-PS₁₆₉/PAA₁₀₀-*b*-PI₁₅₀ blends and PAA₉₉-*b*-PMA₁₀₃-*b*-PS₁₈₈, respectively. A: PAA₉₉-*b*-PS₁₆₉/PAA₁₀₀-*b*-PI₁₅₀ molar ratio of 1:1, and water was added with ultra-fast rate by using pipette addition (>>100 mL/h). Diameter of the overall disk-cylinder nanoparticles are around 80-120 nm. B: Disks assembled from PAA₉₉-*b*-PMA₁₀₃-*b*-PS₁₈₈, amine: acid=0.5:1 with water added in a rate 5 mL/h to 1 mL THF to reach a final relative water composition of 80% water and a total of 5 mL final solution volume. Diameter of the disks is in the range of 60-120 nm. 3D cartoons are drawn to indicate the disk geometry, internal core domain, and chain organization in the disk-shaped nanoparticles. The blue color represents the PAA/amine condensed shell; the green color represents the PS domain in A and the PMA-PS domain in B, respectively; the red color represents the PI domain in A.

Co-assembly results after blends of diblocks and triblock

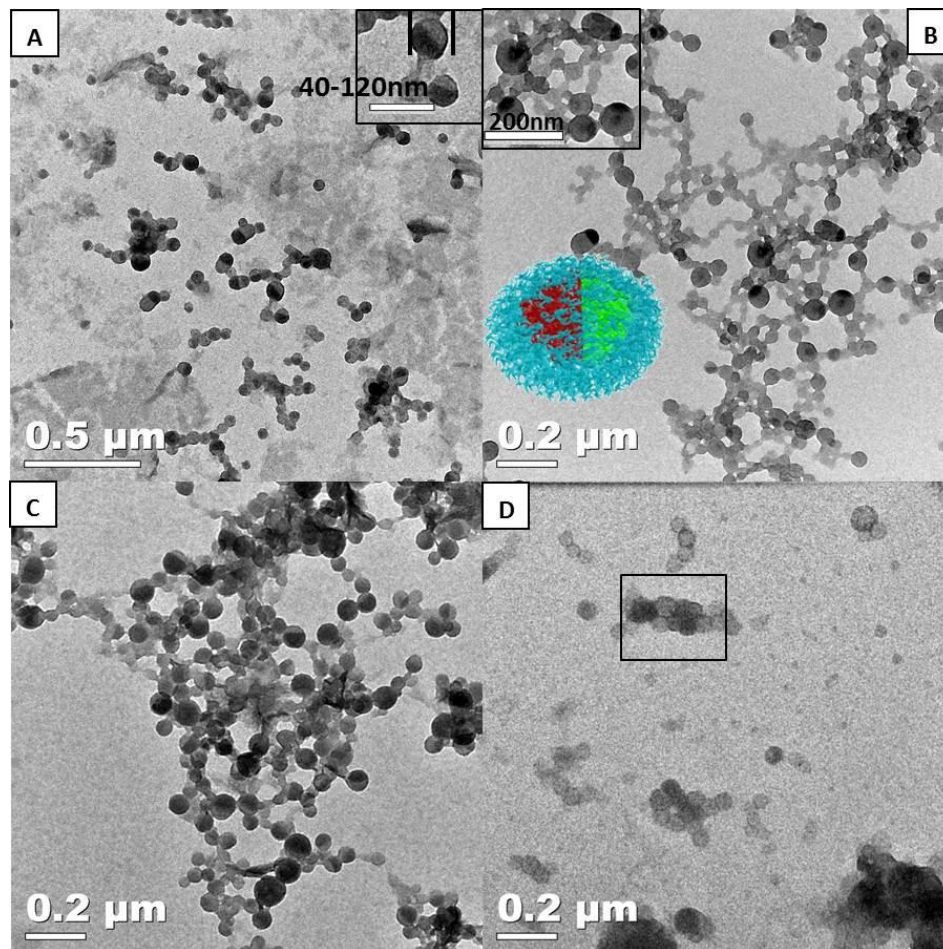


Figure 4.7 Dry-film TEM images of Disk-Disk multicompartiment nanoparticles assembled from the ternary diblock and triblock blend. **A:** ternary blends of PAA₁₀₀-*b*-PI₁₅₀/PAA₉₉-*b*-PS₁₆₉/PAA₉₄-*b*-PMA₁₀₃-*b*-PS₁₈₈ at molar ratio of 9:1:10 (or, an overall molar ratio of 1:1 of each disk-forming system), the volume fractions of different compartments of hybrid disks are designed to be ~50% volume PI phase/50% PMA and PS phases. Water was added with an ultra-fast rate by pipette, H₂O/THF v/v=4:1; **B:** ternary blends of PAA₁₀₀-*b*-PI₁₅₀/PAA₉₉-*b*-PS₁₆₉/PAA₉₉-*b*-PMA₁₀₃-*b*-PS₁₈₈ at molar ratio of 9:1:17, the volume fraction ratio of the dark phase and light phase was targeted to be around 2:8. Water was added in an ultra-fast rate by using pipette, H₂O/THF v/v=4:1. **C:** ternary blends of PAA₁₀₀-*b*-PI₁₅₀/PAA₉₉-*b*-PS₁₆₉/PAA₉₉-*b*-PMA₁₀₃-*b*-PS₁₈₈ at molar ratio of 9:1:5, the volume fractions of dark phase and light phase was around 40%:60%. The determination of the volume fractions of dark phase and light phase will be addressed later in the paper. **D:** Separate populations of disks assembled from blends of diblock and triblock copolymer at extreme slow water addition, at same molar ratio with image A. Separate disks are circled in the image.

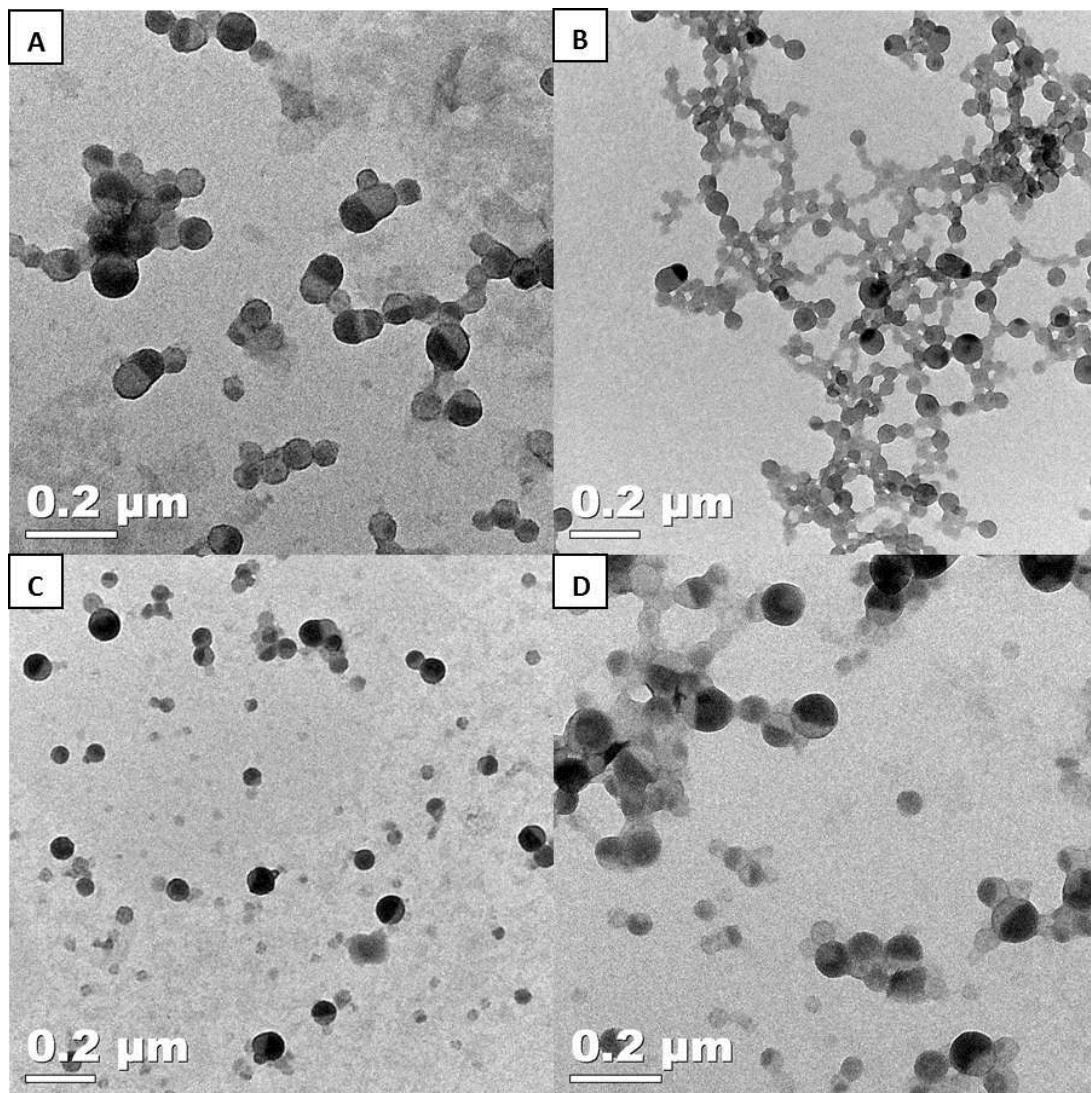


Figure 4.8 Additional higher magnificient dry-film TEM images for the hybrid disk-disk nanoparticles assembled from diblocks and triblock blends. **A:** Same sample as in Fig 4.7A; **B:** Same sample as in Figure 4.7 B; **C,** **D:** Same sample as in Figure 4.7C.

As observed from Figures 4.7 and 4.8, multicompartent disk-disk nanoparticles are assembled at extreme fast water addition rates as expected. By changing the initial blending ratio, one can manipulate the volume fraction ratio of the immiscible hydrophobic phases. At slow water addition rate, separate populations of disks are

assembled, which is consistent with the rate-morphology correlations in the cylinder-cylinder blending system. Another important parameter that needs to be mentioned is the sample aging period needed for the well-defined nanostructures. Three days aging is necessary for this particular blend system, most likely due to the larger molecular weight of the triblock copolymer PAA₉₄-*b*-PMA₁₀₃-*b*-PS₁₈₈ compared with the other smaller molecular weight diblocks. The larger molecular weight, the slower dynamics it needs for the blocks to locally separated. Images taken at earlier time points less than three days show no clear nanophase separation within the nanoparticles.

Tilted-stage TEM characterization of disk shape nanoparticles.

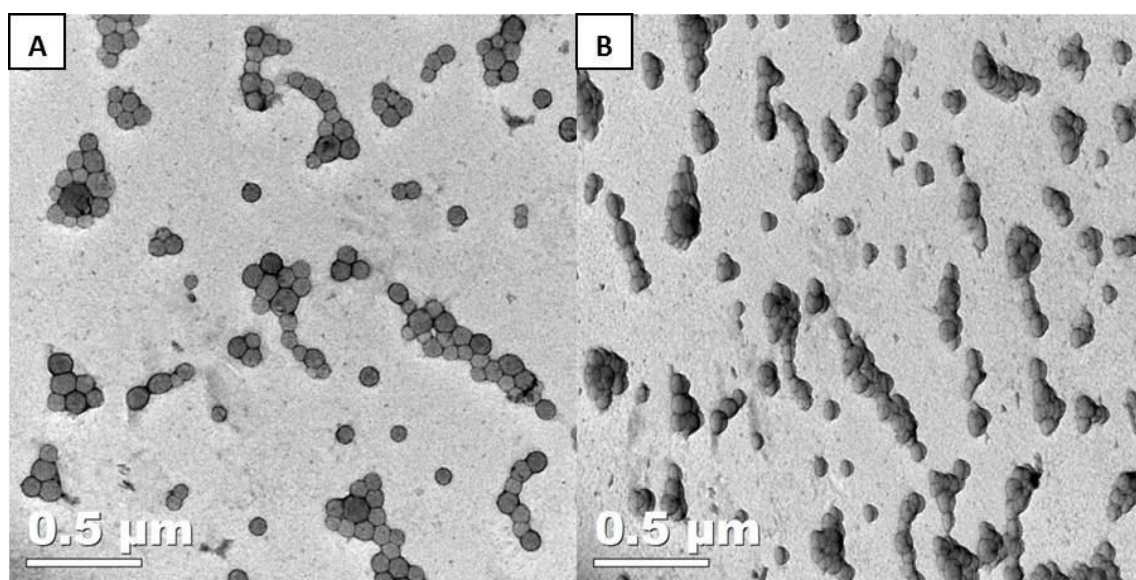


Figure 4.9 Tilt dry-film TEM grids containing the disk structure assembled from PAA₉₄-*b*-PMA₁₀₃-*b*-PS₁₈₈. **A:** zero degree of sample holder. **B:** 60 degree tilted of sample holder.

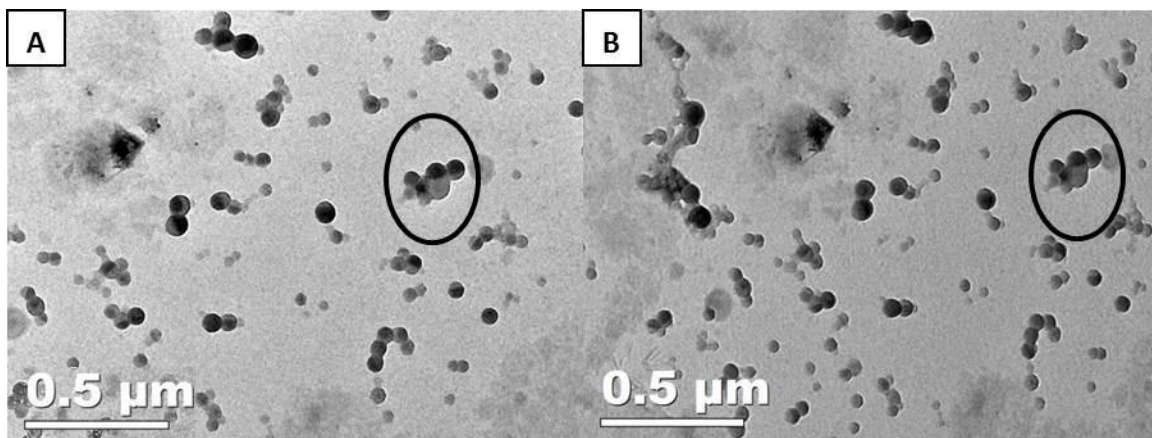


Figure 4.10 Tilt images of dry-film TEM grids containing the disk-disk structure. **A:** hybrid disk-disk assembled from blends of diblocks and triblock, same sample as in the Figure 4.8A. **B:** image taken after holder was tilted at 45°.

To further verify the disk morphology and measure the approximate disk thickness, tilted TEM characterization was performed. If disks exist, the tilting stage will alter the two-dimensional projections with the thin bilayer circles to an elliptical shape. Images with a tilt angle of 45 ° are provided in Fig 4.9 and Fig 4.10, confirming the overall disk shape of the disk-disk nanoparticles.

Small Angle Neutron Scattering measurement results

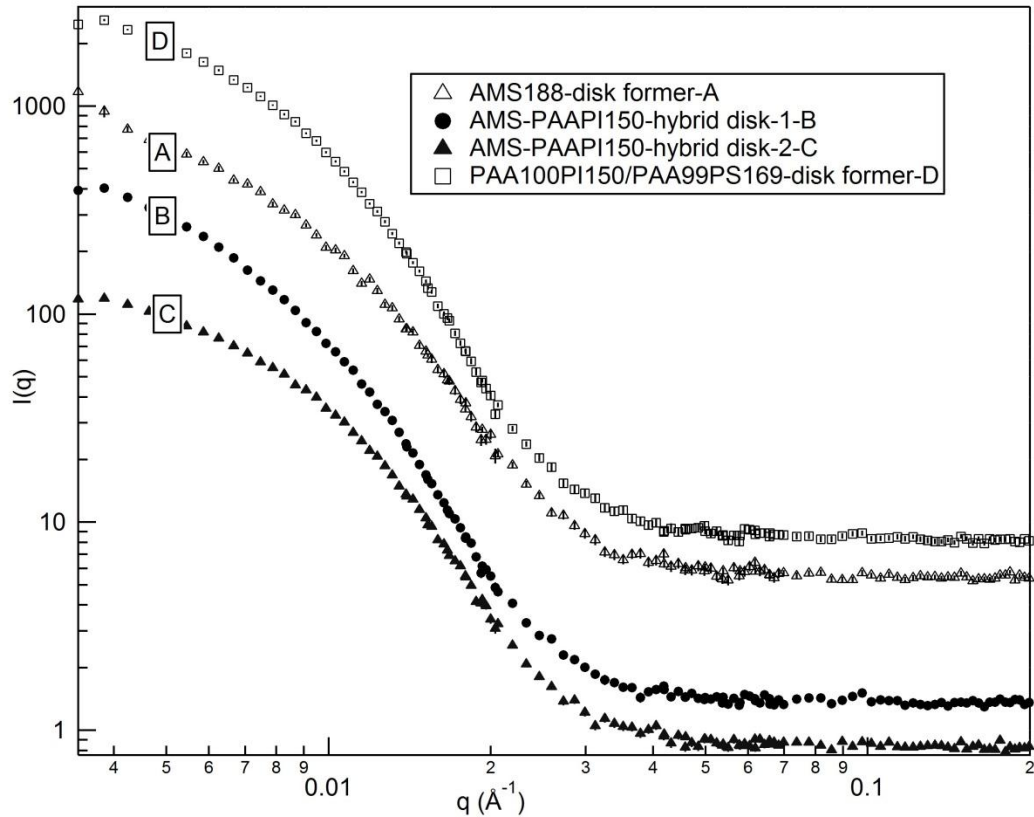


Figure 4.11 Small angle neutron scattering (SANS) data of disk formers assembled from PAA₉₉-*b*-PMA₁₀₃-*b*-PS₁₈₈ (AMS₁₈₈) and blends of PAA₁₀₀-*b*-PI₁₅₀/PAA₉₉-*b*-PS₁₆₉, respectively.

The SANS curves of the two disk formers, hybrid disks at different blending ratios are presented in Figure 4.11. Several nanostructure models were used in attempts to fit the SANS data including the stacked disk form factor model and the multilamellar model. However, no good fitting results are obtained. The lack of a reasonable fit of the SANS data is attributed to the size and shape polydispersity of the nanoparticle system as clearly observed in TEM.

4.4 Ternary blends of diblock copolymers with individual block copolymers that form spheres, cylinders and cylinders, respectively.

One unique advantage of using kinetic control of block copolymer blend solution assembly is that the number of blend units can be arbitrarily changed. Presumably, the diverse morphologies that each building block can exhibit on its own could be combined together into one nanoparticle, producing a wide variety of interesting and new nanostructures. Based on the previous results, complex morphology can be targeted with proper design of the assembly system⁴⁴, taking into account water content, amine condition, water addition rate, and aging time.

In this section, a targeted ternary blend system is discussed where the target nanostructure was conjoining sphere, cylinder and cylinder hybrid particles. The design is based on previous studies. Published results of sphere-cylinder blends *via* different kinetics⁴⁵ reveal that a sphere-former (PAA-*b*-PB) can serve as cylinder cutter to make sphere-short cylinder MCN. In addition, a fast water addition process generally results in the trapping of different block copolymers into one nanoparticle with different hydrophobic blocks locally phase separated into different compartmented domains. So, three diblock copolymers were selected and blended. Based on the acquired knowledge of their individually-formed structures at the same solution conditions, new and asymmetric nanostructures are predicted.

The important reason for selecting PS, PB and PMMA as the three hydrophobic compartments is that they exhibit different Flory-Huggins χ parameters pairwise with one another guaranteeing local phase separation after being trapped inside the same nanoparticle. According to the published data^{46, 47}, the three hydrophobic components as well as their χ parameters are listed as follows:

Table 4.1 χ parameters between hydrophobic block pairs at 25 °

PS/PMMA	PS/PB	PB/PMMA
0.03	0.045	0.071

According to the different interaction parameters between the three components, phase separation between PS, PMMA, and PB blocks with one another is expected within the nanoparticle cores.

4.4.1 Experimental procedures

The solution assembly of single diblock copolymers is the same as described in section 4.2.2. The three diblocks were blended with a molar ratio of 1:1:1 following the kinetic assembly process of amine addition and water addition as described above in 4.2.2. Water was added with an extremely fast rate by using immediate pipette addition. Samples were stirred for one day with images taken subsequently. Cast-film TEM with staining was used for characterization, as described in the Section 4.2.3. Cryo-TEM with staining was used for characterization, in which the OsO₄ vapor staining (0.3 mL) was applied to the solution sample (200 μ L) for 10 minutes before cryo-TEM imaging. The procedure was described in Chapter 3.1.4. PB was staining by using OsO₄, and PS was stained by RuO₄ sequentially.

4.4.2 Experimental Results

Single diblock assembly Results

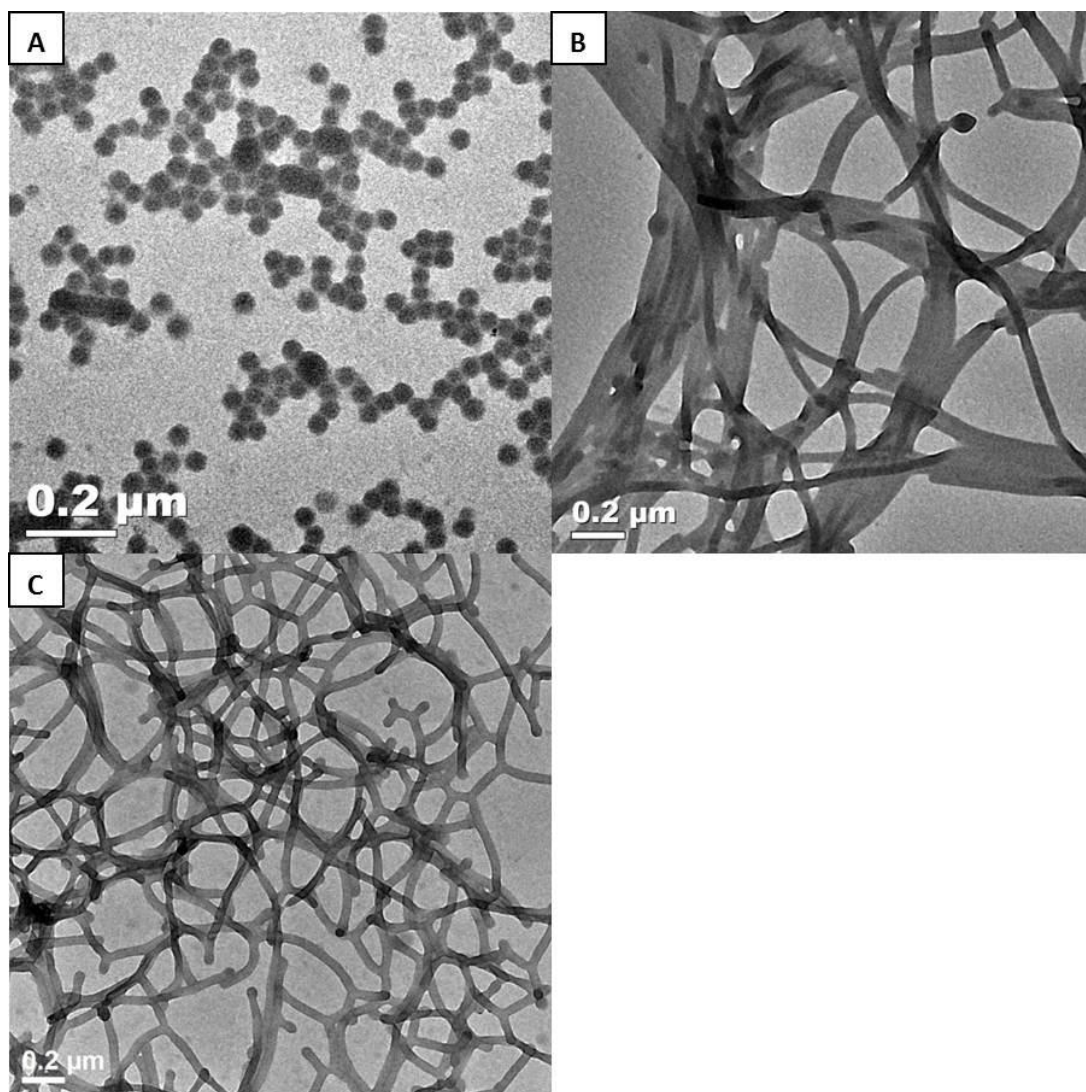


Figure 4.12 Dry-TEM images of micelles assembled from three different diblock copolymers. In all the assemblies: amine: acid=0.5:1, H₂O:THF=4:1, water was added to THF-amine-block copolymer solution (1 mL) to reach 80% relative volume fraction water to THF for a total of 5 mL at a relative medium rate of water addition (10 mL/h). (A): spheres assembled from PAA₇₅-*b*-PB₁₀₄; the diameter of spheres is ~50 nm; (B): cylinders assembled from PAA₉₉-*b*-PS₁₆₉; the diameter of cylinders is ~40 nm; (C): cylinders assembled from PAA₁₀₀-*b*-PMMA₁₇₀; the diameter of cylinders is ~45 nm.

Co-assembly results of three diblock copolymers

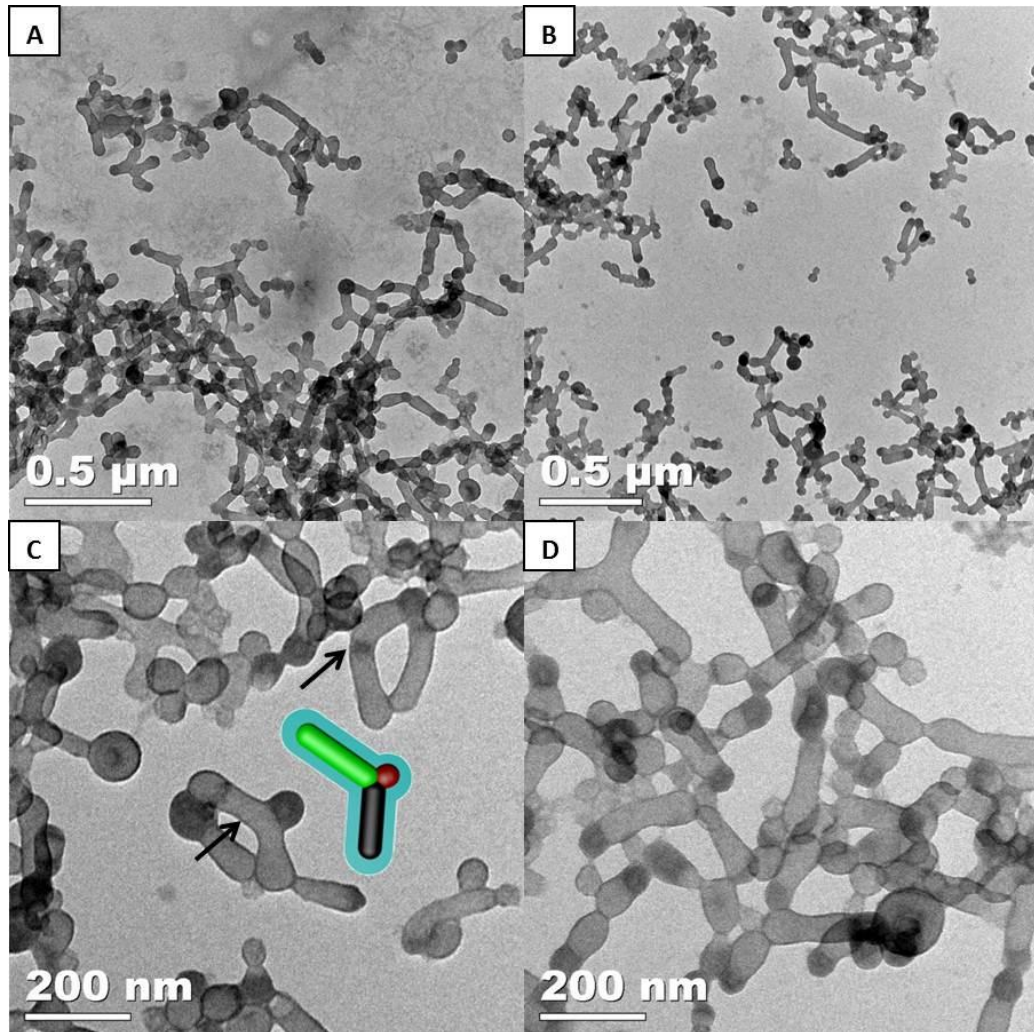


Figure 4.13 A, B: Lower magnification TEM images of asymmetric nanoparticles assembled from ternary blends of diblock copolymers: 1:1:1 molar ratio of PAA₇₅-*b*-PB₁₀₄:PAA₉₉-*b*-PS₁₆₉:PAA₁₀₀-*b*-PMMA₁₇₀. Samples were aged one day after water addition. TEM grids were prepared by dropping the solutions on the grid to make cast film after solution evaporation. OsO₄ vapor was used to stain the PB phase after carbon coated TEM grids were dried. C, D: High Mag TEM images of asymmetric nanoparticles. 3D cartoon represents the possible core-shell packing of asymmetric nanoparticles. The blue color represents PAA/amine shell, the red color represents the PB phase, the dark color represents the PS phase and the green color represents the PMMA phase.

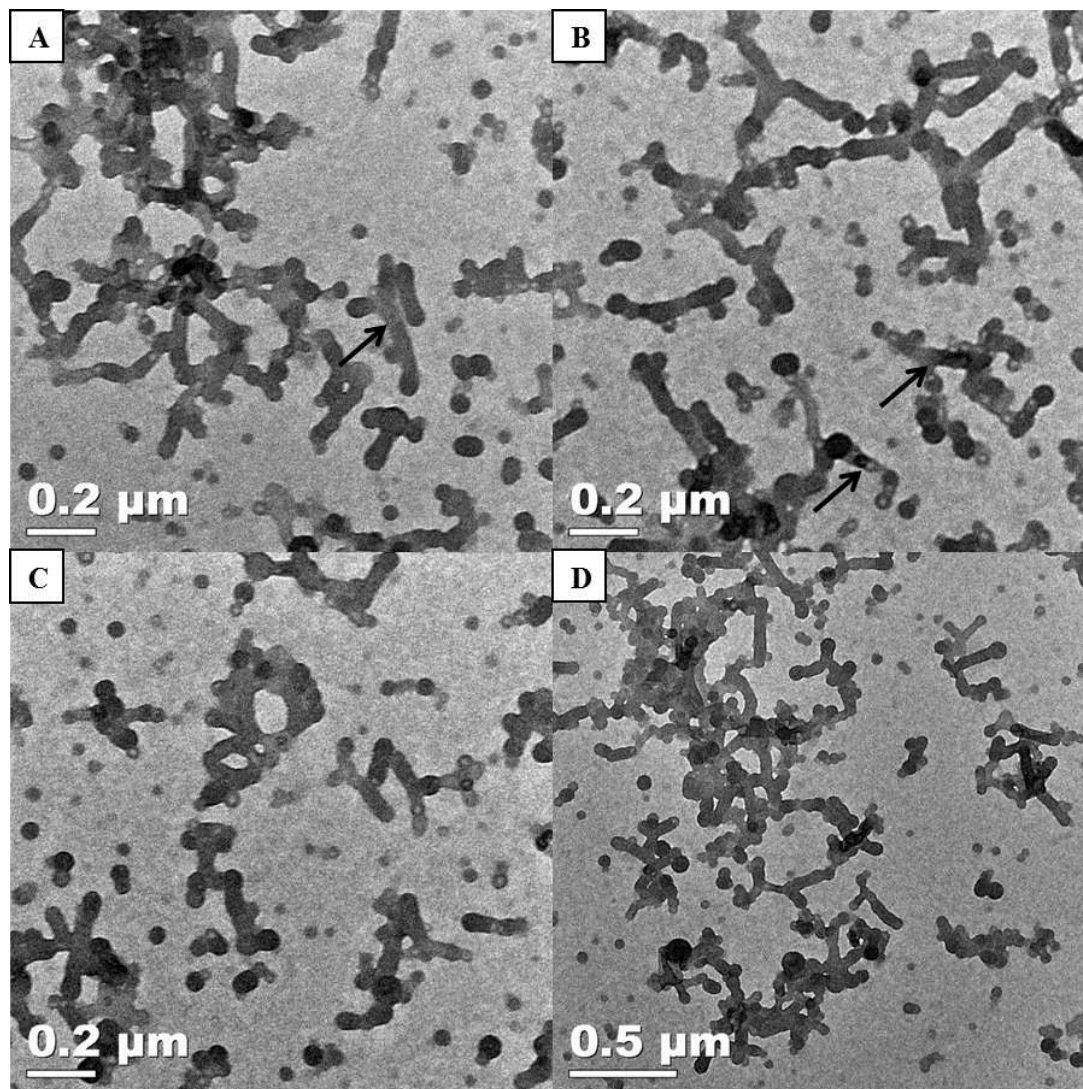


Figure 4.14 Sequential staining using RuO_4 after OsO_4 staining. A, B, C: TEM images of asymmetric nanoparticles. Grids were sequentially stained by OsO_4 and RuO_4 . D: Lower Mag image. Larger domains of dark phases were then observed, comparing with the images in Fig.4.13. Presumably, the PB and PS phases are all stained by sequentially staining using OsO_4 and RuO_4 .

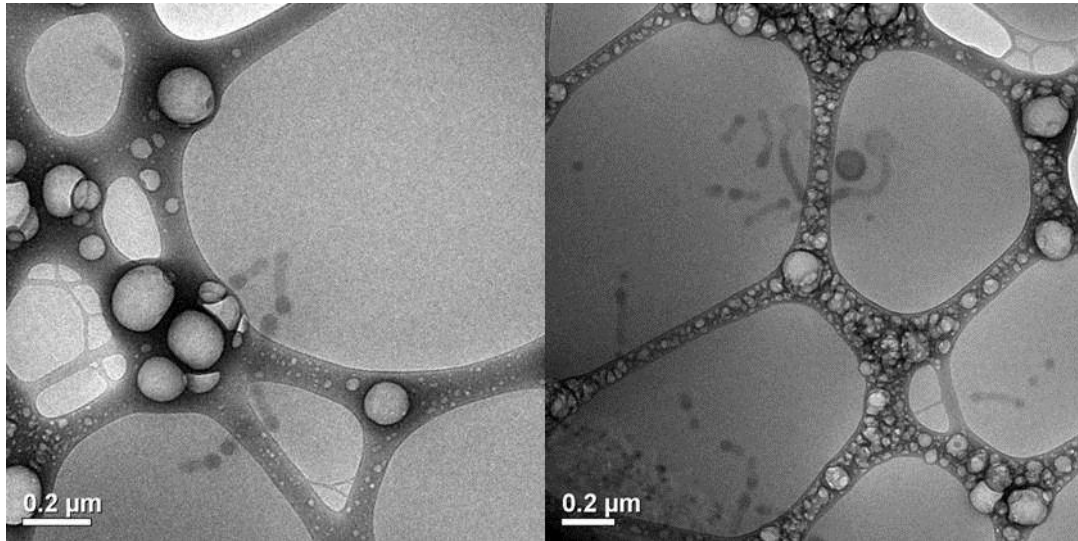


Figure 4.15 Cryo-TEM images of asymmetric nanoparticles from the same sample as in Figure 4.13. The solution was stained by OsO₄ vapor for 10 minutes before cryogenic TEM sample preparation. The dark domain is from PB phase. The light domain is interpreted to be PMMA and PS phases.

In the individual assembly of the diblock copolymers, spheres, cylinders and cylinders clearly are assembled, respectively. After blending together and fast water addition, a complicated mix of nanoparticle structure is observed with many sphere-cylinder-cylinder asymmetric nanoparticles with different hydrophobic phases trapped in the same core. In Figure 4.13.A-D, the PB phase, stained dark by OsO₄, is positioned in a middle bump of a large cylinder to produce an asymmetric nanoparticle. Or, the PB is frequently positioned at the end of cylindrical multicompartiment nanoparticle, as also represented in the 3D cartoon pictures. After sequential staining using RuO₄, larger areas of darker domains were observed in the cylinder sections of the assemblies indicating that both the PB/PS phases were stained within the cylinders.

Due to the difficulties in controlling the length of cylinder micelles, it is difficult to form well-defined sphere-cylinder-cylinder nanoparticles with monodisperse size and shape. More work is needed in order to make controllable ternary blends with

clearly mixed morphology, particularly when blending cylinders. The earlier results of mixed disks are more homogeneous locally compared with the cylinder-containing blends. The ternary blending results enrich the morphological diversity of multicompartiment and multigeometry nanoparticle libraries even exhibiting some asymmetry in nanoparticle formation, which is rare in solution assemblies. However, the limitations of forming well-defined nanostructures *via* blending strategy are also clear. More continuous work is needed to create other, well-defined nanostructures *via* bottom-up assembly strategies.

4.5 Discussion and Conclusion

In this chapter, formation of disk-disk, cylinder-cylinder, and star-like hybrid multicompartiment and multigeometry nanoparticles *via* binary or ternary blends are presented. Specific diblock, triblock copolymer compositions were designed as well as the blending and solution assembly strategy. Water was added with different rates targeting for unblended or blended nanoparticles, resulting in different hybrid nanoparticle systems as expected. This kinetic strategy eliminates the need for synthesis of new block copolymers to achieve the multifunctional nanoparticles. When water is added fast, disk-disk and cylinder-cylinder hybrid multicompartiment nanoparticles are formed. However, when water is added with a slow rate, the blended block copolymers are completely macrophase separated. With ternary blends, sphere-cylinder-cylinder hybrid nanoparticles are assembled. The new results indicate the importance of kinetic control methods. Block copolymers with new types of blocks and length ratios show themselves to be useful in future, designed blends. But, the limitations of the solution blend strategy on constructing hybrid nanoparticles are also revealed. Polydisperse size and shape of complex nanoparticles were observed when three different geometries were combined *via* ternary blends. The achievements of complexity may always result in certain polydispersity *via* simple blends and kinetic control. The following chapter will focus on exploring new chemistry methods to build up multidimensional nanostructure systems.

REFERENCES

1. Y. Mai and A. Eisenberg, *Chem. Soc. Rev.*, 2012, **41**, 5969-5985.
2. S. Jain and F. S. Bates, *Science*, 2003, **300**, 460-464.
3. J. D. Hartgerink, E. Beniash and S. I. Stupp, *Science*, 2001, **294**, 1684-1688.
4. H. Cui, Z. Chen, K. L. Wooley and D. J. Pochan, *Macromolecules*, 2006, **39**, 6599-6607.
5. A. Bernheim-Groswasser, R. Zana and Y. Talmon, *J. Phys. Chem. B*, 2000, **104**, 4005-4009.
6. J. Tanori and M. P. Pileni, *Langmuir*, 1997, **13**, 639-646.
7. H. Cui, Z. Chen, K. L. Wooley and D. J. Pochan, *Macromolecules* 2006, **39**, 6599-6607.
8. Z. Li, M. A. Hillmyer and T. P. Lodge, *Nano Lett.*, 2006, **6**, 1245-1249.
9. X. Wang, G. Guerin, H. Wang, Y. Wang, I. Manners and M. A. Winnik, *Science*, 2007, **317**, 644-647.
10. J. B. Gilroy, T. Gadt, G. R. Whittell, L. Chabanne, J. M. Mitchels, R. M. Richardson, M. A. Winnik and I. Manners, *Nat. Chem.*, 2010, **2**, 565-570.
11. L. Shen, H. Wang, G. Guerin, C. Wu, I. Manners and M. A. Winnik, *Macromolecules*, 2008, **41**, 4380-4389.
12. T. Gädt, N. S. Jeong, G. Cambridge, M. A. Winnik and I. Manners, *Nat. Mater.*, 2009, **8**, 144-150.
13. S. K. Patra, R. Ahmed, G. R. Whittell, D. J. Lunn, E. L. Dunphy, M. A. Winnik and I. Manners, *J. Am. Chem. Soc.*, 2011, **133**, 8842-8845.
14. H. Qiu, V. A. Du, M. A. Winnik and I. Manners, *J. Am. Chem. Soc.*, 2013, **135**, 17739-17742.

15. H. Qiu, G. Cambridge, M. A. Winnik and I. Manners, *J. Am. Chem. Soc.*, 2013, **135**, 12180-12183.
16. S. F. Mohd Yusoff, J. B. Gilroy, G. Cambridge, M. A. Winnik and I. Manners, *Journal of the American Chemical Society*, 2011, **133**, 11220-11230.
17. Z. M. Hudson, D. J. Lunn, M. A. Winnik and I. Manners, *Nat. Commun.*, 2014, **5**, 3372.
18. Z. M. Hudson, C. E. Boott, M. E. Robinson, P. A. Rupar, M. A. Winnik and I. Manners, *Nat. Chem.*, 2014, **6**, 893-898.
19. L. C. Paul A. Rupar, Mitchell A. Winnik, Ian Manners, *Science*, 2012, **337**, 559-562.
20. H. Qiu, Z.M. Hudson, M. A. Winnik, I. Manners, *Science*, 2015, **347**, 1329-1332.
21. R. Savic, L. Luo, A. Eisenberg and D. Maysinger, *Science*, 2003, **300**, 615-618.
22. Y. Geng, P. Dalhaimer, S. Cai, R. Tsai, M. Tewari, T. Minko and D. E. Discher, *Nat. Nanotechnol.*, 2007, **2**, 249-255.
23. A. O. Moughton, M. A. Hillmyer and T. P. Lodge, *Macromolecules*, 2012, **45**, 2-19.
24. F. Schacher, E. Betthausen, A. Walther, H. Schmalz, D. V. Pergushov and A. H. E. Müller, *ACS Nano*, 2009, **3**, 2095-2102.
25. A. H. Groschel, A. Walther, T. I. Lobling, F. H. Schacher, H. Schmalz and A. H. Müller, *Nature*, 2013, **503**, 247-251.
26. F. He, T. Gadt, I. Manners and M. A. Winnik, *J. Am. Chem. Soc.*, 2011, **133**, 9095-9103.
27. Y. Chen, *Macromolecules*, 2012, **45**, 2619-2631.
28. L. Y. Jin, J.-H. Ahn and M. Lee, *J. Am. Chem. Soc.*, 2004, **126**, 12208-12209.
29. L. Ren, F. Ke, Y. Chen, D. Liang and J. Huang, *Macromolecules*, 2008, **41**, 5295-5300.

30. Z. Zhou, Z. Li, Y. Ren, M. A. Hillmyer and T. P. Lodge, *J. Am. Chem. Soc.*, 2003, **125**, 10182-10183.
31. V. Percec, P. Leowanawat, H. J. Sun, O. Kulikov, C. D. Nusbaum, T. M. Tran, A. Bertin, D. A. Wilson, M. Peterca, S. Zhang, N. P. Kamat, K. Vargo, D. Moock, E. D. Johnston, D. A. Hammer, D. J. Pochan, Y. Chen, Y. M. Chabre, T. C. Shiao, M. Bergeron-Brlek, S. Andre, R. Roy, H. J. Gabius and P. A. Heiney, *J. Am. Chem. Soc.*, 2013, **135**, 9055-9077.
32. L. Yin and M. A. Hillmyer, *Macromolecules*, 2011, **44**, 3021-3028.
33. S. Venkataraman, A. L. Lee, H. T. Maune, J. L. Hedrick, V. M. Prabhu and Y. Y. Yang, *Macromolecules*, 2013, **46**, 4839-4846.
34. Y. Shi, W. Zhu, D. Yao, M. Long, B. Peng, K. Zhang and Y. Chen, *ACS Macro Letters*, 2014, **3**, 70-73.
35. Z. Li, Z. Chen, H. Cui, K. Hales, K. Qi, K. L. Wooley and D. J. Pochan, *Langmuir* 2005, **21**, 7533-7539.
36. J. Zhu, S. Zhang, K. Zhang, X. Wang, J. W. Mays, K. L. Wooley and D. J. Pochan, *Nat. Commun.*, 2013, **4**, 2297-2301.
37. S. J. S. Qazi, G. Karlsson and A. R. Rennie, *J. Colloid Interface Sci.*, 2010, **348**, 80-84.
38. K. Liu, Y. Deng, N. Zhang, S. Li, H. Ding, F. Guo, W. Liu, S. Guo and X.-Z. Zhao, *Microfluidics and Nanofluidics*, 2012, **13**, 761-767.
39. I.-H. Lee, P. Amaladass, K.-Y. Yoon, S. Shin, Y.-J. Kim, I. Kim, E. Lee and T.-L. Choi, *J. Am. Chem. Soc.*, 2013, **135**, 17695-17698.
40. J. He, Y. Liu, T. C. Hood, P. Zhang, J. Gong and Z. Nie, *Nanoscale*, 2013, **5**, 5151-5166.
41. Y. Gu, R. M. Dorin and U. Wiesner, *Nano Lett.*, 2013, **13**, 5323-5328.
42. Q. Ma and K. L. Wooley, *Journal of Polymer Science: Part A: Polymer Chemistry*, 2000, **38**, 4805-4820.
43. S. Zhong, H. Cui, Z. Chen, K. L. Wooley and D. J. Pochan, *Soft Matter*, 2008, **4**, 90-94.

44. R. C. Hayward and D. J. Pochan, *Macromolecules*, 2010, **43**, 3577-3584.
45. D. J. Pochan, J. Zhu, K. Zhang, K. L. Wooley, C. Miesch and T. Emrick, *Soft Matter*, 2011, **7**, 2500-2506.
46. T. P. Russell, J. Rex P. Hjelm and P. A. Seeger, *Macromolecules* 1990, **23**, 890-893.
47. R. Stadler, T. Auschra, T. J. Beckmann, U. Krappe, I. Voigt-Martin and L. Leibler-L, *Macromolecules*, 1996, **28**, 3080-3091.

Chapter 5

DESIGN OF FUNCTIONALIZED BLOCK COPOLYMER FOR NANOMATERIAL CONSTRUCTION VIA INTERPARTICLE CROSSLINKING

In this chapter, the design of functionalized block copolymers for hierarchical assembly to form superstructure of blended nanoparticles is presented. In this work, the diblock copolymers are functionalized with thiol groups for post-assembly interparticle crosslinking. The assembly behaviors with and without functionality are compared. The preliminary exploration of two-dimensional and three-dimensional nanoparticle assembly is presented. The thiol functionalized molecule was synthesized in Wooley lab when visiting University of Texas A&M, and the PAA-*b*-PI molecule was synthesized in Mays lab.

5.1 Introduction

Assembly of small building blocks such as atoms, molecules and nanoparticles into macroscopic structures, many times referred to as a “bottom up” assembly strategy, is a topic that covers chemistry, physics and material science^{1,2}. The requirement of highly ordered, well-defined, multifunctional nanostructures limits the efficacy of solution assembly in the successful construction of discrete, hybrid-nanoparticles, let alone multidimensional nanomaterials through interparticle association. Post-assembly particle-particle association is one strategy commonly used to introduce superstructure into nanoparticle systems. As discussed in earlier chapters of this thesis, micelles constructed from synthetic, amphiphilic block copolymers provide the opportunity to achieve this goal³. The post-particle assembly, intermicelle association can be achieved in many ways, such as reported chemical linking between assembled particles⁴, host-guest weak-force association between functionalized

building blocks⁵ and multistep crystalline growth *via* homopolymer and crystalline-core block copolymer blends^{3,6}. Even hydrogels can be produced *via* post-assembly interparticle chemical crosslinking from functionalized micelles^{7,8}. Besides macromolecular solution assemblies, the interparticle association idea is also applied in other materials. Talapin and coworkers have reported a series of work on two-dimensional⁹ or three-dimensional¹⁰ superlattice structures built on ligand-functionalized nanocrystals. For all the programmable interparticle association strategies, well-defined subunits are required for post-assembly subunit linking and definition in the final structure¹¹. In this chapter, chemical reaction is designed to introduce particle-particle linking based on the well-regulated hybrid nanoparticle assembly.

Based on the results presented in Chapter 3 and Chapter 4, controlled multicompartment and multigeometry nanoparticles were constructed *via* tuning of solvent addition rates in designed block copolymer blends. In this chapter, an additional hierarchical multistep assembly method was used to construct targeted superstructure *via* crosslinking of well-defined, anisotropic nanoparticles assembled from functionalized block copolymers. The thiolene reaction between designed functionalized nanoparticles was applied as the strategy to introduce interparticle crosslinking^{12,13}. Thiol-functionalized diblock copolymer HS-PAA-*b*-PS was designed and synthesized. The other block copolymer, PAA-*b*-PI, was designed for blending with HS-PAA-*b*-PS, with similar hydrophilic and hydrophobic block lengths and similarity in assembly size and geometry. Hybrid nanoparticles with an anisotropic shell combining both thiol functionalized PAA and pure PAA were constructed by blending of the two diblock copolymers. An additional block copolymer, Hydroxyethyl acrylate (HEA)-PAA-*b*-PS, was used in nanoparticle assembly in order to provide alkenes on the surface of particles to crosslink with the thiols on other assembled particles for desired interparticle association.

5.1.1 Material Design and Synthesis

The reason for choosing PAA-PS and PAA-PI as the diblock copolymers for individual particles formation originates from the blending results in Chapter 3. PAA₉₀-*b*-PS₁₂₀ was selected as one diblock copolymer. Thiol functionalized HS-PAA-*b*-PS was then prepared. PAA₃₆-*b*-PI₁₆₀ was designed afterward according to the assembly results from functionalized HS-PAA-*b*-PS. Hydroxyethyl acrylate (HEA) modified PAA₉₉-*b*-PS₇₆ was used as a target for reaction with HS-PAA-*b*-PS since it has the diene functionality in the PAA domain. The nanoparticles assembled from HEA-PAA-*b*-PS were small spheres and are designed to react with thiol functionalized, larger nanoparticles to form interparticle associations and nanoparticle superstructures, such as three dimensional agglomerates or large two dimensional sheets (as drawn in the cartoon below).

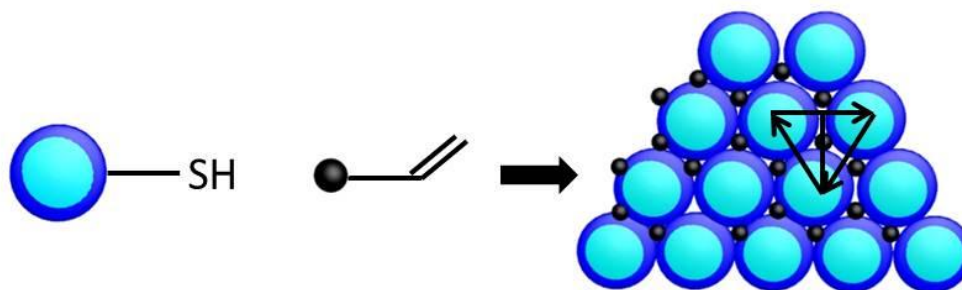
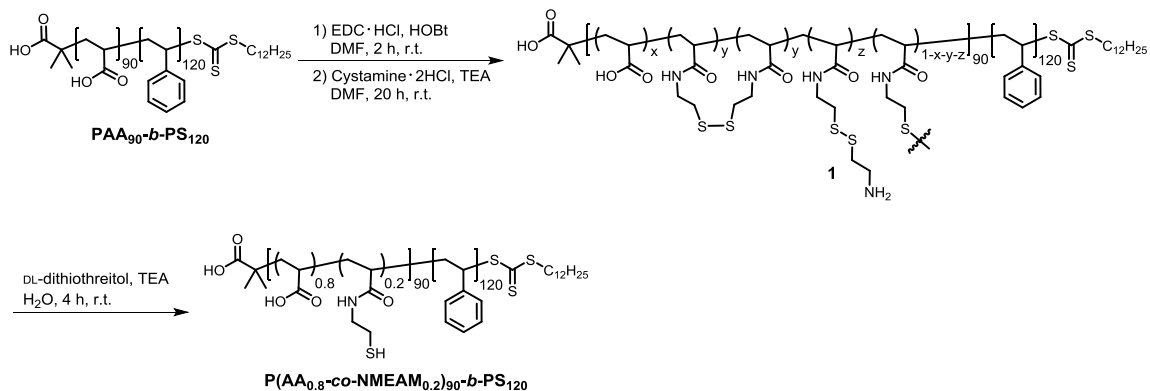


Figure 5.1 Designed interparticle association between hybrid disk nanoparticles with thiol functionality on the periphery and small particles with diene present in the surface. In the left cartoon, the dark blue edge represents the thiol functionalized PAA shell and PS core from HS-PAA-*b*-PS, and the light blue core represents the PAA shell connected to the PI block disk interior from PAA-*b*-PI diblock copolymer when blended with HS-PAA-*b*-PS. In this particular design, the larger particles exhibit a disk geometry with an anisotropic surface (the PAA on the edge contain the thiol functionalities, while the PAA shell in the middle disk domain does not.). In the middle cartoon, the dark sphere represents the small assemblies from HEA modified PAA-*b*-PS with diene on the surface. After thiolene reaction, hybrid disks are presumably linked together through the dark spheres and two-dimensional large sheet-like structure can be formed.

5.1.2 Synthesis of Thiol Functionalized Diblock Copolymer PAA₉₀-*b*-PS₁₂₄



Scheme 5.1 Synthetic scheme for the synthesis of poly(AA_{0.8}-co-NMEAM_{0.2})₉₀-*b*-PS₁₂₀. Throughout the chapter, HS₁₈-PAA₇₂-*b*-PS₁₂₀ was also used to indicate the chemical structure of poly(AA_{0.8}-co-NMEAM_{0.2})₉₀-*b*-PS₁₂₀.

The HS-PAA-*b*-PS was synthesized in Wooley lab by Xun He. Amphiphilic block copolymer poly(acrylic acid)-*b*-polystyrene (PAA₉₀-*b*-PS₁₂₀) was synthesized according to a previously reported method¹⁴. For the synthesis of 1 in scheme 5.1, PAA₉₀-*b*-PS₁₂₀ (49.6 mg, 2.48 μmol), 1-ethyl-3-(3-dimethylaminopropyl)carbodiimide hydrochloride (EDC·HCl, 16.8 mg, 87.6 μmol), hydroxybenzotriazole (HOBT, 11.3 mg, 83.6 μmol) were dissolved in DMF (5 mL) in a flame dried 15 mL round bottom flask and allowed to stir in room temperature for 2 h. To this solution, cystamine dihydrochloride (6.24 mg, 27.7 μmol), triethylamine (83.5 μL, 0.599 mmol) in DMF (1 mL) was added and further allowed to stir for 20 h at room temperature before being transferred to a presoaked dialysis tubing (M_w cut off *ca.* 6000-8000 Da), and dialyzed against nanopure water for 3 days, achieving polymer 1 as a white solid after lyophilization. ¹HNMR was used to characterize the Polymer 1. Polymer 1 (30.0 mg, 1.43 μmol), triethylamine (10 μL, 71.7 μmol) and DL-dithiothreitol (58.9 mg, 0.382 mmol) were dissolved in H₂O (2 mL) in a 5 mL vial and allowed to stir for 4 h at room temperature before being transferred to presoaked dialysis tubing (M_w cut off *ca.* 6000-8000 Da), and dialyzed against nanopure water for 3 days, achieving P(AA_{0.8}-co-NMEAM_{0.2})₉₀-*b*-PS₁₂₀ as a white solid after lyophilization (25.1 mg, 83.6%). ¹H

NMR was used to analyze the polymer 2 and confirm the percentage of thiol functionality. The provided synthesis details are for information purposes.

5.1.3 Synthesis of polyisoprene-*b*-poly(acrylic acid)

*Synthesis of polyisoprene-*b*-poly(*tert*-butyl acrylate)*

The synthesis of PAA-*b*-PI was performed by Christopher Hurley from the collaborating Mays lab. All materials were obtained from Aldrich with the exception of sec-butyllithium (1.4 M in hexanes, Acros), isoprene (Acros), tetrahydrofuran- d_8 (Acros), tetrahydrofuran (Fisher), methanol (Fisher), hexanes (Fisher), aluminum oxide (activated, neutral, Brockmann Grade I, 58 Å, Alfa Aesar), and chloroform- d_1 (Cambridge Isotope Laboratories, Inc.). The detailed method of purification for all monomers, solvents and additives has been previously described in literature. Diblock copolymers of isoprene and *tert*-butyl acrylate (PI-*b*-PtBA) were synthesized by sequential anionic polymerization using high vacuum techniques according to standard protocol^{15, 16}. Deprotection of tertiary butyl group in PI-*b*-PtBA was achieved by using HCl¹⁷.

Characterization of PAA-PI

Size exclusion chromatography (SEC) and ¹H-NMR were performed to characterize the PAA-PI. Data was provided by Christopher Hurley from the Mays lab. SEC was performed using a Tosoh EcoSEC instrument using standard polystyrene with M_n from 580 to 7.5×10^6 g/mol to determine number-average molecular weight, M_n , and the polydispersity index (PDI or \mathcal{D}) of all samples prior to hydrolysis. The polymer was eluted in THF at 40 °C at a flow rate of 0.35 mL/min. ¹H-NMR spectroscopy was performed on Varian Mercury 300 MHz spectrometer with THF- d_8 and chloroform- d_1 as solvents.

PI₁₆₀-*b*-PAA₃₆

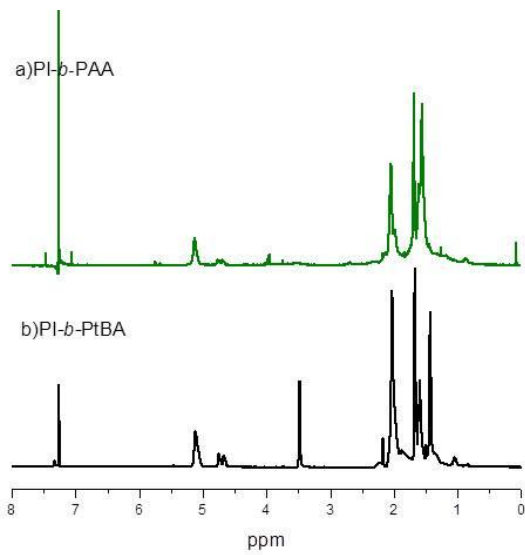


Figure 5.2 NMR result of PI₁₆₀-*b*-PAA₃₆

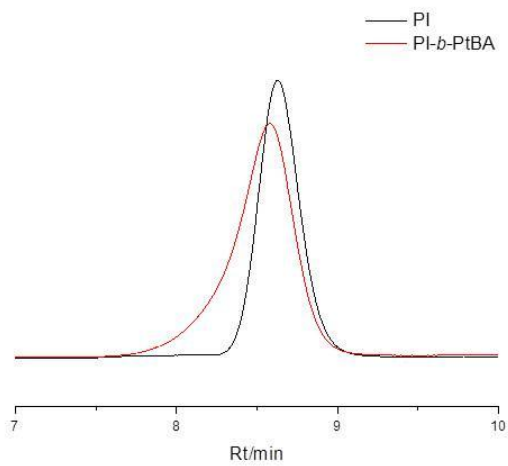


Figure 5.3 GPC result of PI₁₆₀-*b*-PAA₃₆

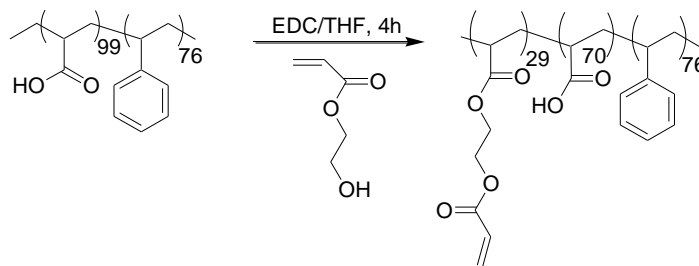
Table 5.1 M_n and \mathcal{D} of PAA-*b*-PI

PI		PI- <i>b</i> -PtBA	
M_n	\mathcal{D}	M_n	\mathcal{D}
10,905 ^a	1.026	20,300 ^b	1.081

^a M_n adjusted by a factor of 1.6 to reflect the accurate value versus the value determined based on polystyrene standards. ^b M_n values given based on polystyrene standards.

5.1.4 Modification of PAA₉₉-*b*-PS₇₆ with hydroxyethyl acrylate (HEA) and characterization

The modification of PAA₉₉-*b*-PS₇₆ with hydroxyethyl acrylate (HEA) was generated according to referenced protocols⁷, in the Pochan lab. Diene is put onto the PAA domain of PAA-*b*-P. Thus the assembled shell also has the diene function that can be used for thiolene reaction with thiol functionalized nanoparticles after assembly. PAA₉₉-*b*-PS₇₆ ($M_n=15100$, $\mathcal{D}=1.05$) is dissolved in THF to form a solution at concentration (2 mg/mL, 8 mg in 4 mL, $5.3e^{-4}$ mmol) and HEA (0.053 mmol, 6 μ L) were dissolved in tetrahydrofuran (THF, 4 mL). The solution was stirred at room temperature for 30 min before the addition of N-(3-dimethylaminopropyl)-N-ethylcarbodiimide (EDC). The mixture was stirred at room temperature in the dark for 4 hours. The sample was then dialyzed against water to remove the remaining impurities from HEA and EDC. The sample in water was then lyophilized to obtain the dried out sample. Small amount of dried out sample was then dissolved in DMSO-*d*₆ for ¹H NMR analysis. ¹H NMR (DMSO-*d*₆): δ 5.9-6.1 CH=CH₂, and 4.0-4.8, CH₂-CH₂ groups in hydroxyethyl acrylate). ¹H NMR analysis indicated a 20 mol% acrylation of the PAA block and the final polymer had a composition of P(AA-g-HEA)-*b*-PS and a M_n of 17874.



Scheme 5.3 Scheme of HEA modification of PAA₉₉-*b*-PS₇₆

5.2 Multistep Self-assembly Experimental Procedures

5.2.1 Self-assembly of Single Diblock Copolymer

*Self-assembly of nonfunctionalized PAA₉₀-*b*-PS₁₂₄ and functionalized HS₁₈-PAA₇₂-*b*-PS₁₂₀*

The added, new functionality in the PAA block of the block copolymer, alters the assembly behavior of the molecules relative to the unfunctionalized diblock. The self-assembly behaviors of PAA₉₀-*b*-PS₁₂₄ and HS₁₈-PAA₇₂-*b*-PS₁₂₀ were compared in this chapter.

The individual polymer solutions were firstly prepared by dissolving each diblock copolymer (PAA₉₀-*b*-PS₁₂₄, HS₁₈-PAA₇₂-*b*-PS₁₂₀) separately in THF to reach a concentration of 2 mg/mL. The solution was stirred for 24 hours for complete dissolution. Organic diamine (1 vol% concentration in THF) was then added to reach a polymer concentration of 0.1 wt% and different amine to acid ratios (0.5:1 or 1:1). Next, water was added to the 1 mL THF solution to reach 80% water concentration with different water addition rates. Final polymer assemblies were formed in 5 mL total mixed solvent (THF/H₂O=1/4 v/v) with a final polymer concentration at 0.018 wt%.

Test of thiol functionality stability

To test the free thiol stability in different solvent environment, small molecule cystamine was dissolved in different acidic or basic buffer solutions with a concentration of 10 μM . UV-vis was used to detect the absorption of dithiolide functionality that is possibly formed in different solution environments.

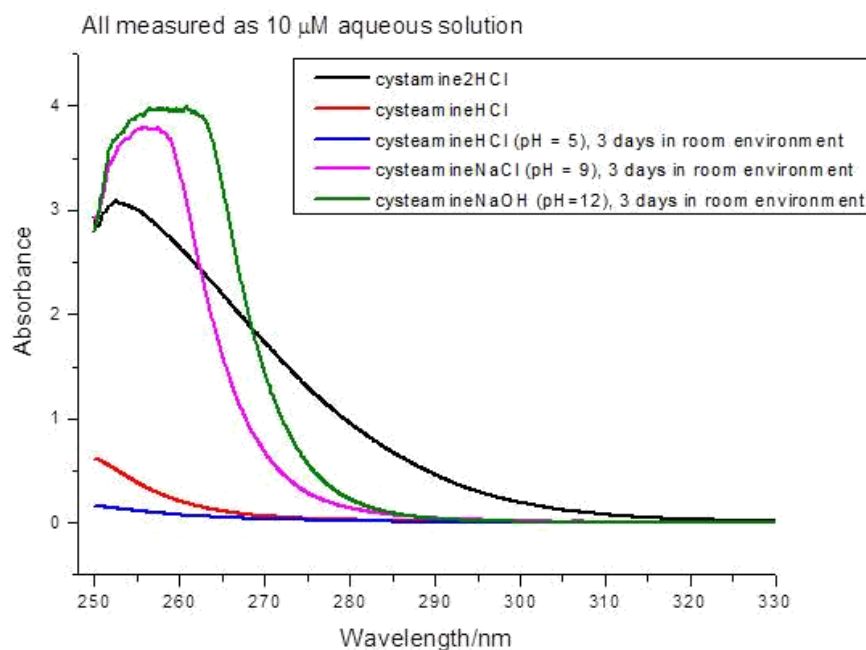


Figure 5.4 UV-vis spectroscopy of cystamine in different buffer solutions. Data provided by Xun He

This characterization was completed by Xun He from Wooley lab. The peak at ca. 260 nm is assigned as the absorption of S-S. This graph indicates that SH of cystamine is stable in slightly acidic environment (pH = 5) but prone to oxidation in basic environments (pH = 9 or 12). In all assembly experiments, the amine to acid ratio was either 0.5:1 or 1:1, meaning that the solution condition is slightly acidic. We believe that the thiol functionality is free during the assembly and are reactive for post-assembly crosslinking.

Self-assembly procedure of PAA₃₆-b-PI₁₆₀

The polymer was firstly prepared by dissolving PAA₃₆-b-PI₁₆₀ to reach a concentration of 2 mg/mL. The solution was stirred for 24 hours for complete dissolution. Organic diamine (1 vol% concentration in THF) was then added to reach a polymer concentration of 0.1 wt% and different amine to acid ratios (0.5:1, 1:1). Next, water was added to the 1 mL THF solution to reach 80% water concentration through different water addition rates. Final polymer assemblies were obtained in 5 mL total mixed solvent volume (THF/H₂O=1/4 v/v) with a final polymer concentration at 0.02 wt%.

Self-assembly procedure of HEA₂₉-PAA₇₀-b-PS₇₆

The polymer solution was prepared by dissolving HEA₂₉-PAA₇₀-b-PS₇₆ in THF to reach a concentration of 2 mg/mL. The solution was stirred for 24 hours for complete dissolution. Organic diamine (1 vol% concentration in THF) was then added to reach a polymer concentration of 0.1 wt% and amine to acid ratio 1:1. Next, water was added to the 1 mL THF solution to reach 80% water concentration with a slow water addition rate (1 mL/h). Final polymer assemblies were thus obtained in 5 mL total mixed solvent (THF/H₂O=1/4 v/v) with a final polymer concentration at 0.018 wt%.

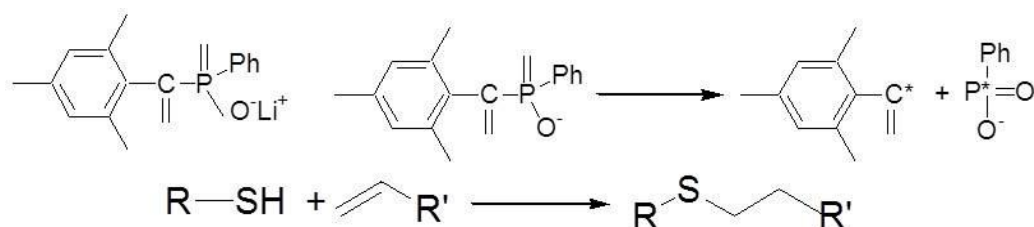
5.2.2 Co-assembly of PAA₃₆-PI₁₆₀ and Functionalized HS₁₈-PAA₇₂-b-PS₁₂₀

Based on the assembly results of single diblock copolymer PAA₃₆-b-PI₁₆₀ and HS₁₈-PAA₇₂-b-PS₁₂₀, co-assembly of the two diblock copolymers was performed. The solutions of two individual diblock copolymers were made and subsequently stirred for 24 h to allow for sufficient mixing. Diamine was then added to reach an amine to acid ratio of 0.5:1, and extra THF was added in the meantime to reach a polymer weight percent at 0.1 wt%. After the solution was stirred for 24 h, water was added to trigger the self-assembly. 1.2 mL water was added to 0.3 mL THF block copolymer

solution with a fast rate (30 mL/h) to initiate the coassembly and hybrid nanoparticle formation in 80% H₂O/20% THF solution, with the polymer concentration at 0.018 wt%. The solution was aged for one day before imaging of the hybrid nanoparticles.

5.2.3 Interparticle Association via Thiolene Reaction

In this multistep assembly, interparticle association was generated after the formation of hybrid nanoparticles and the formation of diene functionalized small particles. The hybrid nanoparticle solution and the diene functionalized small sphere solution were mixed with the ratio of 9:1 (0.45 mL: 0.05 mL). Lap was used as the photo initiator for the thiolene reaction. Lap was mixed in the solution to reach a concentration at 0.067 wt%. Lap is used widely as a highly water-soluble initiator with strong absorbance at 365 nm. The mixed solution was positioned under a UV lamp with the light at 365 nm wavelength for 15 minutes.



Scheme 5.4 Chemical structure of Lap and the mechanism of the thiolene reaction. The chemical structure of Lap initiator (upper left); the initiating mechanism of forming radicals for thiolene reaction (upper right). The mechanism of thiolene reaction was (bottom).

5.2.4 TEM and Cryo-TEM Experiments

The procedure for cast-film TEM was described in Chapter 3. Cryo-TEM imaging process was described previously in Chapter 3. All solution assemblies were aged one day before imaging.

5.3 Results and Discussions

5.3.1 Self-assembly of Single Diblock Copolymers

*Self-assembly of non-functionalized and functionalized PAA-*b*-PS*

The assembled nanoparticles of nonfunctionalized PAA-*b*-PS and functionalized PAA-*b*-PS were compared, as shown in Figure 5.5 A, B. In the solution conditions with amine to acid equals to 0.5:1 and 80% water conditions, the thiol functionalized PAA-*b*-PS was assembled to stacked disk structures and the PAA-*b*-PS was assembled to cylinder structures. The introduction of thiol functions altered the assembly behavior and the lower-curvature disk structures are attributed to the decrease of the hydrophilic domain, compared with the nonfunctionalized PAA-*b*-PS. With a higher amine to acid condition (1:1), disk-like structure was formed with thiol functionalized PAA-*b*-PS. Compared with the lower amine condition with stacked disks, the saturated amine to acid ratio attribute to the discrete disk formation¹⁸. The diameter of the disks is between 60 to 80 nm, which is larger than the diameter of the cylinders and indicates the disk-like structure rather than spheres breaking up from cylinders. In addition, overlapped disks are also observed in Figure 5.5 C and D. All these results indicated that disk-like nanoparticles are assembled from thiol functionalized PAA-*b*-PS, and this structure will be taken advantages of in the co-assembly of hybrid multicompartment disk nanoparticles.

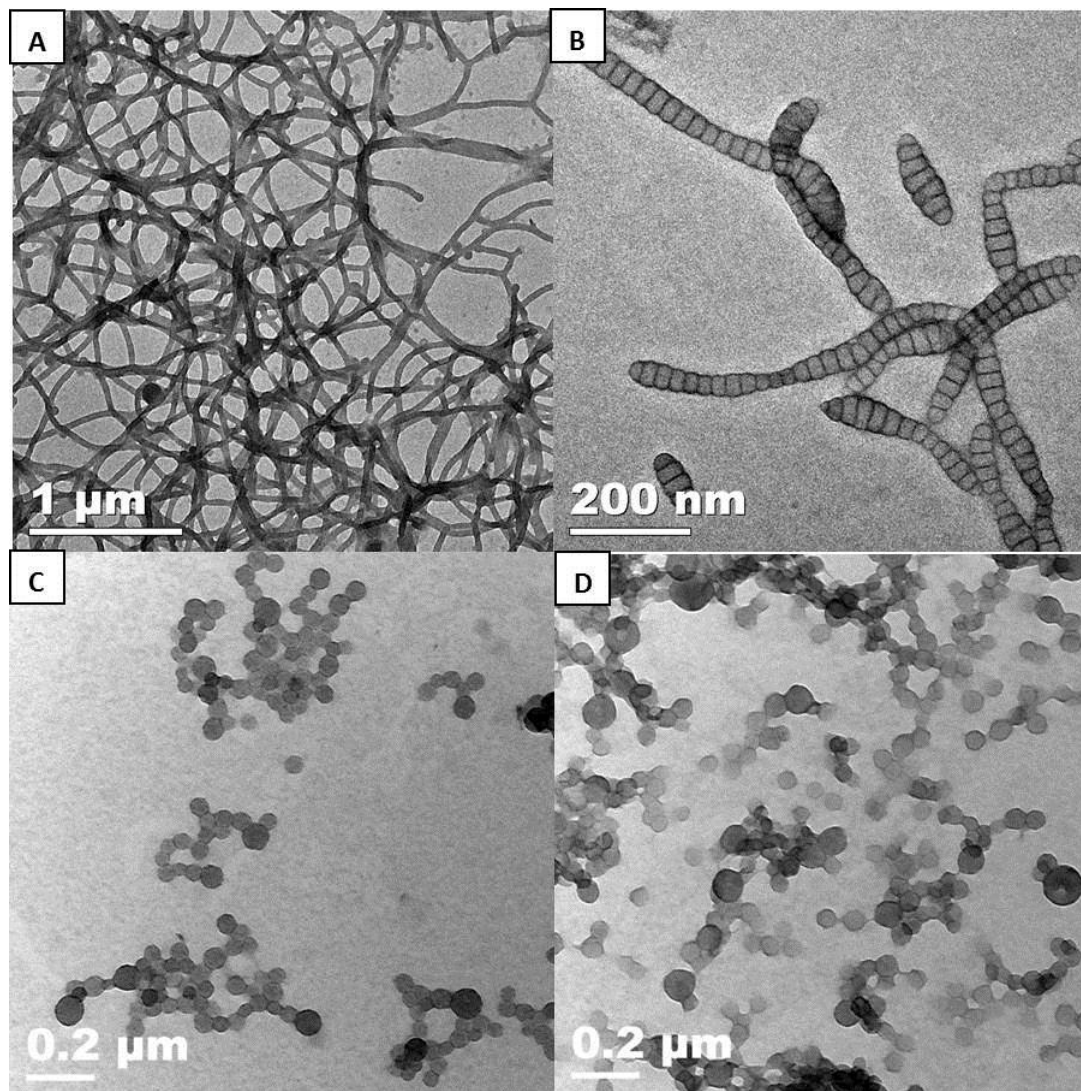


Figure 5.5 TEM images of the solution assemblies of PAA₉₀-*b*-PS₁₂₄ and HS₁₈-PAA₇₂-*b*-PS₁₂₀. A: Cylinders assembled from PAA₉₀-*b*-PS₁₂₄ with diamine: acid=0.5:1, 80% H₂O/20% THF. The diameter of the cylinders is 45 nm. Water was added with the rate of 1 mL/h. B: Stacked disks assembled from HS₁₈-PAA₇₂-*b*-PS₁₂₀ with diamine: acid=0.5:1, 80% H₂O/20% THF, water was added in a slow rate of 1 mL/h. C, D: disk structure assembled from HS₁₈-PAA₇₂-*b*-PS₁₂₀ with diamine: acid=1:1, 80% H₂O/20% THF. Water was added into THF with a slow rate at 1 mL/h. The diameter range of the disks is between 60 nm-80 nm.

Self-assembly of PAA₃₆-b-PI₁₆₀

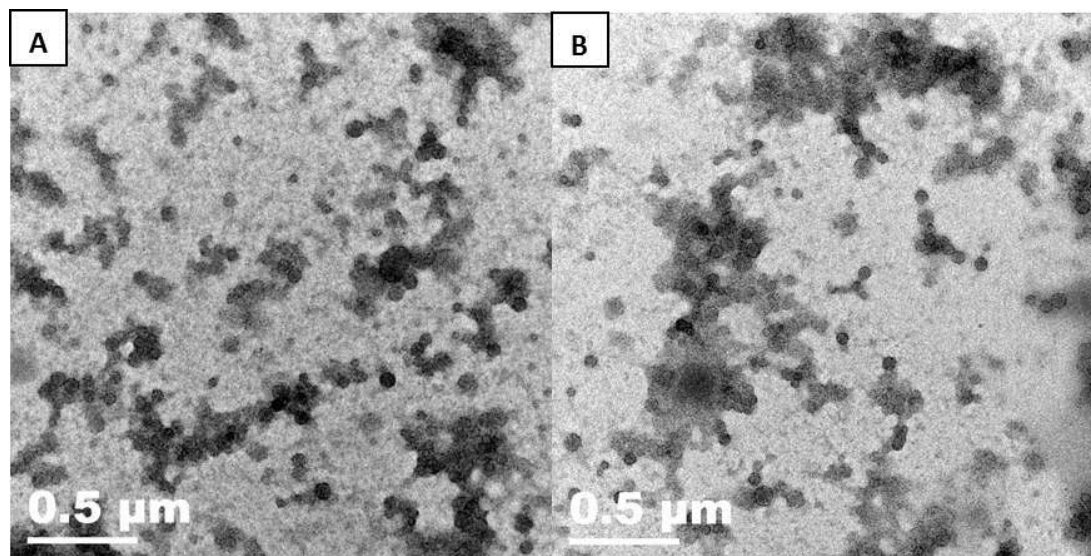


Figure 5.6 TEM images of nanoparticles assembled from PAA₃₆-b-PI₁₆₀. A, B: TEM images of nanoparticles assembled from PAA₃₆-b-PI₁₆₀, with amine to acid=1:1, 80% H₂O/20% THF. The diameters of the particles are around 70 to 80 nm.

Self-assembly of HEA₂₉-PAA₇₀-b-PS₇₆

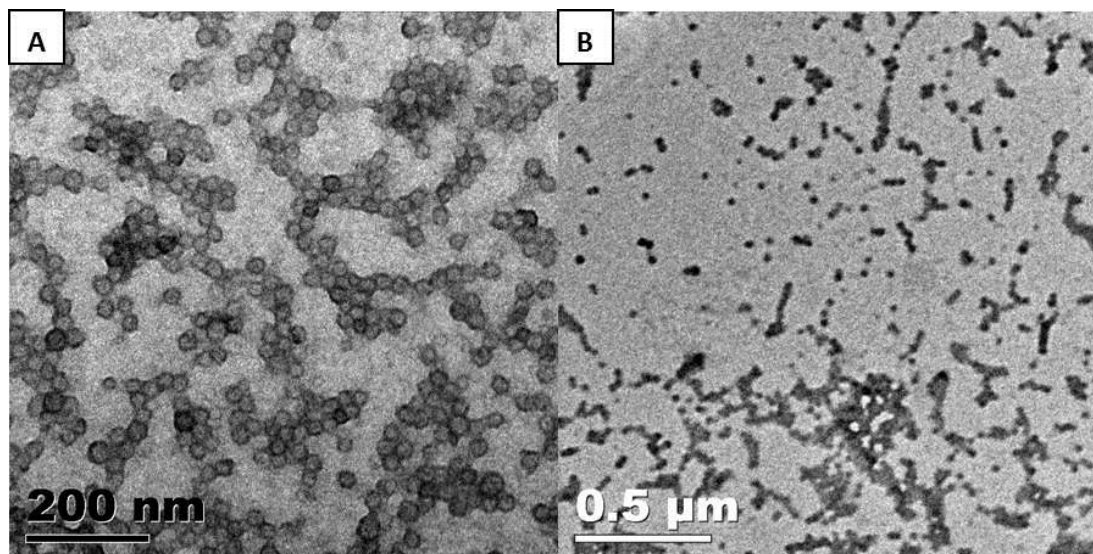


Figure 5.7 TEM images of the spherical particles assembled from HEA₂₉-PAA₇₀-b-PS₇₆. **A:** cast-film TEM images of the spheres assembled from HEA₂₉-PAA₇₀-b-PS₇₆. Images were stained using uranyl acetate. **B:** cast-film TEM images of the spheres assembled from HEA₂₉-PAA₇₀-b-PS₇₆. Images were not stained. The diameter of the spheres is 30 nm.

As shown in Figure 5.6, nanoparticles are assembled from PAA₃₀-b-PI₁₆₀ with the amine to acid ratio at 1:1 and 80% water. The diameters of the nanoparticles are ~70 nm. As shown in Figure 5.7, spheres were assembled from HEA₂₉-PAA₇₀-b-PS₇₆. The spherical nanoparticles with small size were designed to be used as crosslinkers to introduce interparticle crosslinking with thiol-functionalized hybrid nanoparticles.

5.3.2 Co-assembly of HS₁₈-PAA₇₂-b-PS₁₂₀ and PAA₃₆-b-PI₁₆₀

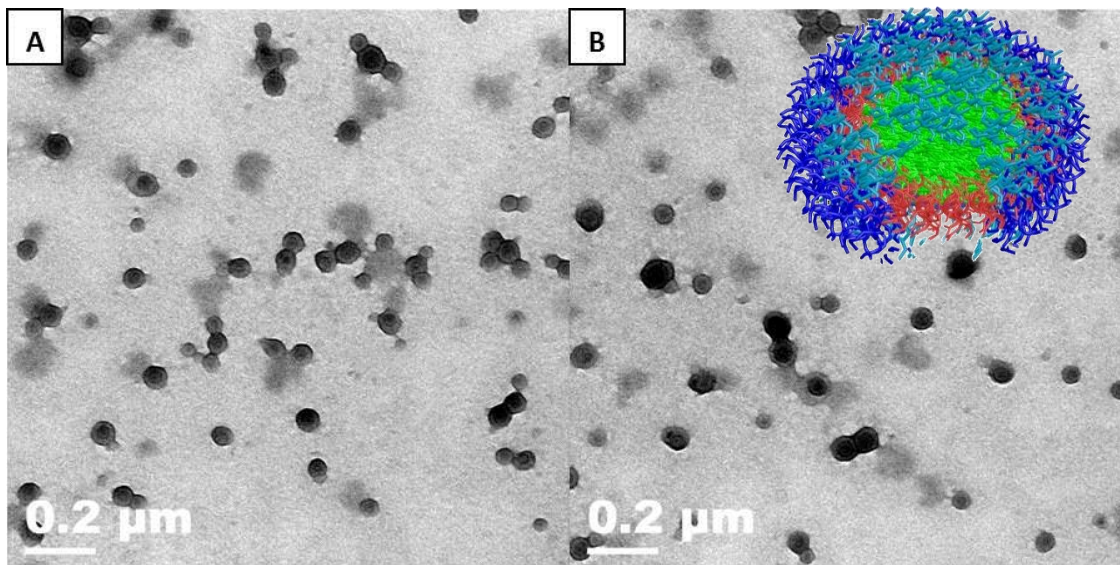


Figure 5.8 TEM images of hybrid disks assembled from blends of $\text{HS}_{18}\text{-PAA}_{72}\text{-}b\text{-PS}_{120}$ and $\text{PAA}_{36}\text{-PI}_{160}$. $\text{HS}_{18}\text{-PAA}_{72}\text{-}b\text{-PS}_{120}$ and $\text{PAA}_{36}\text{-}b\text{-PI}_{160}$ were blended with the molar ratio 1:1, amine: acid=0.5:1, 80% $\text{H}_2\text{O}/20\%$ THF, 0.4 mL water was added to 0.1 mL in a rate of 30 mL/h, OsO_4 was used for staining the PI domain. A, B: cast-film TEM images of hybrid disks in different imaging areas. The inserted 3D cartoon represents for the hybrid disk-like nanoparticle with anisotropic surface. The dark blue edge represents the thiol functionalized PAA from $\text{HS}_{18}\text{-PAA}_{72}\text{-}b\text{-PS}_{120}$, the lighter blue color represents the PAA block from $\text{PAA}_{36}\text{-}b\text{-PI}_{160}$, the red color represents the PS block, and the inner green color represents the PI block.

Fast water addition was applied to trap the different diblock copolymers into one nanoparticle. As shown in Figure 5.8, disk-like nanoparticles having a dark core inside and light edge outside were assembled. The dark core is attributed to the PI block stained by OsO_4 , and the light rim is attributed to the PS block. This local hydrophobic block nanophase separation guarantees that the anisotropic shell of the hybrid nanoparticles, meaning the thiol functionalized PAA chains from $\text{HS}_{18}\text{-PAA}_{72}\text{-}b\text{-PS}_{120}$ are positioned on the disk edges and the PAA chains from $\text{PAA}_{36}\text{-}b\text{-PI}_{160}$ are positioned in the middle surface of the disk, as shown in the 3D cartoon.

Inter-particle crosslinking after photoinitiation

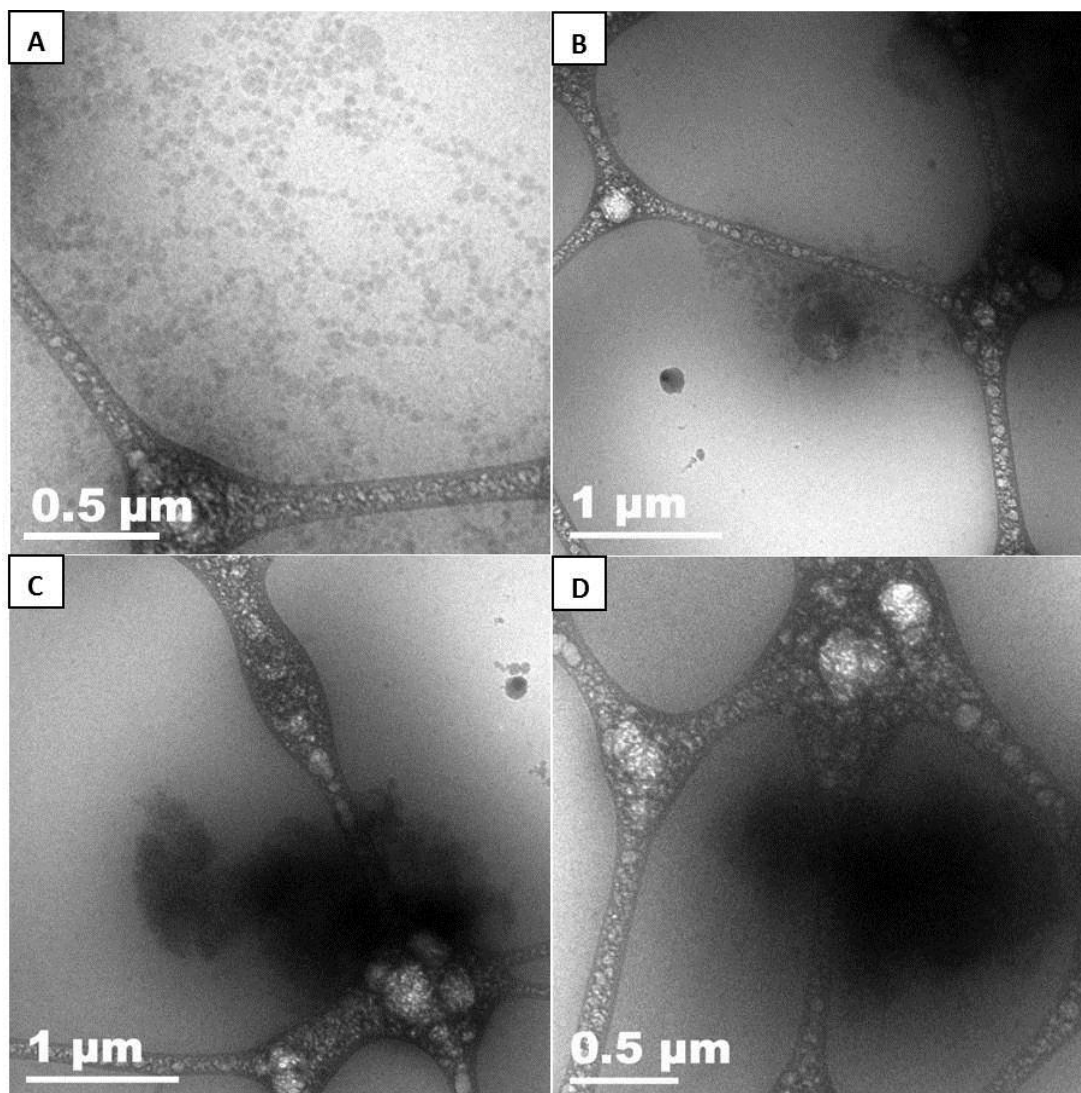


Figure 5.9 Cryo-TEM images of solution assemblies after photo initiating thiolene reaction. A: cryo-TEM images of unstained solution assemblies after photo initiation, showing a type of 2D planar structure. B: 2D planar structure in different imaging area. C: cryo-TEM image of the same solution assembly sample. Solution was stained by OsO₄. D: cryo-TEM image of the same solution assembly sample, in different image are. Three-dimensional agglomerates were observed. Two-dimensional planar sheets and three-dimensional agglomerates are observed after photo-initiated crosslinking by cryo-TEM.

UV-initiated photo crosslinking was applied to introduce crosslinking between the thiol functionalized hybrid disks assembled from mixing of HS₁₈-PAA₇₂-*b*-PS₁₂₀ and PAA₃₆-*b*-PI₁₆₀ and the diene functionalized smaller nanoparticles. The solution changes from clear to cloudy after photo initiating. The exploration indicated that interparticle crosslinking happened after photo-initiation. And, it is apparent that more work needs to do to observe the internal hybrid disk structure, and disk-sphere linking pattern inside the three-dimensional agglomerate.

5.4 Conclusion

Continuous work on designing new functionalized diblock copolymers for hierarchical multi-step assembly was presented in this chapter. Kinetic control, targeted manipulation of solvent addition rates and post-assembly inter-particle crosslinking were applied in assembly of nanoparticle superstructures. Hybrid disk-like nanoparticles with anisotropic surface properties were assembled from blends of thiol functionalized HS₁₈-PAA₇₂-*b*-PS₁₂₀ diblock and its dimensionally matched diblock PAA₃₀-*b*-PI₁₆₀. Preliminary studies showed that two-dimensional networks and three dimensional nanoparticle agglomerates were assembled *via* particle-particle crosslinking. The research paved the way to construct other nanoparticle agglomerates with well-defined packing geometries, such as the linking of hybrid vesicle nanoparticles described in chapter 3 or the linking of hybrid toroidal nanostructures *via* blends of functionalized diblocks. The work presented here demonstrated the rational design of molecules, multicompartment nanoparticle assembly *via* targeted kinetics and post-assembly particle crosslinking strategy. Research on this concept, on the exploration of new chemistry methods to provide functionalized building blocks and on the hierarchical assembly of multidimensional, multicompartment and multigeometry nanoparticles, is in progress.

REFERENCES

1. Q. Chen, S. C. Bae and S. Granick, *Nature*, 2011, **469**, 381-384.
2. Q. Chen, J. K. Whitmer, S. Jiang, S. C. Bae, E. Luijten and S. Granick, *Science*, 2011, **331**, 199-202.
3. H. Qiu, Z. M. Hudson, M. A. Winnik and I. Manners, *Science*, 2015, **347**, 1329-1332.
4. P. A. Rugar, L. Chabanne, M. A. Winnik and I. Manners, *Science*, 2012, **337**, 559-562.
5. J. Zhu, S. Zhang, F. Zhang, K. L. Wooley and D. J. Pochan, *Adv. Funct. Mater.*, 2013, **23**, 1767-1773.
6. T. G. M. v. d. V. Georgios Rizis, and Adi Eisenberg, *Angew. Chem. Int. Ed.*, 2014, **53**, 1-5.
7. L. Xiao, C. Liu, J. Zhu, D. J. Pochan and X. Jia, *Soft matter*, 2010, **6**, 5293-5297.
8. C. Zhou, M. A. Hillmyer and T. P. Lodge, *J. Am. Chem. Soc.*, 2012, **134**, 10365-10368.
9. E. V. Shevchenko, D. V. Talapin, N. A. Kotov, S. O'Brien and C. B. Murray, *Nature*, 2006, **439**, 55-59.
10. A. Nag, M. V. Kovalenko, J. S. Lee, W. Liu, B. Spokoyny and D. V. Talapin, *J. Am. Chem. Soc.*, 2011, **133**, 10612-10620.
11. L. Cademartiri and K. J. Bishop, *Nat. Mater.*, 2015, **14**, 2-9.
12. W. S. Etsuro Majima, *Makromol. Chem*, 1991, **192**, 2307-2315.
13. B. D. Fairbanks, M. P. Schwartz, A. E. Halevi, C. R. Nuttelman, C. N. Bowman and K. S. Anseth, *Adv. Mater.*, 2009, **21**, 5005-5010.
14. F. Zhang, M. Elsbahy, S. Zhang, L. Y. Lin, J. Zou and K. L. Wooley, *Nanoscale*, 2013, **5**, 3220-3225.

15. D. Uhrig and J. W. Mays, *Journal of Polymer Science Part A: Polymer Chemistry*, 2005, **43**, 6179-6222.
16. X. Wang, J. He and Y. Yang, *Journal of Polymer Science Part A: Polymer Chemistry*, 2007, **45**, 4818-4828.
17. X. Wang, J. Chen, K. Hong and J. W. Mays, *ACS Macro Letters*, 2012, **1**, 743-747.
18. Z. Li, Z. Chen, H. Cui, K. Hales, K. L. Wooley and D. J. Pochan, *Langmuir*, 2007, **23**, 4689-4694.

Chapter 6

COLLABORATIVE WORK ON NANOSTRUCTURE CHARACTERIZATION

In this chapter, collaborative work on construction and characterization of solution assemblies is elaborated. The solution assembly of macromolecules, dendrimers and other large amphiphiles is discussed. The assembly strategies as well as the various kinds of assembled nanostructures observed by *in-situ* imaging are presented. I was working with the lab of Prof. Jan van Hest from Radboud University, and this was the thesis work of Silvie Meeuwissen. Silvie Meeuwissen generated the synthesis and assembly, and I was working on the cryo-TEM imaging. I was working with the lab of Virgil Percec from University of Pennsylvania on dendrimer solution assemblies. The Percec lab members generated the molecule synthesis and self-assembly, and I was participating with the cryo-TEM imaging in UD. Parts of the work were reproduced or adopted with permissions from S. A. Meeuwissen, K. T. Kim, Y. Chen *et al.*, *Angew. Chem. Int. Ed.* 2011; Virgil Percec, *et al.*, *J. Am. Chem. Soc.*, 2013; Shaodong Zhang, *et al.*, *ACS Nano*, 2014; Shaodong Zhang, *et al.*, *PNAS*, 2014.

6.1 Polymersome Stomatocytes assembled from PEG₄₄-PS₂₉₂.

6.1.1 Introduction

Amphiphilic molecules, such as phospholipids, can self-assemble into various membranous or vesicular nanostructures. For example, tough vesicles¹ and other structures have been reported. The permeability and mechanical properties of vesicles assembled from natural molecules like observed in natural cells are comparatively better biologically than artificial materials. The material properties of vesicular

nanoparticles may influence the potential behavior of a synthetic vesicle being an efficient drug delivery vehicle. Inspired by small amphiphiles, the construction of higher molecular weight, large amphiphilic block copolymers is a large area of research. The vesicles assembled from small amphiphiles having a bilayer of molecules in the vesicle wall are named liposomes while vesicles assembled from block copolymers having bilayers of molecules are called polymersomes. Many methods now exist to achieve well-defined, nearly monodisperse and even exotic vesicular structures. For example, people have used extrusion methods to make nearly monodisperse vesicles from polydisperse precursors². Giant amphiphiles are used in vesicle assembly occurred in selective solvent^{3, 4}. Polymersomes are also shown to experience shape transformations and to show considerable morphological diversity relative to solution condition changes. Most vesicle self-assembly methods produce kinetically-trapped polymersome structures that are not easily transformable, especially when a glassy hydrophobic block is included. In this section, the successful utilization of a reverse dialysis of vesicles, which were initially dispersed in aqueous solution against organic cosolvent, resulted in stable, reproducible and interesting morphological transformations into stomatocyte vesicles. Cryo-TEM was used to image the highlighted structures. This work was collaborated with Silvie Meeuwissen from the Jan van Hest group at Radboud University.

6.1.2 Chemical Structure of Diblock Copolymers and Material Synthesis

and permeable vesicular membrane had to be regenerated. THF and dioxane were considered as good candidates for the recovery of a flexible polymer membrane due to their ability of plasticizing on PS and miscibility with water. Then, a THF/dioxane mixture blended with water (v/v, 1:1) was used as the dialysis agent for the stomatocyte aqueous solutions. It is predicted that the swelling degree of the membranes would introduce rich shape transitions of the initial vesicular structure. Different THF/dioxane mixing ratios were then used to trigger the swelling of the PS domain. The concentrated, aqueous stomatocyte vesicle structures were dialyzed against mixtures of water (50% v) and THF/dioxane (75:25, 55:45, 25:75). At different time points, a small amount of solution (20 μL) was withdrawn and then quickly added to a large amount of water (1000 μL). The PS block was quickly vitrified and the morphology was preserved. Cryo-TEM, normal TEM and cryo-SEM were used to characterize the morphologies at different THF/dioxane ratios and dialysis time points.

6.1.4 Results and Discussion

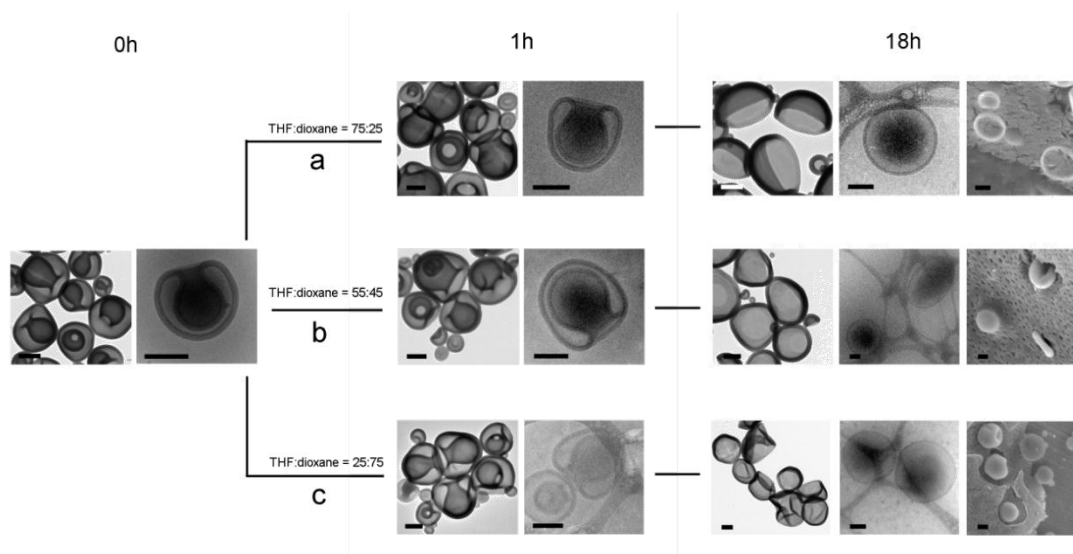


Figure 6.2 Shape transformation of stomatocytes of PEG-*b*-PS block copolymers over time illustrated by ambient TEM (left at 0 h, 1 h and 18 h), cryo-TEM (right at 1 h, middle at 18 h) and cryo-SEM images (right at 18 h). The stomatocytes were dialyzed against a mixture of water and organic solvent (1/1, v/v) using three different ratios of THF to dioxane by volume: a) 75:25, b) 55:45, and c) 25:75. Scale bars: 200 nm. Figures adapted from reference⁵, with copyright approved from Wiley 2011. The cryo-TEM images were obtained in UD Keck lab by Yingchao Chen. The SEM and cryo-SEM data was provided by Silvie Meeuwissen from Radboud University.

The morphologies at different solvent conditions and time points are provided in Figure 6.2. As can be seen in the images, in the mixing ratio of THF/dioxane 75:25, the average estimated wall thickness of the vesicles after 18 hours of dialysis was 46 ± 3 nm ($n = 50$). Compared to the initial bilayer membrane of 26 ± 2 nm ($n = 50$), the walls are 77% thicker than a normal vesicle. This increase, together with the perfectly round shape, indicated the formation of completely collapsed structure. After dialysis for 1 hour, the first morphology changes were observed with open-mouth stomatocytes. After longer time dialysis (18 hours), eventually, stable, round vesicular nanoparticles are formed. The formation of the kippah morphology was due to the

effect of the PS segment swelling in the high volume fraction of THF. The membrane became weak enough to be permeable to organic solvent as well as water to form the exotic structure.

When THF and dioxane was mixed at 55:45 volume ratio, completely different morphology transitions were captured at different dialysis time points by cryogenic TEM. The stomatocytes were transformed into a uniconcave discocyte morphology. The opening of the stomatocytes expanded in one hour. And, after 18 hours dialysis, ellipse-shaped vesicles were observed as shown in Figure 6.3b. When THF and dioxane was mixed at 25:75 by volume, the transition status toward completely inflated vesicles (Figure 6.2C) was complete, as described in literature⁵.

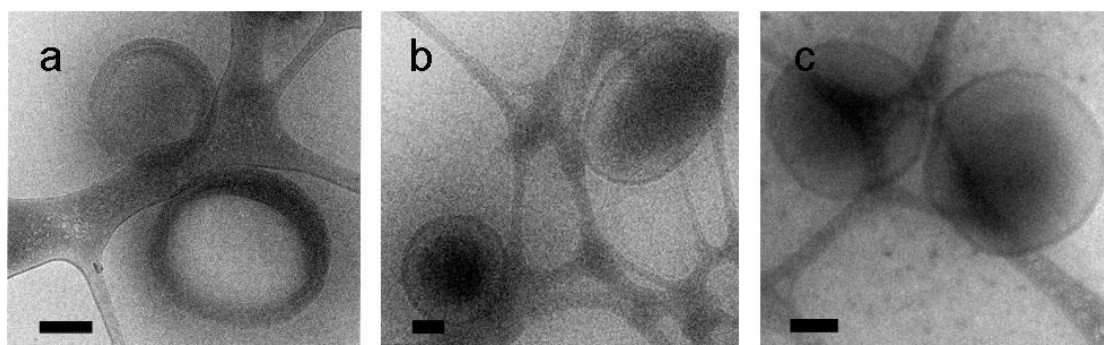


Figure 6.3 Cryo-TEM images of stomatocytes. The stomatocytes were dialyzed for 18 h in MilliQ water/(THF:dioxane) (v/v:v) is a) 50/(75:25); b) 50/(50:50) and c) 50/(25:75). Scale bars a-c: 200 nm. Figures adapted from reference⁵, with copyright approved from Wiley 2011. The images were taken in UD Keck lab by Yingchao Chen.

By tracking the in-situ morphologies in solution using cryogenic TEM, the controlled morphology transition into unusual, stable structures was captured *via* gradual introduction the organic solvent to the thick-wall vesicle solution.

6.2 Self-Assembly of Amphiphilic Janus Glycodendrimers into Glycodendrimersomes and other Complex Architectures.

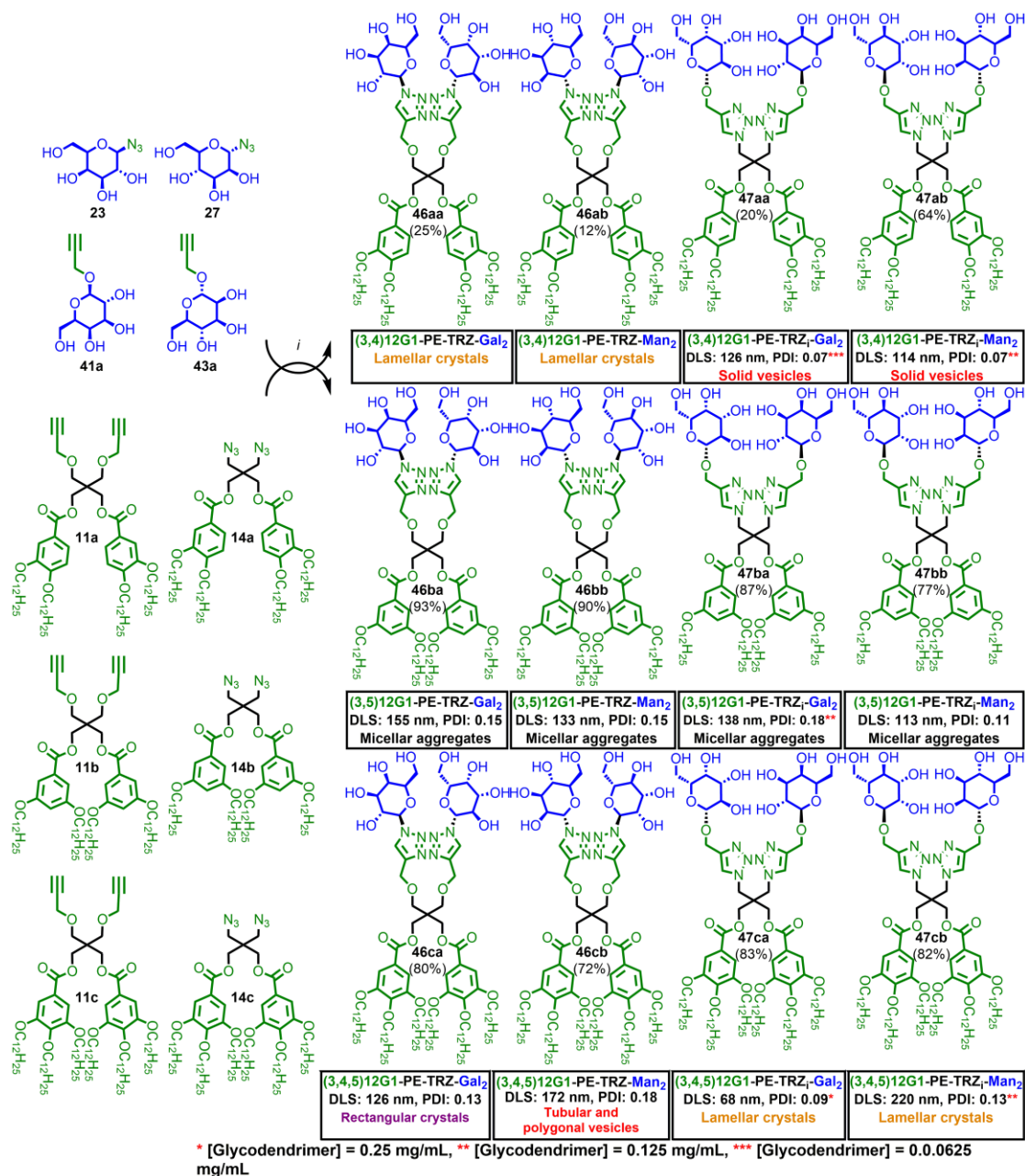
6.2.1 Introduction

Amphiphilic dendrimers are a family of large amphiphiles that can be solution self-assembled into different nanostructures. Different from block copolymers which have slow chain dynamics and polydisperse assemblies, large amphiphiles were readily assembled into solution assemblies with stable structure and less polydispersity in size and shape. More important, the solvent processing methods for achieving stable nanostructures from these amphiphiles are relatively simple and kinetically faster due to the quicker chain dynamics relative to block copolymers. In this section, injections of organic solutions into water were performed for the assembly of the interesting nanostructures.

Several libraries of amphiphilic Janus dendrimers with the carbohydrates d-mannose, d-galactose and d-lactose as their hydrophilic component were synthesized. Their self-assembly behavior by simple injection of their THF or ethanol solution into water or buffer was analyzed by cryo-TEM. A diversity of hard/crystalline and soft/fluid supramolecular assemblies were observed, including unilamellar spherical, polygonal and tubular vesicles denoted glycodendrimersomes, aggregates of spherical and rod-like micelles named glycodendrimermicelles, cubosomes denoted glycodendrimercubosomes, as well as lamellar and rectangular crystals. This work was performed in collaboration with the Percec research group at University of Pennsylvania.

6.2.2 Molecular structure of Amphiphilic Dendrimers and their Self-assembly Behaviors

Modular Synthesis of Two Constitutional Isomeric Libraries Containing Twelve Amphiphilic Janus Glycodendrimers Based on D-Mannose and D-Galactose.



Scheme 6.1 Modular Synthesis of the Constitutional Isomeric Libraries 1 (**46aa** to **46cb**) and 2 (**47aa** to **47cb**) Containing twelve Amphiphilic Janus Glycodendrimers with D-Mannose and D-Galactose and the summary of their self-Assembly by the injection of their THF solution into water. Scheme adapted from reference⁷, with

copyright approved from ACS publications 2013. The molecule structure scheme was provide by the Percec lab.

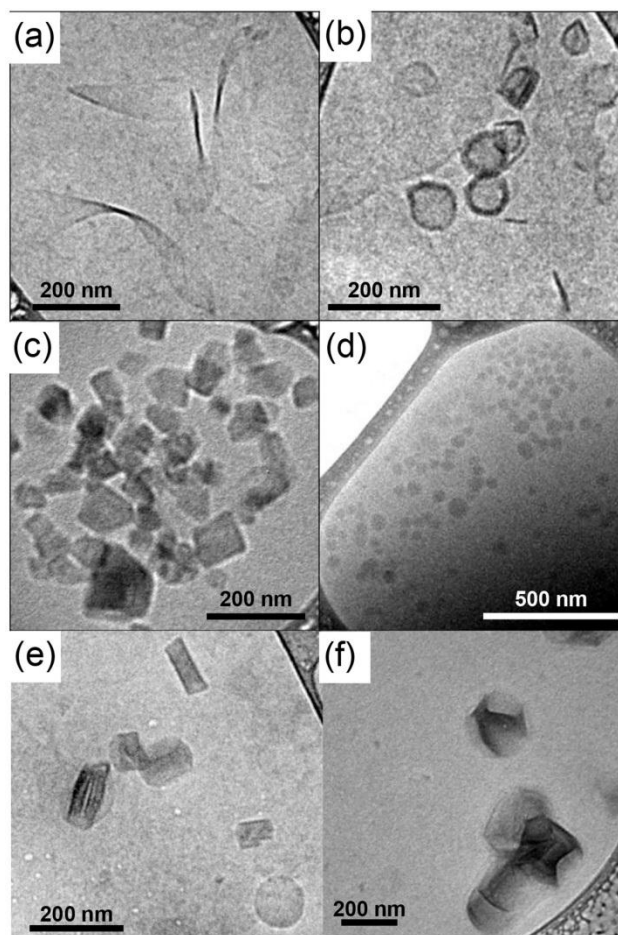


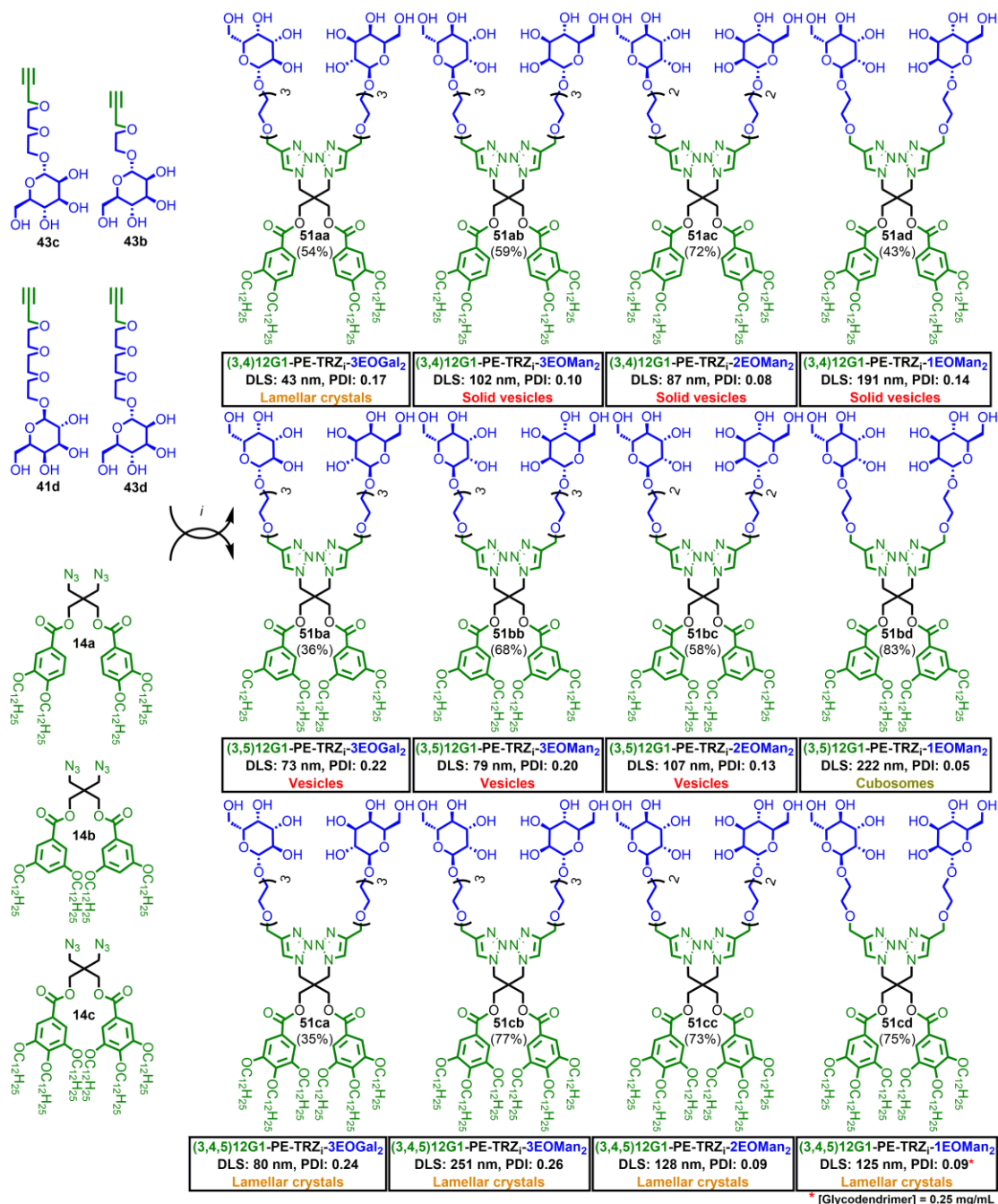
Figure 6.4 Selected Cryo-TEM images of lamellar crystals assembled from (a) (3,4)12G₁-PE-TRZ-Gal₂ 46aa; (b) solid glycodendrimerosomes assembled from (3,4)12G₁-PE-TRZ_i-Man₂ 47ab; (c) rectangular crystals assembled from (3,4,5)12G₁-PE-TRZ-Gal₂ 46ca; (d) glycodendrimermicelles assembled from (3,5)12G₁-PE-TRZ-Man₂ 46bb; (e, f) mixture of tubular and polygonal glycodendrimerosomes and glycodendrimermicelles assembled from (3,4,5)12G₁-PE-TRZ-Gal₂ 46cb. Figures adapted from reference⁷, with copyright approved from ACS publications 2013. The images a, b, d were obtained by yingchao chen at UD keck lab. The images b, c, e were obtained by Hao-jan from UPenn.

The self-assembly experiments were generated by direct injection of 100 μL THF solution of all Janus glycodendrimers with the molecular structures presented in scheme 6.1 (10 mg/mL) into Millipore water (2 mL) followed by 5 seconds of vortex mixing. Self-assembly of final structures were then observed. The structures of these supramolecular assemblies were determined by cryo-TEM and are also summarized in Figure 6.4. It was observed that these Janus dendrimers self-assemble into lamellar crystals (Figure 6.4a), solid vesicles named solid glycodendrimersomes (Figure 6.4b), rectangular crystals (Figure 6.4c), micellar aggregates (Figure 6.4d), tubular and polygonal glycodendrimersomes (Figure 6.4 e,f).

The 2D sheet-like morphology indicates that the membrane is crystalline and stiff, which prevents the closing process required to form a 3D vesicle (Figure 6.4a). A solid vesicle is a 3D hollow structure constructed from a unilamellar bilayer membrane in a similar way as the regular fluid/soft vesicles (Figure 6.4b). However, the sharp edges/corners of the structure indicate that its membrane is stiff and results from a crystalline or semicrystalline structure. Another untraditional assembled nanostructure is the glycodendrimermicelle (Figure 6.4d), whose diameter dimension is much larger than the dimension of two molecular lengths. It was determined that the glycodendrimermicelle is a filled particle or droplet consisting of a Janus dendrimer-rich phase suspended in water similar to an oil droplet in water. The mechanism of forming these glycodendrimermicelle is interpreted to be the fact that the segment phase separation process is kinetically slow or the driving force is not strong enough to form unilamellar structures in this specific molecule. The compound 46cb formed a mixed morphology by the injection method. Overall, the results indicate that the kinetic rates for the formation of all morphologies are similar (Figure 6.4). After quick injection, stable nanostructures are formed in near aqueous solutions (water 95%, organic solvent 5%).

Modular synthesis and analysis of library containing twelve Janus glycodendrimers with linear hydrophobic n-alkyl groups and D-mannose and D-galactose connected by mono-, di- and triethylene glycol spacers.

Several libraries of dendrimers were synthesized in the lab of Prof. Percec, UPenn, containing linear n-alkyl groups as the hydrophobic component. A succinic ester spacer was incorporated between the hydrophobic fragments. The previously presented libraries generated mostly hard assemblies and tubular vesicles. However, the replacement of the linear n-alkyl groups with a branched hydrophobic segment together with a triethylene glycol spacer produced only vesicles (Figure 6.5). The monoethylene glycol, diethylene glycol and triethylene glycol spacers were combined to generate library 5 containing twelve janus glycodendrimers with linear hydrophobic groups and glycol spacers⁷.



Scheme 6.2 Modular synthesis and molecular structure of the Library 5. Molecules (51aa to 51cd) contain twelve amphiphilic Janus glycodendrimers with linear n-Alkyl Groups and D-mannose and D-galactose connected *via* mono-, di- and triethylene glycol spacers and the summary of self-assembly by injection of the THF or EtOH

solution into water. Approved copy right from ACS publication. Figures adapted from reference⁷, with copyright approved from ACS publication.

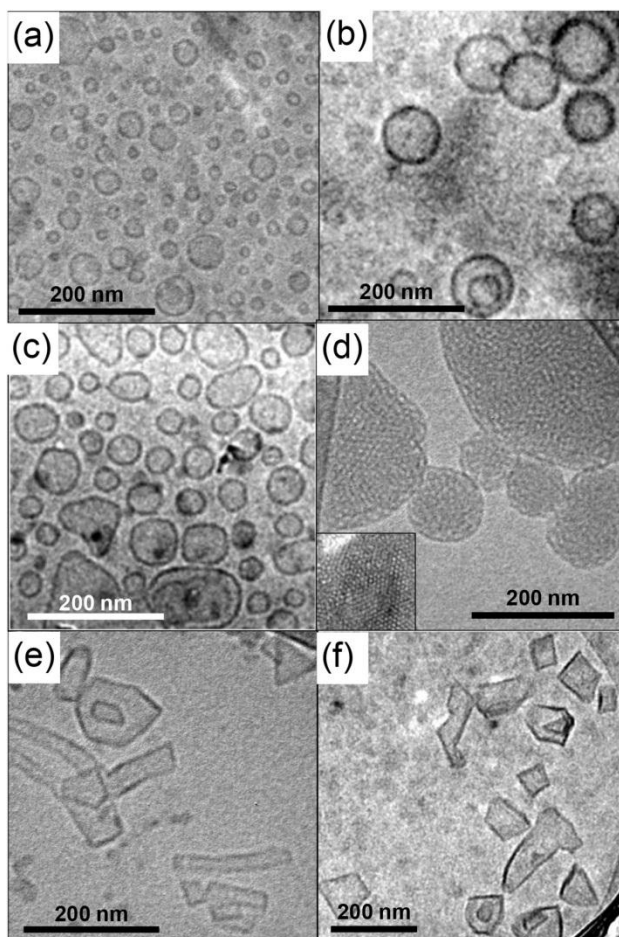


Figure 6.5 Selected Cryo-TEM images of glycodendrimerosomes assembled from (a) $(3,5)_{12}G_1$ -PE-TRZ_i-3EOGal₂ 51ba, (b) $(3,5)_{12}G_1$ -PE-TRZ_i-3EOMan₂ 51bb, and (c) $(3,5)_{12}G_1$ -PE-TRZ_i-2EOMan₂ 51bc; glycodendrimercubosomes assembled from (d) $(3,5)_{12}G_1$ -PE-TRZ_i-1EOMan₂ 51bd; lamellar crystals assembled from (e) $(3,4,5)_{12}G_1$ -PE-TRZ_i-3EOGal₂ 51ca and (f) $(3,4,5)_{12}G_1$ -PE-TRZ_i-3EOMan₂ 51cb. Figure adapted from reference⁷, with copyright approved from ACS publications 2013. The cryo-TEM images d,e,f were obtained from UD keck lab by Yingchao Chen; the cryo-TEM images a, b,c were provided by the Percec lab at UPenn.

All Janus glycodendrimers in scheme 6.2 are soluble both in THF and ethanol in the concentration range from 0.25 to 0.5 mg/ml. The self-assembly process is also generated by direct injection of the THF solution to water. The top row in this library from scheme 6.2 demonstrated that 3,4-replaced hydrophobic segments of the Janus dendrimer produced lamellar crystals for 51 aa and solid vesicles for 51 ab, 51 ac and 51 ad. The 3,5-disubstituted molecules produced soft vesicles for 51ba, 51bb and 51bc and cubosomes for 51bd. The transition from 3,5-disubstituted to 3,4,5-trisubstituted changes the assemblies in water from soft to hard and generated polygonal vesicles for 51ca and lamellar crystals for 51cb, 51cc and 51cd. Moreover, the assembled nanostructures depending on the 3,4-, 3,5- and 3,4,5-substitution pattern are in line with the molecular mechanism of unilamellar structure formation reported previously⁸.

6.2.3 Conclusions of Glycodendrimer Assembly

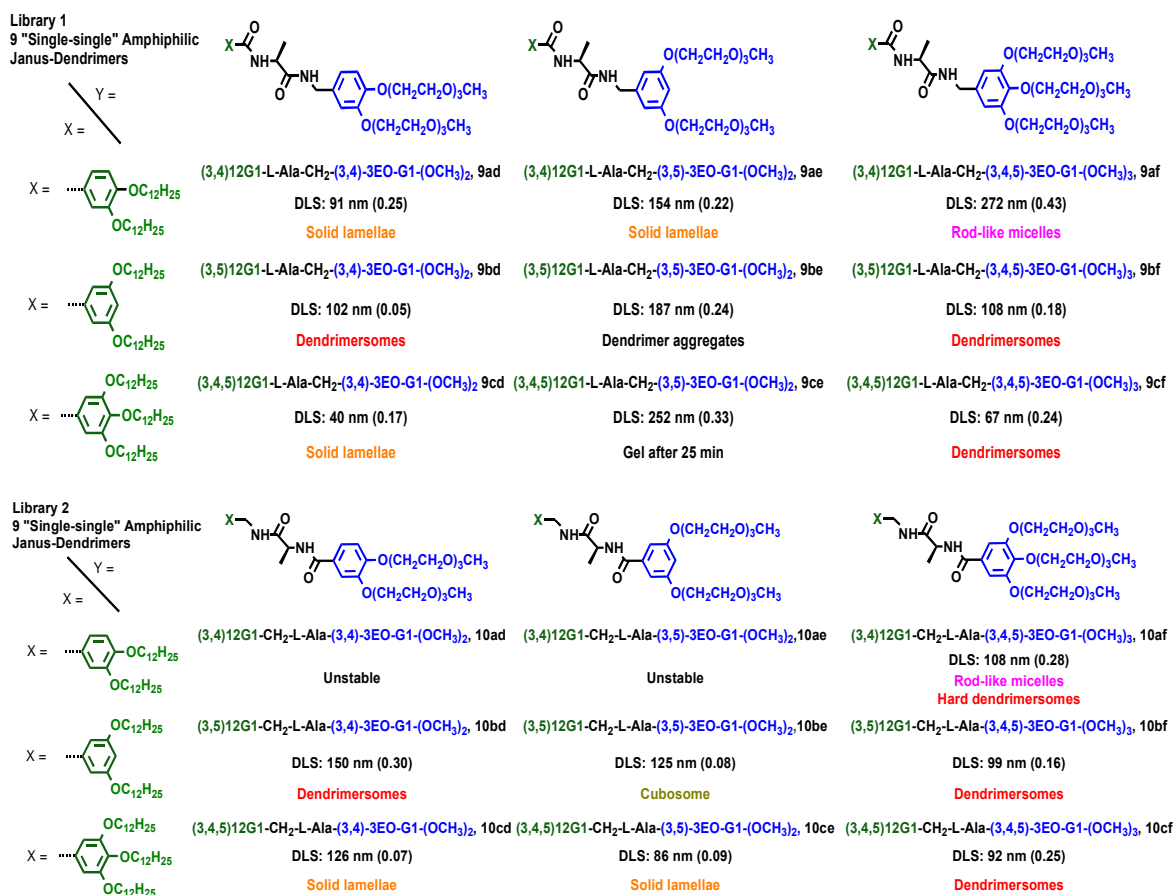
The modular synthesis of libraries of glycodendrimers containing amphiphilic Janus glycodendrimers with the carbohydrates d-mannose, d-galactose and d-lactose in their hydrophilic part has been synthesized by an accelerated synthesis strategy. The self-assembly behaviors of certain libraries were highlighted here. The self-assembly processes were generated by simple injection of polymer THF solution into water. Cryo-TEM was used to scan and analyze the assembled structures.

Soft and hard nanostructures were formed including unilamellar spherical, polygonal and tubular glycodendrimersomes, aggregates of soft glycodendrimermicelles, glycodendrimercubosomes as well as lamellar and rectangular crystals. Some unique structures, like the bicontinuous cubosomes, were also discovered.

6.3 “Single-Single” Amphiphilic Janus Dendrimers Self-Assemble into Narrow Distribution Dendrimersomes with Predictable Size

As discussed in the previous section, most of the amphiphilic Janus dendrimers used for the assembly of dendrimersomes were constructed from combinations of twin-hydrophobic and twin-hydrophilic dendrons, named “twin-twin” amphiphilic Janus dendrimers. While “twin-twin” amphiphilic Janus dendrimers and glycodendrimers have been shown to produce dendrimersomes^{8, 9} and glycodendrimersomes⁷, the synthesis of a “single” hydrophilic and a “single” hydrophobic Dendron would reduce the time of synthesis and be of considerable interest for broader applications. In this section, the modular synthesis of libraries of “single-single” amphiphilic Janus dendrimers and their solution assemblies are presented, with the discovery of a linear relationship between dendrimer concentration and vesicle size.

6.3.1 Molecular Architectures



Scheme 6.3 Self-Assembly of "Single-Single" Amphiphilic Janus Dendrimers from Libraries 1 and 2^a. ^aShort notations and the summary of the assemblies in water. The diameter (in nm), Scheme adapted from reference¹⁰, with copyright approved from ACS 2014. The molecular scheme was provided by the Percec lab.

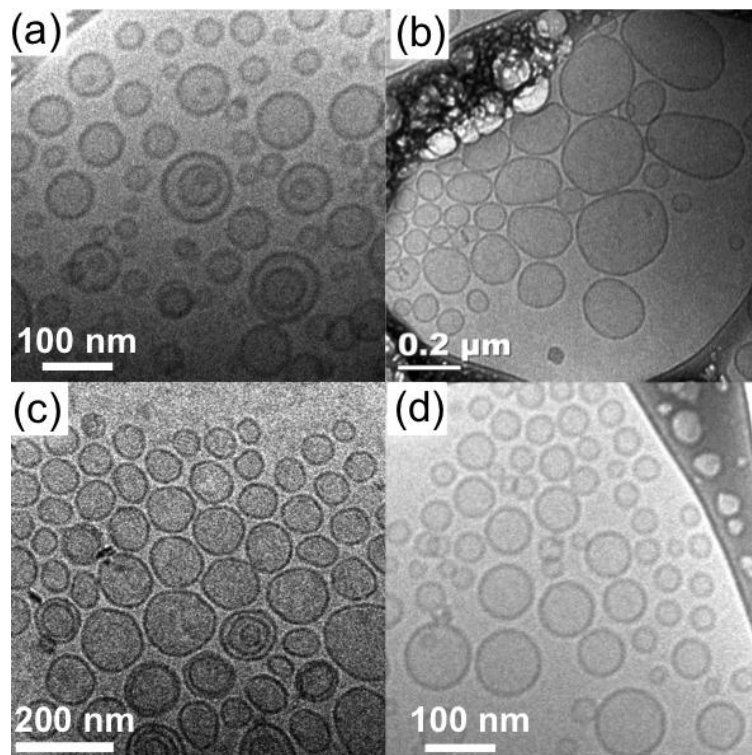
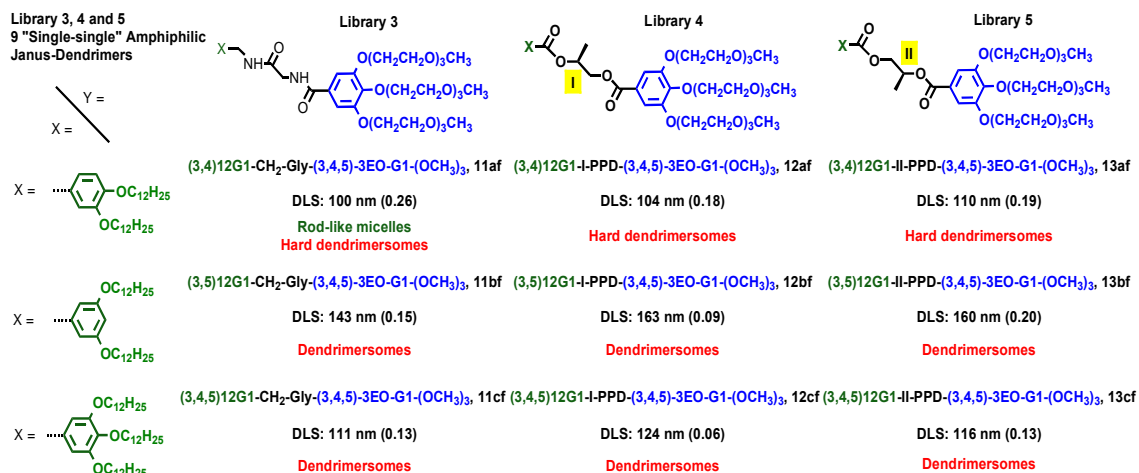


Figure 6.6 Selected cryo-TEM images of the self-assembled morphologies from libraries 1 and 2. (a) (3,4,5)12G1-L-Ala-CH₂-(3,4,5)-3EO-G1-(OCH₃)₃, **9cf**. (b) (3,5)12G1-CH₂-L-Ala-(3,4)-3EO-G1-(OCH₃)₂, **10bd**; (c) (3,5)12G1-L-CH₂-Ala-(3,4,5)-3EO-G1-(OCH₃)₃, **10bf**; (d) (3,4,5)12G1-L-Ala-CH₂-(3,4,5)-3EO-G1-(OCH₃)₃, **10cf**. Image adapted from reference¹⁰, with copyright approved from ACS 2014. The cryo-TEM images were obtained in UD by Yingchao Chen, Haojan Sun and Shaodong Zhang.

Cryo-TEM images of dendrimersomes self-assembled by the “single-single” amphiphilic Janus dendrimers **9cf**, **10bd**, **10bf** and **10cf** from Libraries 1 and 2 are presented in Figures 6.6. Mostly bilayer vesicles were assembled in aqueous solutions.



Scheme 6.4 Structures of the “Single-Single” Amphiphilic Janus Dendrimers From Libraries 3, 4 and 5^a. ^aShort notations and the summary of their assemblies in water at 25 °C. The diameter (in nm), polydispersity (in between brackets) determined by DLS (0.5 mg/mL in water solution), and the morphologies in water determined by cryo-TEM are indicated. Scheme adapted from reference¹⁰, with copyright approved from ACS 2014. The molecule structure scheme was provided by the Percec lab.

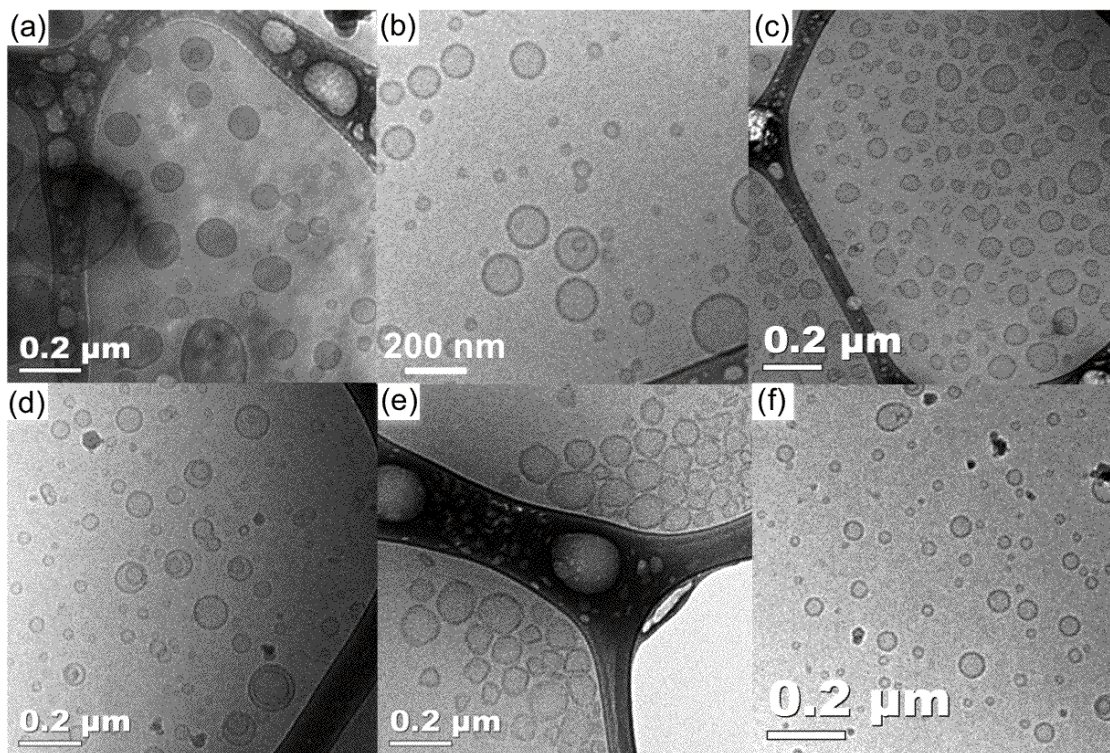


Figure 6.7 Representative cryo-TEM images of self-assembled morphologies in libraries 3, 4 and 5. (a) (3,5) $12G_1$ -CH₂-Gly-(3,4,5) G_1 -3EOMe₃, **11bf**; (b) (3,4,5) $12G_1$ -CH₂-Gly-(3,4,5) G_1 -3EOMe₃, **11cf**; (c) (3,4) $12G_1$ -I-PPD-(3,4,5) G_1 -3EOMe₃, **12af**; (d) (3,4,5) $12G_1$ -I-PPD-(3,4,5) G_1 -3EOMe₃, **12cf**; (e) (3,4) $12G_1$ -II-PPD-(3,4,5) G_1 -3EOMe₃, **13af**; (f) (3,4,5) $12G_1$ -II-PPD-(3,4,5) G_1 -3EOMe₃, **13cf**. Image adapted from reference¹⁰, with copyright approved from ACS 2014. The images a-c were obtained in UD by Yingchao Chen, Hao-jan sun and Shaodong Zhang. The images d-f were provided by the Percec lab at UPenn.

Representative cryo-TEM images of the assemblies produced by the “single-single” amphiphilic Janus dendrimers from Libraries 3, 4 and 5 are shown in Figure 6.7. All of them, except (3,4)- $12G_1$ -CH₂-Gly-(3,4,5)-3EO-G₁-(OCH₃)₃ **11af**, self-assemble into hard and soft dendrimersomes. In Library 3, (3,5) $12G_1$ -CH₂-Gly-(3,4,5)-3EO-G₁-(OCH₃)₃ **11bf** and (3,4,5) $12G_1$ -CH₂-Gly-(3,4,5)-3EO-G₁-(OCH₃)₃ **11cf** self-assemble into soft dendrimersomes with smooth and fluid surface (Figure 6.7a and 6.7b). (3,4) $12G_1$ -I-PPD-(3,4,5)-3EO-G₁-(OCH₃)₃ **12af** from Library 4 self-

assembles into hard dendrimersomes with sharp edges and corners (Figure 6.8c), while (3,5)12G₁-I-PPD-(3,4,5)-3EO-G₁-(OCH₃)₃ **12bf** and (3,4,5)12G₁-I-PPD-(3,4,5)-3EO-G₁-(OCH₃)₃ **12cf** self-assemble into soft dendrimersomes (Figure 6.8d). (3,4)12G₁-II-PPD-(3,4,5)-3EO-G₁-(OCH₃)₃ **13af** from Library 5 also forms hard dendrimersomes (Figure 6.8e), while (3,5)12G₁-II-PPD-(3,4,5)-3EO-G₁-(OCH₃)₃ **13bf** and (3,4,5)12G₁-II-PPD-(3,4,5)-3EO-G₁-(OCH₃)₃ **13cf** self-assemble into soft dendrimersomes (Figure 6.7f).

During the imaging processes, it was found that the size of the assembled vesicles varies when different polymer concentrations were used. The size and concentration correlations were revealed in detail by cryo-TEM. DLS was also used to characterize the global size and size distribution, and it is reported in the full paper. Theoretical explanations and predictions of the size-concentration correlations were also discussed in the full paper¹⁰. It is apparent that the size of the vesicles increases from 61 nm to 245 nm as the concentration increases, which is consistent with the predictions from theoretical equations.

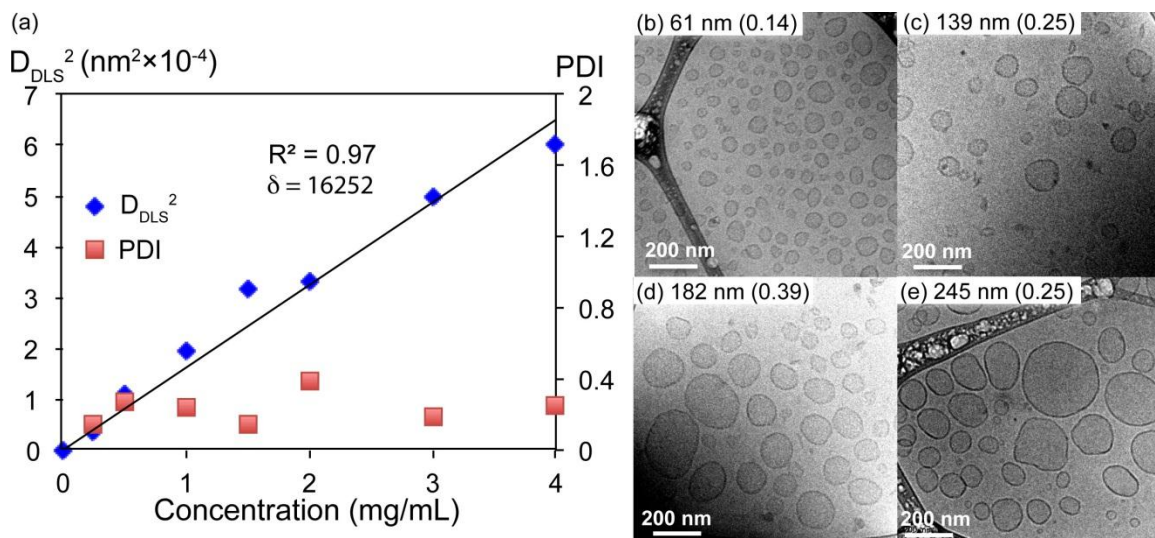


Figure 6.8 The concentration dependence of the size of dendrimersomes formed by (3,4)12G₁-I-PPD-(3,4,5)-3EO-G₁-(OCH₃)₃, 12af. (a) Square diameter-concentration relationship of the dendrimersomes. Cryo-TEM images of the dendrimersomes with the indicated size (in nm) and polydispersity index (PDI, in between brackets) at final concentration of (b) 0.25 mg/mL; (c) 1 mg/mL; (d) 2 mg/mL; (e) 4 mg/mL. Image adapted from reference¹⁰, with copyright approved from ACS 2014. The DLS data was provided by the Percec lab, and the images b and c were generated at UD.

6.3.2 Conclusions

Five libraries of “single-single” amphiphilic Janus dendrimers were synthesized. Their assemblies were obtained by injection of their ethanol solution into water, generating various nanostructures including soft and hard dendrimersomes, cubosomes, solid lamellar, and rod-like micelles, all characterized by cryo-TEM. By employing the methodology developed for their “twin-twin” homologues,¹¹ the size of the dendrimersomes assembled by these “single-single” amphiphilic Janus dendrimers were predictable for wide range of concentrations while their size distribution is narrow. This predictability provides a methodology to prepare vesicles with desired

size by simply choosing a specific concentration of the amphiphiles in the applicable range.

6.4 Self-assembly of Amphiphilic Janus Dendrimers into Uniform Onion-like Dendrimersomes with Predictable Size and Number of Internalized Bilayers

6.4.1 Introduction

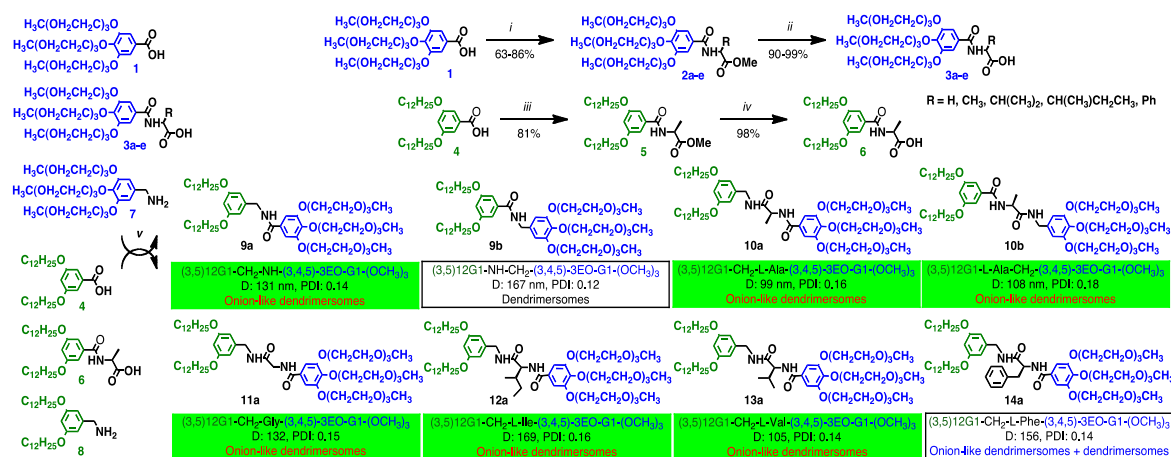
Many natural molecules assemble into single-bilayer membrane structures such as lipids and glycolipids, with the final membranes containing other molecules such as cholesterol, transmembrane proteins, and glycoproteins. Gram-negative bacteria and cell nuclei exhibit an assembled structure of a double-bilayer membrane¹². More complex membrane structures are achieved in cells and their various organelles^{13, 14}. Natural assemblies inspired molecule design to mimic the complex membrane structures. And there are many encountered bilayer membrane structures generated from artificial molecules. For instance, liposomes self-assembled from phospholipids are the initial mimics of single-bilayer biological membranes¹⁵, while they exhibit polydispersity in size, weak mechanical properties, as well as permeable and unstable properties¹⁶. Polymersomes, in contrast, can be assembled from amphiphilic block copolymers and display better mechanical properties for potential applications, but are still highly polydisperse and have lower biocompatibility^{17, 18}. Janus glycodendrimers can also be assembled into bilayer dendrimersomes mimicking the glycan ligands showing^{8, 9}. And it is promising for wider application and better manipulation that the size/shape of dendrimersomes *via* concentration-structure correlations can be predicted¹⁰.

Nature contains onion-like vesicles from cell molecules as reported previously^{19, 20}. Man-made, amphiphilic, Janus glycodendrimers self-assemble into glycodendrimersomes that mimic the glycan ligands of biological membranes⁷. By taking advantages of the previous study, a constitutional library synthesized by a modular approach has been employed to discover six “single-single” amphiphilic

Janus dendrimer primary structures, that self-assemble into stable and monodisperse onion-like vesicles with predictable dimension and number of internal bilayers. These vesicles are assembled by simple injection of a solution of Janus dendrimers (in water-miscible-solvent) into water or buffers²¹.

The onion-like dendrimersomes studied here are assembled by simple injection of polymer organic solution into pure water with uniform structures produced. Compared with direct injection, people have also used more complicated extrusion-hydration method to produce multilayer vesicles from block copolymers and have produced onion-like vesicles that are more polydisperse^{22, 23}. The report of low dispersity, stable, and easily made onion-like vesicles are presented here, and the unique structures are characterized by in-situ cryogenic TEM.

6.4.2 Molecular Structures of Dendrimers



Scheme 6.5 Molecular structures of Amphiphilic Janus Dendrimers.^{a,b} Reagents and conditions: (i) RCH(NH₂)COOCH₃·HCl, THF, 23 °C, 6-8 h; (ii and iv) KOH, EtOH:H₂O, reflux, 1-4 h; (iii and v) THF, 23 °C, 8 h. ^bThe diameter (D, in nm), polydispersity (PDI) of the dendrimersomes are measured by DLS (0.5 mg/mL in water solution). The indicated structures in water were determined by cryo-TEM. Scheme adapted from reference²¹, with copyright approved from PNAS 2014. The

molecule scheme was provided by the Percec lab.

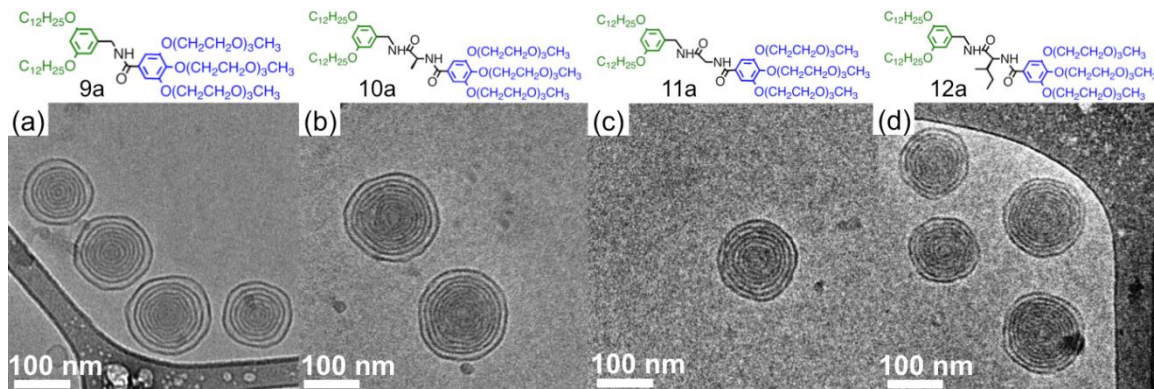


Figure 6.9 Multilayer onion-like vesicles assembled from dendrimers. Images adapted from reference²¹, with copyright approved from PNAS 2014. The image c was obtained at UD and images a, b, d were obtained at UPenn.

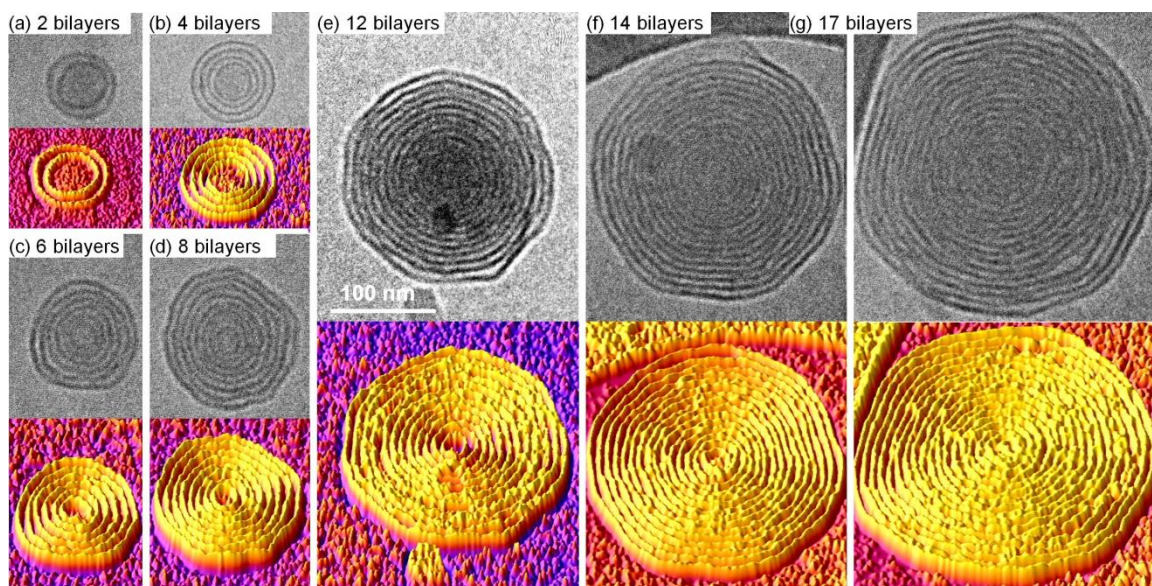


Figure 6.10 Cryo-TEM images and 3D modeling of multilayer onion-like vesicles with predictable layer numbers. The images (a-b) were obtained at UD and the images (c-g) were obtained at UPenn.

A tetrahydrofuran (THF) solution of each single-single amphiphilic Janus compound from scheme 6.5 (100 μ L) was injected into 2 mL of Millipore water. This method is referred to as direct injection. The size and size distribution of the resulting assemblies analyzed by dynamic light scattering (DLS) and the structures determined by cryogenic-transmission electron microscopy (cryo-TEM) are summarized in the full paper. The primary structure of the amphiphilic Janus compounds was onion-like dendrimersomes and was discovered by screening this constitutional isomeric library. Two pairs of constitutional isomers, i.e., (3,5)₁₂G₁-CH₂-NH-(3,4,5)-3EO-G₁-(OCH₃)₃, 9a vs (3,5)₁₂G₁-NH-CH₂-(3,4,5)-3EO-G₁-(OCH₃)₃, 9b and (3,5)₁₂G₁-CH₂-L-Ala-(3,4,5)-3EO-G₁-(OCH₃)₃, 10a vs (3,5)₁₂G₁-L-Ala-CH₂-(3,4,5)-3EO-G₁-(OCH₃)₃, 10b were compared to study the constitutional isomeric effect on their self-assembled structure. The two Janus compounds 9a and 10a with (3,5)₁₂G₁-CH₂-pattern self-assembled into onion-like dendrimersomes (Fig. 6.9 A and B). It was found that the spacing between their bilayers was identical, 10.0 \pm 0.7 nm (Fig. 6.10). This observation indicates that the number of bilayers of the onion-like dendrimersomes is proportional to their diameter. On the other hand, the other two constitutional isomers 9b, 10b with -CH₂-(3,4,5)-3EO-G₁-(OCH₃)₃- self-assembled, respectively, into single-bilayer and onion-like vesicles with different spacing between adjacent bilayers. More investigation is required to understand this constitutional isomeric effect. Nevertheless, four more amino acid-containing amphiphilic Janus dendrimers 11a, 12a, 13a, and 14a were designed with (3,5)₁₂G₁-CH₂-, which self-assembled into regular onion-like vesicles (Fig. 6.9 C and D). Only 14a formed a mixture of single-bilayer and onion-like vesicles. The onion-like dendrimersomes self-assembled from 12a also exhibit uniform spacing between the bilayers, 10.3 \pm 0.7 nm (Fig. 6.9). When the amide group from the structure of the Janus compound was replaced with an ester group (28) only single-bilayer vesicles were obtained²¹.

Similar concentration-structure correlations, as discussed earlier, were observed in these libraries¹⁰. Onion-like vesicles were found to exhibit similar size-concentration dependence. This dependence is exemplified with the onion-like

structures formed from $(3,5)_{12}G_1\text{-CH}_2\text{-L-Ala-(3,4,5)-3EO-G}_1\text{-(OCH}_3)_3$, 10a. Their diameter increased from 63 to 289 nm with their concentration ranging from 0.025 to 2.5 mg/mL, as illustrated by the cryo-TEM images with indicated concentrations in full paper²¹. At very low concentration (0.025 mg/mL) onion-like dendrimersomes exhibited only two bilayers (Fig. 6.10A). Therefore, their structure provides a simple mimic of the double-lamellar membrane of Gram-negative bacteria^{12, 13} that survive in a more dilute environment than other biological membranes. The number of bilayers increased gradually to 4 at 0.1 mg/mL (Fig. 6.10B), 6 at 0.2 mg/mL (Fig. 6.10C), and up to 17 when the concentration increased to 2.5 mg/mL (Fig. 6.10G). Experimental data of the film thickness measurements reported in the literature based on closely related sample preparations show that the film thickness is ~100 nm at the center and up to ~430 nm near the edge. Judging from the observation of the darker or transparent central part of the onion-like vesicles, we estimated the thickness of the vitrified ice films to be ~100 nm at the center and ~350 nm near the edge of the hole. These values agree with literature data²⁴.

6.5 Conclusions

Collaborative work on 1) the self-assembly of block copolymers with large hydrophobic blocks and, 2) glycodendrimers or amphiphilic Janus dendrimers in solution has been elaborated here. In the first collaboration, various stomatocyte intermediate structures were constructed with the membrane instabilities of thick-walled vesicles through solvent condition fluctuations. It was shown that membranes with a glassy hydrophobic segment are no longer merely destined to just attain a spherical vesicle morphology. Upon gradual introduction of plasticizing organic solvent molecules, the membrane becomes permeable and responsive to the environment in a controlled approach. Rapid quenching of the membrane enables the entrapment of desired, transient structures. The degree of flexibility introduced to the system has an influence on the final morphology. Slow solvent exchange was used to introduce the morphology transitions in the described system.

In the second collaboration the characterization of solution assemblies of amphiphilic Janus glycodendrimers with three types of biogenic carbohydrates was described. Lamellar crystals, rectangular crystals, tubular and polygonal glycodendrimersomes, and several types of vesicles (polygonal, unilamellar spherical and solid) were characterized using cryogenic TEM. In addition, the self-assembly behaviors of six primary structures of single-single amphiphilic Janus dendrimers were studied. Uniform onion-like dendrimersomes were characterized by cryo-TEM. These onion-like vesicles were assembled by two extremely easy-to-handle direct and reverse injection methods. It has been demonstrated that the size and the number of bilayers of the onion-like vesicles are predictable by the final concentration of the Janus dendrimer. At low concentration, double-bilayer vesicles are formed, whereas at higher concentrations they form multilayer onion-like vesicles. The onion-like dendrimersomes provide mimics of various biological membranes. In all the dendrimer assembly, water was directly added to the THF/dendrimer solution to introduce the self-assembly with the nanostructures being stable over a long time.

Generally, two assembly strategies were explored. First, complicated nanostructures were formed through the self-assembly of macromolecules with large molecular weight *via* slow solvent exchange pathway. Secondly, relatively uniform nanostructures were formed through the self-assembly of giant amphiphiles with relatively small molecular weight *via* fast solvent exchange pathway. All the newly developed nanostructures were characterized by cryo-TEM.

REFERENCES

1. B. M. Discher, Y.-Y. Won, D. S. Ege, J. C.-M. Lee, F. S. Bates, D. E. Discher and D. A. Hammer, *Science*, 1999, **284**, 1143-1146.
2. R. Tangirala, R. Revanur, T. P. Russell and T. Emrick, *Langmuir*, 2007, **23**, 965-969.
3. X. Yu, W.-B. Zhang, K. Yue, X. Li, H. Liu, Y. Xin, C.-L. Wang, C. Wesdemiotis and S. Z. D. Cheng, *J. Am. Chem. Soc.*, 2012, **134**, 7780-7787.
4. X. Yu, S. Zhong, X. Li, Y. Tu, S. Yang, R. M. V. Horn, C. Ni, D. J. Pochan, R. P. Quirk, C. Wesdemiotis, W.-B. Zhang and S. Z. D. Cheng, *J. Am. Chem. Soc.*, 2010, **132**, 16741-16744.
5. S. A. Meeuwissen, K. T. Kim, Y. Chen, D. J. Pochan and J. C. M. v. Hest, *Angew. Chem. Int. Ed.*, 2011, **50**, 7070-7073.
6. K. T. Kim, J. Zhu, S. A. Meeuwissen, J. J. L. M. Cornelissen, D. J. Pochan, R. J. M. Nolte and J. C. M. v. Hest, *J. Am. Chem. Soc.*, 2010, **132**, 12522-12524.
7. V. Percec, P. Leowanawat, H. J. Sun, O. Kulikov, C. D. Nusbaum, T. M. Tran, A. Bertin, D. A. Wilson, M. Peterca, S. Zhang, N. P. Kamat, K. Vargo, D. Moock, E. D. Johnston, D. A. Hammer, D. J. Pochan, Y. Chen, Y. M. Chabre, T. C. Shiao, M. Bergeron-Brlek, S. Andre, R. Roy, H. J. Gabius and P. A. Heiney, *J. Am. Chem. Soc.*, 2013, **135**, 9055-9077.
8. M. Peterca, V. Percec, P. Leowanawat and A. Bertin, *J. Am. Chem. Soc.*, 2011, **133**, 20507-20520.
9. V. Percec, D. A. Wilson, P. Leowanawat, C. J. Wilson, A. D. Hughes, M. S. Kaucher, D. A. Hammer, D. H. Levine, A. J. Kim, F. S. Bates, K. P. Davis, T. P. Lodge, M. L. Klein, R. H. DeVane, E. Aqad, B. M. Rosen, A. O. Argintaru,

- M. J. Sienkowska, K. Rissanen, S. Nummelin and J. Ropponen, *Science*, 2010, **328**, 1009-1014.
10. S. Zhang, H.-J. Sun, A. D. Hughes, B. Draghici, J. Lejnieks, P. Leowanawat, A. Bertin, L. O. D. Leon, O. V. Kulikov, Y. Chen, D. J. Pochan, P. A. Heiney and V. Percec, *ACS Nano*, 2014, **8**, 1554-1565.
 11. M. Peterca, V. Percec, P. Leowanawat and A. Bertin, *J. Am. Chem. Soc.*, 2011, **133**, 20507–20520.
 12. E. Kellenberger and A. Ryter, *J. Biophysic and Biochem. cytol.*, 1958, **4**, 323-330.
 13. T. J. Beveridge, *J. Bacteriology*, 1999, **181**, 4725-4733.
 14. B. Burke and J. Ellenberg, *Nat. Rev. Mol. Cell Bio*, 2002, **3**, 487-497.
 15. A. d. Bangham, M. M. Standish and J. C. Watkins, *J. Mol. Biol.*, 1965, **13**, 238-252.
 16. H. Ringsdorf, B. Schlarb and J. Venzmer, *Angew. Chem. Int. Ed.*, 1988, **27**, 113-158.
 17. S. F. M. V. Dongen, H.-P. M. d. Hoog, R. J. R. W. Peters, M. Nallani, R. J. M. Nolte and J. C. M. V. Hest, *Chem. Rev.*, 2009, **109**, 6212-6274.
 18. X. Zhang, P. Tanner, A. Graff, C. G. Palivan and W. Meier, *J. Polym. Sci. A: Polym. Chem.*, 2012, **50**, 2293-2318.
 19. S.-H. Choi, F. S. Bates and T. P. Lodge, *Macromolecules*, 2011, **44**, 3594-3604.
 20. M. Mar í é C. Bonduelle and S. Lecommandoux, *Chem. Soc. Rev.*, 2013, **42**, 512-529.
 21. S. Zhang, H.-J. Sun, A. D. Hughes, R.-O. Moussodia, A. Bertin, Y. Chen, D. J. Pochan, P. A. Heiney, M. L. Klein and V. Percec, *Proc. Natl. Acad. Sci.*, 2014, **111**, 9058-9063.
 22. K. T. Kim, J. Zhu, S. A. Meeuwissen, J. J. L. M. Cornelissen, D. J. Pochan, R. J. M. Nolte and a. J. C. M. v. Hest, *J. Am. Chem. Soc.*, 2010, **132**, 12522-12524.

23. R. C. MacDonald, R. I. MacDonald, B. P. M. Menco, K. Takeshita, N. K. Subbarao and L. r. Hu, *Biochimica et Biophysica Acta*, 1991, 297-303.
24. I. Angert, C. Burmester, C. Dinges, H. Rose and R. Schroder, *Ultramicroscopy*, 1996, **63**, 181-192.

Chapter 7

THESIS SUMMARY AND FUTURE WORK

7.1 Thesis Summary

Similar to small amphiphile analogs, amphiphilic block copolymers can self-assemble into various, well-defined nanostructures in selective solvent mixtures. Recently, multicompartment and multigeometry nanoparticles have attracted more attention due to their potential nanofunctional applications. To achieve the construction of multicompartment and multigeometry nanoparticles with new shapes, polymer blends and kinetic control of the self-assembly process were studied. The slow chain dynamics inherent to polymeric assemblies is one advantage that can be used to form kinetically-trapped and pathway-dependent nanostructures. Therefore, optimization of the assembly parameters to create new shaped, well-defined and reproducible multicompartment and multigeometry solution assemblies are required. This dissertation demonstrated the design, self-assembly and kinetic study of macromolecular, amphiphilic molecules with the ultimate aim of potentially being used as multifunctional nanoreactors, nanocarriers or other applications.

In this dissertation, several diblock copolymers with a common hydrophilic block and different, immiscible hydrophobic blocks were designed. The effects of solvent processing rates affecting the morphology of the solution assemblies were explored in detail. Multicompartment and multigeometry nanoparticles have been assembled under targeted kinetic control with newly designed molecules. The new shapes include vesicle-cylinders, hybrid vesicles, disk-cylinders, hybrid cylinders, hybrid disks, asymmetric star-like cylinders and three-dimensional, ill-defined aggregates. Overall, the work presented here helps define better control of solution assemblies and offers a basis for the rational design of novel nanomaterials.

7.1.1 Revealing Effects of Solvent Processing Rates on Block Copolymer Assemblies

In Chapter 3, the water addition rate was evaluated as the main controlling parameter in kinetic control self-assembly. Two diblock copolymers having similar block lengths and relative hydrophilic-hydrophobic length ratios were designed. Overall rate-morphology correlations showed that smaller blended nano-objects with high curvatures are formed from these block copolymers at faster water addition rates. The size dispersity of the hybrid nanoparticles also becomes smaller at faster water addition rate. The morphology evolution of hybrid vesicles was presented to fully understand the advantages of kinetic control methods. Nanoparticles with nontraditional shapes were observed after long-time aging of the solution assemblies. The detected gross differences in assembly behaviors showed the importance of kinetic control. By taking advantage of the revealed rate-morphology rule, other hybrid multicompartment nanoparticles were assembled with other molecule blends including the hybrid cylinders, hybrid disks and star-like cylinders as presented in Chapter 4.

Experimentally, four slow *vs.* fast water addition rates were used based on a common beginning solution volume of 1 mL and a final solution volume of 5 mL. In Chapter 3 there is a description of how to determine water addition rates if one desires a different initial volume of polymer solution. When using diblock copolymers with longer block lengths, it is predicted that slower water addition rates need to be used for the assembly of defined nanostructures. For instance, a diblock copolymer PAA₂₀₀-PS₃₀₀ was synthesized with the ability to form big spheres (diameter=70 nm) at amine: acid=0.5:1 and 80% H₂O condition. PAA₂₀₀-PI₃₀₀ was synthesized with the ability to form big vesicles (wall thickness=80nm). After blending the two block copolymers, separated spherical and vesicle nanoparticles are predicted with extremely slow water addition rates while hybrid/blended nanoparticles are predicted with faster water addition rates. However, compared with the lower molecular weight PAA₉₉-PS₁₆₉/PAA₁₀₀-PI₁₅₀ blend system, slower water addition rate is suggested if one want

to make hybrid nanoparticles by blending PAA₂₀₀-PS₃₀₀ with PAA₂₀₀-PI₃₀₀ because the larger molecular weight diblocks have even slower chain dynamics in solution as well as more PAA chain length to be complexed with added organic amines and, therefore, are likely to be more easily trapped together across a wider variety of water addition rates. The tweaking of the solution assembly parameters needs real experimental investigation along with simulation work to help to predict useful parameter ranges in future nanoparticle assembly.

The formation of separate, unblended nanoparticles with slow water addition rates exhibit lower free interfacial energies within particles compared with the hybrid nanoparticles formed with fast water addition rates. For example, the separate sphere and cylinder nanoparticles have no intraparticle, high-energy PI/PS, PB/PS, or PS/PMMA interfaces^{1,2}. Hybrid nanoparticles that contain high interfacial energy interfaces within the hydrophobic cores require fast solvent mixing processes to trap the immiscible hydrophobic blocks in the same particle cores. The faster addition rates, the higher free energy the solution assembly will adopt, Figure 7.1. Most solution assemblies are kinetically-trapped, metastable structures due to the assembly process combined with the slow chain exchange rate of high molecular weight block copolymers. However, block copolymers kinetically trapped in a nanoparticle can relax/phase separate over time in order to further lower the system free energy. Additionally, in more rare rates (as also shown in Figure 7.1) separate particles can join together physically to form interparticle, hybrid nanostructures to further lower the system free energy.

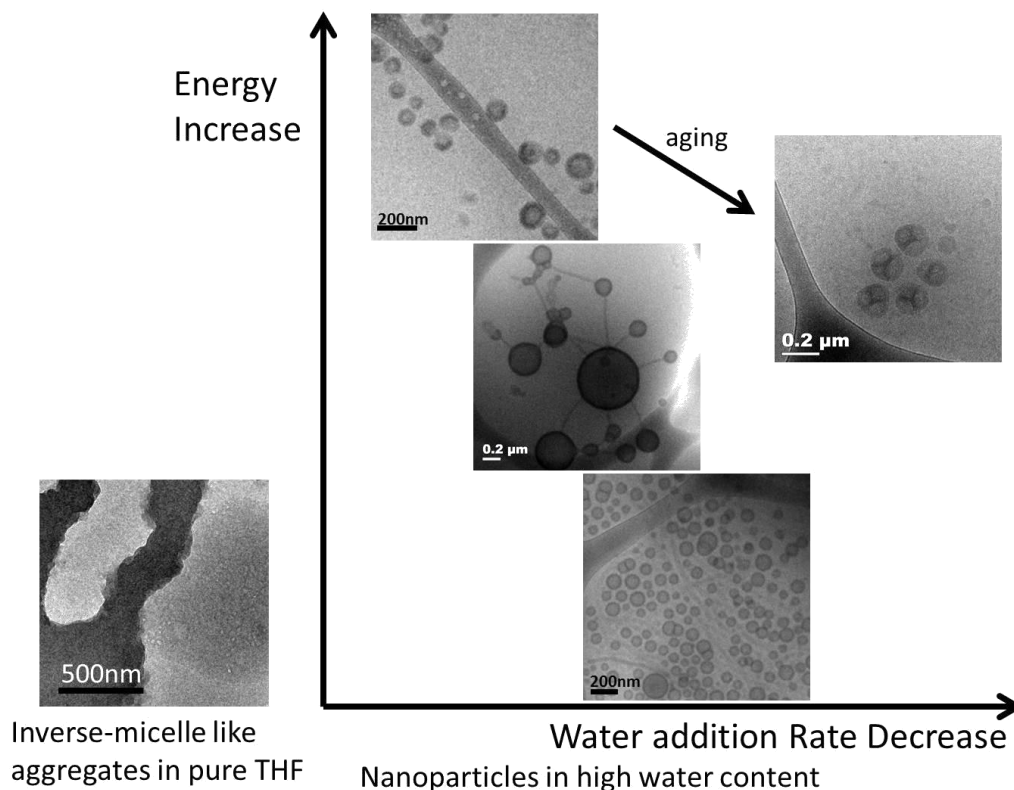


Figure 7.1 Varied morphologies assembled from blends of PAA-PI and PAA-PS in different water addition rates. The y axis represents the relative free energy of the formed nanoparticle system. Higher energy is observed when water addition rate is faster.

7.1.2 Construction of Multicompartment and Multigeometry Nanoparticles

A multicompartment and multigeometry nanoparticle morphological library has been presented in this dissertation. As indicated in Figure 7.2, multicompartment nanoparticles featuring common and uncommon^{3,4} geometries have been constructed. Here, the common geometries include spheres, cylinders, and vesicles. The uncommon geometries are referred to disks and toroids.

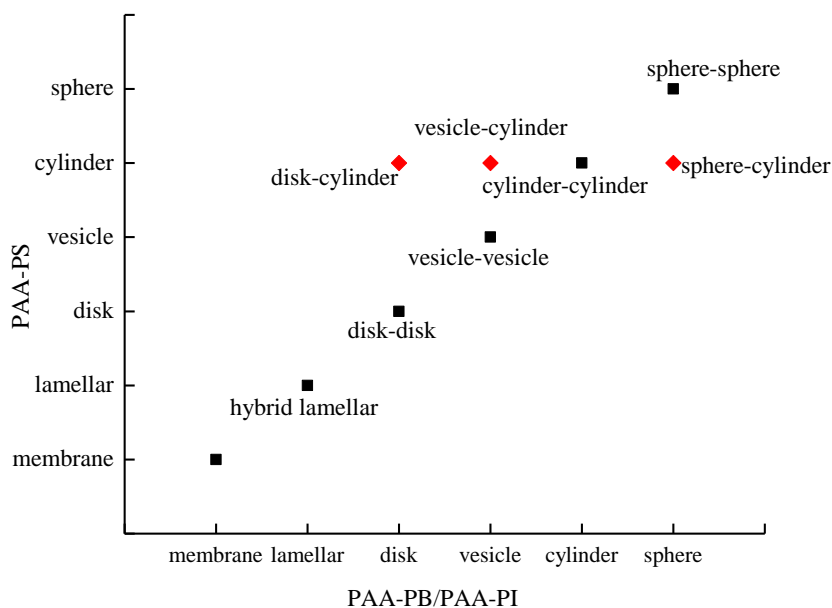


Figure 7.2 Construction of Multicompartment and Multigeometry nanoparticles via block copolymer blends. The black square represents the multicompartment nanoparticles. The red square represents the multicompartment and multigeometry nanoparticles.

The newly constructed hybrid nanoparticles, in addition to previously published results³⁻⁵, reveal the importance of material design and kinetic control methods^{6,7}. A critical exploration of the limitations of the blending strategy has also been presented such as in the co-assembly of two cylinder-forming block copolymers.

According to the blend scheme that was presented in Chapter 3 and 4, combination of diblock copolymers with different morphologies in the same solution conditions (amine: acid ratio, H₂O content) were shown to provide successful construction of new shapes of multicompartment and multigeometry nanoparticles. A list of diblock copolymers were designed targeting for specific morphologies in the same solution condition (amine: acid=0.5:1, 80% H₂O), Table 7.1.

Table 7.1 Diblock copolymers and their assembled nanostructures (amine: acid=0.5:1, 80% H₂O)

PAA-PS	Structures	Diameter/ wall thickness (nm)	PAA-PB	Structures	Diameters
PAA ₁₅₀ -PS ₅₀	S	30	PAA ₇₅ -PB ₁₄₀	S	50
PAA ₉₄ -PS ₁₂₄	S+C	40	PAA ₈₃ -PB ₂₀₄	C	83
PAA ₉₉ -PS ₁₆₉	C	40	PAA ₉₇ -PB ₂₇₀	C+V	108
PAA ₉₉ -PS ₂₄₀	C	45	PAA-PMMA		
PAA ₇₀ -PS ₅₅₅	V	65	PAA ₁₀₅ -PMMA ₁₀₀	C	43
PAA ₁₂₄ -PS ₁₄₀₀	Giant M		PAA ₁₀₀ -PMMA ₁₇₀	C	45
PAA ₂₀₀ -PS ₃₀₀	S	70	PAA ₁₄₂ -PMMA ₁₅₆	C	50

PAA-PI	Structures	Diameter/wall thickness (nm)
PAA ₇₅ -PI ₁₀₀	S+C	50
PAA ₁₀₀ -PI ₁₀₀	V+C	V: 30; C:40
PAA ₁₀₀ -PI ₁₅₀	V	35
PAA ₇₅ -PI ₁₅₀	V+C+S	V: 40; C: 70; S: 60-70

S represents for sphere; C represents for cylinder; V represents for vesicle; Giant M represents for giant membrane.

The explored nanostructures from the listed diblock copolymers can be referred to in the design of new block copolymers with targeted shapes and sizes. The longer hydrophobic block length that one block copolymer has, the lower curvature it will form in the same solution condition as a block copolymer with shorter hydrophobic block length.

7.1.3 Exploration of Interparticle Crosslinking via Designed Functionalized Molecules

The typical lack of interparticle physical association and the successful construction of hybrid nanoparticles with patches/domains after hybrid particle construction motivated the design of functionalized building blocks for post-assembly interparticle linking. Due to local immiscible blocks and consequent nanophase separation, hybrid nanoparticles with multiple hydrophobic phases in the core are formed under fast kinetic control. The incorporation of functionalized diblock copolymers facilitated the formation of hybrid disk-like nanoparticles with a patchy and anisotropic surface. Post-assembly, interparticle crosslinking resulted in three dimensional nanoparticle agglomerates. The understanding of the influences of functionality on the assembly behavior, and the exploration of possible nanoparticle associations hopefully will inspire future material design and supernanoparticle construction with other geometries.

7.2 Recommendations for Future Work

7.2.1 Multidimensional Superstructure Construction via Hybrid Nanoparticle subunits containing Patchy, Anisotropic Surfaces

The successful optimization of solution assembly parameters offers targeted hybrid nanoparticles with different geometries through interparticle assembly. Further study on exploration of new kinds of designed functionalized building units, and achievements of three-dimensional or two-dimensional superstructures, are warranted. For instance, the reported hybrid spheres, hybrid vesicles, and hybrid disks are great building blocks for further particle-particle association. As shown in the Figure 7.3, designed giant sphere-small sphere hybrid nanoparticles are constructed from blends of diblock copolymer. The dark blue spheres represent the solution assemblies from diblock copolymer with longer block length while the light blue spheres represent the solution assemblies from diblock copolymer with shorter block lengths. By tuning the

blending ratios, giant sphere-small sphere dimer, trimer, triangle particles and tetrahedral particles are predicted. The important idea is that: functionality of the block copolymers forming the dark blue spheres will result in the hybrid nanoparticles with reactive patches on the surface. Initiation of the interparticle chemical reaction, especially those that can occur in water/THF mixed solvent conditions, will promote the linking of the dark spheres to form two dimensional nanoparticle arrays. Similarly, dimers with the light blue reactive patches will also facilitate the targeted formation of nanoparticle arrays with an end-to-end linking fashion. Importantly, the realization of one-dimensional, two-dimensional arrays or three-dimensional networks asks for subunits with monodisperse sizes and shapes and surface properties. The current, multiple step assembly needs more achievement of accurately controlled subunits formation in each step⁸.

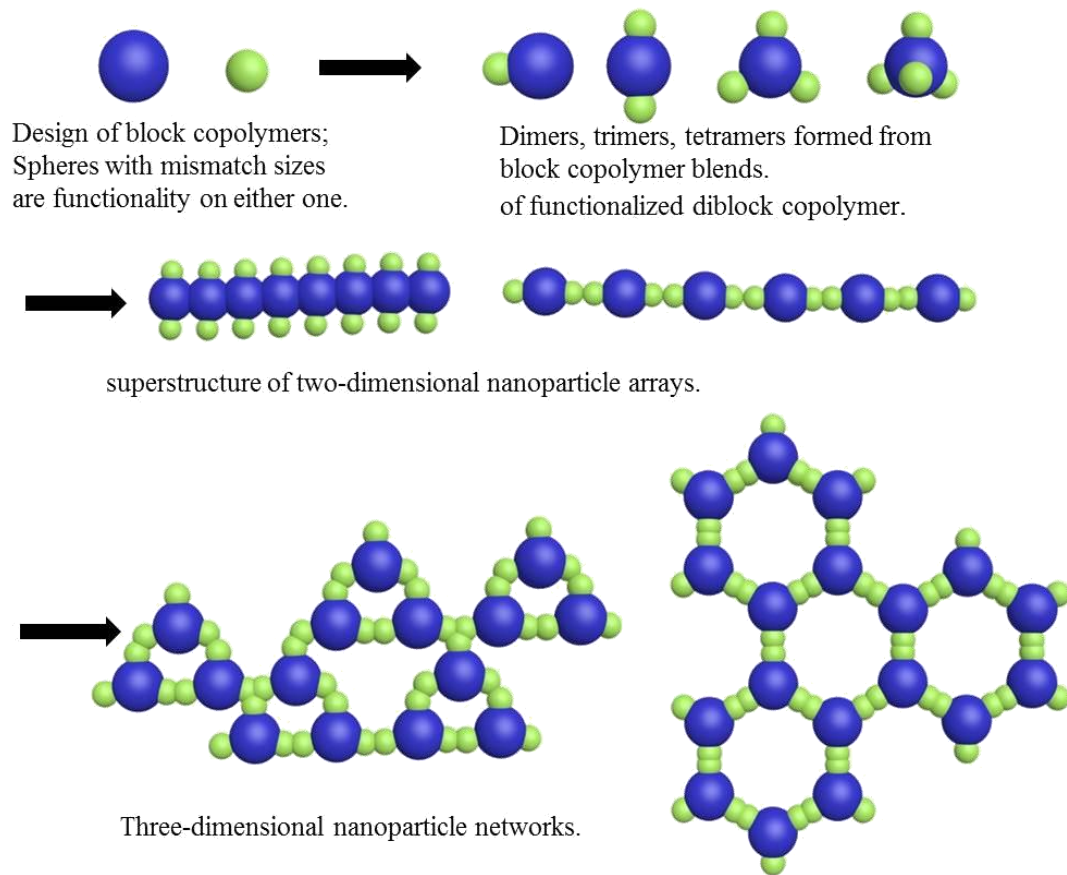


Figure 7.3 Sphere-sphere superstructures from hybrid sphere nanoparticles *via* multistep assembly.

Table 7.2 Designed diblock copolymers targeting specific sizes and shapes

Diblock	Predicted structures	Size (diameter, nm)
PAA ₃₀₀ -PS ₃₀₀	S	80-90
PAA ₃₀₀ -PI ₂₀₀	S	~100
PAA ₁₅₀ -PI ₁₀₀	S	50
PAA ₁₅₀ -PMMA ₁₀₀	S	45-50

Table 7.3 Predicted block length of SH-PAA-PS for achieving different geometries

Non-functionalized	Morphology	Functionalized	Morphology
PAA ₉₀ -PS ₁₂₀	Cylinder	20% thiol(HS ₁₈ -PAA ₇₂ -PS ₁₂₀)	Lamellar, disk
		10% thiol (predicted)	Vesicle (predicted)
PAA ₂₀₀ -PS ₁₂₀	Sphere	Variations of thiol functions	Sphere, cylinder



Figure 7.4 Three dimensional toroidal flowers build from hybrid toroids.

Similarly, hybrid toroids are predicted from blends of PAA₉₉-PMA₁₀₃-PS₄₄⁹ and functionalized PAA-PI with the reactive interparticle functionalities in the PAA domain. The PAA-PI block length is predicted to be in the range of PAA₁₅₀-PI₁₀₀ with the ability to form spherical structures, Table 7.4. As shown in Figure 7.3, the dark color domain in the hybrid toroids represents the PI block, and the grey color domain represents the PMA-PS blocks. The red color ring represents the PAA/diamine condensed shell. The small branch extended outside represents the reactive functionalities from functionalized PAA-PI molecules. With fast water addition kinetics, hybrid toroids are assembled with the immiscible hydrophobic blocks trapped inside and the patchy surface formed outside. Then, triggering the interparticle reaction will result in the linking of the hybrid toroids and the three dimensional toroidal flower-like structure, as shown in Figure 7.4. The proposed strategy above can also be applied to the formation of hybrid nanoparticles with other geometries. Newly designed block copolymer with specific block lengths and functionalities are anticipated to assemble into hybrid vesicles under fast water kinetic addition. Then, hybrid vesicles with anisotropic surfaces can be possibly linked together to form three-dimensional packed agglomerates. With the tuning of the volume fraction of the patchy area, one can build up different packing fashions of the hybrid nanoparticles, similar as the study of colloidal assembly with different valences¹⁰⁻¹².

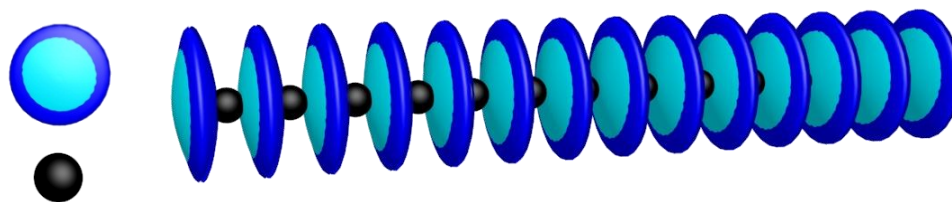


Figure 7.5 Packing disks assembled from hybrid disks with anisotropic and functionalized surface and gold nanoparticles.

The design of new functionalized block copolymers is required to achieve the interparticle crosslinking after hybrid nanoparticle assembly. The current assembly study of the new developed thiol functionalized PAA-PS helps the design of thiol functionalized diblocks with other length to achieve the desired geometries. For instance, the thiol functionality increased the hydrophobicity of the whole amphiphile. Thus, increasing the hydrophilic block length will promote the formation of different assemblies due to the introduction of the thiol. As shown in Table 7.1, one can design the different block lengths to achieve the anticipated geometries.

In addition, following the work from Chapter 5, if functionalized diblock copolymers were designed to form the inner domain of disk-cylinders as shown in Figure 7.5, then arrays of packed hybrid disks are predicted to be designed by reaction between hybrid disks and functionalized spheres.

Other robust chemistry methods to provide functionality on the PAA block are also suggested. For instance, the Fox group has recently reported the click chemistry reaction between *trans*-cyclooctene (TCO) and tetrazine (Tz) derivatives that has significant fast reaction speed (k_2 284000 M⁻¹ s⁻¹)^{13, 14}. The successful functionality of diblock/triblock copolymers with the TCO and Tz will provide promising building blocks for hierarchical inter-particles reaction after the formation of hybrid, well-defined nanoparticles.

Imaging of the particle aggregation process via dynamic in-situ TEM

The dynamic process of nanoparticle association is constantly one interesting and evolving topic¹⁵. As it is proposed above, the nanoparticles with anisotropic surfaces will be able to associate together if robust chemical reactions are designed between the hybrid nanoparticle subunits. The dynamic association process of the particles is still a mystery and could be revealed by dynamic, in-situ TEM imaging¹⁵.

7.2.2 Complicated Morphology Transformations via long term aging under fast kinetic control

Under fast water addition, different, immiscible hydrophobic phases are kinetically trapped inside of one particle. The nanoparticles are metastable and may change over long time aging. As discussed in the Chapter 3, asymmetric nanoparticles with exotic shapes are formed from the aging of the hybrid vesicles. It then provides an interesting morphological transformation example of metastable nanoparticles under fast kinetic water addition. Further study is needed on assembled hybrid nanoparticles with other geometries, which will possibly transform to novel structures over long time aging.

7.2.3 Summary of Future Directions

The avenues outlined above will provide new insight into block copolymer self-assembly necessary to create new, well-defined, reproducible nanoparticles for potential multifunctional applications. Specifically, further design of functionalized diblock copolymers for hybrid nanoparticle assembly and post-assembly interparticle association will empower the construction of large scale, multidimensional suprananostructures¹⁶. Morphology transformation over long time aging under fast water addition is an interesting branch to dive into. The incorporation of other functionalized or degradable block copolymers into the blend system is also suggested. Together, these approaches will figure essential structure-property relationships for

broader applications of polymeric nano-assemblies and guide the rational design of molecules and solution-assembly. The comprehensive understanding of the processing pathways and assembly results presented in this dissertation are important for new, emerging nanotechnologies.

REFERENCES

1. J. Zhu and R. C. Hayward, *Macromolecules*, 2008, **41**, 7794-7797.
2. A. F.M.BARTON, *CRC Handbook of Solubility Parameters and other Cohesion Parameters, Second Edition*, CRC Press, 1991.
3. D. J. Pochan, J. Zhu, K. Zhang, K. L. Wooley, C. Miesch and T. Emrick, *Soft Matter*, 2011, **7**, 2500-2506.
4. J. Zhu, S. Zhang, F. Zhang, K. L. Wooley and D. J. Pochan, *Adv. Funct. Mater.*, 2013, **23**, 1767-1773.
5. J. Zhu, S. Zhang, K. Zhang, X. Wang, J. W. Mays, K. L. Wooley and D. J. Pochan, *Nat. Commun.*, 2013, **4**, 2297-2301.
6. L. Zhang, J. Lin and S. Lin, *J. Phys. Chem. B*, 2007, **111**, 9209-9217.
7. X. Li, P. Tang, F. Qiu, H. Zhang and Y. Yang, *Journal of Physical Chemistry B*, 2006, **110**, 2024-2030.
8. H. Qiu, Z.M. Hudson, Mitchell A. Winnik and Ian Manners, *Science*, 2015, **347**, 1329-1332.
9. D. J. Pochan, Z. Chen, H. Cui, K. Hales, K. Qi and K. L. Wooley., *Science*, 2004, **306**, 94-97.
10. S. Sacanna, M. Korpics, K. Rodriguez, L. Colon-Melendez, S.-H. Kim, D. J. Pine and G.-R. Yi, *Nat. Commun.*, 2013, **4**, 1688-1693.
11. S. Sacanna, D. J. Pine and G.-R. Yi, *Soft Matter*, 2013, **9**, 8096-8102.
12. Y. Wang, Y. Wang, D. R. Breed, V. N. Manoharan, L. Feng, A. D. Hollingsworth, M. Weck and D. J. Pine, *Nature*, 2012, **491**, 51-55.
13. H. Zhang, K. T. Dicker, X. Xu, X. Jia and J. M. Fox, *ACS macro letters*, 2014, **3**, 727-731.

14. J. L. Seitchik, J. C. Peeler, M. T. Taylor, M. L. Blackman, T. W. Rhoads, R. B. Cooley, C. Refakis, J. M. Fox and R. A. Mehl, *J. Am. Chem. Soc.*, 2012, **134**, 2898-2901.
15. Q. Chen, J. M. Smith, J. Park, K. Kim, D. Ho, H. I. Rasool, A. Zettl and A. P. Alivisatos, *Nano Lett.*, 2013, **13**, 4556-4561.
16. A. H. Groschel, A. Walther, T. I. Lobling, F. H. Schacher, H. Schmalz and A. H. Müller, *Nature*, 2013, **503**, 247-251.

Appendix A

FORM FACTOR FITTING RESULTS OF SAXS TRACES

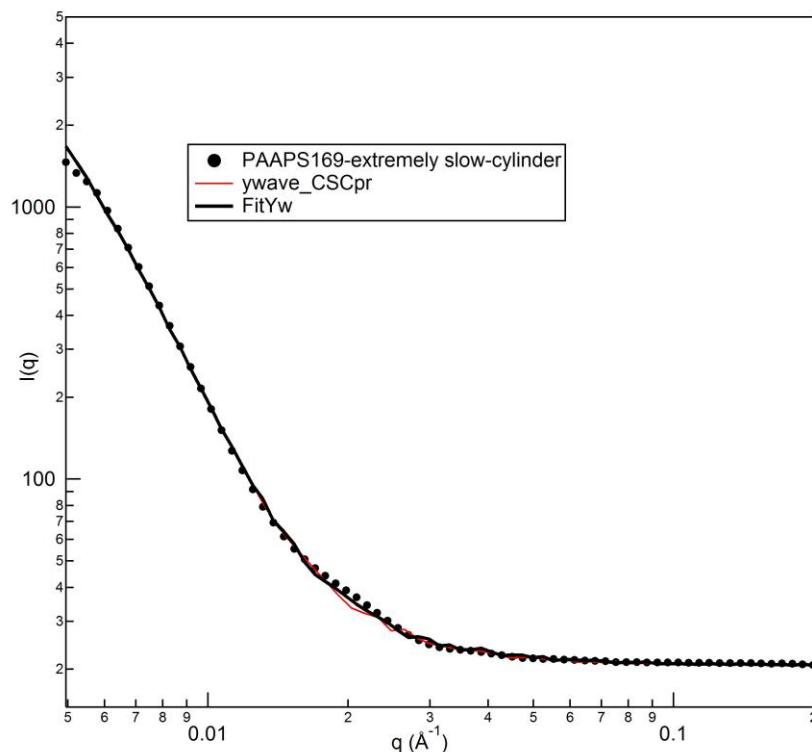


Figure A1 Form factor fitting of the pure cylinders assembled from PAA-PS, with the extreme slow water addition rate. Core-shell cylinder form factor was used to fit the SAXS trace corresponding to the cylinder nanostructures. The SAXS trace is according to the Figure 3. 2B.

The initial scattering length density (\AA^{-1}) used for PAA, PAA/EDDA, PS, and the final THF/H₂O mixture for fitting purpose are $9.44\text{e-}6$, $9.50\text{e-}6$, $8.31\text{e-}6$, $9.24\text{e-}6$ respectively. The core radius was set at 200 \AA for the purpose of fitting; the core length was set at 1000 \AA and the shell thickness was set at 20 \AA .

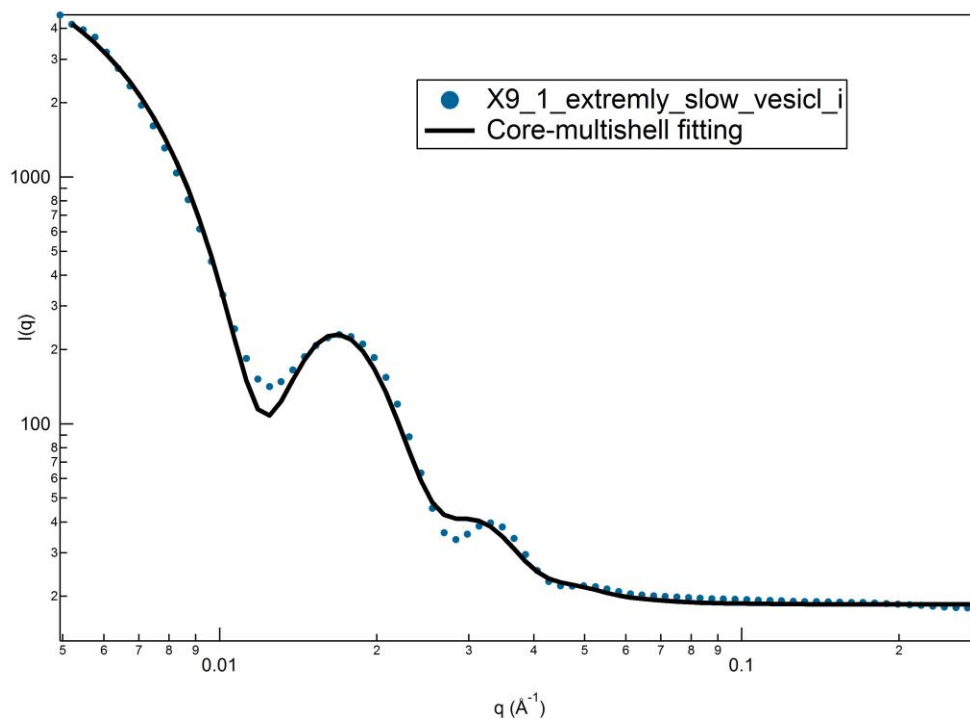


Figure A2 Form factor fitting of the separate populations of vesicle and cylinder nanoparticles formed at extremely slow water addition, with the PAA-PI/PAA-PS blend ratio at 9:1, vesicles are in the dominant volume ratio. The SAXS trace is corresponding to the TEM image of Figure 3.8A.

The initial scattering length density (\AA^{-1}) used for PAA, PAA/EDDA, PS, PI and the final THF/H₂O mixture for fitting purpose are 9.44e^{-6} , 9.50e^{-6} , 8.31e^{-6} , 6.46e^{-6} and 9.24e^{-6} respectively. In the multishell core model: the SLD for the core was set at 9.24e^{-6} with the radius initially set at 250 \AA with the range from 100-700 \AA ; the SLD for the first layer was set at 9.50e^{-6} with the radius initially set at 20 \AA with the range from 20-50 \AA , and the SLD and radius set for the third layer are the same as the first layer. The SLD for the second layer was set at 6.46e^{-6} , corresponding to the SLD of the PI core, and the radius was set at 250 \AA initially with the range from 200-400 \AA .

Appendix B

COPYRIGHT PERMISSIONS

Permissions for Chapter 1

Figure 1.1, 1.2

This Agreement between yingchao chen ("You") and John Wiley and Sons ("John Wiley and Sons") consists of your license details and the terms and conditions provided by John Wiley and Sons and Copyright Clearance Center.

License Number	3553890383719
License date	Jan 21, 2015
Licensed Content Publisher	John Wiley and Sons
Licensed Content Publication	Wiley Books
Licensed Content Title	Surfactant Science and Technology, 3rd Edition
Licensed Content Author	Drew Myers
Licensed Content Date	Oct 1, 2005
Pages	400
Type of use	Dissertation/Thesis
Requestor type	University/Academic
Format	Print and electronic
Portion	Figure/table
Number of figures/tables	2
Original Wiley figure/table number(s)	Figure 1.1; Figure 4.6
Will you be translating?	No
Title of your thesis / dissertation	hybrid nanoparticle formation via block copolymer blends and kinetic control

Expected completion date Feb 2015

Expected size (number of pages) 1

Requestor Location yingchao chen
201 Dupont Hall
Material Science and Engineering
University of Delaware
NEWARK, DE 19716
United States
Attn: yingchao chen

Billing Type Invoice

Billing Address yingchao chen
201 Dupont Hall
Material Science and Engineering
University of Delaware
NEWARK, DE 19716
United States
Attn: yingchao chen

Total 0.00 USD

Terms and Conditions

Figure 1.3, cryo-TEM images:

Thank you very much for your order.

This is a License Agreement between yingchao chen ("You") and The American Association for the Advancement of Science ("The American Association for the Advancement of Science"). The license consists of your order details, the terms and conditions provided by The American Association for the Advancement of Science, and the [payment terms and conditions](#).

[Get the printable license](#).

License Number	3582690029146
License date	Mar 05, 2015
Licensed content publisher	The American Association for the Advancement of Science
Licensed content publication	Science

Licensed content title	On the Origins of Morphological Complexity in Block Copolymer Surfactants
Licensed content author	Sumeet Jain, Frank S. Bates
Licensed content date	Apr 18, 2003
Volume number	300
Issue number	5618
Type of Use	Thesis / Dissertation
Requestor type	Scientist/individual at a research institution
Format	Print and electronic
Portion	Figure
Number of figures/tables	3
Order reference number	None
Title of your thesis / dissertation	hybrid nanoparticle construction via kinetic control of block copolymer blends
Expected completion date	Apr 2015
Estimated size(pages)	1
Total	0.00 USD

Figure 1.4



Title: Toroidal Triblock Copolymer Assemblies
Author: Darrin J. Pochan, Zhiyun Chen, Honggang Cui, Kelly Hales, Kai Qi, Karen L. Wooley
Publication: Science
Publisher: The American Association for the Advancement of Science
Date: Oct 1, 2004
 Copyright © 2004, American Association for the Advancement of Science

Logged in as:
 yingchao chen
 Account #:
 3000881260

[LOGOUT](#)

Order Completed

Thank you very much for your order.

This is a License Agreement between yingchao chen ("You") and The American Association for the Advancement of Science ("The American Association for the Advancement of Science"). The license consists of your order details, the terms and conditions provided by The American Association for the Advancement of Science, and the [payment terms and conditions](#).

[Get the printable license.](#)

License Number	3555420323882
License date	Jan 24, 2015
Licensed content publisher	The American Association for the Advancement of Science
Licensed content publication	Science
Licensed content title	Toroidal Triblock Copolymer Assemblies
Licensed content author	Darrin J. Pochan, Zhiyun Chen, Honggang Cui, Kelly Hales, Kai Qi, Karen L. Wooley
Licensed content date	Oct 1, 2004
Volume number	306
Issue number	5693
Type of Use	Thesis / Dissertation
Requestor type	Scientist/individual at a research institution
Format	Print and electronic
Portion	Figure
Number of figures/tables	2
Order reference number	None
Title of your thesis / dissertation	hybrid nanoparticle formation via block copolymer blends and kinetic control
Expected completion date	Feb 2015
Estimated size(pages)	1

Total 0.00 USD

Title: Helix self-assembly through the coiling of cylindrical micelles

Author: Sheng Zhong,Honggang Cui,Zhiyun Chen,Karen L. Wooley,Darrin J. Pochan

Publication: Soft Matter

Publisher: Royal Society of Chemistry

Date: Nov 8, 2007

Copyright © 2007, Royal Society of Chemistry

Logged in as:
yingchao chen

Account #:
3000881260

LOGOUT

Order Completed

Thank you very much for your order.

This is a License Agreement between yingchao chen ("You") and Royal Society of Chemistry. The license consists of your order details, the terms and conditions provided by Royal Society of Chemistry, and the [payment terms and conditions](#).

[Get the printable license.](#)

License Number	3555420626369
License date	Jan 24, 2015
Licensed content publisher	Royal Society of Chemistry
Licensed content publication	Soft Matter
Licensed content title	Helix self-assembly through the coiling of cylindrical micelles
Licensed content author	Sheng Zhong,Honggang Cui,Zhiyun Chen,Karen L. Wooley,Darrin J. Pochan
Licensed content date	Nov 8, 2007
Volume number	4

Issue number	1
Type of Use	Thesis/Dissertation
Requestor type	academic/educational
Portion	figures/tables/images
Number of figures/tables/images	2
Distribution quantity	100
Format	print and electronic
Will you be translating?	no
Order reference number	None
Title of the thesis/dissertation	hybrid nanoparticle formation via block copolymer blends and kinetic control
Expected completion date	Feb 2015
Estimated size	1
Total	0.00 USD

Order Completed

Thank you for your order.

This Agreement between yingchao chen ("You") and John Wiley and Sons ("John Wiley and Sons") consists of your license details and the terms and conditions provided by John Wiley and Sons and Copyright Clearance Center.

Your confirmation email will contain your order number for future reference.

[Get the printable license.](#)

License Number	3555421049982
License date	Jan 24, 2015
Licensed Content Publisher	John Wiley and Sons
Licensed Content Publication	Angewandte Chemie
Licensed Content Title	Self-Assembled ABC Triblock Copolymer Double and Triple Helices

Licensed Content Author	John Dupont,Guojun Liu,Ken-ichi Niihara,Ryuhei Kimoto,Hiroshi Jinnai
Licensed Content Date	Jul 7, 2009
Licensed Content Pages	4
Type of use	Dissertation/Thesis
Requestor type	University/Academic
Format	Print and electronic
Portion	Figure/table
Number of figures/tables	3
Original Wiley figure/table number(s)	Figure 1.
Will you be translating?	No
Title of your thesis / dissertation	hybrid nanoparticle formation via block copolymer blends and kinetic control
Expected completion date	Feb 2015
Expected size (number of pages)	1
Requestor Location	yingchao chen 201 Dupont Hall Material Science and Engineering University of Delaware NEWARK, DE 19716 United States Attn: yingchao chen
Billing Type	Invoice
Billing address	yingchao chen 201 Dupont Hall Material Science and Engineering University of Delaware NEWARK, DE 19716 United States Attn: yingchao chen
Total	0.00 USD

Title: Mechanistic Insights for Block Copolymer Morphologies: How Do Worms Form Vesicles?
Author: Adam Blanz, Jeppe Madsen, Giuseppe Battaglia, et al
Publication: Journal of the American Chemical Society
Publisher: American Chemical Society
Date: Oct 1, 2011
Copyright © 2011, American Chemical Society

Logged in as:
yingchao chen
Account #:
3000881260

LOGOUT

PERMISSION/LICENSE IS GRANTED FOR YOUR ORDER AT NO CHARGE

This type of permission/license, instead of the standard Terms & Conditions, is sent to you because no fee is being charged for your order. Please note the following:

- Permission is granted for your request in both print and electronic formats, and translations.
- If figures and/or tables were requested, they may be adapted or used in part.
- Please print this page for your records and send a copy of it to your publisher/graduate school.
- Appropriate credit for the requested material should be given as follows: "Reprinted (adapted) with permission from (COMPLETE REFERENCE CITATION). Copyright (YEAR) American Chemical Society." Insert appropriate information in place of the capitalized words.
- One-time permission is granted only for the use specified in your request. No additional uses are granted (such as derivative works or other editions). For any other uses, please submit a new request.

If credit is given to another source for the material you requested, permission must be obtained from that source.



Title: Synthesis and Self-Assembly of RGD-Functionalized PEO-PB Amphiphiles
Author: John A. Zupancich, Frank S. Bates, Marc A. Hillmyer

Logged in as:
yingchao chen
Account #:
3000881260

LOGOUT

Publication: Biomacromolecules
Publisher: American Chemical Society
Date: Jun 1, 2009
Copyright © 2009, American Chemical Society

PERMISSION/LICENSE IS GRANTED FOR YOUR ORDER AT NO CHARGE

This type of permission/license, instead of the standard Terms & Conditions, is sent to you because no fee is being charged for your order. Please note the following:

- Permission is granted for your request in both print and electronic formats, and translations.
- If figures and/or tables were requested, they may be adapted or used in part.
- Please print this page for your records and send a copy of it to your publisher/graduate school.
- Appropriate credit for the requested material should be given as follows: "Reprinted (adapted) with permission from (COMPLETE REFERENCE CITATION). Copyright (YEAR) American Chemical Society." Insert appropriate information in place of the capitalized words.
- One-time permission is granted only for the use specified in your request. No additional uses are granted (such as derivative works or other editions). For any other uses, please submit a new request.

If credit is given to another source for the material you requested, permission must be obtained from that source.



ACS Publications
Most Trusted. Most Cited. Most Read.

Title: Water-Soluble Monodisperse Core-Shell Nanorings: Their Tailorable Preparation and Interactions with Oppositely Charged Spheres of a Similar Diameter
Author: Kaka Zhang, Han Miao, Daoyong Chen
Publication: Journal of the American Chemical Society
Publisher: American Chemical Society
Date: Nov 1, 2014
Copyright © 2014, American Chemical Society

Logged in as:
yingchao chen
Account #:
3000881260

[LOGOUT](#)

PERMISSION/LICENSE IS GRANTED FOR YOUR ORDER AT NO CHARGE

This type of permission/license, instead of the standard Terms & Conditions, is sent to you because

no fee is being charged for your order. Please note the following:

- Permission is granted for your request in both print and electronic formats, and translations.
- If figures and/or tables were requested, they may be adapted or used in part.
- Please print this page for your records and send a copy of it to your publisher/graduate school.
- Appropriate credit for the requested material should be given as follows: "Reprinted (adapted) with permission from (COMPLETE REFERENCE CITATION). Copyright (YEAR) American Chemical Society." Insert appropriate information in place of the capitalized words.
- One-time permission is granted only for the use specified in your request. No additional uses are granted (such as derivative works or other editions). For any other uses, please submit a new request.

If credit is given to another source for the material you requested, permission must be obtained from that source.

Figure 1.5

Title: Pathway toward Large Two-Dimensional Hexagonally Patterned Colloidal Nanosheets in Solution

Author: Bo Ni, Mingjun Huang, Ziran Chen, et al

Publication: Journal of the American Chemical Society

Publisher: American Chemical Society

Date: Feb 1, 2015

Copyright © 2015, American Chemical Society

PERMISSION/LICENSE IS GRANTED FOR YOUR ORDER AT NO CHARGE

This type of permission/license, instead of the standard Terms & Conditions, is sent to you because no fee is being charged for your order. Please note the following:

- Permission is granted for your request in both print and electronic formats, and translations.
- If figures and/or tables were requested, they may be adapted or used in part.
- Please print this page for your records and send a copy of it to your publisher/graduate school.
- Appropriate credit for the requested material should be given as follows: "Reprinted (adapted) with permission from (COMPLETE REFERENCE CITATION). Copyright

(YEAR) American Chemical Society." Insert appropriate information in place of the capitalized words.

- One-time permission is granted only for the use specified in your request. No additional uses are granted (such as derivative works or other editions). For any other uses, please submit a new request.

Figure 1.6

Shape Transformations of
Membrane Vesicles from
Amphiphilic Triblock
Copolymers: A Dissipative
Particle Dynamics
Simulation Study

Author: Xuejin Li, Igor V.
Pivkin, Haojun
Liang, et al

Publication: Macromolecules

Publisher: American
Chemical Society

Date: Apr 1, 2009

Copyright © 2009, American Chemical Society

PERMISSION/LICENSE IS GRANTED FOR YOUR ORDER AT NO CHARGE

This type of permission/license, instead of the standard Terms & Conditions, is sent to you because no fee is being charged for your order. Please note the following:

- Permission is granted for your request in both print and electronic formats, and translations.
- If figures and/or tables were requested, they may be adapted or used in part.
- Please print this page for your records and send a copy of it to your publisher/graduate school.
- Appropriate credit for the requested material should be given as follows: "Reprinted (adapted) with permission from (COMPLETE REFERENCE CITATION). Copyright (YEAR) American Chemical Society." Insert appropriate information in place of the capitalized words.
- One-time permission is granted only for the use specified in your request. No additional uses are granted (such as derivative works or other editions). For any other uses, please submit a new request.

If credit is given to another source for the material you requested, permission must be obtained from that source.

Figure 1.7

Thank you for your order.

This Agreement between yingchao chen ("You") and John Wiley and Sons ("John Wiley and Sons") consists of your license details and the terms and conditions provided by John Wiley and Sons and Copyright Clearance Center.

Your confirmation email will contain your order number for future reference.

[Get the printable license.](#)

License Number	3582730350378
License date	Mar 05, 2015
Licensed Content Publisher	John Wiley and Sons
Licensed Content Publication	Macromolecular Chemistry and Physics
Licensed Content Title	Multicompartment Micelles: Has the Long-Standing Dream Become a Reality?
Licensed Content Author	Jean-François Lutz, André Laschewsky
Licensed Content Date	Apr 19, 2005
Licensed Content Pages	5
Type of use	Dissertation/Thesis
Requestor type	University/Academic
Format	Print and electronic
Portion	Figure/table
Number of figures/tables	1
Original Wiley figure/table number(s)	figure 1
Will you be translating?	No
Title of your thesis / dissertation	hybrid nanoparticle construction via kinetic control of block copolymer blends
Expected completion date	Apr 2015
Expected size (number of pages)	1
Requestor Location	yingchao chen 201 Dupont Hall Material Science and Engineering University of Delaware NEWARK, DE 19716 United States Attn: yingchao chen

Billing Type	Invoice
Billing address	yingchao chen 201 Dupont Hall Material Science and Engineering University of Delaware NEWARK, DE 19716 United States Attn: yingchao chen

Figure 1.8

Thank you for your order.

This Agreement between yingchao chen ("You") and John Wiley and Sons ("John Wiley and Sons") consists of your license details and the terms and conditions provided by John Wiley and Sons and Copyright Clearance Center.

Your confirmation email will contain your order number for future reference.

[Get the printable license.](#)

License Number	3582730868341
License date	Mar 05, 2015
Licensed Content Publisher	John Wiley and Sons
Licensed Content Publication	Angewandte Chemie International Edition
Licensed Content Title	Multicompartment Micelles Formed by Self-Assembly of Linear ABC Triblock Copolymers in Aqueous Medium
Licensed Content Author	Stephan Kubowicz, Jean-François Baussard, Jean-François Lutz, Andreas F. Thünemann, Hans von Berlepsch, André Laschewsky
Licensed Content Date	Jul 20, 2005
Licensed Content Pages	4
Type of use	Dissertation/Thesis
Requestor type	University/Academic
Format	Print and electronic
Portion	Figure/table
Number of figures/tables	1
Original Wiley figure/table number(s)	1
Will you be translating?	No
Title of your thesis / dissertation	hybrid nanoparticle construction via kinetic control of block copolymer blends
Expected completion date	Apr 2015
Expected size (number of pages)	1

Requestor Location	yingchao chen 201 Dupont Hall Material Science and Engineering University of Delaware NEWARK, DE 19716 United States Attn: yingchao chen
Billing Type	Invoice
Billing address	yingchao chen 201 Dupont Hall Material Science and Engineering University of Delaware NEWARK, DE 19716 United States Attn: yingchao chen
Total	0.00 USD

Figure 1.9

itle: Morphologies of
Multicompartment Micelles
Formed by ABC Miktoarm Star
Terpolymers

Author: Zhibo Li, Marc A. Hillmyer,
Timothy P. Lodge

Publication: Langmuir

Publisher: American Chemical Society

Date: Oct 1, 2006

Copyright © 2006, American Chemical Society

PERMISSION/LICENSE IS GRANTED FOR YOUR ORDER AT NO CHARGE

This type of permission/license, instead of the standard Terms & Conditions, is sent to you because no fee is being charged for your order. Please note the following:

- Permission is granted for your request in both print and electronic formats, and translations.
- If figures and/or tables were requested, they may be adapted or used in part.
- Please print this page for your records and send a copy of it to your publisher/graduate school.
- Appropriate credit for the requested material should be given as follows: "Reprinted (adapted) with permission from (COMPLETE REFERENCE CITATION). Copyright (YEAR) American Chemical Society." Insert appropriate information in place of the capitalized words.
- One-time permission is granted only for the use specified in your request. No additional uses are granted (such as derivative works or other editions). For any other uses, please submit a new request.

If credit is given to another source for the material you requested, permission must be obtained from that source.

Figure 1.10

Title: Self-Assembly of Janus Cylinders
into Hierarchical Superstructures

Author: Andreas Walther, Markus
Drechsler, Sabine Rosenfeldt, et
al

Publication: Journal of the American
Chemical Society

Publisher: American Chemical Society

Date: Apr 1, 2009

Copyright © 2009, American Chemical Society

PERMISSION/LICENSE IS GRANTED FOR YOUR ORDER AT NO CHARGE

This type of permission/license, instead of the standard Terms & Conditions, is sent to you because no fee is being charged for your order. Please note the following:

- Permission is granted for your request in both print and electronic formats, and translations.
- If figures and/or tables were requested, they may be adapted or used in part.
- Please print this page for your records and send a copy of it to your publisher/graduate school.
- Appropriate credit for the requested material should be given as follows: "Reprinted (adapted) with permission from (COMPLETE REFERENCE CITATION). Copyright (YEAR) American Chemical Society." Insert appropriate information in place of the capitalized words.
- One-time permission is granted only for the use specified in your request. No additional uses are granted (such as derivative works or other editions). For any other uses, please submit a new request.

If credit is given to another source for the material you requested, permission must be obtained from that source.

Figure 1.11

Title: Multicompartment Core Micelles
of Triblock Terpolymers in
Organic Media

Author: Felix Schacher, Andreas
Walther, Markus Ruppel, et al

Publication: Macromolecules

Publisher: American Chemical Society

Date: May 1, 2009

Copyright © 2009, American Chemical Society

PERMISSION/LICENSE IS GRANTED FOR YOUR ORDER AT NO CHARGE

This type of permission/license, instead of the standard Terms & Conditions, is sent to you because no fee is being charged for your order. Please note the following:

- Permission is granted for your request in both print and electronic formats, and translations.
- If figures and/or tables were requested, they may be adapted or used in part.
- Please print this page for your records and send a copy of it to your publisher/graduate school.
- Appropriate credit for the requested material should be given as follows: "Reprinted (adapted) with permission from (COMPLETE REFERENCE CITATION). Copyright (YEAR) American Chemical Society." Insert appropriate information in place of the capitalized words.
- One-time permission is granted only for the use specified in your request. No additional uses are granted (such as derivative works or other editions). For any other uses, please submit a new request.

If credit is given to another source for the material you requested, permission must be obtained from that source.

Figure 1.12

Title: Dynamic Multicompartment-
Core Micelles in Aqueous Media

Author: Felix Schacher, Andreas
Walther, Axel H. E. Müller

Publication: Langmuir

Publisher: American Chemical Society

Date: Sep 1, 2009

Copyright © 2009, American Chemical Society

PERMISSION/LICENSE IS GRANTED FOR YOUR ORDER AT NO CHARGE

This type of permission/license, instead of the standard Terms & Conditions, is sent to you because no fee is being charged for your order. Please note the following:

- Permission is granted for your request in both print and electronic formats, and translations.

- If figures and/or tables were requested, they may be adapted or used in part.
- Please print this page for your records and send a copy of it to your publisher/graduate school.
- Appropriate credit for the requested material should be given as follows: "Reprinted (adapted) with permission from (COMPLETE REFERENCE CITATION). Copyright (YEAR) American Chemical Society." Insert appropriate information in place of the capitalized words.
- One-time permission is granted only for the use specified in your request. No additional uses are granted (such as derivative works or other editions). For any other uses, please submit a new request.

If credit is given to another source for the material you requested, permission must be obtained from that source.

Figure 1.13

Title: Undulated Multicompartment
Cylinders by the Controlled and
Directed Stacking of Polymer
Micelles with a
Compartmentalized Corona

Author: Bing Fang, Andreas
Walther, Andrea Wolf, Youyong
Xu, Jiayin Yuan, Axel H. E. Müller

Publication: Angewandte Chemie
International Edition

Publisher: John Wiley and Sons

Date: Mar 12, 2009

Copyright © 2009 WILEY-VCH Verlag GmbH & Co.
KGaA, Weinheim

Order Completed

Thank you for your order.

This Agreement between yingchao chen ("You") and John Wiley and Sons ("John Wiley and Sons") consists of your license details and the terms and conditions provided by John Wiley and Sons and Copyright Clearance Center.

Your confirmation email will contain your order number for future reference.

[Get the printable license.](#)

License Number	3582760145135
License date	Mar 05, 2015
Licensed Content Publisher	John Wiley and Sons

Licensed Content Publication	Angewandte Chemie International Edition
Licensed Content Title	Undulated Multicompartment Cylinders by the Controlled and Directed Stacking of Polymer Micelles with a Compartmentalized Corona
Licensed Content Author	Bing Fang, Andreas Walther, Andrea Wolf, Youyong Xu, Jiayin Yuan, Axel H. E. Müller
Licensed Content Date	Mar 12, 2009
Licensed Content Pages	4
Type of use	Dissertation/Thesis
Requestor type	University/Academic
Format	Print and electronic
Portion	Figure/table
Number of figures/tables	1
Original Wiley figure/table number(s)	1
Will you be translating?	No
Title of your thesis / dissertation	hybrid nanoparticle construction via kinetic control of block copolymer blends
Expected completion date	Apr 2015
Expected size (number of pages)	1
Requestor Location	yingchao chen 201 Dupont Hall Material Science and Engineering University of Delaware NEWARK, DE 19716 United States Attn: yingchao chen
Billing Type	Invoice
Billing address	yingchao chen 201 Dupont Hall Material Science and Engineering University of Delaware NEWARK, DE 19716 United States Attn: yingchao chen
Total	0.00 USD

Figure 1.14

Title: Interpolyelectrolyte Complexes of Dynamic Multicompartment Micelles

Author: Felix Schacher, Eva Betthausen, Andreas Walther, et al

Publication: ACS Nano

Publisher: American Chemical Society

Date: Aug 1, 2009

Copyright © 2009, American Chemical Society

Logged in as:
yingchao chen
Account #:
3000881260

[LOGOUT](#)

PERMISSION/LICENSE IS GRANTED FOR YOUR ORDER AT NO CHARGE

This type of permission/license, instead of the standard Terms & Conditions, is sent to you because no fee is being charged for your order. Please note the following:

- Permission is granted for your request in both print and electronic formats, and translations.
- If figures and/or tables were requested, they may be adapted or used in part.
- Please print this page for your records and send a copy of it to your publisher/graduate school.
- Appropriate credit for the requested material should be given as follows: "Reprinted (adapted) with permission from (COMPLETE REFERENCE CITATION). Copyright (YEAR) American Chemical Society." Insert appropriate information in place of the capitalized words.
- One-time permission is granted only for the use specified in your request. No additional uses are granted (such as derivative works or other editions). For any other uses, please submit a new request.

If credit is given to another source for the material you requested, permission must be obtained from that source.

Figure 1.15

Title: Non-Centrosymmetric Cylindrical Micelles by Unidirectional Growth

Author: Paul A. Rupar, Laurent Chabanne, Mitchell A. Winnik, Ian Manners

Publication: Science

Publisher: The American Association for the Advancement of Science

Date: Aug 3, 2012

Copyright © 2012, American Association for the Advancement of Science

Logged in as:
yingchao chen
Account #:
3000881260

LOGOUT

Order Completed

Thank you very much for your order.

This is a License Agreement between yingchao chen ("You") and The American Association for the Advancement of Science ("The American Association for the Advancement of Science"). The license consists of your order details, the terms and conditions provided by The American Association for the Advancement of Science, and the [payment terms and conditions](#).

[Get the printable license](#).

License Number	3582761142027
License date	Mar 05, 2015
Licensed content publisher	The American Association for the Advancement of Science
Licensed content publication	Science
Licensed content title	Non-Centrosymmetric Cylindrical Micelles by Unidirectional Growth
Licensed content author	Paul A. Rugar, Laurent Chabanne, Mitchell A. Winnik, Ian Manners
Licensed content date	Aug 3, 2012
Volume number	337
Issue number	6094
Type of Use	Thesis / Dissertation
Requestor type	Scientist/individual at a research institution
Format	Print and electronic
Portion	Figure
Number of figures/tables	1
Order reference number	None
Title of your thesis / dissertation	hybrid nanoparticle construction via kinetic control of block copolymer blends
Expected completion date	Apr 2015
Estimated size(pages)	1
Total	0.00 USD

Figure 1.16

Title: Block copolymer micelles for delivery of cancer therapy: Transport at the whole body, tissue and cellular levels

Author: Andrew S. Mikhail, Christine Allen

Publication: Journal of Controlled Release

Publisher: Elsevier

Date: 15 September 2009

Copyright © 2009 Elsevier B.V. All rights reserved.

Logged in as:
yingchao chen
Account #:
3000881260

[LOGOUT](#)

Order Completed

Thank you very much for your order.

This is a License Agreement between yingchao chen ("You") and Elsevier ("Elsevier"). The license consists of your order details, the terms and conditions provided by Elsevier, and the [payment terms and conditions](#).

[Get the printable license.](#)

License Number	3582770543459
License date	Mar 05, 2015
Licensed content publisher	Elsevier
Licensed content publication	Journal of Controlled Release
Licensed content title	Block copolymer micelles for delivery of cancer therapy: Transport at the whole body, tissue and cellular levels

Licensed content author	Andrew S. Mikhail,Christine Allen
Licensed content date	15 September 2009
Licensed content volume number	138
Licensed content issue number	3
Number of pages	10
Type of Use	reuse in a thesis/dissertation
Portion	figures/tables/illustrations
Number of figures/tables/illustrations	1
Format	both print and electronic
Are you the author of this Elsevier article?	No
Will you be translating?	No
Original figure numbers	figure 1
Title of your thesis/dissertation	hybrid nanoparticle construction via kinetic control of block copolymer blends
Expected completion date	Apr 2015
Estimated size (number of pages)	1
Elsevier VAT number	GB 494 6272 12
Permissions price	0.00 USD
VAT/Local Sales Tax	0.00 USD / 0.00 GBP
Total	0.00 USD

Figure 1.17

Title: Shape effects of filaments versus spherical particles in flow and drug delivery

Author: Yan Geng, Paul Dalhaimer, Shenshen Cai, Richard Tsai, Manorama Tewari et al.

Publication: Nature Nanotechnology

Publisher: Nature Publishing Group

Date: Mar 25, 2007

Copyright © 2007, Rights Managed by Nature Publishing Group

Logged in as:
yingchao chen
Account #:
3000881260

LOGOUT

Review Order

Please review the order details and the associated [terms and conditions](#).

Licensed content publisher	Nature Publishing Group
Licensed content publication	Nature Nanotechnology
Licensed content title	Shape effects of filaments versus spherical particles in flow and drug delivery
Licensed content author	Yan Geng, Paul Dalhaimer, Shenshen Cai, Richard Tsai, Manorama Tewari et al.
Licensed content date	Mar 25, 2007
Type of Use	reuse in a dissertation / thesis

Volume number	2
Issue number	4
Requestor type	academic/educational
Format	print and electronic
Portion	figures/tables/illustrations
Number of figures/tables/illustrations	1
High-res required	no
Figures	figure 1
Author of this NPG article	no
Your reference number	None
Title of your thesis / dissertation	hybrid nanoparticle construction via kinetic control of block copolymer blends
Expected completion date	Apr 2015
Estimated size (number of pages)	1
Total	0.00 USD

Figure 1.18

Title: Toward Intelligent Nanosize Bioreactors: A pH-Switchable, Channel-Equipped, Functional Polymer Nanocontainer

Author: Pavel Broz, Sergey Driamov, Joerg Ziegler, et al

Publication: Nano Letters

Publisher: American Chemical Society

Date: Oct 1, 2006

Copyright © 2006, American Chemical Society

Logged in as:
yingchao chen
Account #:
3000881260

[LOGOUT](#)

PERMISSION/LICENSE IS GRANTED FOR YOUR ORDER AT NO CHARGE

This type of permission/license, instead of the standard Terms & Conditions, is sent to you because no fee is being charged for your order. Please note the following:

- Permission is granted for your request in both print and electronic formats, and translations.
- If figures and/or tables were requested, they may be adapted or used in part.
- Please print this page for your records and send a copy of it to your publisher/graduate school.
- Appropriate credit for the requested material should be given as follows: "Reprinted (adapted) with permission from (COMPLETE REFERENCE CITATION). Copyright (YEAR) American Chemical Society." Insert appropriate information in place of the capitalized words.
- One-time permission is granted only for the use specified in your request. No additional uses are granted (such as derivative works or other editions). For any other uses, please

submit a new request.

If credit is given to another source for the material you requested, permission must be obtained from that source.

Permissions for Chapter 2

Figure 2.7

Title: Cryo-EM Study of the Chromatin Fiber Reveals a Double Helix Twisted by Tetranucleosomal Units

Author: Feng Song, Ping Chen, Dapeng Sun, Mingzhu Wang, Liping Dong, Dan Liang, Rui-Ming Xu, Ping Zhu, Guohong Li

Publication: Science

Publisher: The American Association for the Advancement of Science

Date: Apr 25, 2014

Copyright © 2014, American Association for the Advancement of Science

Order Completed

Thank you very much for your order.

This is a License Agreement between yingchao chen ("You") and The American Association for the Advancement of Science ("The American Association for the Advancement of Science"). The license consists of your order details, the terms and conditions provided by The American Association for the Advancement of Science, and the [payment terms and conditions](#).

[Get the printable license.](#)

License Number	3582780217178
License date	Mar 05, 2015
Licensed content publisher	The American Association for the Advancement of Science
Licensed content publication	Science
Licensed content title	Cryo-EM Study of the Chromatin Fiber Reveals a Double Helix Twisted by Tetranucleosomal Units
Licensed content author	Feng Song, Ping Chen, Dapeng Sun, Mingzhu Wang, Liping Dong, Dan Liang, Rui-Ming Xu, Ping Zhu, Guohong Li

Licensed content date	Apr 25, 2014
Volume number	344
Issue number	6182
Type of Use	Thesis / Dissertation
Requestor type	Scientist/individual at a research institution
Format	Print and electronic
Portion	Figure
Number of figures/tables	1
Order reference number	None
Title of your thesis / dissertation	hybrid nanoparticle construction via kinetic control of block copolymer blends
Expected completion date	Apr 2015
Estimated size(pages)	1
Total	0.00 USD

Figure 2.8

Title: Aqueous Self-Assembly of Giant Bottlebrush Block Copolymer Surfactants as Shape-Tunable Building Blocks

Author: Ryan Fenyves, Marc Schmutz, Ian J. Horner, et al

Publication: Journal of the American Chemical Society

Publisher: American Chemical Society

Date: May 1, 2014

Copyright © 2014, American Chemical Society

Logged in as:
yingchao chen
Account #:
3000881260

[LOGOUT](#)

PERMISSION/LICENSE IS GRANTED FOR YOUR ORDER AT NO CHARGE

This type of permission/license, instead of the standard Terms & Conditions, is sent to you because no fee is being charged for your order. Please note the following:

- Permission is granted for your request in both print and electronic formats, and translations.
- If figures and/or tables were requested, they may be adapted or used in part.
- Please print this page for your records and send a copy of it to your publisher/graduate school.
- Appropriate credit for the requested material should be given as follows: "Reprinted (adapted) with permission from (COMPLETE REFERENCE CITATION). Copyright (YEAR) American Chemical Society." Insert appropriate information in place of the capitalized words.
- One-time permission is granted only for the use specified in your request. No additional uses are granted (such as derivative works or other editions). For any other uses, please

submit a new request.

If credit is given to another source for the material you requested, permission must be obtained from that source.

Figure 2.9

Title: Temperature-Responsive
Nanospheres with Bicontinuous
Internal Structures from a
Semicrystalline Amphiphilic
Block Copolymer

Author: Beulah E. McKenzie, Fabio
Nudelman, Paul H. H. Bomans,
et al

Publication: Journal of the American
Chemical Society

Publisher: American Chemical Society

Date: Aug 1, 2010

Copyright © 2010, American Chemical Society

Logged in as:
yingchao chen
Account #:
3000881260

LOGOUT

PERMISSION/LICENSE IS GRANTED FOR YOUR ORDER AT NO CHARGE

This type of permission/license, instead of the standard Terms & Conditions, is sent to you because no fee is being charged for your order. Please note the following:

- Permission is granted for your request in both print and electronic formats, and translations.
- If figures and/or tables were requested, they may be adapted or used in part.
- Please print this page for your records and send a copy of it to your publisher/graduate school.
- Appropriate credit for the requested material should be given as follows: "Reprinted (adapted) with permission from (COMPLETE REFERENCE CITATION). Copyright (YEAR) American Chemical Society." Insert appropriate information in place of the capitalized words.
- One-time permission is granted only for the use specified in your request. No additional uses are granted (such as derivative works or other editions). For any other uses, please submit a new request.

If credit is given to another source for the material you requested, permission must be obtained from that source.

Figure 2.10

Title: Hidden Structural Features of Multicompartment Micelles Revealed by Cryogenic Transmission Electron Tomography

Author: Tina I. Löbbling, Johannes S. Haataja, Christopher V. Synatschke, et al

Publication: ACS Nano

Publisher: American Chemical Society

Date: Nov 1, 2014

Copyright © 2014, American Chemical Society

Logged in as:
yingchao chen
Account #:
3000881260

LOGOUT

PERMISSION/LICENSE IS GRANTED FOR YOUR ORDER AT NO CHARGE

This type of permission/license, instead of the standard Terms & Conditions, is sent to you because no fee is being charged for your order. Please note the following:

- Permission is granted for your request in both print and electronic formats, and translations.
- If figures and/or tables were requested, they may be adapted or used in part.
- Please print this page for your records and send a copy of it to your publisher/graduate school.
- Appropriate credit for the requested material should be given as follows: "Reprinted (adapted) with permission from (COMPLETE REFERENCE CITATION). Copyright (YEAR) American Chemical Society." Insert appropriate information in place of the capitalized words.
- One-time permission is granted only for the use specified in your request. No additional uses are granted (such as derivative works or other editions). For any other uses, please submit a new request.

If credit is given to another source for the material you requested, permission must be obtained from that source.

Permissions for Chapter 6
Figure 6.1, Figure 6.2, Figure 6.3

Title: Controlled Shape Transformation of Polymersome Stomatocytes

Author: Silvie A. Meeuwissen, Kyoung Taek Kim, Yingchao Chen, Darrin J. Pochan, Jan C. M. van Hest

Publication: Angewandte Chemie International Edition

Logged in as:
yingchao chen

LOGOUT

Publisher: John Wiley and Sons

Date: Jun 17, 2011

Copyright © 2011 WILEY-VCH Verlag GmbH & Co.
KGaA, Weinheim

Order Completed

Thank you for your order.

This Agreement between yingchao chen ("You") and John Wiley and Sons ("John Wiley and Sons") consists of your license details and the terms and conditions provided by John Wiley and Sons and Copyright Clearance Center.

Your confirmation email will contain your order number for future reference.

[Get the printable license.](#)

License Number	3553761061001
License date	Jan 21, 2015
Licensed Content Publisher	John Wiley and Sons
Licensed Content Publication	Angewandte Chemie International Edition
Licensed Content Title	Controlled Shape Transformation of Polymersome Stomatocytes
Licensed Content Author	Silvie A. Meeuwissen,Kyoung Taek Kim,Yingchao Chen,Darrin J. Pochan,Jan C. M. van Hest
Licensed Content Date	Jun 17, 2011
Licensed Content Pages	4
Type of use	Dissertation/Thesis
Requestor type	Author of this Wiley article
Format	Print and electronic
Portion	Figure/table
Number of figures/tables	4
Original Wiley figure/table number(s)	Figure1, Figure 2
Will you be translating?	No
Title of your thesis / dissertation	hybrid nanoparticle formation via block copolymer blends and kinetic control
Expected completion date	Feb 2015
Expected size (number of pages)	None
Requestor Location	yingchao chen 201 Dupont Hall Material Science and Engineering University of Delaware NEWARK, DE 19716 United States Attn: yingchao chen
Billing Type	Invoice
Billing address	yingchao chen 201 Dupont Hall Material Science and Engineering University of Delaware

NEWARK, DE 19716
United States
Attn: yingchao chen

Total 0.00 USD

[ORDER MORE](#) [CLOSE WINDOW](#)

Copyright © 2015 [Copyright Clearance Center, Inc.](#) All Rights Reserved. [Privacy statement.](#)
Comments? We would like to hear from you. E-mail us at customercare@copyright.com



ACS Publications Title:
Most Trusted. Most Cited. Most Read.

Modular Synthesis of
Amphiphilic Janus
Glycodendrimers and Their Self-
Assembly into
Glycodendrimersomes and Other
Complex Architectures with
Bioactivity to Biomedically
Relevant Lectins

Author: Virgil Percec, Pawaret
Leowanawat, Hao-Jan Sun, et al

Publication: Journal of the American
Chemical Society

Publisher: American Chemical Society

Date: Jun 1, 2013

Copyright © 2013, American Chemical Society

Logged in as:
yingchao chen

[LOGOUT](#)

PERMISSION/LICENSE IS GRANTED FOR YOUR ORDER AT NO CHARGE

This type of permission/license, instead of the standard Terms & Conditions, is sent to you because no fee is being charged for your order. Please note the following:

- Permission is granted for your request in both print and electronic formats, and translations.
- If figures and/or tables were requested, they may be adapted or used in part.
- Please print this page for your records and send a copy of it to your publisher/graduate school.
- Appropriate credit for the requested material should be given as follows: "Reprinted (adapted) with permission from (COMPLETE REFERENCE CITATION). Copyright (YEAR) American Chemical Society." Insert appropriate information in place of the capitalized words.
- One-time permission is granted only for the use specified in your request. No additional uses are granted (such as derivative works or other editions). For any other uses, please submit a new request.

Scheme 6.6, Figure 6.10, Figure 6.11.

As a PNAS author, you and your employing institution or company retain extensive rights for use of your materials and intellectual property. You retain these rights and permissions without having to obtain explicit permission from PNAS, provided that you cite the original source:

- The right to post a [PDF of your article](#) on [your Web site](#) or that of your employer's institution (provided that the institution is nonprofit).
- The right to make [electronic or hard copies of articles](#) for your personal use, including classroom use, or for the personal use of colleagues, provided those copies are not for sale and are not distributed in a systematic way outside of your employing institution.
- The right to post and update a preprint version of your article on a public electronic server such as the Web. See the information on [electronic preprints](#) below.
- The right to permit others to use your original figures or tables published in PNAS for noncommercial and educational use (i.e., in a review article, in a book that is not for sale), provided that the original source is cited. Third parties need not ask PNAS for permission to use figures and tables for such use.
- The right, after publication in PNAS, to use all or part of your article in a printed compilation of your own works, such as collected writings or lecture notes.
- If your article is a "work for hire" made within the scope of your employment, your employer may use all or part of the information in your article for intracompany use.
- The right to include your article in your thesis or dissertation.
- The right to present all or part of your paper at a meeting or conference, including ones that are webcast, and to give copies of your paper to meeting attendees before or after publication in PNAS. For interactions with the media prior to publication, see the [PNAS Policy on Media Coverage](#).
- The right to publish a new or extended version of your paper provided that it is sufficiently different to be considered a new work.
- The right to expand your article into book-length form for publication.
- The right to reuse your original figures and tables in your future works.
- Patent and trademark rights or rights to any process or procedure described in your article. For other uses by authors, please contact PNAS at PNASpermissions@nas.edu.